Turbulent Boundary Layer on a Rough Surface with Pressure Gradient and Surface Heating.

by

Abd-El-Hamid Hamed AWAD, B.Sc.(Eng).

August 1966

A thesis submitted for the Degree of Doctor of Philosophy in the Faculty of Engineering of the University of London.

Summary

The boundary layer on a surface with square cavities as roughness elements was examined in the presence of mild favourable and adverse pressure gradients and surface heating. The range of Reynolds numbers covered extended to about 2×10^6, the reference airspeed being about 100 ft/sec and the plate length 3 ft.

Velocity and temperature profiles were found similar for cavity or protrusion type roughness, with their origin below the crest of roughness elements (or top of cavities).

The "law of the wall" was generally valid for a small region of the measured profiles. The presentation of the profiles was found best defined by the velocity-defect form, with 'G' as parameter. Limited success was achieved using the method of computing the skin-friction coefficients from velocity measurements.

The skin-friction coefficients were strongly influenced by the pressure gradients, and responded differently when applying surface heating, depending on the sign of pressure gradient present.

The relation $G(\pi)$ differed from that of the smooth surface, due to the higher values of H in the present work.

The temperature profiles were affected by roughness and pressure gradient, and were far from "similar" to the velocity profiles. A new presentation is suggested.

The heat-transfer coefficients were slightly influenced by the applied preesure gradients, and strongly affected by the wall temperature gradient. The present theories for smooth surfaces compared poorly with the obtained values of heat-transfer coefficients after a stepwise wall-temperature discontinuity was applied.

The measured longitudinal velocity fluctuations were higher than those for a smooth surface, and had a clear "peak" near the origin of the velocity profiles. The applied pressure gradients had small effect on $\overline{u'^2}$ particularly near the surface.

The measured $\overline{u'v'}$ (y) show sharp increase near the surface, but τ/τ_w agrees closely with that of a smooth surface elsewhere.

The effect of abrupt change in surface roughness was examined.

Available data for different roughness geometries were correlated.

Finally, heat and friction characteristics of a rough wall were linked.

Acknowledgements

The author gratefully acknowledges the unfailing guidance and encouragement given by his supervisor, Dr. A.J. Taylor-Russell throughout the course of this study.

The author wishes to thank Mr.W.H.Davies and the Aeronautics Department Workshop staff for their patient care in the construction of the model.

The author wishes to express his appreciation of the help given by Miss Rogers, Cranley Typing Office, who typed the thesis, and Mr. J.P.O'Leary who carried out the photographic work.

The author gratefully acknowledges the financial support of Cairo University, whose grant made possible the present study.

LIST OF CONTENTS

Nomenclature

A	Constant appearing in the velocity defect profile relationship,
B	Constant; heat-transfer coefficient of the roughness-dominated region;
C	Constant,
C_f	Local skin-friction coefficient ($\tau w / \frac{1}{2} \rho e U e^2$),
c_p	Specific heat at constant pressure,
C_p	Pressure coefficient ($= (P-Po) / \frac{1}{2} \rho e U^2_{ref}$),
D	Pitch of roughness elements,
G	Velocity-defect shape parameter ($= \int_0^\infty \left(\frac{U_e - U}{u_\tau}\right)^2 d \frac{y u_\tau}{\delta_{1u} U_e}$)
H	Boundary-layer shape parameter ($= \delta_1/\delta_2$),
Hu	" " " " ($= \delta_{1u}/\delta_{2u}$),
k	Height of roughness elements,
k_s	Equivalent height of sand roughness,
l	Length
Nu	Nusselt number ($Qw\, x / \lambda\, (Tw - Te)$),
Nuo	Nusselt number for a smooth surface,
P	Static pressure,
P_o	Reference pressure (wall pressure at x = 34 ins),
P_r	Prandtl number ($= \mu\, c_p / \lambda$),
Q_w	Surface heat-input per unit area,
R	Reynolds number (Ul/ν),

S_t	Heat transfer coefficient ($Q_w/\rho_e U_e c_p(Tw-Ta)$,
T	Absolute temperature (^oK),
Ta	Absolute adiabatic-wall temperature,
Te	Absolute temperature of air flow outside the boundary layer,
Tr	Absolute reference temperature,
Tw	Absolute wall temperature,
U	Mean velocity in the direction of x,
U_d	Velocity defect (= $(Ue - U)/u_\tau$)
U_e	Mean velocity in the direction of x in the free stream,
U_{ref}	" " " " " " " " " " " at x = 34 ins.,
u_τ	Friction velocity ($\sqrt{\tau w/\rho}$),
u'	Fluctuating velocity component in the direction of x,
V	Mean velocity in the direction of y,
v'	Fluctuating velocity component in the direction of y,
W'	Fluctuating velocity component in the direction of z,
x	Distance along the plate in the direction of the main flow, measured from the beginning of roughness.
y	Distance along the perpendicular to the plate,
z	Distance along the plate perpendicular to the direction of the main flow,
δ	Thickness of the dynamic boundary layer ($\delta_{0.99}$),
δ_1	Boundary layer displacement thickness $\left(= \int_0^\infty 1 - \frac{\rho U}{\rho U_e} \, dy\right)$
δ_{1u}	" " " " $\left(= \int_0^\infty 1 - \frac{U}{U_e} \, dy\right)$

δ_2 Momentum thickness $\left(= \int_0^\infty \frac{\rho U}{\rho_e U_e}\left(1 - \frac{U}{U_e}\right) dy\right)$

δ_{2u} " " $\left(= \int_0^\infty U/U_e\left(1 - \frac{U}{U_e}\right) dy\right)$

δ_3 Energy thickness $\left(= \int_0^\infty \frac{\rho U}{\rho_e U_e}\left(1 - \left(\frac{U}{U_e}\right)^2\right) dy\right)$

δ_{3u} " " $\left(= \int_0^\infty \frac{U}{U_e}\left(1 - \left(\frac{U}{U_e}\right)^2\right) dy\right)$

Δ Thickness of the thermal boundary layer ($\Delta_{.99}$),

Δ_1 Thermal - displacement thickness $\left(= \int_0^\infty \frac{\rho}{\rho_e}\left(1 - \bar{\theta}\right) dy\right)$

Δ_2 Enthalpy thickness $\left(= \int_0^\infty \frac{\rho U}{\rho_e U_e}\left(1 - \bar{\theta}\right) dy\right)$

θ Temperature (°C),

θ_a Adiabatic-wall temperature (°C),

θ_e Temperature of air flow outside the boundary layer,

θ_w Wall temperature,

θ' Fluctuation component of temperature,

$\bar{\theta}$ Non-dimensional temperature in the boundary layer $\left(\equiv (\theta_w - \theta)/(\theta_w - \theta_e)\right)$

λ Coefficient of thermal conductivity for air,

μ Molecular viscosity,

ν Kinematic viscosity ($= \mu / \rho$),

Π Pressure gradient parameter $\left(\frac{\delta_1}{\tau_w} \frac{dP}{dx}\right)$,

ρ Density of air,

ρ_e Density of air outside the boundary layer,

τ Shear stress in the boundary layer,

τ_w Shear stress at the wall ($\frac{1}{2} \rho_e U_e^2 C_f$)

Note:- In Appendix II only, the following symbols were used;

Y instead of $10^3 . y$, (where y is in inches),

U " $10^3 . U/U_e$, and ,

T " $10^3 . \bar{\theta}$.

I. INTRODUCTION

I.1 - Purpose and Scope of Investigation:

Surface roughness has a very important influence on the frinctional resistance and heat transfer characteristics of surfaces. Because most of the materials in engineering use can hardly be considered as hydraulically smooth; especially at high Reynolds numbers; the investigation of such characteristics has many practical uses in aeronautics and many other fields.

Although the study of the effect of roughness has occupied many investigators, most studies were based on results from flow in pipes, or over flat plates with either heat transfer or pressure gradient, but rarely in the presence of both.

The present study is therefore aimed at better knowledge on the effect of heat transfer and pressure gradient, on the characteristics of turbulent boundary layers on rough surfaces.

The present work was carried out using a flat plate with square cavities, of constant pattern and dimensions, as roughness elements. Two arbitrary pressure distributions were chosen, one approximately constant, changing to favourable towards the trailing edge of the 3 ft. long plate, and one adverse changing to constant.

Three cases were studied for each pressure distribution, the unheated plate, the isothermally heated, and the case where the plate temperature undergoes a stepwise discontinuity.

Shear-stress profiles were measured for both pressure distributions. The plate was then unheated.

Some of the shear-stress profiles were of the boundary layer experiencing an abrupt change in surface roughness.

I.2 - Review of Relevant Literature:

It is not an easy task to mention all the work done in connection with rough surfaces. However, a brief account on some of the work will be given.

J. Nikuradse (1) experimented systematically on pipes with sand roughness. Variation of pipe diameter and sand-grain sizes, enabled him to achieve a range of r/k_s from 15 to 500. Nikuradse identified three roughness regimes. The hydraulically-smooth ($0 \leq k_s u_\tau/\nu \leq 5$) has a resistance coefficient as unique function of Reynolds number. The resistance of the transition regime is function of both Reynolds number and k_s/r. The resistance of the completely rough regime ($k_s u_\tau/\nu > 70$) is a unique function of k_s/r. Nikuradse also found that the velocity-defect profile for a smooth wall is still applicable for a rough surface, irrespective of the height of roughness elements.

N..Scholz(1) found that the semi-logarithmic linear relationship, known as "the law of the wall", is applicable for rough surfaces, except that the line is shifted downwards by $\Delta U/u_\tau$ which depends upon the value of $k_s u_\tau/\nu$.

H. Schlichting worked on plates having artificial roughness, for which he determined the equivalent sand-roughness height. His experiments covered spheres, cones, spherical segments, and short angles fixed on a smooth surface. The heights and spacing for each type were varied. Schlichting found that C_f is constant for the same values of x/k_s in the completely rough regime, irrespective of the Reynolds number R_x $(\equiv U_e x/\nu)$.

Schlichting also plotted the iso-velocity curves behind a row of spheres, which clearly show that the velocity behind a roughness element, was much larger than that at the same height from the plate, measured in the gap between the spheres (see Fig.21.15(1)). Schlichting called this phenomena "the negative wake effect". He stated that a body placed in a boundary layer, produces an effect different from that caused by a body placed in the free stream. This effect was explained by the existence of a secondary flow as calculated by F. Schultz-Grunow.

Wieghardt (1) experiemnted, as Schlichting, on artificial roughness elements over flat plates. He used circular cavities and rectangular ribs as roughness elements. It was found that, for circular cavities, the increment of the drag coefficient passes by a maximum at a ratio of height to diameter of the cavities. This maximum occurred at 0.5 ratio approximately (see Fig.21.14(1)).

Hama (2) used four different wire screens at a constant pressure over a flat plate. The wire-mesh length varied from 1 to 1/28 of an inch, and the ratios of wire-diameter to mesh length were 0.207, 0.216, 0.207 and 0.210 respectively. Hama plotted the shift of the semi-logarithmic relation $\Delta U/u_\tau$ against log $k u_\tau/\nu$ for the results he obtained, and those of Sarpkaya for channel flow. The relationship was found linear for $k u_\tau/\nu > 30$. For lower values, Hama achieved some points which lied below the extrapolation of the line.

Brunello (3) used three plates with spheres at the maximum possible density. The sphere diameters were 0.2, 0.4 and 0.6mm respectively, and the plates were lightly heated to 12°C approximately above that of the main stream. No pressure gradient was applied. Brunello's results show that the velocity profiles exhibited a tendency to increase their thickness with increase of the sphere diameters used. Brunello started his experiments with a smooth surface, for which good agreement between velocity and temperature profiles was found. This was not so for rough surfaces, which exhibited marked dissimilarity, which increased with the increase of the sphere diameters. Skin friction and heat transfer were both greater for the rough surfaces, than those for a smooth surface, and increased as the height of roughness elements increased.

Reynolds analogy applied reasonably for the smooth surface, but the ratio $2S_t/C_f$ decreased as the height of roughness increased.

Brunello found, as Schlichting did, that C_f remained unaltered for constant x/k, and similarly for S_t with slight discrepancy. The skin-friction coefficients for the three rough plates agreed with those of the plates with sand grains of equal sizes as the spheres.

Brunello chose a fictitious origin for the x-axis, which he used for the calculation of $R_{x'}$. Skin-friction and heat-transfer coefficients could be expressed in the form $C\left(R_{x'}\right)^{-1/5}$.

J. Doenecke (4) succeeded Brunello, using similar surface heating, and no pressure gradient was applied. He examined four different rough plates, two were provided with cavities, and two with protrusions. The plates with cavities were essentially short cylindrical elements, standing with their crests level with the surface of the smooth leading edge. The other plates had two-dimensional square ribs of different sizes, but with the same pitch.

Doenecke gave a sketch of a stationary eddy behind the square ribs, with its centre situated at about 0.6 the height of roughness for k = 3mm and D = 12.5mm. He also stated that the temperture variation is very small within the eddy, but behaves like that of a smooth surface beyond it. His velocity profiles were similar when plotted in the form $\frac{U}{U_e}(y/\delta_2)$ and so was the case for the temperature profiles $\bar{\theta}(y/\Delta_2)$.

Doenecke concluded that the temperature profiles were more curved than those of the velocity $(\delta_1 > \Delta_1 , \delta_2 > \Delta_2)$, and that the curves $\frac{\overline{u'v'}}{U_e^2}(y)$ had the same behaviour as those of $\frac{\overline{\theta'v'}}{U_e T_e}(y)$. He found that $2 S_t / C_f$ decreases as the roughness height increases, as previously found by Brunello.

Also working on two-dimensional square ribs, were Perry and Joubert (5), who experimented in the presence of two different arbitrary adverse-pressure gradients on a flat plate. In their paper, the authors proposed a graphical method for computing the skin-friction coefficients, based on the assumption that a logarithmic law of the wall exists for rough surfaces, although shifted, and that the wake hypothesis introduced by D. Coles is applicable. The authors compared between the results obtained by using the proposed method, and those obtained by using the two-dimensional momentum integral equation for some profiles. The two methods only disagreed at the downstream end of the plate, where the pressure gradient was milder than upstream. The validity of that method for the present experiments is discussed in § III.

D. Bettermann, E. Brun and P. Gougat (6) used the results obtained in (4), and two more plates with square ribs, to define a form of velocity and temperature profiles. The authors found that the law of the wall show large scatter, and thought the profiles are best represented by $U/U_e = a(y/\delta_2)^m$ and $\bar{\theta} = b(y/\Delta_2)^n$ respectively. The constants a, b, m and n varied from one plate to another.

II. INSTRUMENTATION AND EXPERIMENTAL TECHNIQUE

II.1 - Wind Tunnel:

The experiments were carried out using the Imperial College 3' x 2' wind tunnel. The working section measures 40 inches high by 24 inches wide, and is 12 ft. long. Excluding the corner fillets, the wind tunnel contraction ratio is 9.

The tunnel is provided with five screens of 30 meshes/inch, of wire diameter 0.01", producing a blockage coefficient of 0.49. The air-speed is controlled by a variable speed motor coupled to the fan-shaft. It attains a maximum of 140 ft/sec. approximately in the working section, at maximum motor speed of 1600 r.p.m. With empty tunnel, the air speed is about 2% higher at the bottom of the working section than at the top. Due to the vibrations at high motor speeds, the air speed was chosen about 100 ft/sec throughout the experiments.

The turbulence level was 0.25% on the centre line of the working section, when the tunnel was empty and at the air speed of 100 ft/sec.

A sketch of the tunnel is given on Fig.II 1.1.

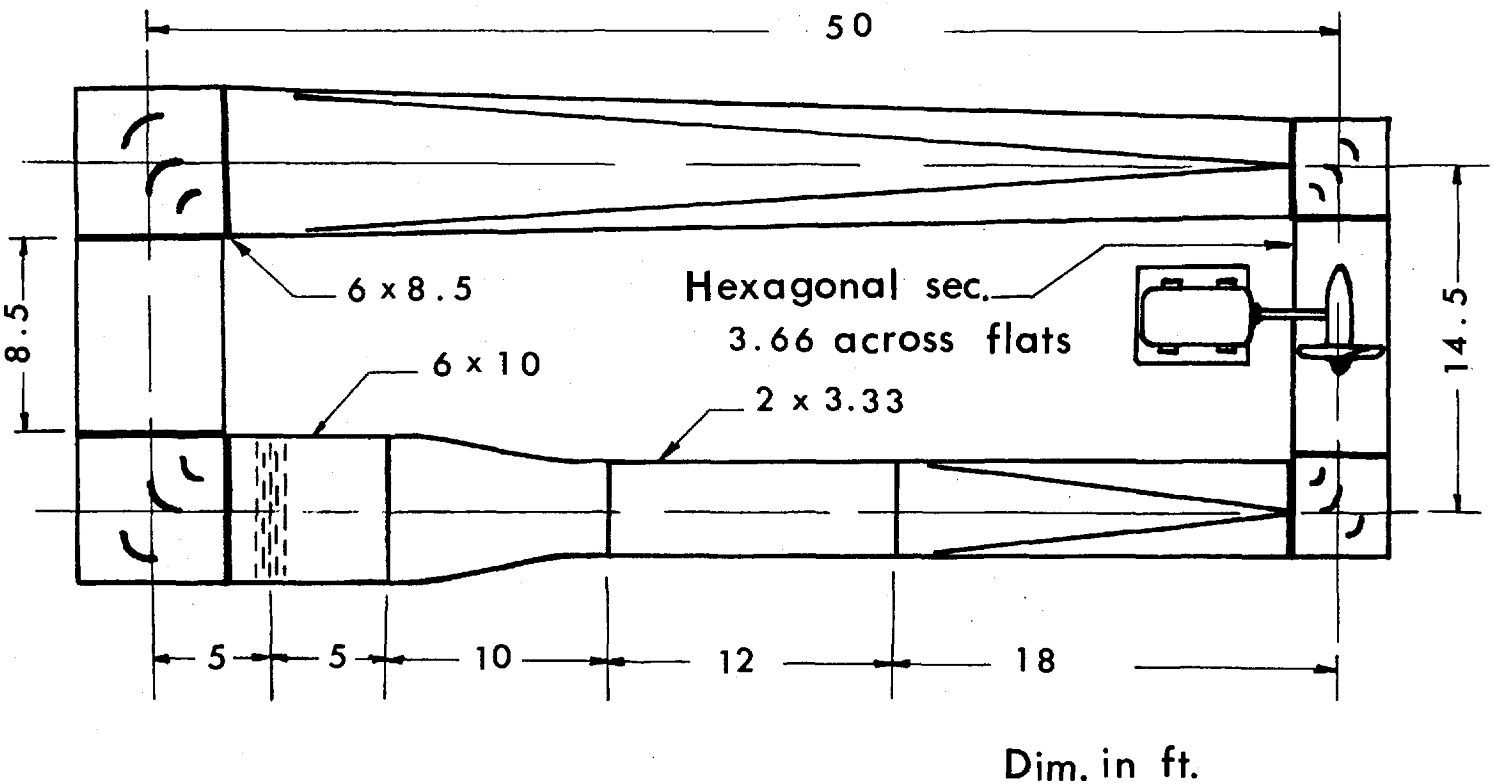

Fig. II.1.1_ Wind Tunnel layout.

II.2 - <u>Model Construction</u>:

The model consists of a flat plate $37\frac{5}{16}$ in. long by $25\frac{1}{2}$ in. wide, and $\frac{1}{4}$ in. thick. The plate was provided with $\frac{3}{8}$ in. square cavities, $\frac{1}{8}$in. deep. The pitch of roughness pattern measured $\frac{9}{16}$ in, as shown on Fig. II.2.1

The plate was realised by tightly riveting a perforated $\frac{1}{8}$ in. thick commercial aluminium plate, on a smooth one of the same thickness and material.

The plate was placed vertically in the working section of the tunnel, between 6 ft. long horizontal end plates, as shown in Fig.II.2.2.

As it was to be heated, the plate was mounted freely with a clearance of $\frac{1}{8}$ in. in both ways, to allow for thermal expansion without deformation of the plate (Fig.II.2.3).

The plate was also recessed by $2\frac{1}{2}$ ins. from the side walls of the tunnel, to avoid any interference from the boundary layer of the tunnel-walls. A leading-edge bleed was provided. Its surface was left smooth, and measured $10\frac{1}{4}$ ins. upstream of the rough plate. This is shown on Fig. II.2.4.

The plate had sixty pressure tubes. They were arranged in fours at fifteen stations along the x-axis. The tubes were connected to vertical alchol manometers,

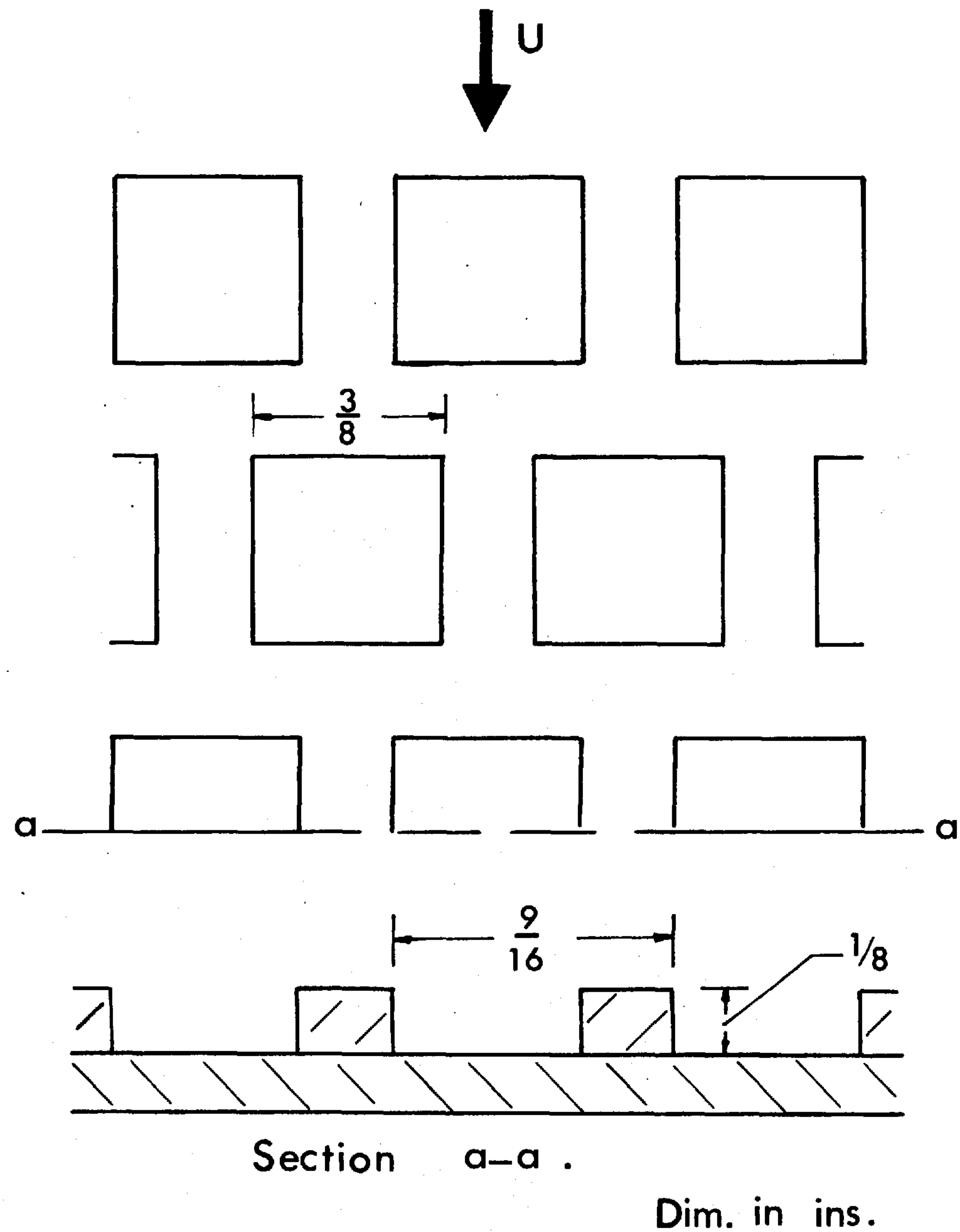

Fig. II.2.1_ Detail of the roughness.

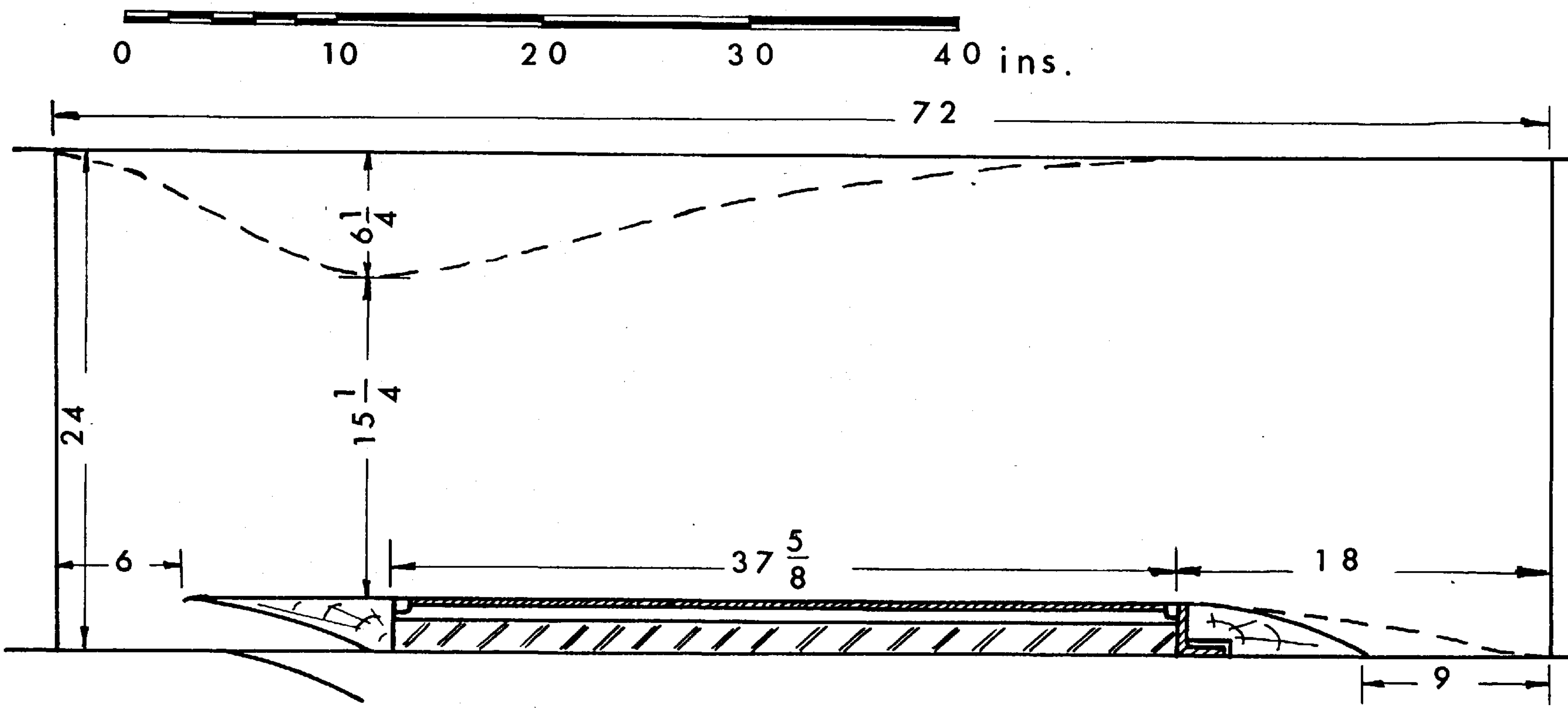

Fig. II.2.2_ Plate mounting in the wind tunnel.

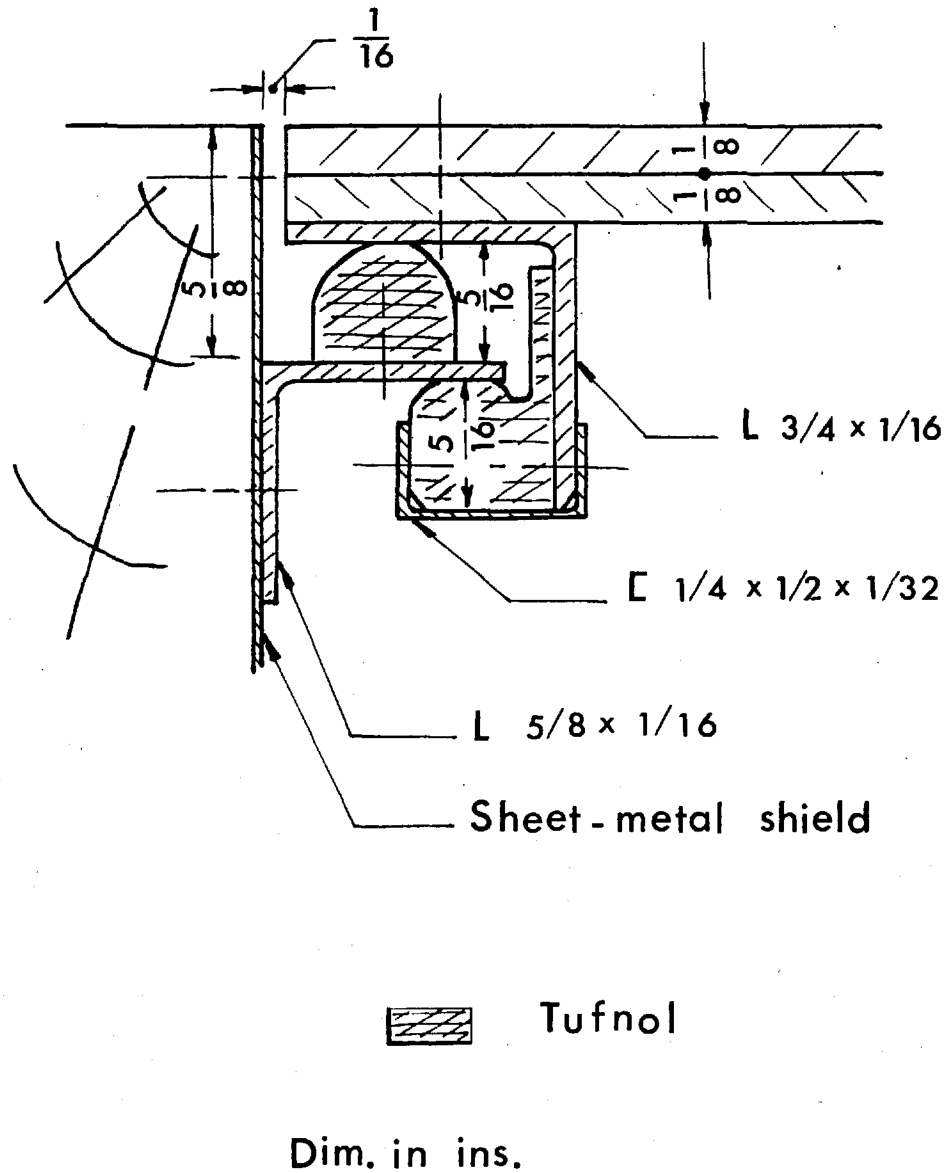

Fig. II.2.3_ Detail of plate's edge support.

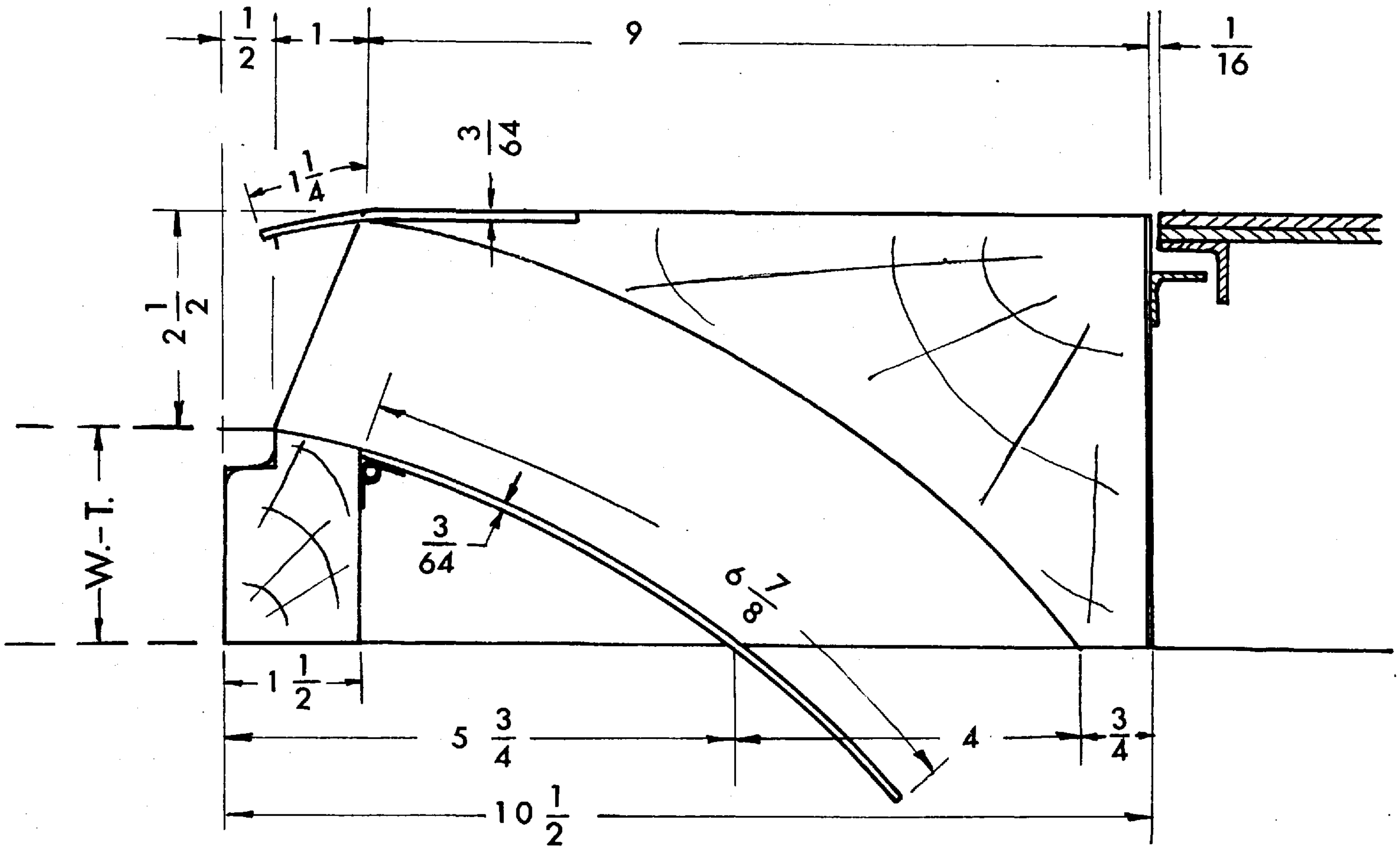

Fig. II.2.4_ Detail of bleed for tunnel-wall boundary layer.

partly by silicone tubing to withstand the heat. One of the tubes was placed, on the centre-line of the plate, level with the top of cavities, and another level with the bottom. The other two tubes were 6¼ ins. above and below the centre-line, level with the top of cavities.

The heating system consists of 48 Cressall metal cased mica wound heating elements. Each heater measured 7¼ x 2 ins., with power rating 215 watts approximately. They were mounted in vertical rows of three, on the back of the plate. This is shown by Fig.II.2.5.

A thermocouple joint was inserted in a pop rivet between each two successive heaters. They were fixed in position by a mixture of aluminium saw-dust and Araldite. This arrangement gave electric resistances of 3 to 5 ohms between the plate and the joint. A sketch is shown on Fig.II.2.6. The thermocouple materials were high conductivity copper against Ferry*, which gave better linearity in calibration than some other arrangements. A typical calibration curve is shown on Fig. II.2.7.

* Ferry is the trade name of a 45-55 nickel-copper alloy resistance wire of Messrs. Henry Wiggin & Co.Ltd.

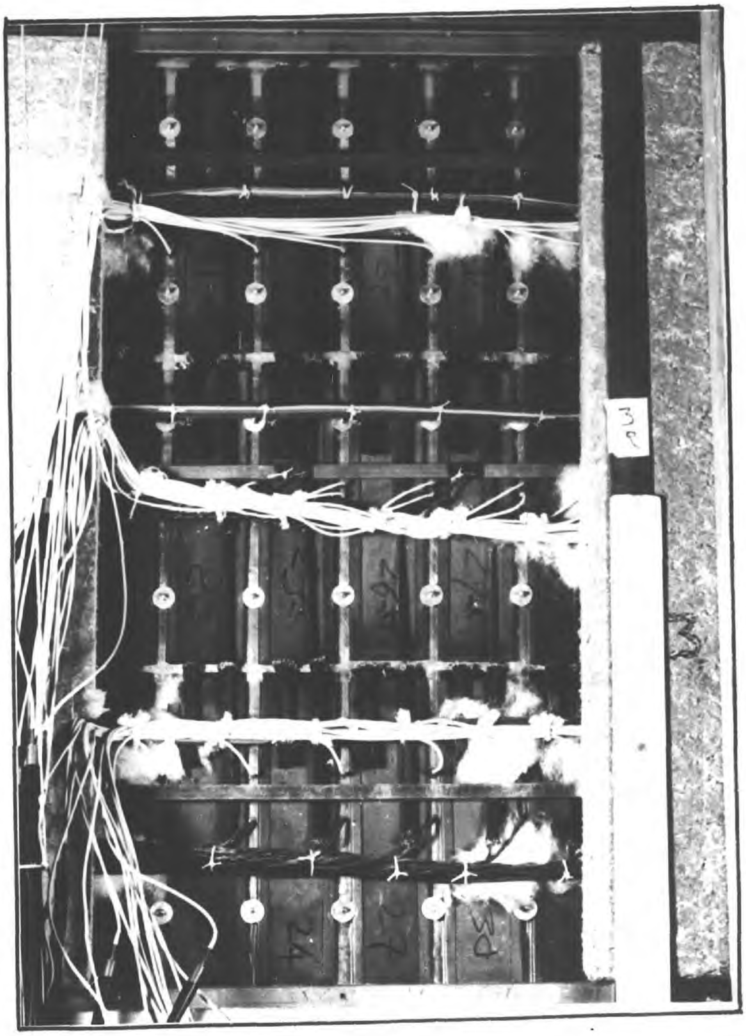

Fig.II.2.5 _ Heating elements mounted on the plate.

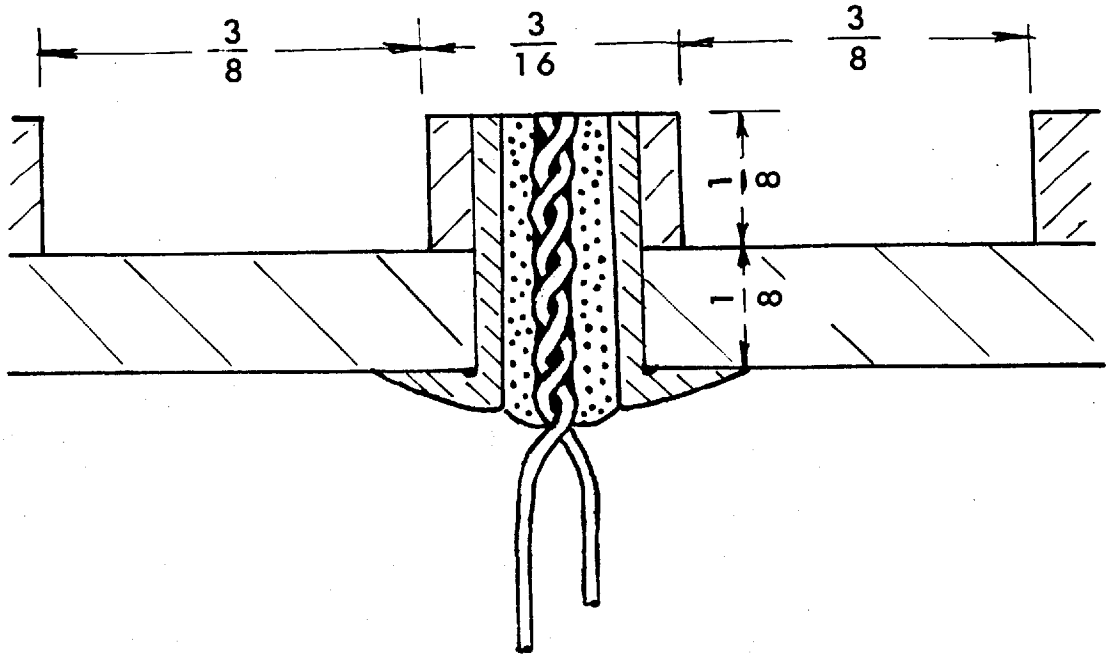

Fig. II.2.6 _ Sketch of hot-junction for a typical thermocouple.

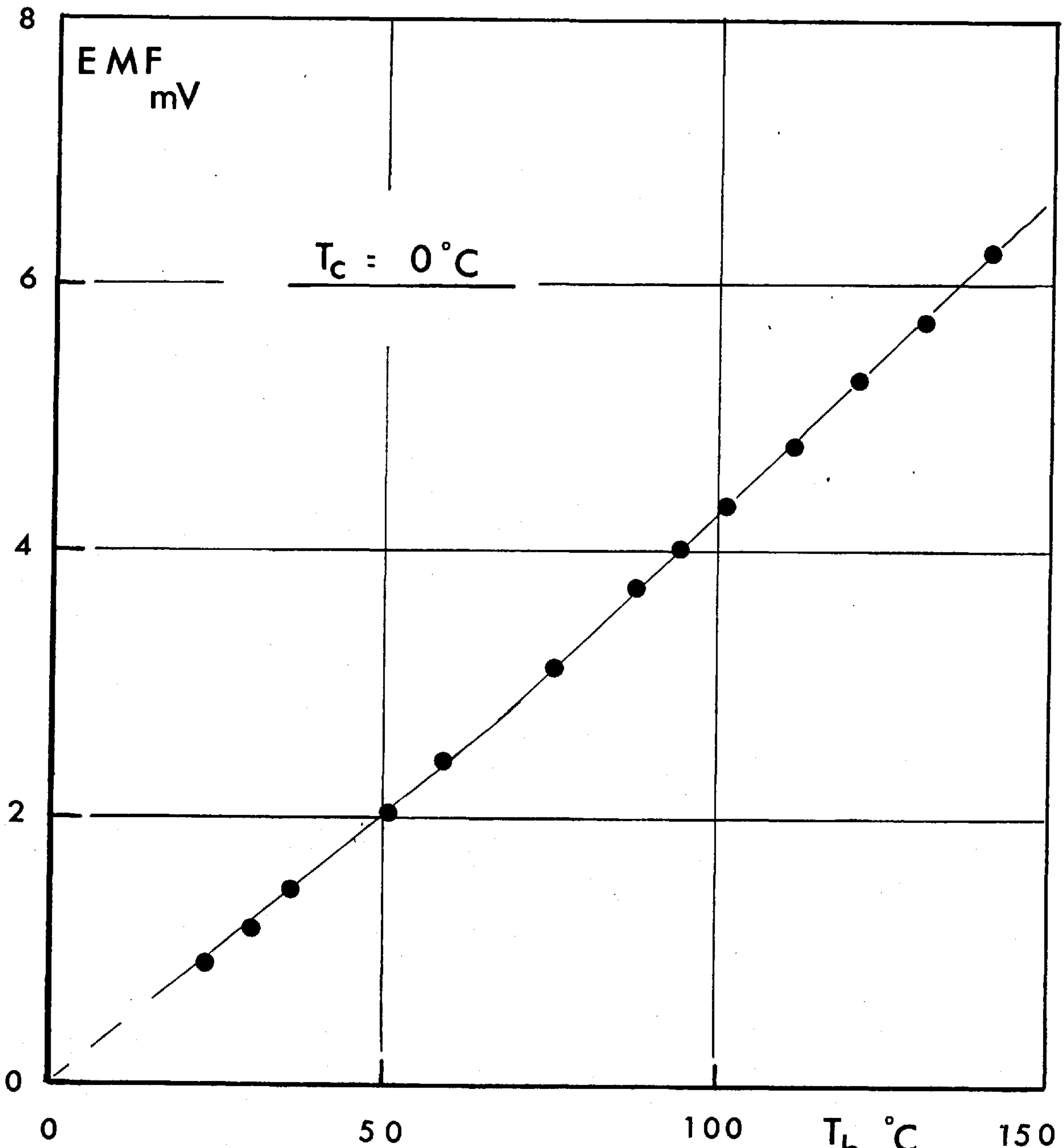

Fig. II.2.7_ Thermocouple calibration curve.

Each of the heaters was controlled separately by a set of nine Cressall mica wound strip resistors, connected in series with the heater. These ranged from 0.75 to 192 ohms. Each resistance was controlled by a parallel on/off switch. The resistors and switches were mounted in a box, which was ventilated by two axial fans.

The adjustment -box is shown on Fig. II.2.8 and II.2.9., and a circuit diagram is given on Fig. II.2.10.

An air gap of ½ in. was left behind the heaters. After that a 1½ in. thick asbestos block was fixed.

A row of eight thermocouples was placed along the centre-line, immediately close to the hot side of the asbestos block. Three thermocouples were close to the cold side of the asbestos block.

The adverse pressure distribution was achieved by placing a profile surface on the opposite side of the tunnel wall, as shown by the broken line on Fig. II.2.2.

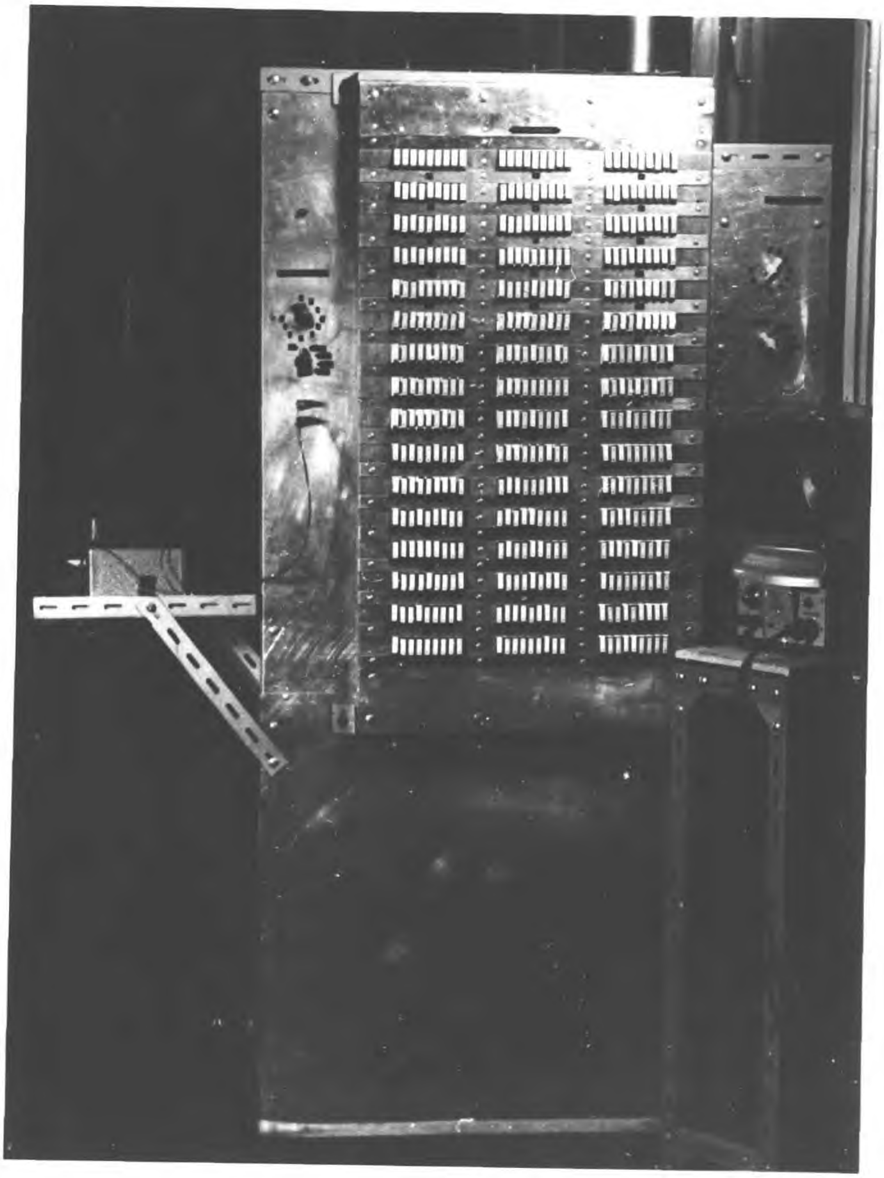

Fig. II.2.8_ Box for heating adjustment.

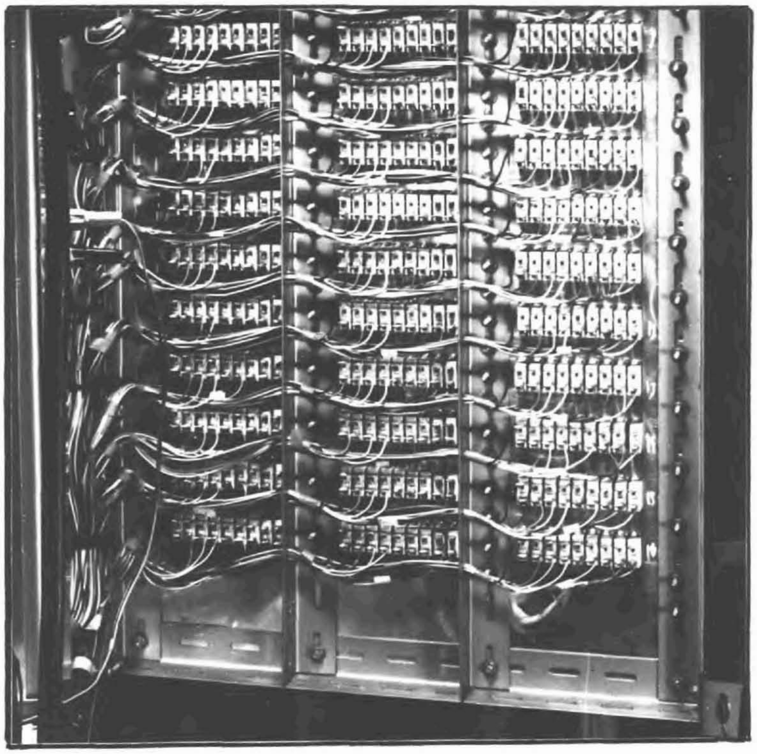

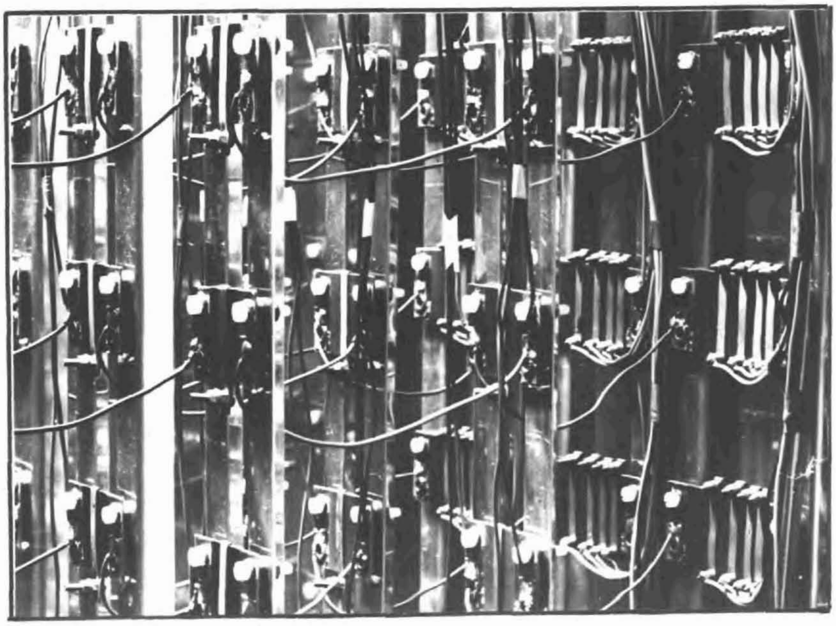

Fig. II.2.9_ Part of the inside elements of the adjustment box.

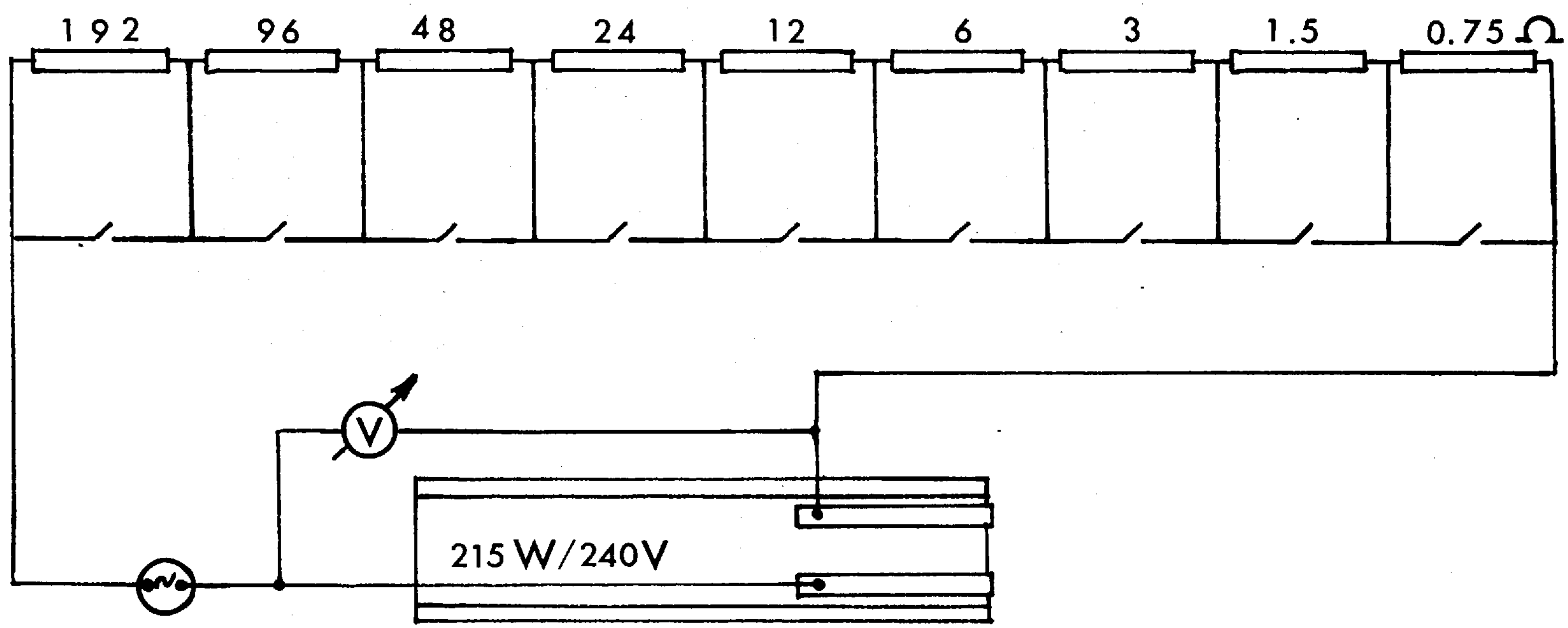

Fig. II.2.10_ Electric circuit diagram for a typical heater.

II.3 - Measurement of Velocity and Temperature Profiles:

Velocity and temperature profiles were measured by a special hot-wire probe. It consists of two steel needles, bent forward to avoid interference of the probe, to form the wire support. A third straight needle was connected to a simple electric light-signal, to indicate the distance from the plate. The three needles had 0.027 in. shank diameter, and held by an Araldite casting. The Araldite was shaped to a streamline cross-section, which in turn was matched to a streamline steel tube 0.625 x 0.2 in. A probe is shown on Fig. II.3.1.

The hot-wire material used was Platinum Wollaston wire of 0.0001 in. core-diameter.

The wires were given a slight curvature, when soldered, to allow for the vibrations. The etched part was 0.45 to 0.6 mm, and was kept straight.

A detailed account on hot wire preparation is given in (12) and (14).

The probes were connected to a model 55A ol DISA constant temperature anemometer (7).

To discuss the method of measurement of the velocity and temperature profiles, the calibration formula will be

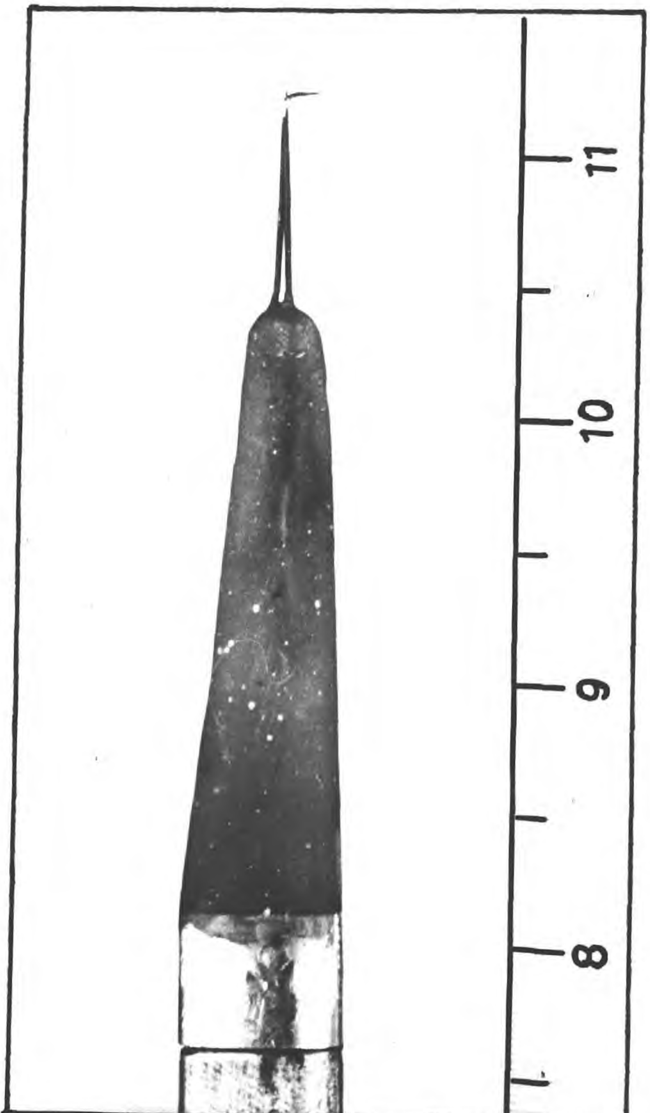

Fig. II. 3.1_ Probe for velocity and temperature profiles.

given. It can be written as:

$$0.24\frac{V^2}{R_w} = l\,[T_w - T_a]\left(\lambda + 2\sqrt{\lambda \rho c_p d U}\right).$$

where: V is the D.C. voltage across the wire,

R_W the wire operating-resistance,

l the wire length,

T_W the wire operating-temperature,

T_a the ambient temperature of air, and

d the wire diameter.

This relation can be expressed in the form:

$$V^2 = (T_w - T_a)(A + B\sqrt{U}) .$$

where A and B are constants for a particular wire.

$V^2(\sqrt{U})$ was found to be linear* for platinum wires, in the range $(T_w - T_a) \geqslant 140\,^\circ C$.

We can then construct an array of wire calibration curve with wire-temperatures as parameter, similar to the sketch on Fig.II.3.2.

The operating resistances corresponding to the different temperatures could be found according to the relation:

$$R_w = R_a\,(1 + \alpha\,(T_w - T_a))$$

where R_a is the wire resistance at ambient temperature,

α platinum temperature coefficient of resistance.

*Except for very low air speeds of O(1)ft/sec.

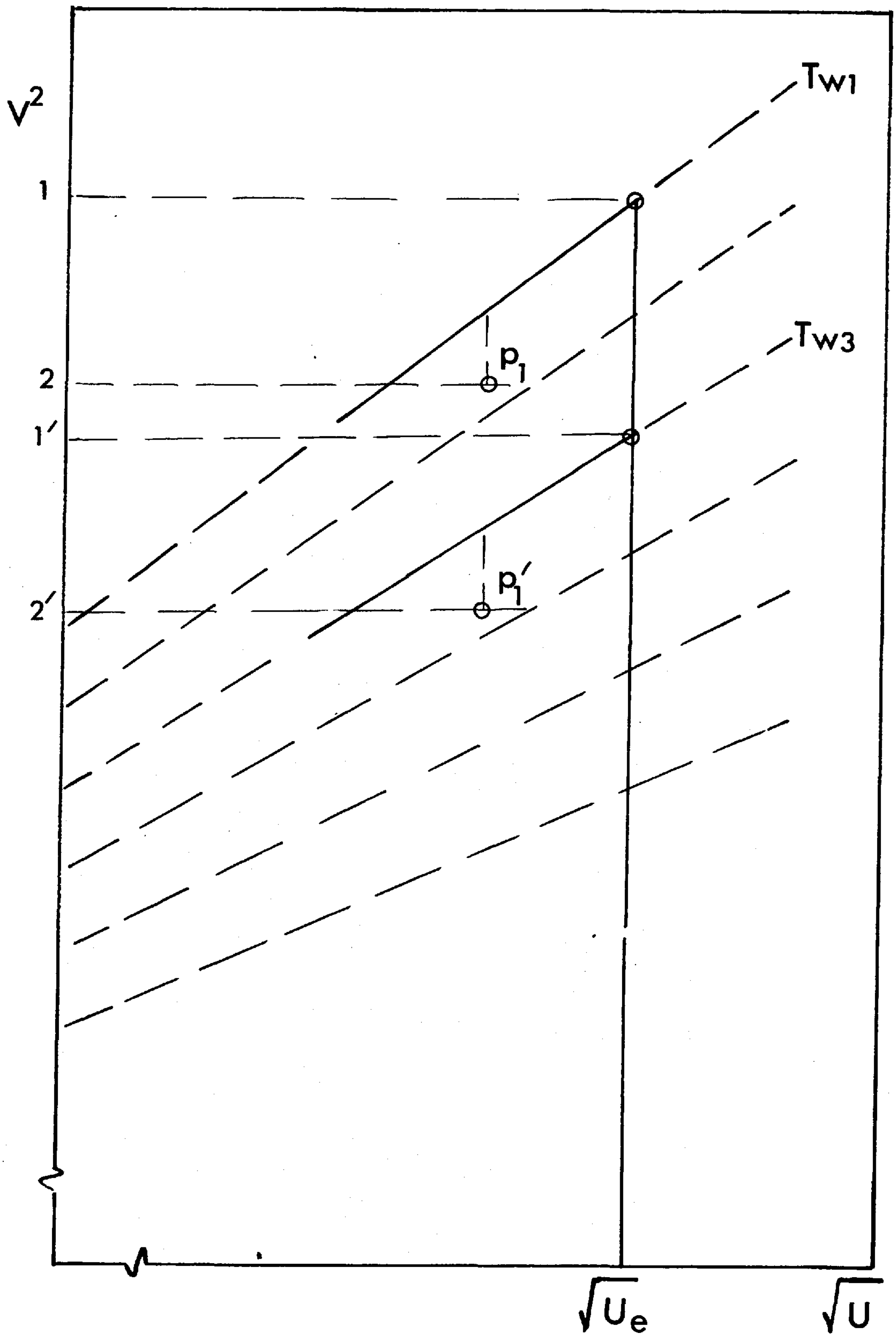

Fig.II.3.2 – Measurement of velocity and temperature.

The coefficient α was taken to be 0.00367/°C(8).

The output voltage, at two different wire-operating temperatures, is then recorded for each position in the boundary layer, along the y-axis.

A restriction on the possible combinations of velocity and temperature is achieved by starting from the outer edge of the boundary layer. There, it is certain that, the temperature is that of the free stream. Supposing we choose T_{w1} and T_{w3} as the two wire-operating temperatures, it is then possible to locate $\sqrt{U_e}$ from V_1 and $V_{1'}$ directly. Moving to the next point inward in the boundary layer, the air is bound to have a temperature equal to or greater than, θ_e. The velocity will be equal to or less than U_e. This argument fixes the two boundaries shown by the two complete lines in Fig.II.3.2 This construction enables us to choose the points P_1 and $P_{1'}$, satisfying the condition of having the same velocity and the same temperature difference from that of the free stream.

The two wire operating temperatures were chosen to be 270° and 250°C above that of the ambient when surface heating was applied, and 260°C above the ambient when no heating was applied.

II.4 - Measurement of Turbulent Quantities:

The longitudinal component of fluctuations was measured by means of the probe described in § II.3, using the DISA constant temperature anemometer.

An X-wire probe was used for the measurement of the shear-stress profiles (see Fig. II.4.1). The wires were at right angles to each other. The two operating temperatures were matched until a similar, or not very different, slopes were achieved throughout the range of measurements.

Using one DISA random signal indicator and correlator type 55 A 06, the correlation coefficients were calculated from the measured sums of and differences betweeen the two signals.

The measurement procedure and computation formulae for both $\overline{u'^2}$ and $\overline{u'v'}$, can be found in (7), (10) and (32).

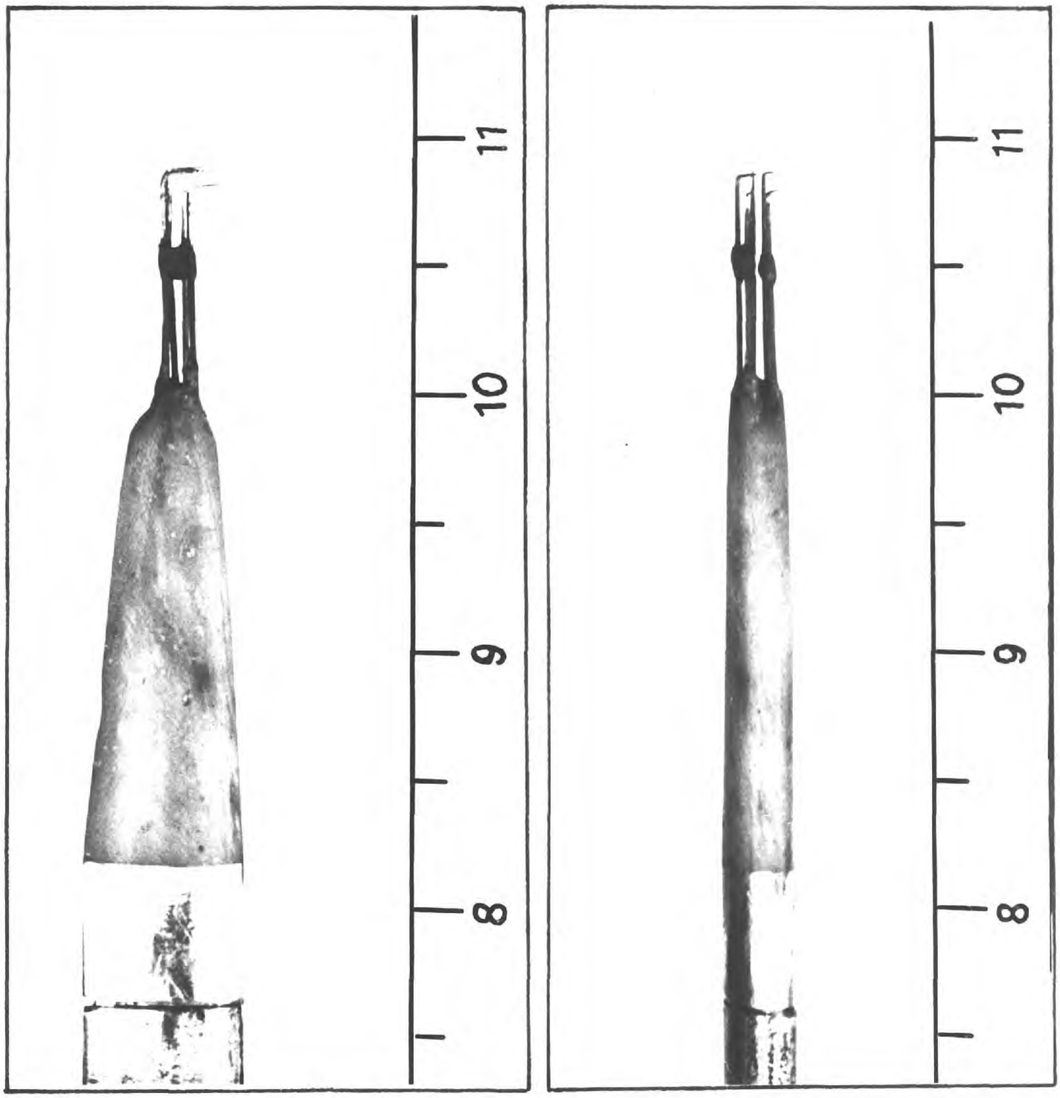

Fig. II.4.1_ Shear-stress probe.

II.5 - Measurement of Heat-transfer Coefficients:

It is thought that by keeping similar temperatures of the three thermocouples on the same distance along x, the top and bottom heaters will take care of end effects, the heaters being arranged in rows of three; the one in the middle will be dissipating heat to the air flow only.

It is possible by measuring the resistances of the heaters and recording the voltage across them, to calculate the heat input to the air flow, after deducing the heat lost through the asbestos block*. The formulae used are,

$$Q_w = \frac{C}{s} \quad \frac{V^2}{R} - \frac{k}{t} \left(T_i - T_o \right), \quad \text{and}$$

$$S_t = Q_w / \rho_e U_e c_p (T_w - T_e)$$

where C is a conversion factor,

s the area covered by a heater ($=\frac{1}{8}$ ft^2),

V the voltage across the heater,

R the resistance of the heater,

k the coefficient of conductivity of the asbestos,

t the thickness of asbestos block,

T_i hot-side temperature of asbestos, and

T_o cold-side temperature of asbestos.

* Conductivity of the asbestos block was taken as that quoted by the manufacturers (11).

II.6 - Displacement of Probes:

The probes mentioned in §§ II.3 and II.4 were mounted on a 0.625 x 0.2 in. stream line steel tubing, connected on the opposite side of the tunnel wall to a micrometric head shown on Fig. II.6.1. The probe displacement could be directed along the y-axis to the nearest 0.0005 in. The micrometric head could be moved in the x-direction by turning a lead screw of 20 threads/inch, using a large dial connected to the turning handle.

The head assembly was mounted on a heavy 2 x 4 ins. aluminium channel supported on a tunnel window, which was provided with a central slot covered with masking tape. The window was also provided with some vertical slots to allow for traverses which might be required below or above the centre line of the plate.

The distance from the plate was detected by the electric light signal, a method which was repeatable better than 0.001 in. in all cases.

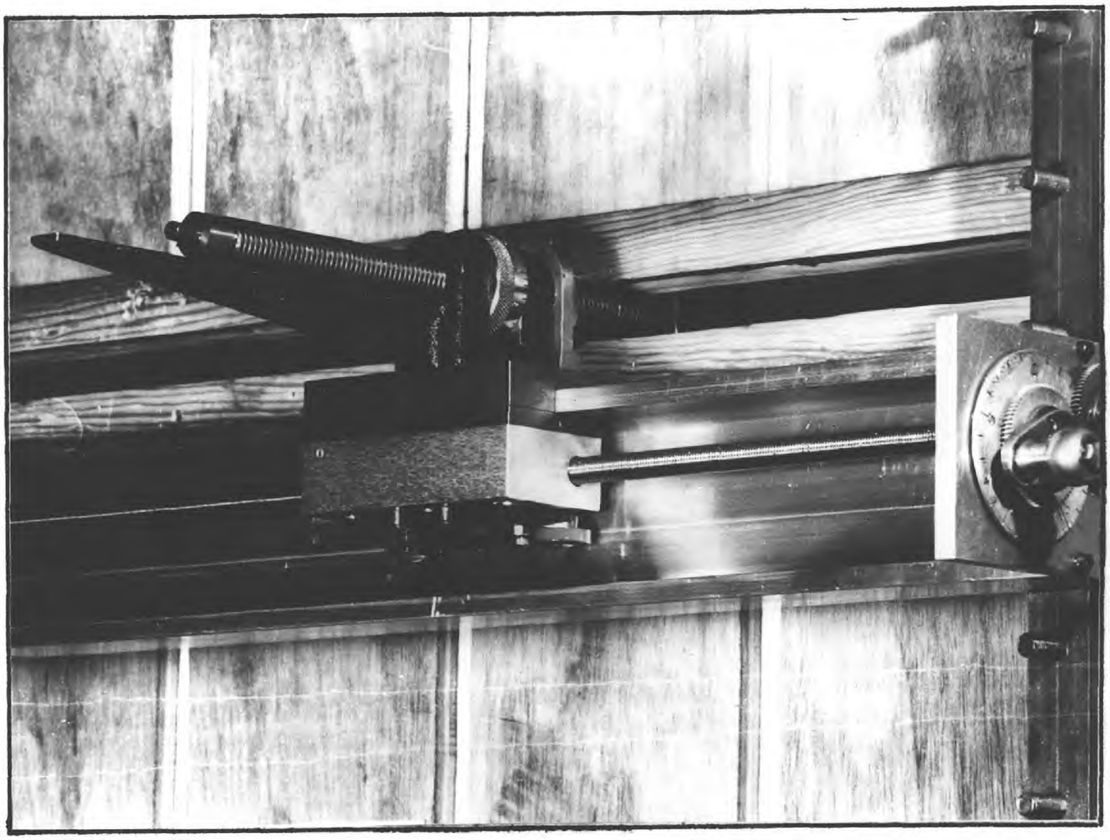

Fig. II.6.1_ Device for probe displacement.

II.7 - Accuracy of Measurements:

II.7.1 - Velocity and temperature profiles

The values of velocity and temperature determined from the hot-wire calibration curves, were within $\pm$ 0.02 $(\mathrm{ft/sec})^{\frac{1}{2}}$ and $\pm$ 0.5°C respectively. T_e was measured to the nearest 0.2°C.

As for Tw, a value of $\pm$ 1.5°C covers all measurements, considering $\pm$ 1% error due to thermocouples, and $\pm$ 1% for the PYE galvanometer used to measure their EMF.

Great care was taken to start the measurements only after the temperatures settled in the air flow and on the plate.

We can then write,

$$\frac{\Delta(U/U_e)}{U/U_e} = \frac{2\,\Delta(\sqrt{U})}{\sqrt{U}} + \frac{2\,\Delta(\sqrt{U_e})}{\sqrt{U_e}} .$$

The value of $\sqrt{U}$ changes from 4 to 10 approximately, which correspond to an error on (U/U_e) ranging from $\pm$ 1.4% near the origin to $\pm$ 0.8% at the outside edge of the boundary layer.

For the temperature profiles, we can use the expression,

$$\frac{\Delta\bar{\theta}}{\bar{\theta}} = \Delta T_w\left(\frac{1}{T_w - T} - \frac{1}{T_w - T_e}\right) + \Delta T_e\left(\frac{1}{T_w - T_e}\right) + \Delta T\left(\frac{1}{T_w - T_e}\right).$$

Taking an average value of 70°C for ($T_W - T_e$), and considering that ($T_W - T$) varies from 30°C to 70°C approximately, $\Delta\bar{\theta}/\bar{\theta}$ varies accordingly from $\pm$ 4.5% to $\pm$ 1%, between the origin of the boundary layer and its outer edge.

If the temperature profile is curved enough, the high inaccuracy is confined to a very thin layer not more than 0.5 Δ_2 or an average value of 0.07δ, where $\bar{\theta}$ is about 0.5 and the error reduces to $\pm$ 2%.

II.7.2 - Turbulent quantities

At no air flow, it was always found that the fluctuating component suffered a zero error amounting to about 1 mV, a value which could not be reduced and was mainly due to amplifier noise.

Such noise was thought to remain constant in magnitude for the whole range of measurements. It is very difficult to say exactly how much this noise affected the values of $\overline{u'v'}$, when the sum and difference amplifiers involved in the correlator were considered. It was thought that it would amount to the same order of magnitude as the error on $\overline{u'^2}$ which can be written as,

$$\frac{\Delta\left(\sqrt{\overline{u'^2}}/U_e\right)}{\sqrt{\overline{u'^2}}/U_e} = \frac{\Delta\left(\sqrt{\overline{u'^2}}/U\right)}{\sqrt{\overline{u'^2}}/U} + \frac{\Delta\left(U/U_e\right)}{U/U_e} .$$

Near the origin of the boundary layer, the error was $\pm$ 2.4%, and at 0.8 δ it was $\pm$ 5.8% approximately.

II.7.3 - Heat-transfer coefficients

The heat-transfer coefficient can be obtained from the expression*;

$$S_t = \left(C \cdot \frac{V^2}{R} \right) / \left(\rho_e U_e c_p (T_w - T_e) \right) .$$

The resistance of each heater was measured to the nearest 0.01 of an ohm, and also their respective inductances. This resulted in a power factor of 0.99985 at 50 cycles per second.

*The inaccuracy on the heat dissipated through the asbestos blocks is ignored in the present discussion only, as they amounted to about 0.02 of Q_w. They were fully accounted for in computing the values of S_t.

The resistance of the heaters was guaranteed by the manufacturers not to change by more than $\pm$ 5% of their original values in the range of temperature 20^{o} to $400^{o}C$.

Considering the range of operating temperatures used here, the inaccuracy on the resistance of the heaters will be estimated $\pm$ 2% of their values at room temperature.

The voltages across the heaters were measured by an AVO-meter, the inaccuracy of which is $\pm$ 2.25% in the range of measurements*.

Also, as it was discussed before, the inaccuracy on U_e is of the order $\pm$ 0.4%, and on $(T_w - T_e)$ is $\pm$ 2.3%

We can then state the total inaccuracy on the calculated heat-transfer coefficients to be,

$$\Delta S_t / S_t = 2\frac{\Delta V}{V} + \frac{\Delta R}{R} + \frac{\Delta U_e}{U_e} + \frac{\Delta (T_w - T_e)}{(T_w - T_e)} .$$

from which we get,

$$\Delta S_t / S_t = \pm 9.2\% .$$

* The particular meter used had an accuracy of 99% in the range of the present measurements, but the larger value of inaccuracy quoted by the manufacturers was retained to see how serious the error can become, if that did not remain so during the actual measurements.

III. RESULTS AND DISCUSSION

III.1. - Field of Experiments:

A rough plate was used throughout the course of the present work, at six different conditions, referred to subsequently as cases.

The first three cases were those of the plate with approximately zero pressure gradient, which changed to a mild favourable one towards the last third of the plate. The rest of three cases concerned the plate with mild adverse pressure gradient changing to approximately constant pressure towards the last third of the plate.

Each set of the above mentioned three cases included the investigation of unheated plate, an isothermal plate heating to a temperature such that $T_w / T_e \cong 1.2$, and the case of heating to $T_w / T_e \cong 1.2$ to 1.3 with a gradual step near the middle of the plate.

Fig. III.1.1 to III.1.6 represent the pressure coefficients measured at the wall with the reference velocity at the downstream end of the plate, while Fig. III.1.7 to III.1.10 show the wall temperature distribution for the heated cases.

For the unheated cases, the mean velocity profiles and the longitudinal fluctuating component were measured;

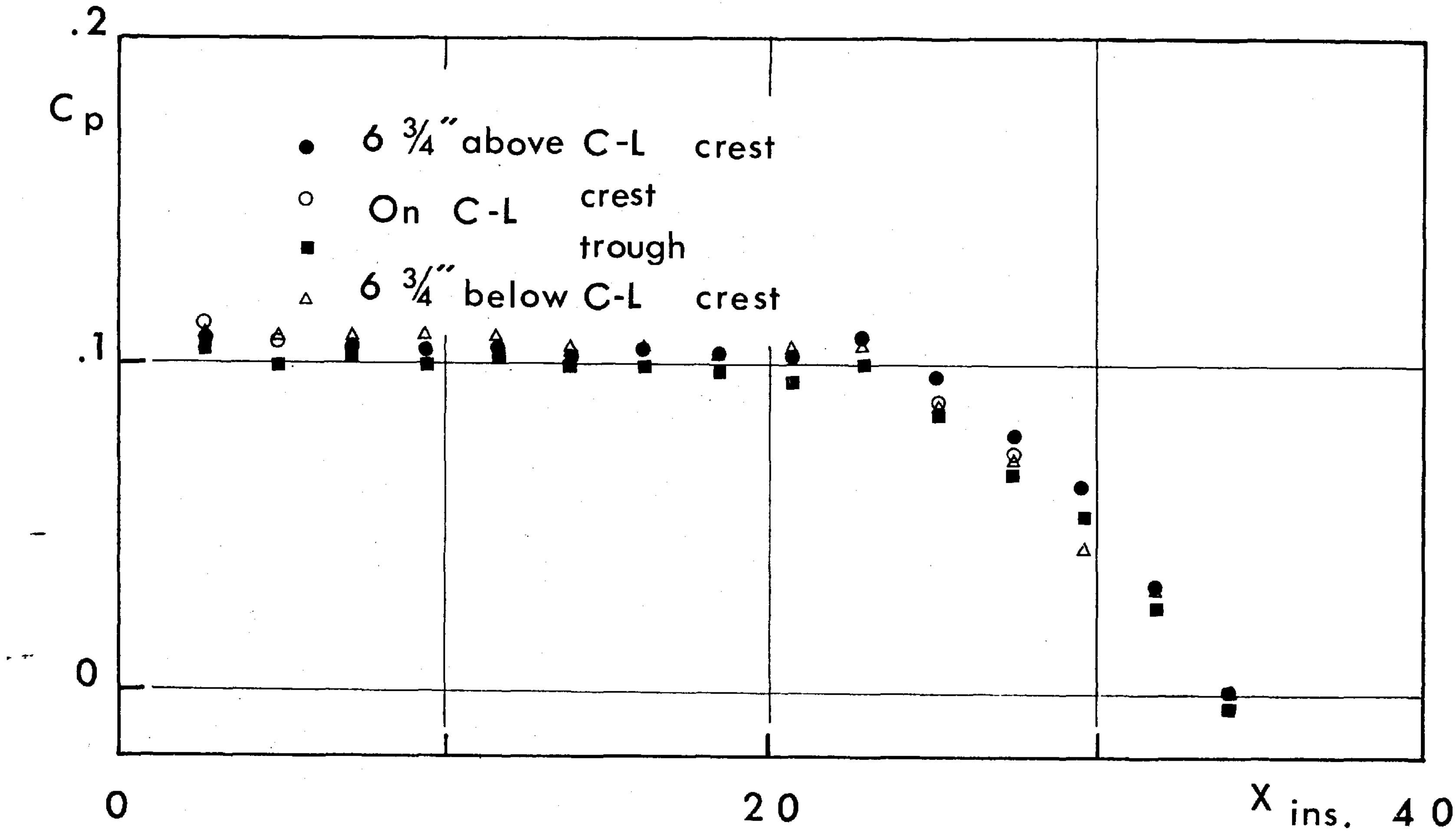

Fig. III.1.1_ Pressure distribution _ Case I_A .

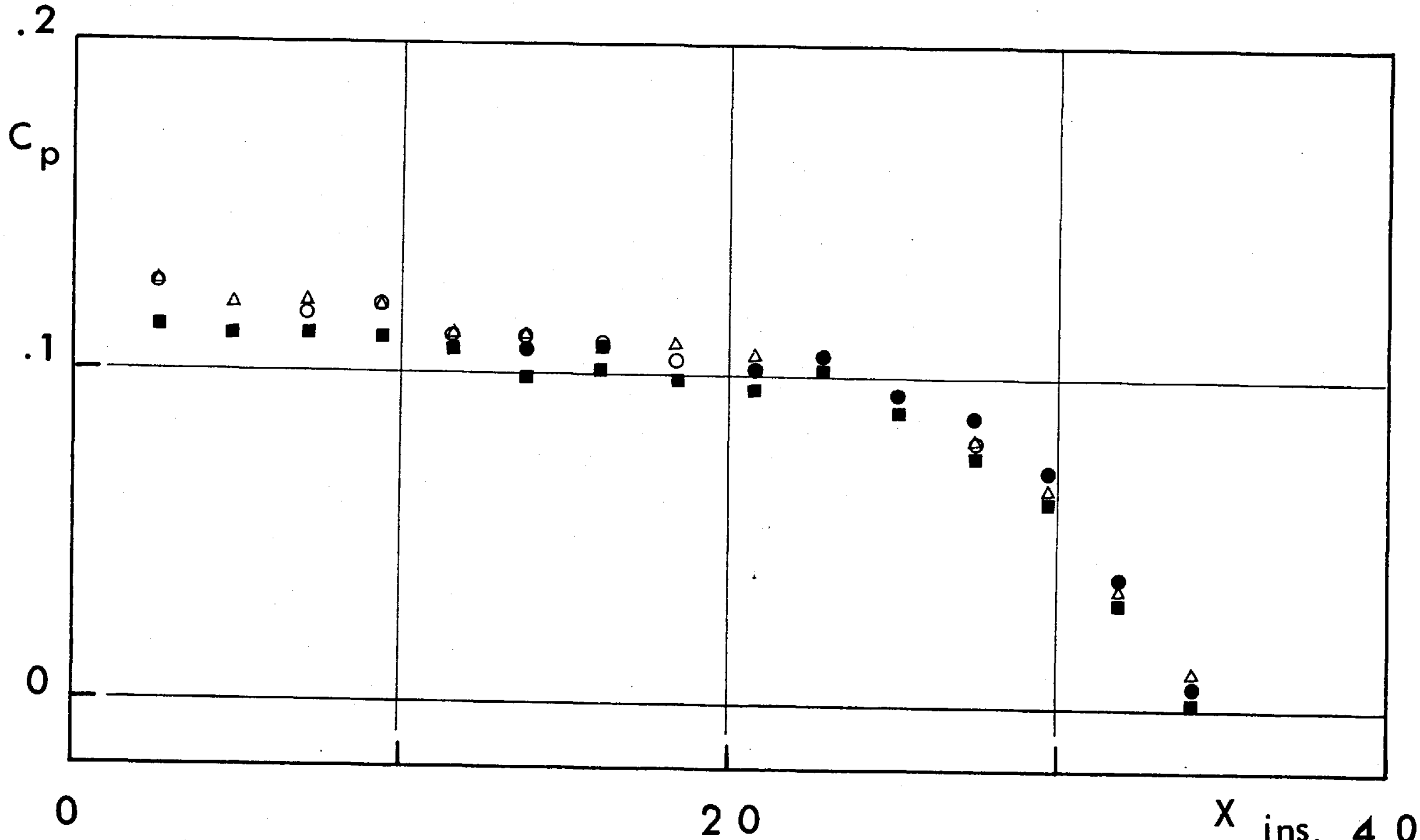

Fig. III.1.2 _ Pressure distribution _ Case I_B .

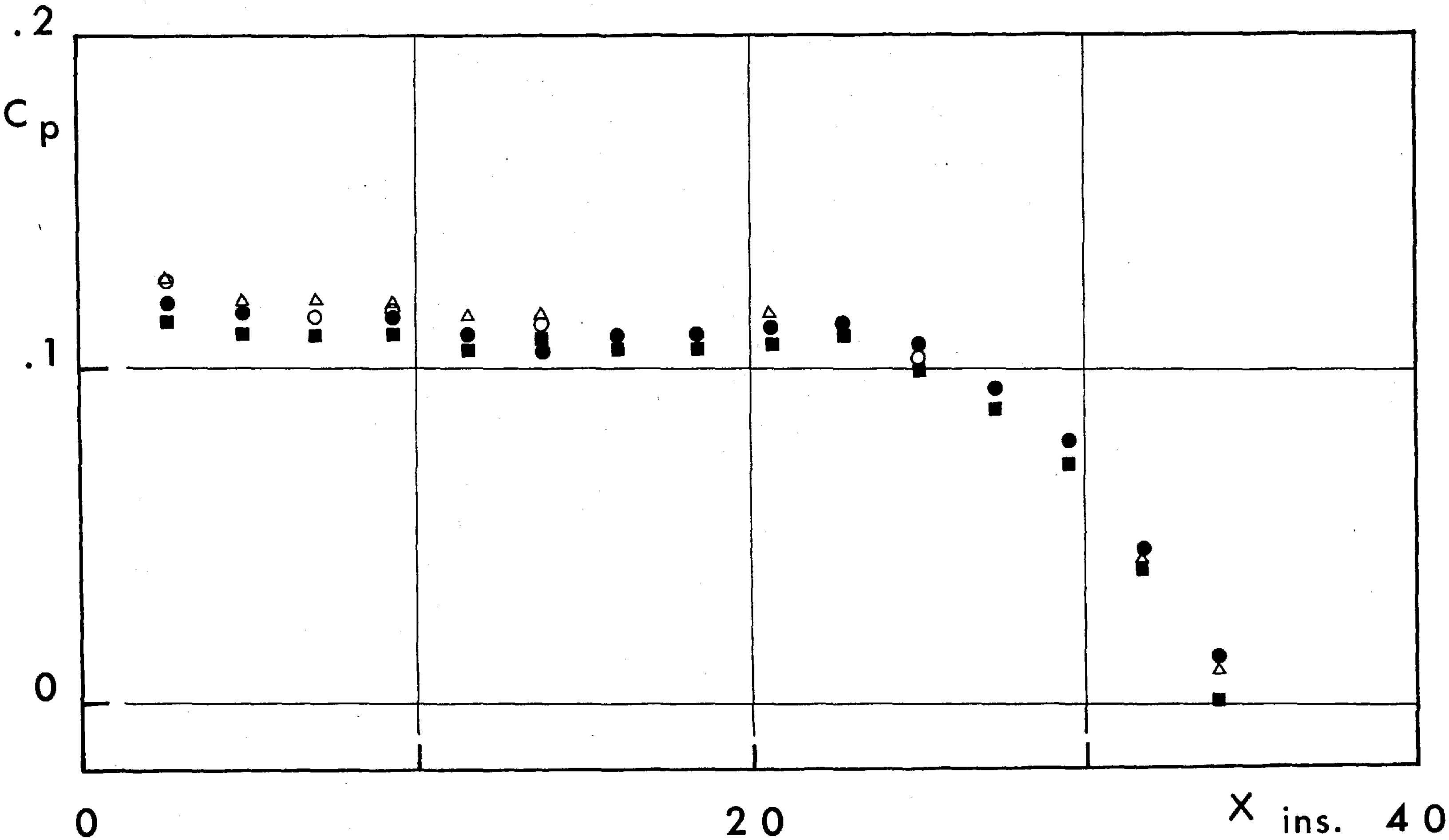

Fig. III.1.3 _ Pressure distribution _ Case I_C .

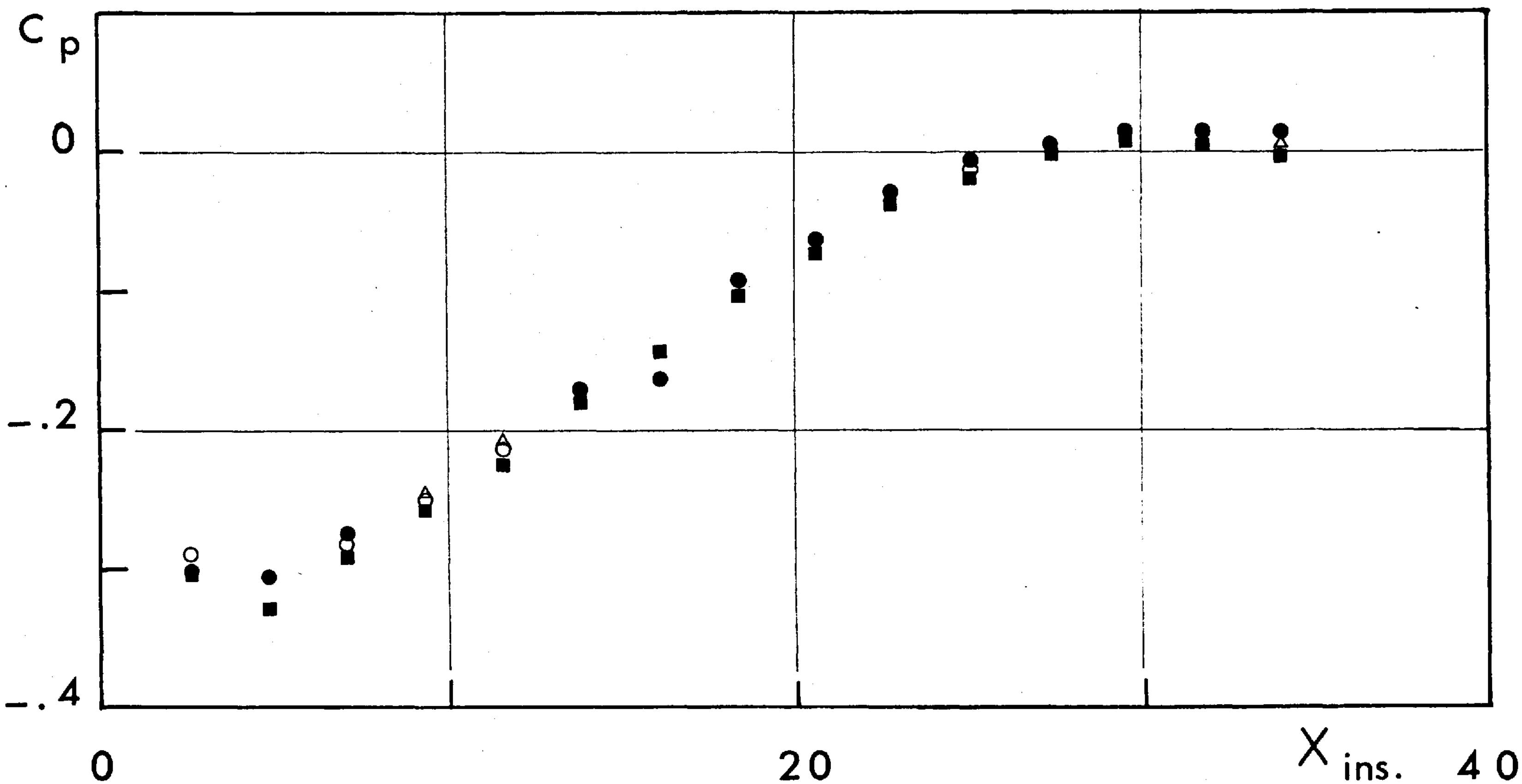

Fig. III.1.4 – Pressure distribution – Case II_A .

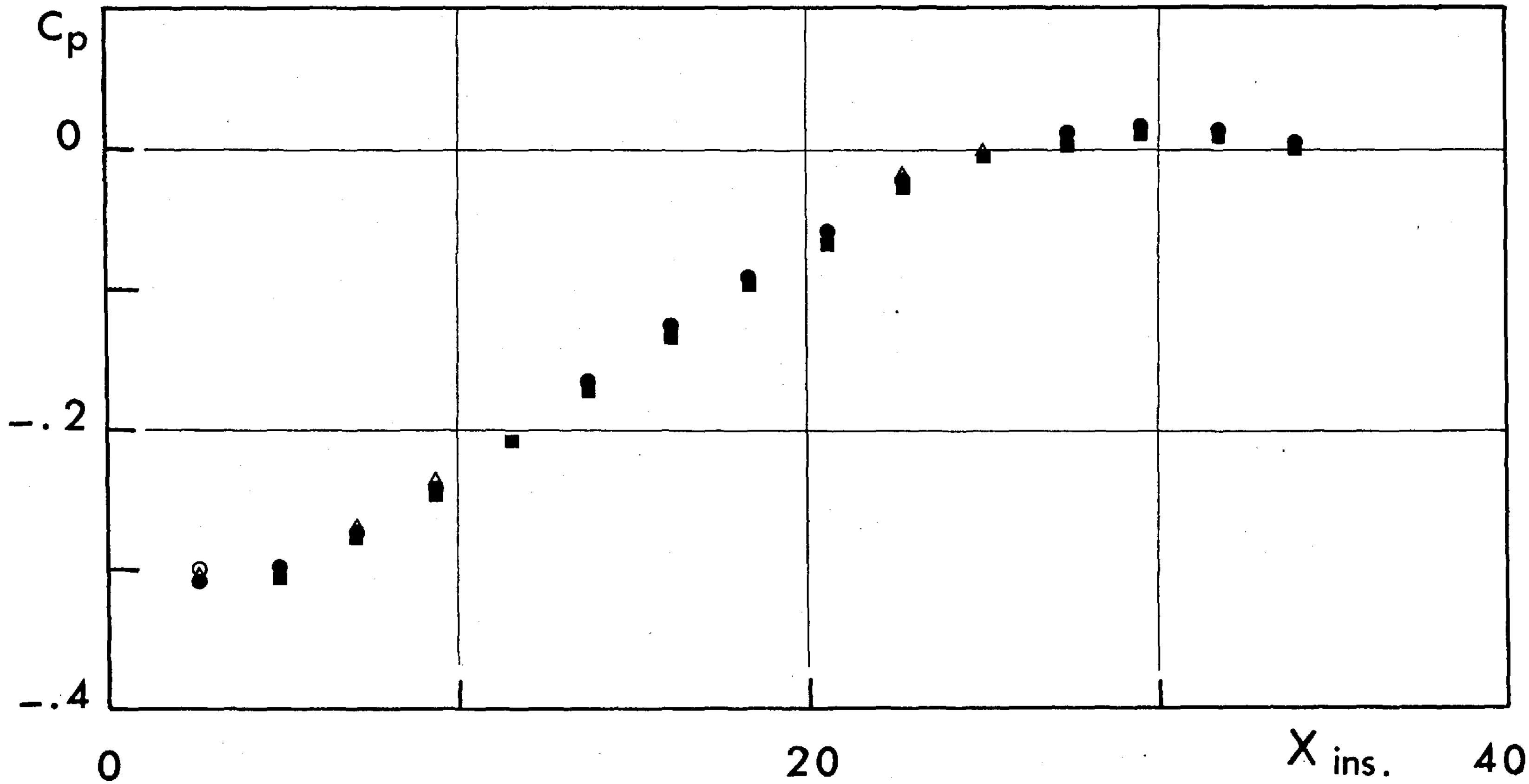

Fig. III.1.5 _ Pressure distribution _ Case II_B .

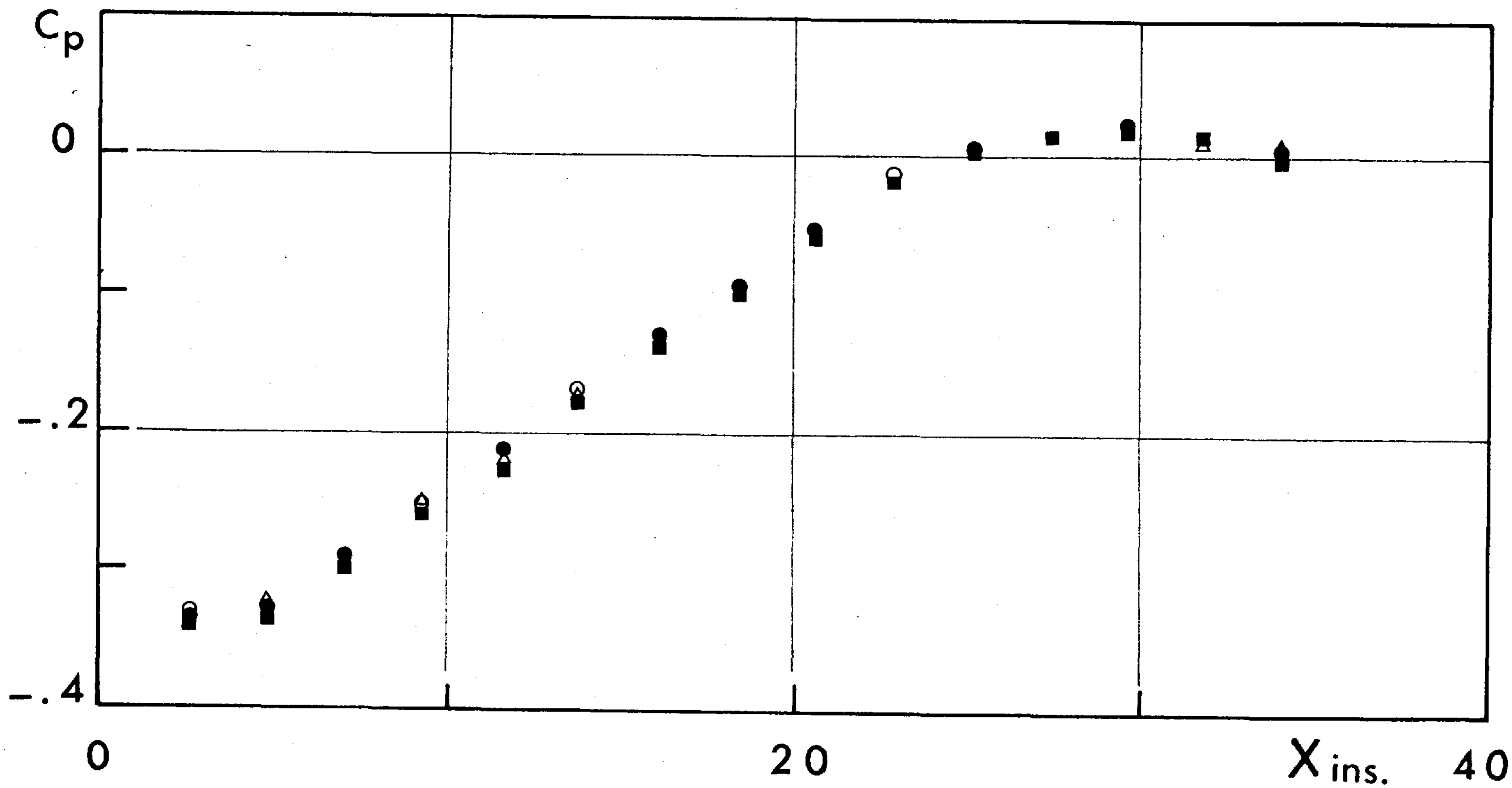

Fig. III.1.6 _ Pressure distribution _ Case II_C

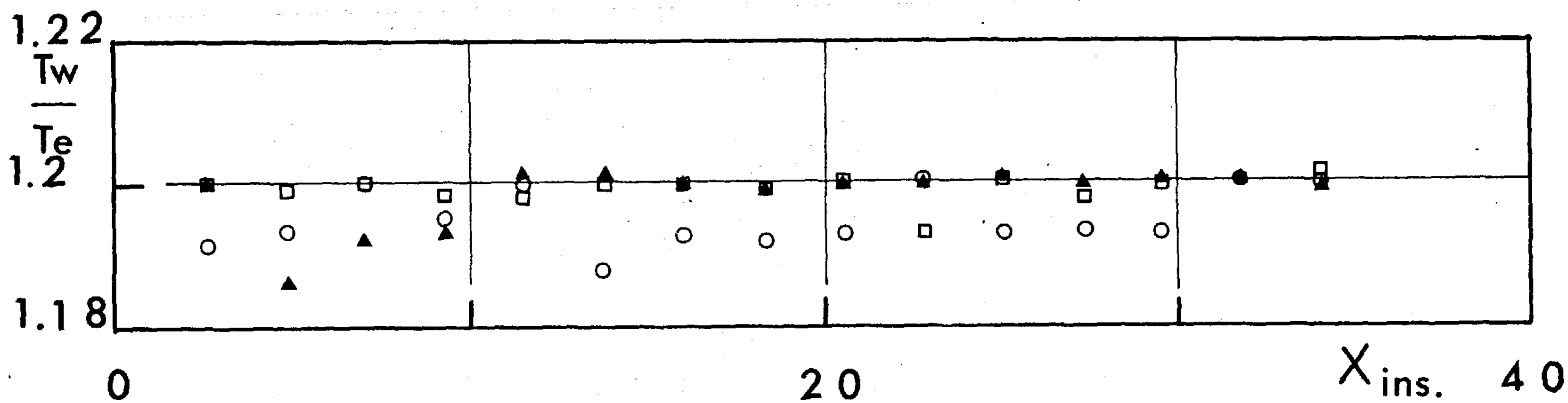

Fig. III.1.7 _ Wall-temperature distribution _ Case I_B .

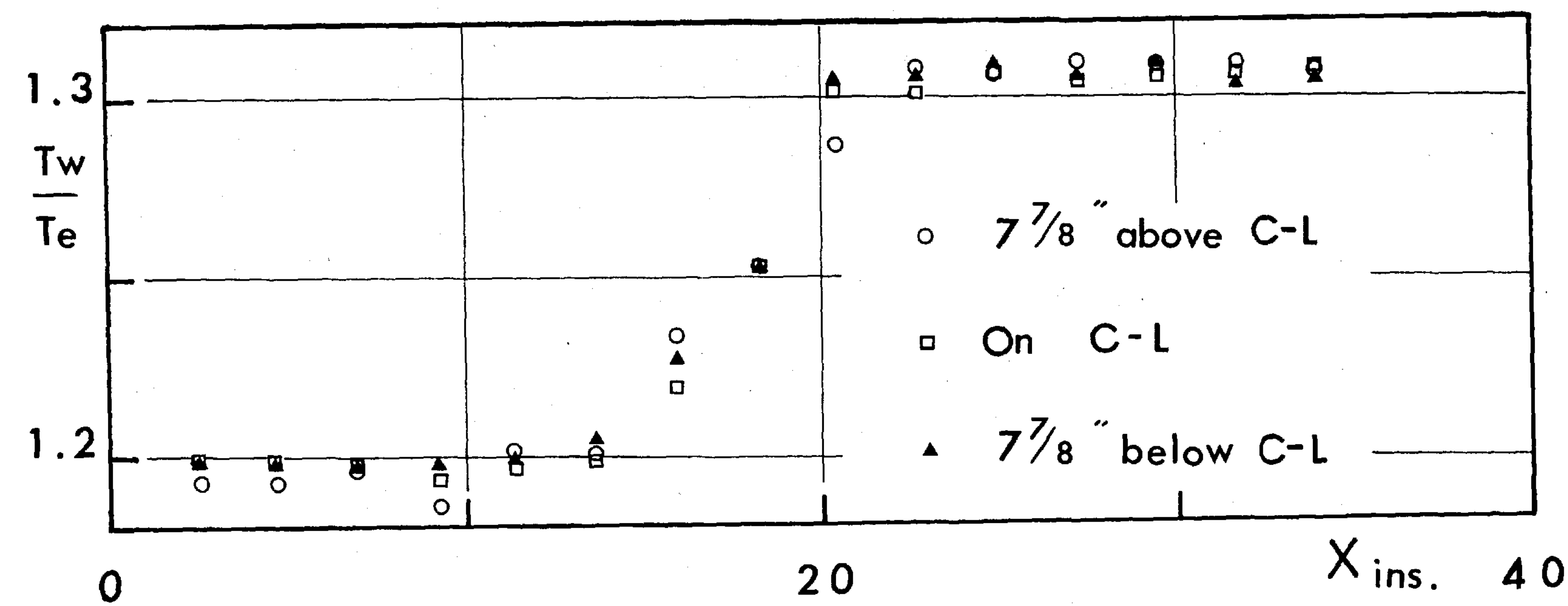

Fig. III.1.8 _ Wall-temperature distribution _ Case I_C .

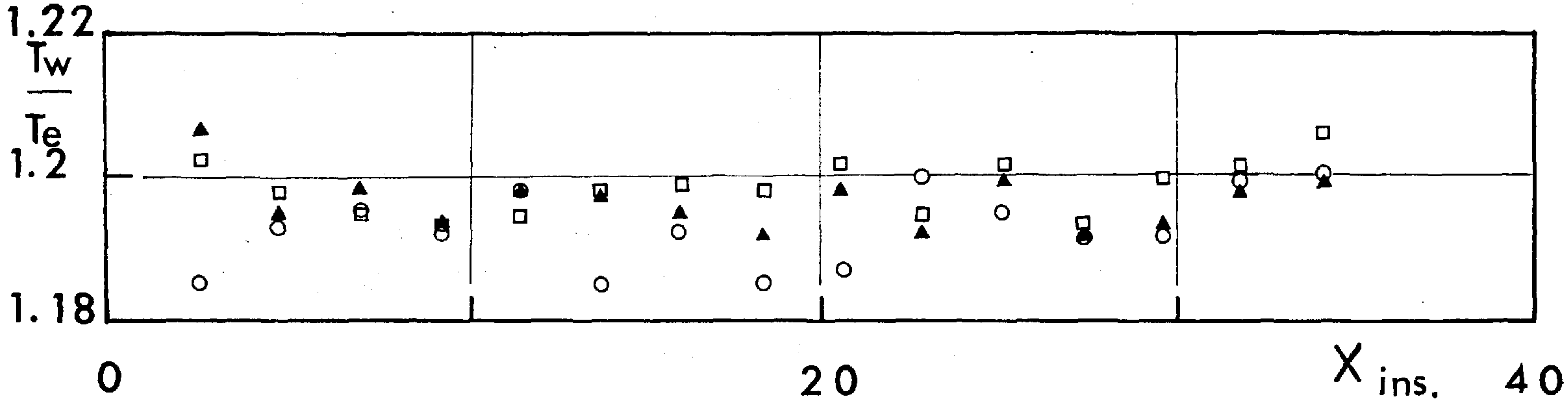

Fig. III.1.9 _ Wall-temperature distribution _ Case II_B .

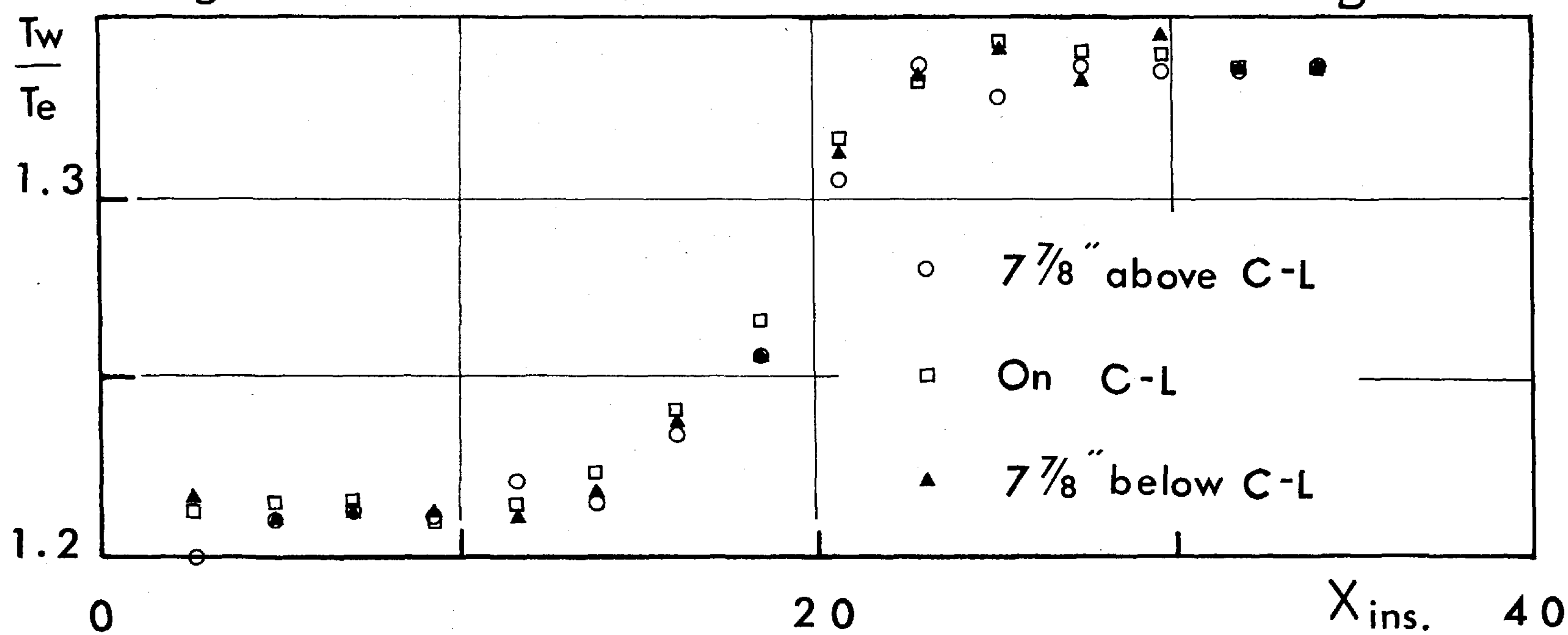

Fig. III.1.10 _ Wall-temperature distribution _ Case II_C .

and for the heated plate, the mean velocity and temperature profiles were measured. The longitudinal fluctuations were also recorded for the heated cases, but to serve only in a qualitative comparison.

The turbulent shear-stresses were measured for both pressure gradients, but when no surface heating was applied.

It was possible to obtain some measurements of the shear stress across boundary layers, experiencing an abrupt change in surface condition, from rough to smooth, or vice versa. This was done by sticking self-adhesive polythene sheet on the first or the second half of the plate*.

* The term "smoother" should have really been used instead. The polythene sheet could not be prevented completely from sagging in the cavities. However, the depth of sagging was not more than 0.005 in. anywhere on the covered part of the plate.

III.2. - The Dynamic Boundary Layer:

The present section deals with the velocity profiles and skin-friction coefficients for all the examined cases. The temperature profiles will be examined in the next section.

III.2.1. - Velocity profiles behind roughness elements:

Bodies placed in the free air stream will generate wakes, but placed in a boundary layer they cause displacement of the steamlines towards and behind them.

Schlichting described this phenomena as "the negative wake effect", which was explained by the existence of secondary flow. This effect can be clearly seen from the shape of constant velocity lines measured by Schlichting behind a row of spheres (Fig.21.15(1)) and the secondary flow calculated later by Schultz - Grunow.

The eddy behind a roughness element was visualised by White (30) and Wieghardt (33). Its existence was noted later by Doenecke (4), in that it satisfies the condition of continuity of the fluid in the volume behind the roughness element, with its centre coinciding with the origin of the velocity profile. Doenecke also sketched the pattern of the behaviour of velocity behind a roughness element, similar to that given on Fig.III.2.1.

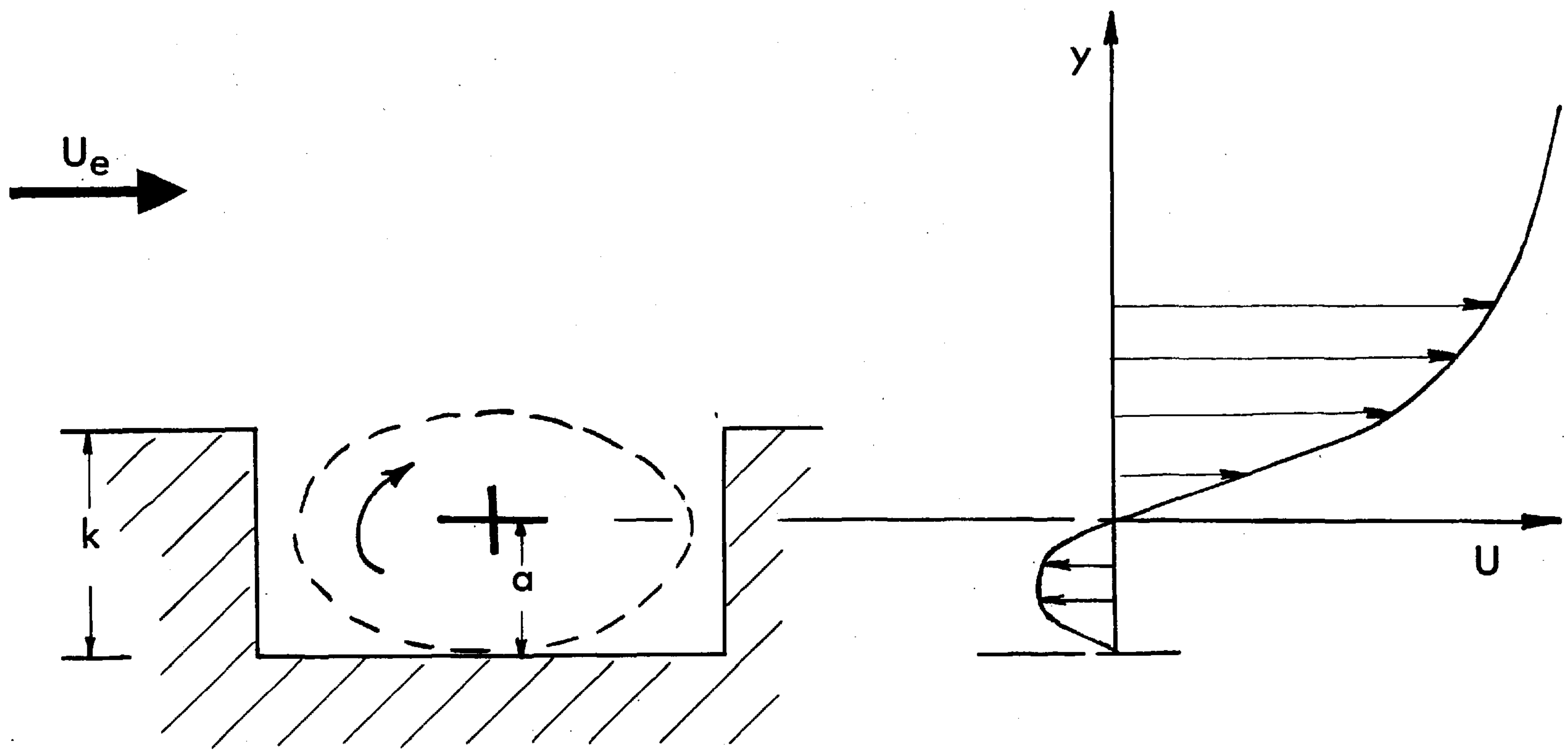

Fig. III. 2.1 _ Velocity profiles behind roughness elements .

The height of the centre of eddy for a plate with 3 mm two-dimensional square ribs, spaced by 12.5 mm. was given as equal to 1.7 to 1.9 mm from the trough of the roughness element (4).

In the present work, the velocity profiles were measured at the centre of a cavity, starting at about 0.05 in. from the trough, using the single-wire probes earlier described.

A curve of $U(y)$ was then plotted for each profile, and the origin of the boundary layer was chosen as the first point on the straight part of the profile. An example of this choice is given on Fig.III.2.2. The readings before the chosen origin were ignored as they are thought meaningless.

The origin of the velocity profile thus obtained, was found to be about 0.050 $\pm$ 0.005 in. below the crest of the $\frac{1}{8}$ in. cavities.

The origin of the velocity profiles which could be measured from the surface unoccupied by the cavities, is clearly the surface itself; but the measurements carried out at the centre of a cavity along the centre-line of the plate made the recording of the viscous sub-layer more feasible.

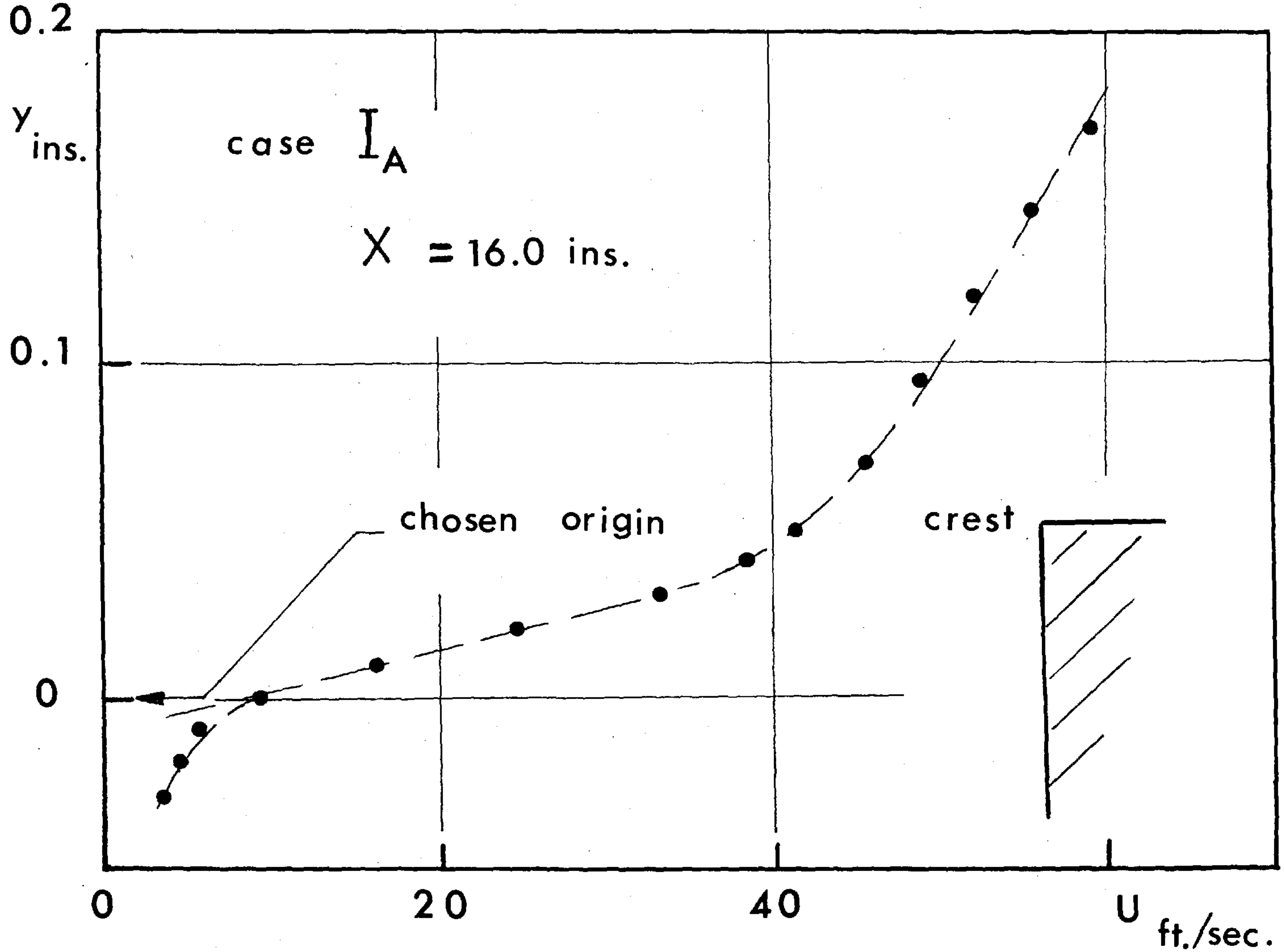

Fig. III.2.2 _ Choice of origin for velocity profiles .

The eddies inside cavities or behind protrusions participate in momentum dissipation in the same manner, forming, with the secondary flow, the main difference between a rough and a smooth surface.

III.2.2 - Boundary layer thicknesses:

The thicknesses of the boundary layer δ_1 , δ_2 and δ_3 were computed from the measured velocity profiles by the trapezoidal method, using the Imperial College IBM 7090 computer, as the rest of routine calculations.

For the heated plate, the thicknesses δ_{1u} , δ_{2u} and δ_{3u} were also calculated.

These various integral terms are plotted as function of x on Fig. III.2.3 to III.2.12, and are tabulated numerically in Appendix I.

Tables of measured velocity and temperature profiles are given in Appendix II.

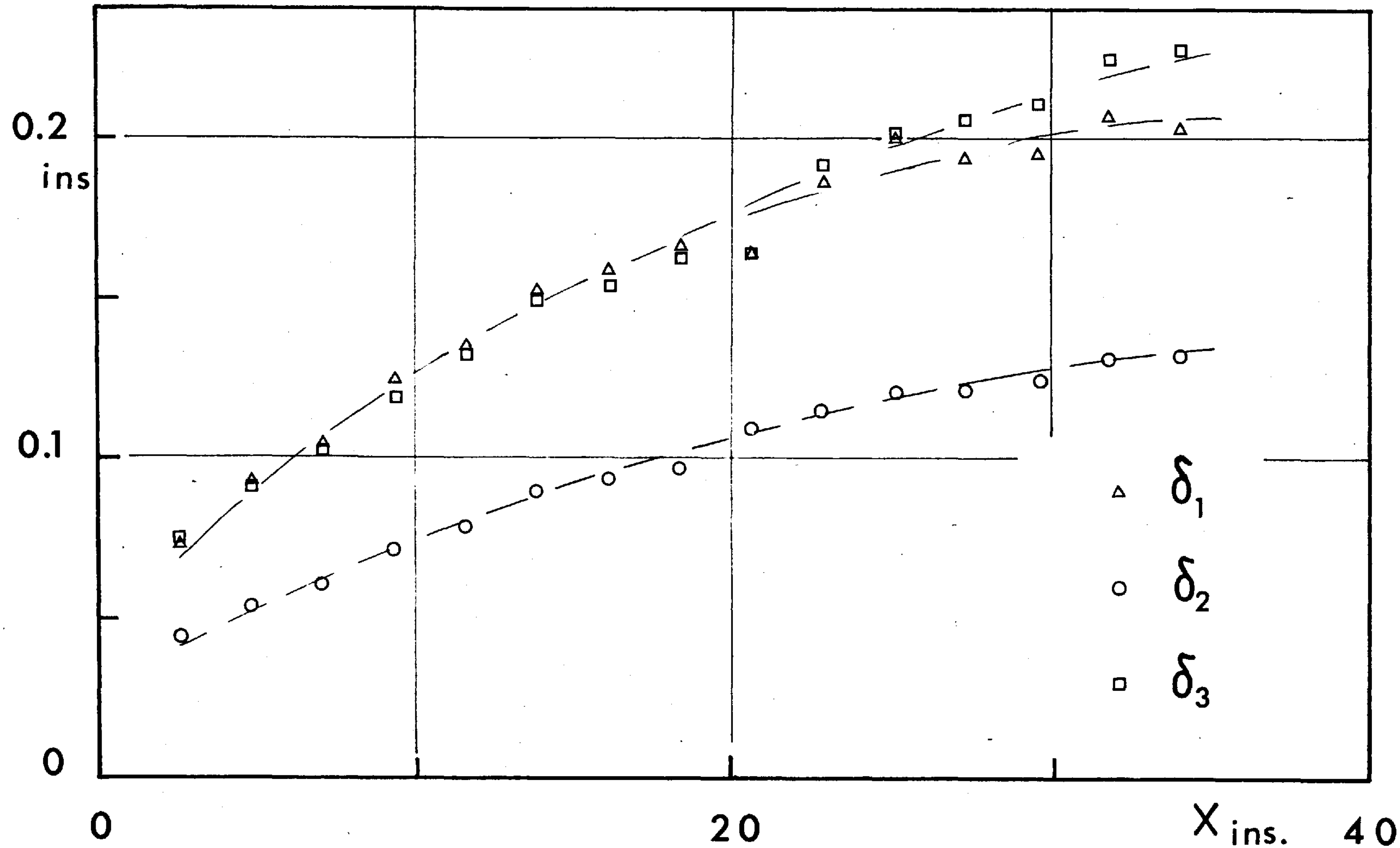

Fig. III.2.3_ Boundary layer thicknesses_ Case I_A .

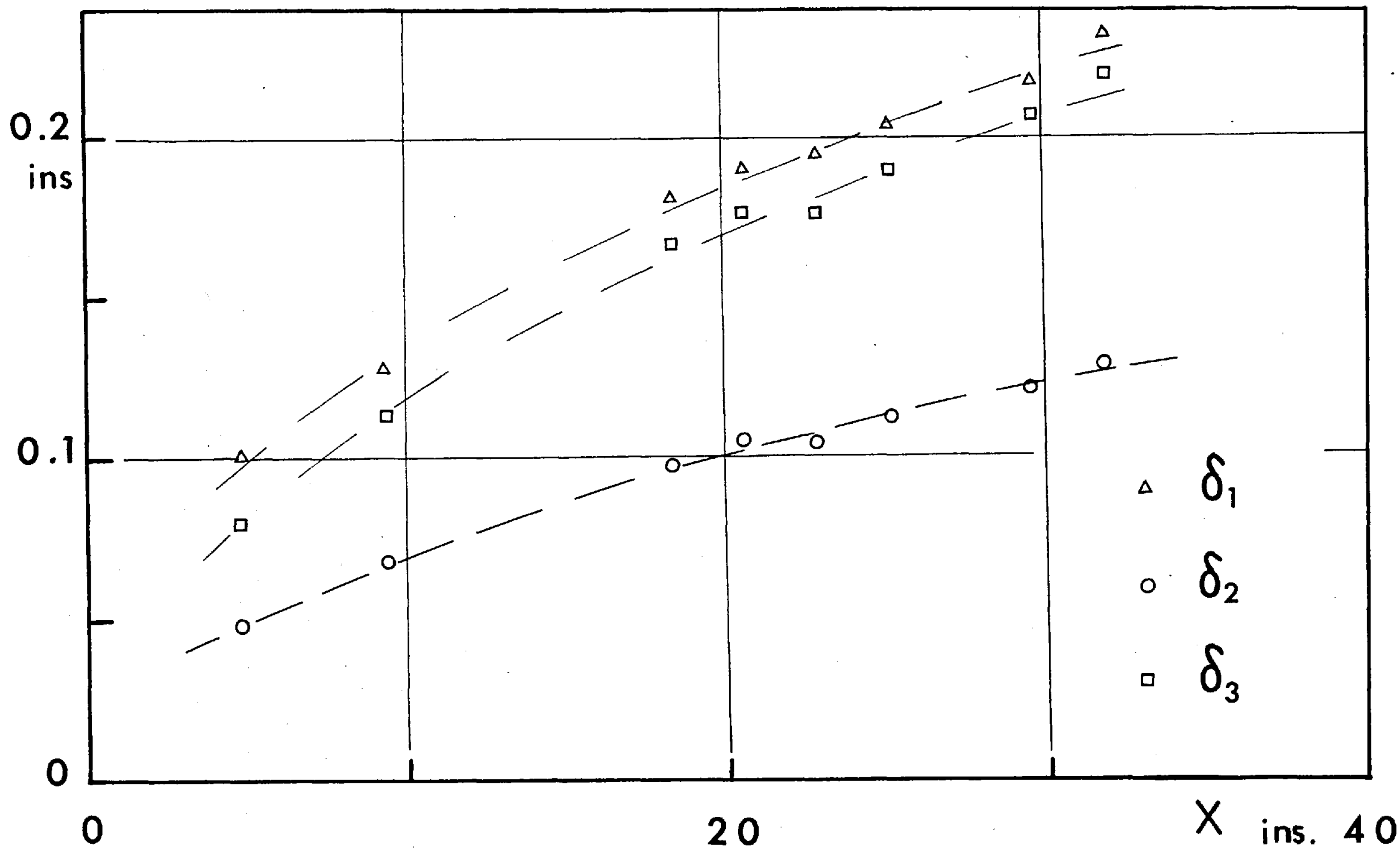

Fig. III.2.4 _ Boundary layer thicknesses _ Case I_B .

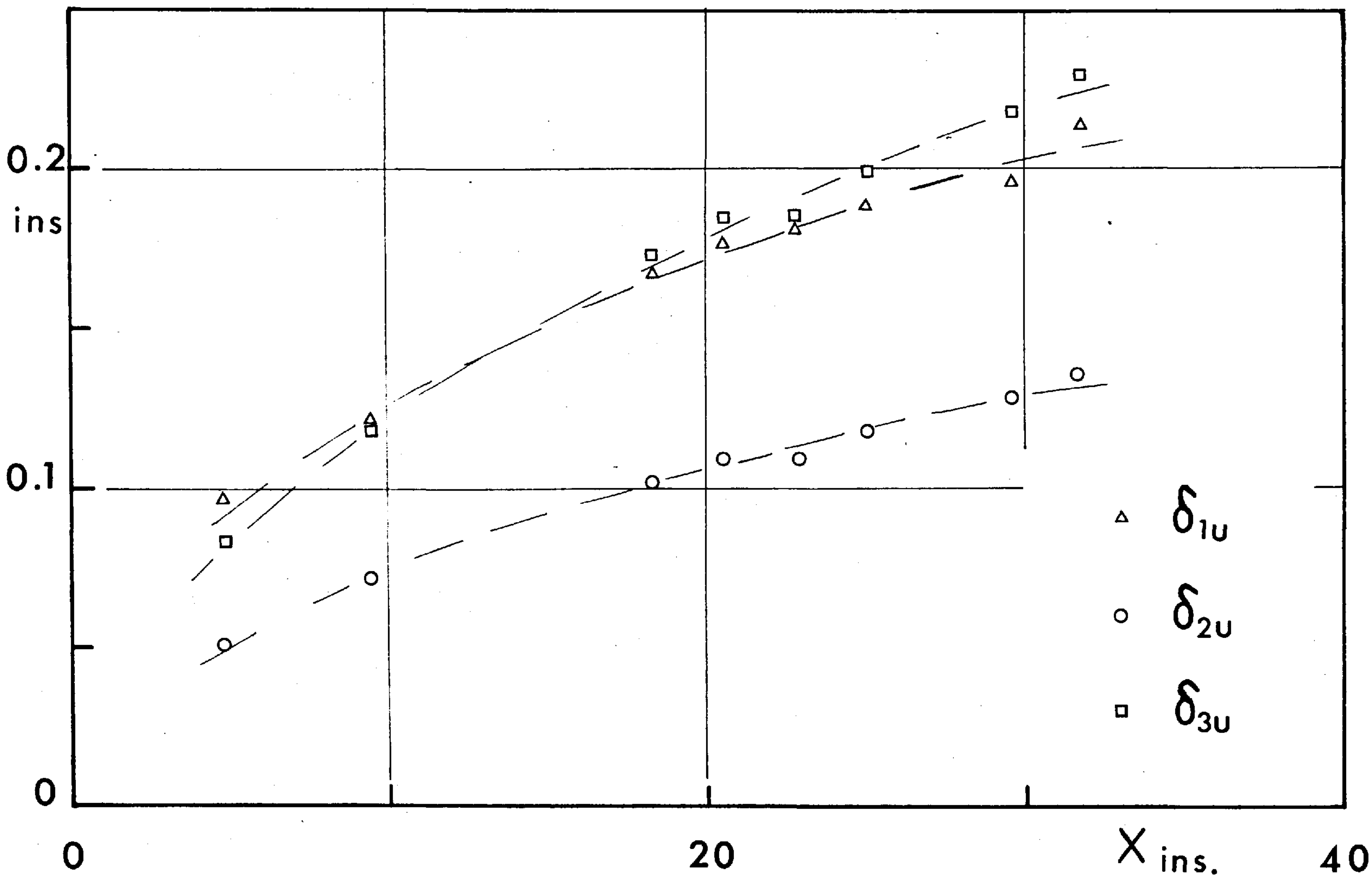

Fig. III.2.5_ Boundary layer thicknesses _ Case I_B .

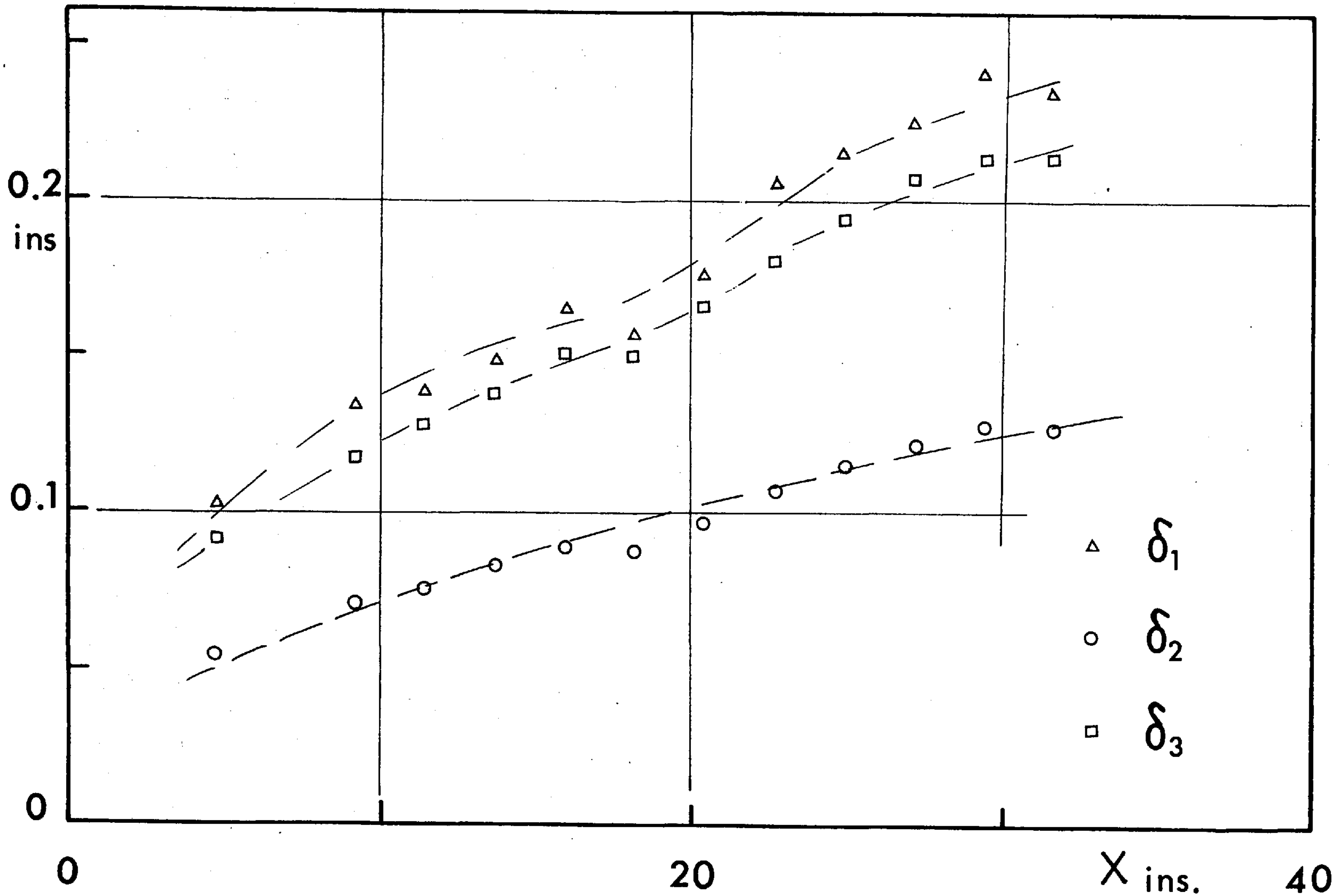

Fig. III.2.6 _ Boundary layer thicknesses _ Case I_C .

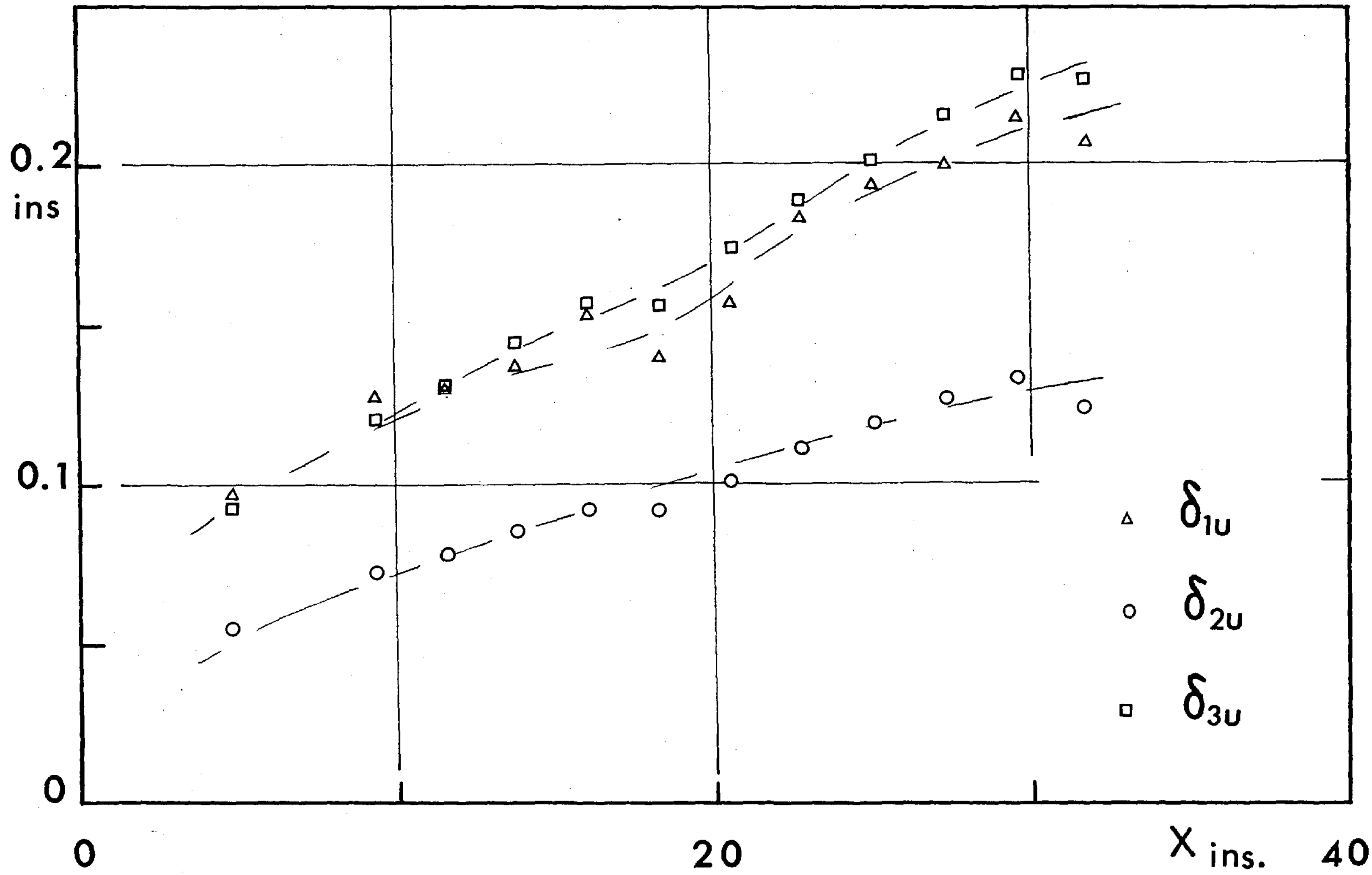

Fig. III.2.7_ Bondary layer thicknesses _ Case I_C .

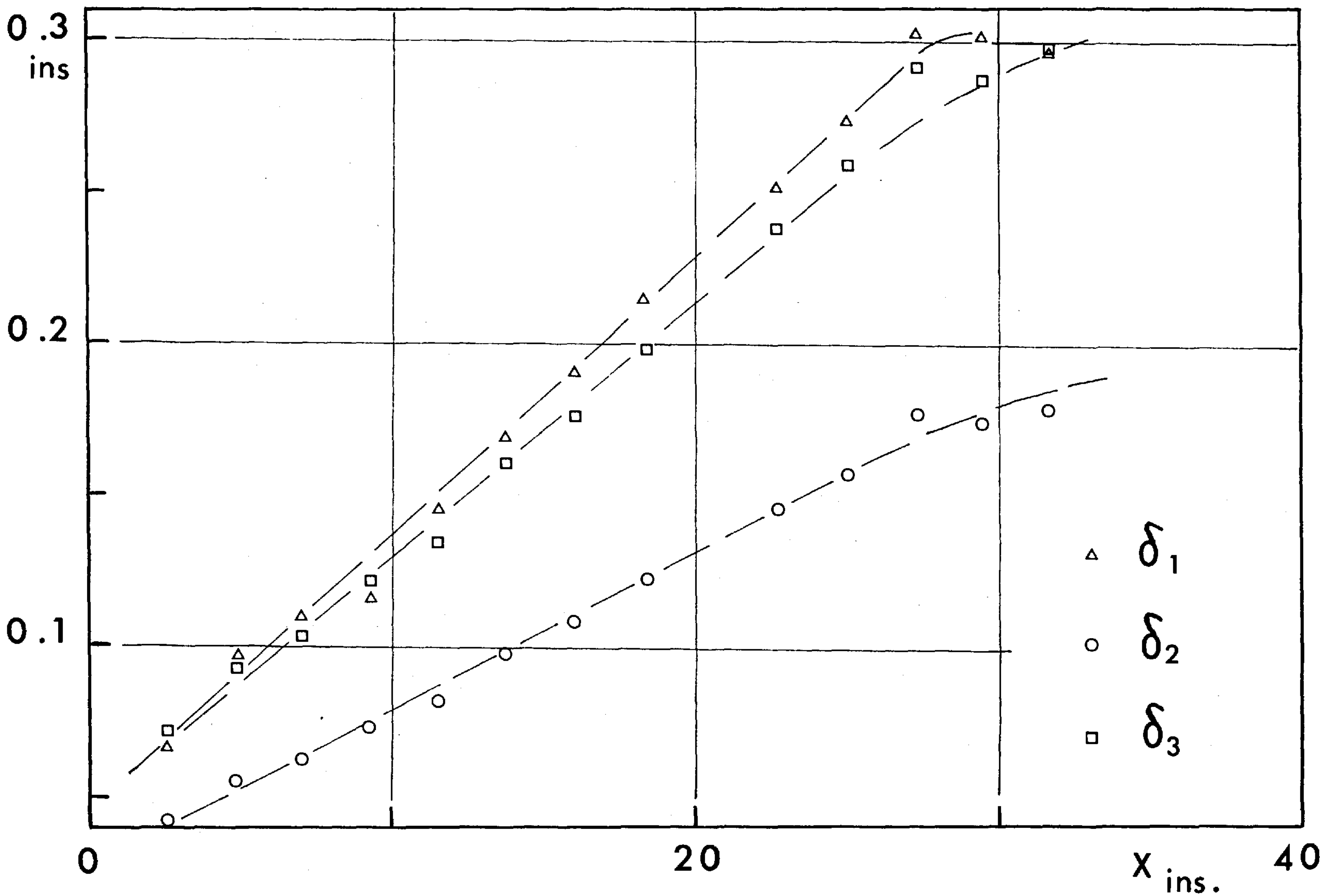

Fig. III.2.8 _ Boundary layer thicknesses _ Case II_A .

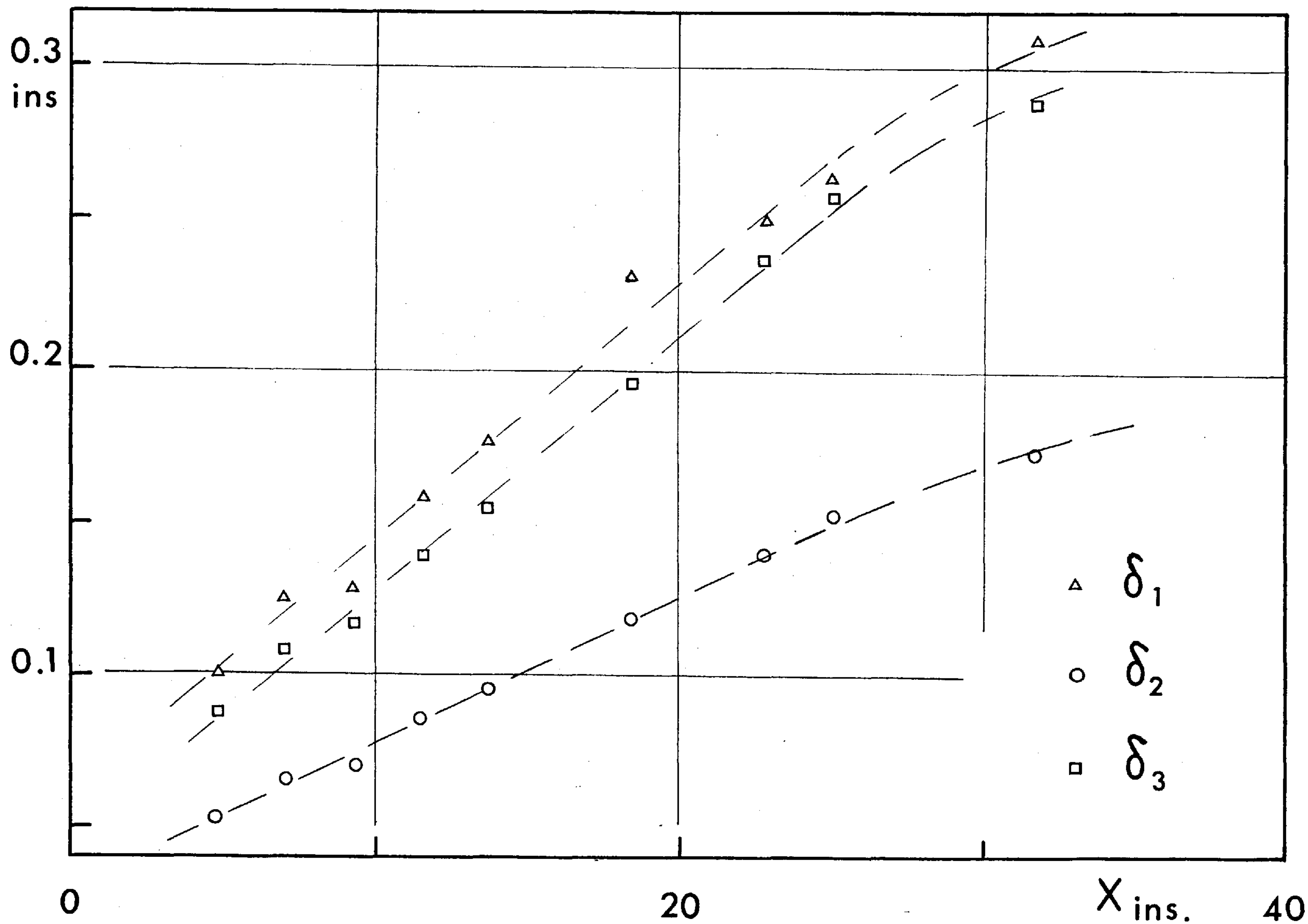

Fig. III.2.9 _ Boundary layer thicknesses _ Case II_B .

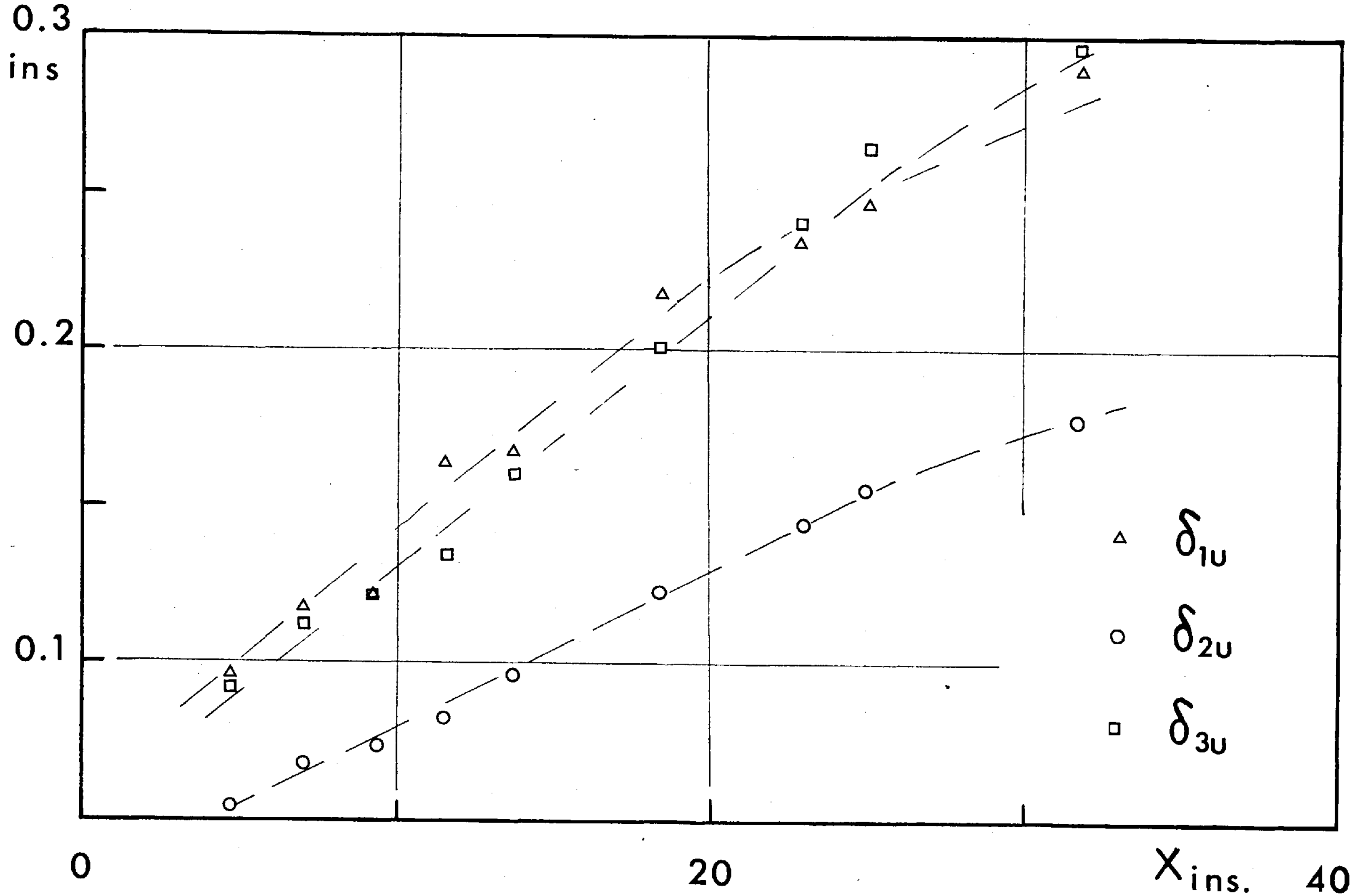

Fig. III.2.10 _ Boundary layer thicknesses _ Case II_B .

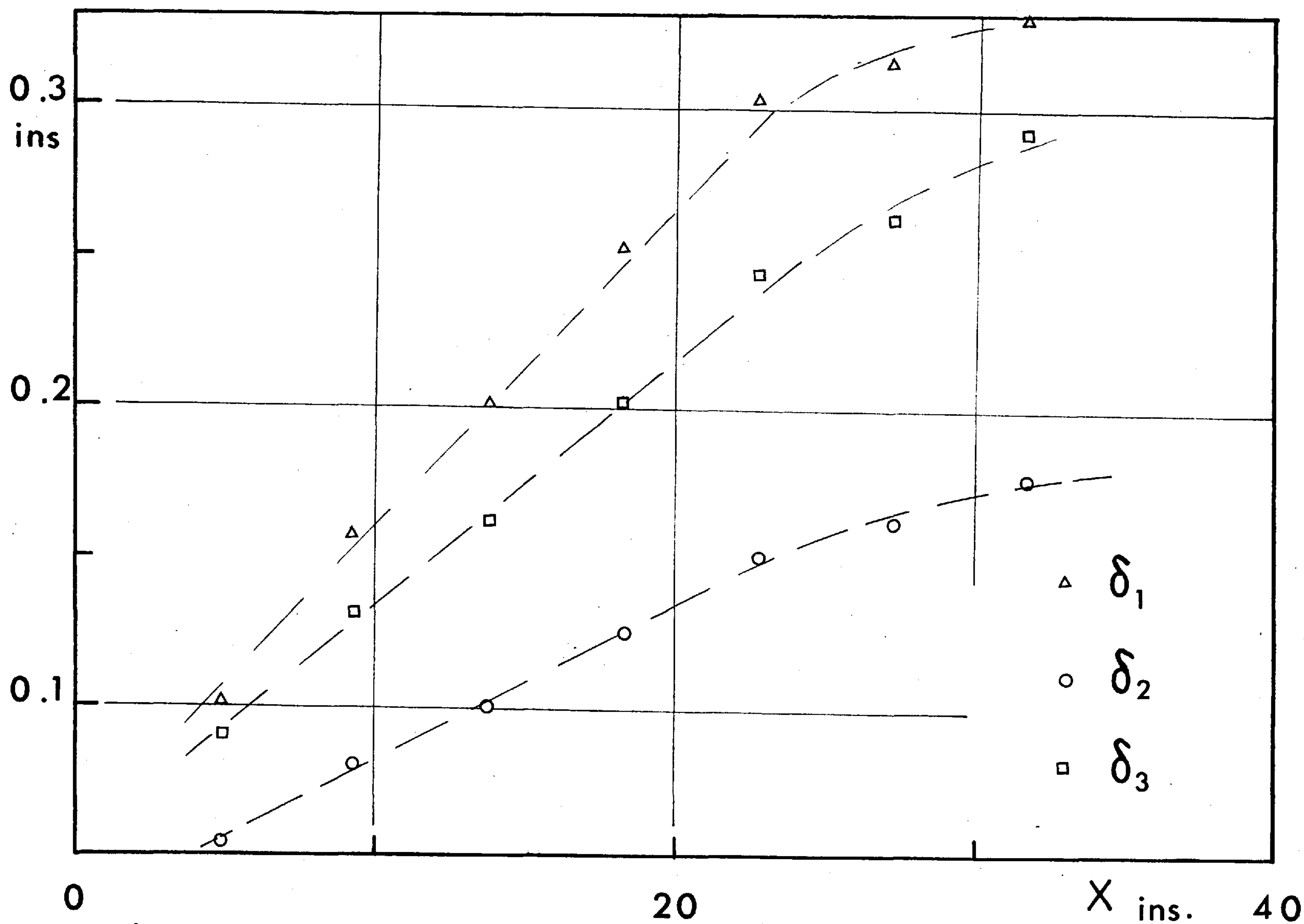

Fig. III.2.11 _ Boundary layer thicknesses _ Case II_C .

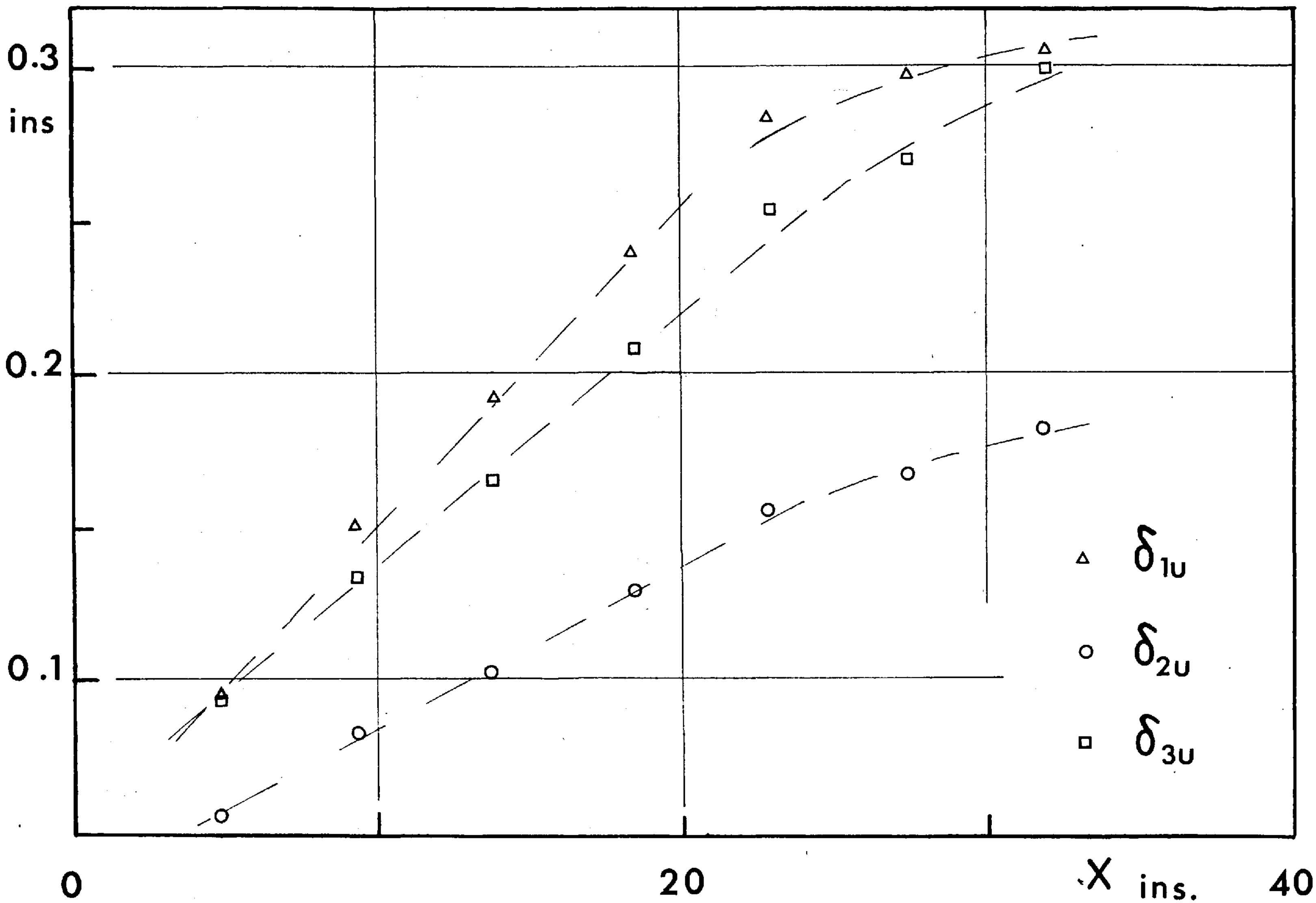

Fig. III.2.12 _ Boundary layer thicknesses _ Case II_C .

III.2.3 - <u>Calculation of the skin-friction coefficients:</u>

The skin-friction coefficients were calculated from the values of boundary-layer thicknesses computed as described in § III.2.2, and the obtained wall-pressure coefficients. The von-Karman two-dimensional momentum integral equation was used. It can be written as,

$$C_f = 2\frac{d\delta_2}{dx} + 2(H+2)\frac{\delta_2}{U_e}\frac{dU_e}{dx} .$$

The above equation is unmistakably valid, only under certain assumptions, and consequently has its limitations. For example, the effect of normal fluctuations $\overline{v'^2}$ is neglected, and the pressure across the boundary layer is considered constant. In fact, the static pressure is,

$$P_y = P_{wall} + \int_0^y \rho\, \overline{v'^2}\, dy \quad \text{(see (17) for example).}$$

The effect of velocity fluctuations and their correlations is not taken into account in calculating the momentum differences.

With adverse pressure gradients, two terms of the same order of magnitude are subtracted from each other, and the slight inaccuracy on one of the terms, or both, may be magnified quite easily.

Finally, the existence of three-dimensionality in the flow, alters the meaning of the above equation (see (18) for example).

The effect of the first factor, in our experiments and within the limited measurements of fluctuating components performed, was found to be at most an order of magnitude less than that of skin-friction coefficients.

Care was taken, as much as possible, in obtaining the graphical differentiations.

Three-dimensionality could have one, or both, of two main causes; that air is flowing unsymmetrically over the plate, or from natural convection from the heated plate which was mounted vertically in the working section of the wind-tunnel.

The boundary layer* was measured, by a provisional total-head probe flattened to 0.020 in. outside thickness approximately connected to a Betz micromanometer, at $3\frac{5}{8}$, $15\frac{7}{16}$ and $21\frac{1}{16}$ in. along the x-axis; 0, ± 4 and ± 8 in. along the z-axis**. It was found that the velocity profiles at the same distance along x, agree closely with each other, within the limits of accuracy of measurements.

Although the region covered above has no significant

* IA

** The origin of z being the centre-line of the plate.

pressure gradient, and might not be fully representative of all the cases, especially those with positive pressure gradient, the wall pressures of the plate seem to suggest that there could not be serious, if any, cross flow.

On the other hand, the order of magnitude of the effect of buoyancy on the skin-friction could be seen from the demonstration of E. Pohlhausen (see (1) for example), on the natural convection from a vertical hot plate. The vertical air velocity was expressed as,

$$w = 4\nu\sqrt{z+h}\; C^2 \zeta'(\eta)$$

where : h is half the height of the plate,

$$C = \left[\frac{g}{4\nu^2}\;\frac{T_w - T_e}{T_e}\right]^{\frac{1}{4}}$$

$$\zeta'(\eta) = \frac{w}{2\sqrt{g(z+h)}}\sqrt{\frac{T_e}{T_w - T_e}} \quad , \text{ and,}$$

$$\eta = C\,y\,/\,(z+h)^{\frac{1}{4}} \quad .$$

The maximum value of $\zeta'(\eta)$ for Pr = 0.73, occurs at $\eta \cong 1$ and has the value of 0.27 (Fig.14.23 (1)). The maximum vertical air speed at the centre of the plate would then be,

$$(w_o)_{max.} \cong 1.67 \;\; ft/sec \quad ,$$

for

$$T_w / T_e \cong 1.3 \quad .$$

The above estimate shows that the deviation of stream lines at the centre of the plate due to surface heating could reach a maximum value of 1°, with $\frac{\partial w}{\partial z}$ very much less than $\partial u/\partial y$, the latter being at least of $O(10^3)$, while $\frac{\partial w}{\partial z}$ is of $O(1)$.

The obtained values of skin-friction coefficients and of $2\frac{d\delta_2}{dx}$ for the examined cases are shown on Fig. III.2.13 to III.2.18.

Skin-friction co-efficients will also be discussed later in § III.4.

III.2.4 - <u>The effect of surface-heating on the skin-friction coefficients:</u>

Examining the obtained results of $C_f(x)$, it is noticed that the effect of surface heating on the computed values of C_f, is either a reduction or an increase.

For example, the effect of heating was of relatively small importance in the presence of no, or very small, pressure gradient, in the range of heating applied. Generally speaking, the heating has the effect of reducing C_f obtained for the unheated plate*, in similar pressure

*Near adiabatic at such low speeds.

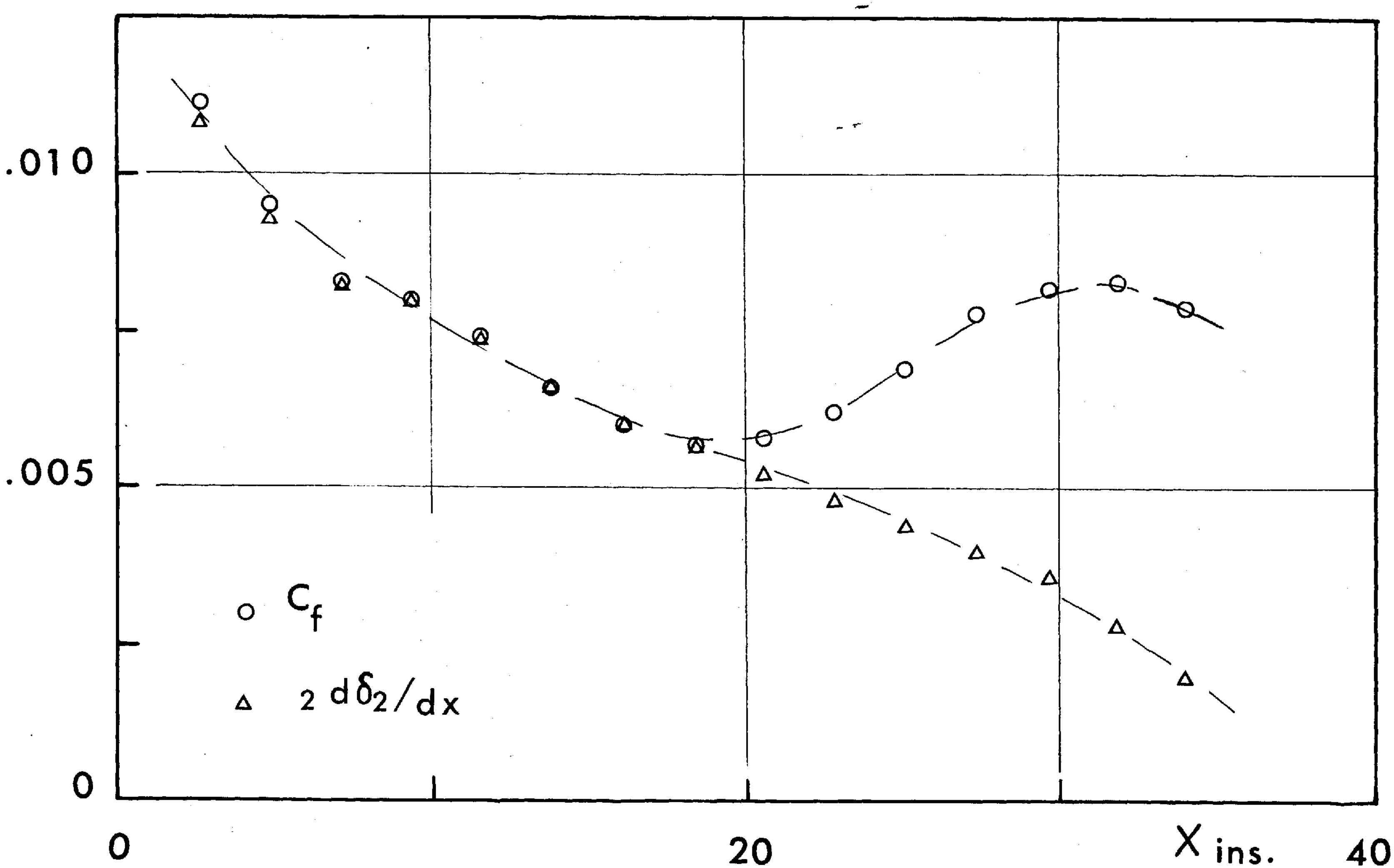

Fig. III. 2.13 _ Skin friction coefficients _ Case I_A .

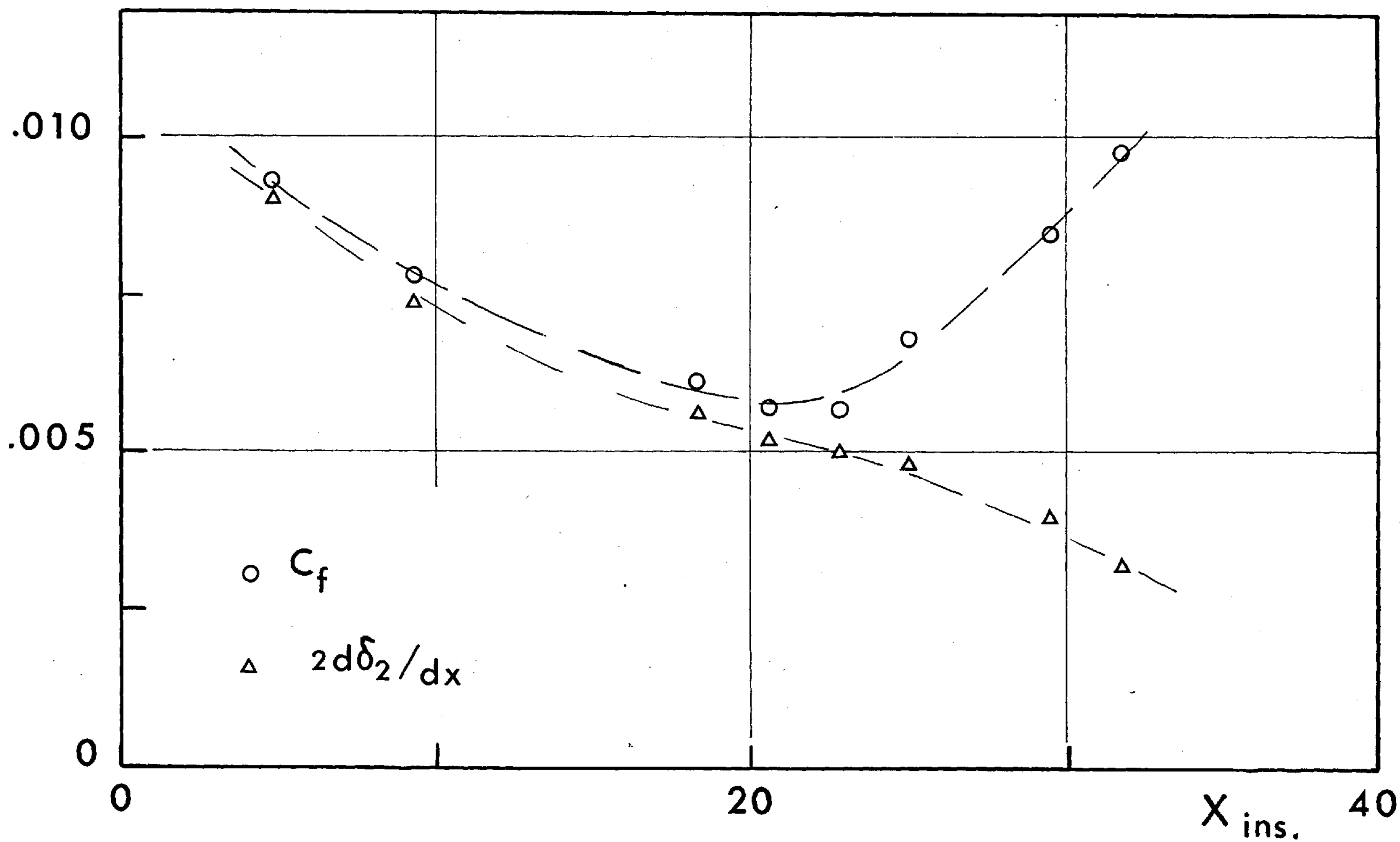

Fig. III. 2.14 _ Skin friction coefficients _ Case I_B .

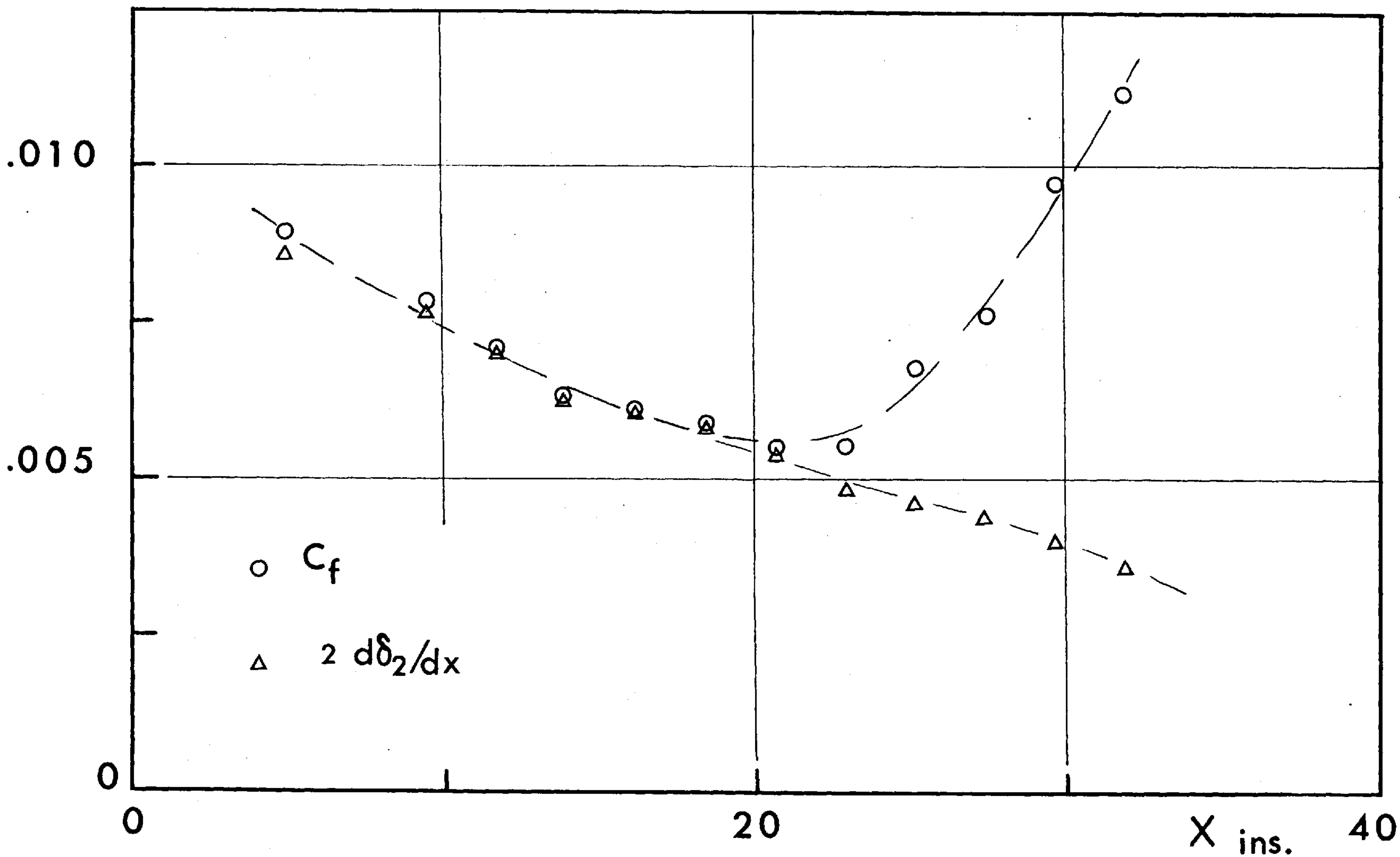

Fig. III. 2.15 _ Skin friction coeffecients _ Case I_C .

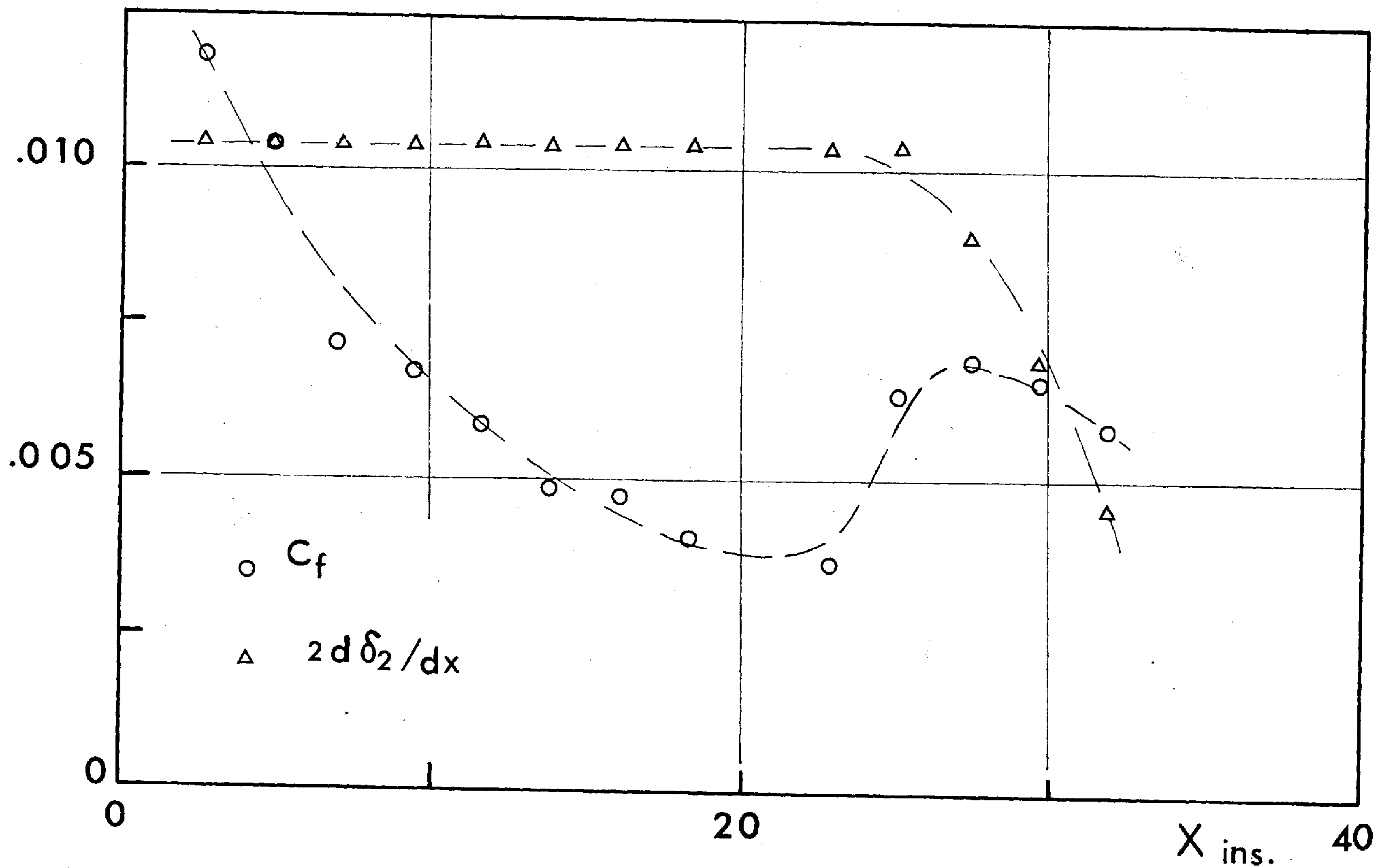

Fig. III.2.16 _ Skin friction coeffecients _ Case II_A .

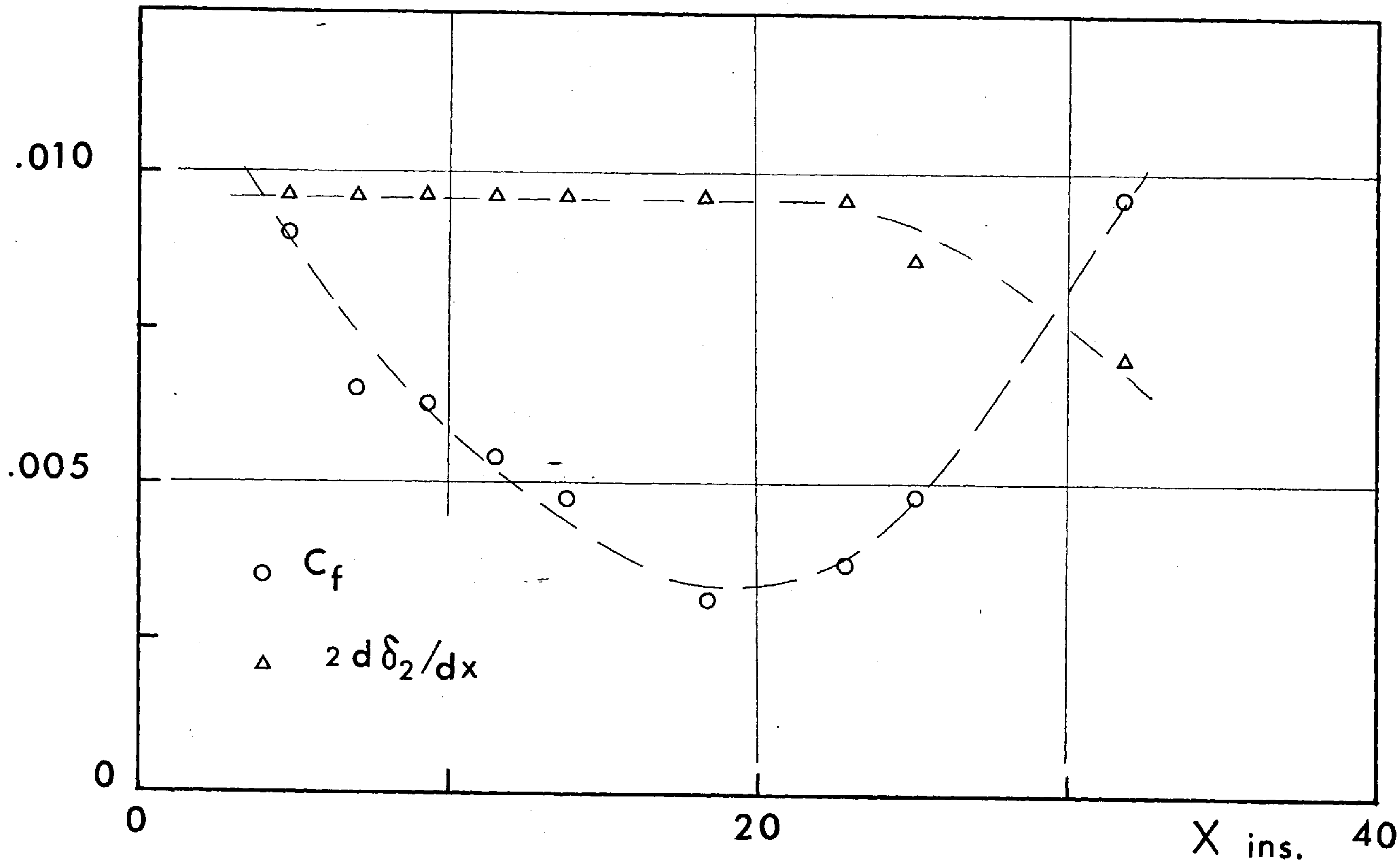

Fig. III.2.17 _ Skin friction coefficients _ Case II_B .

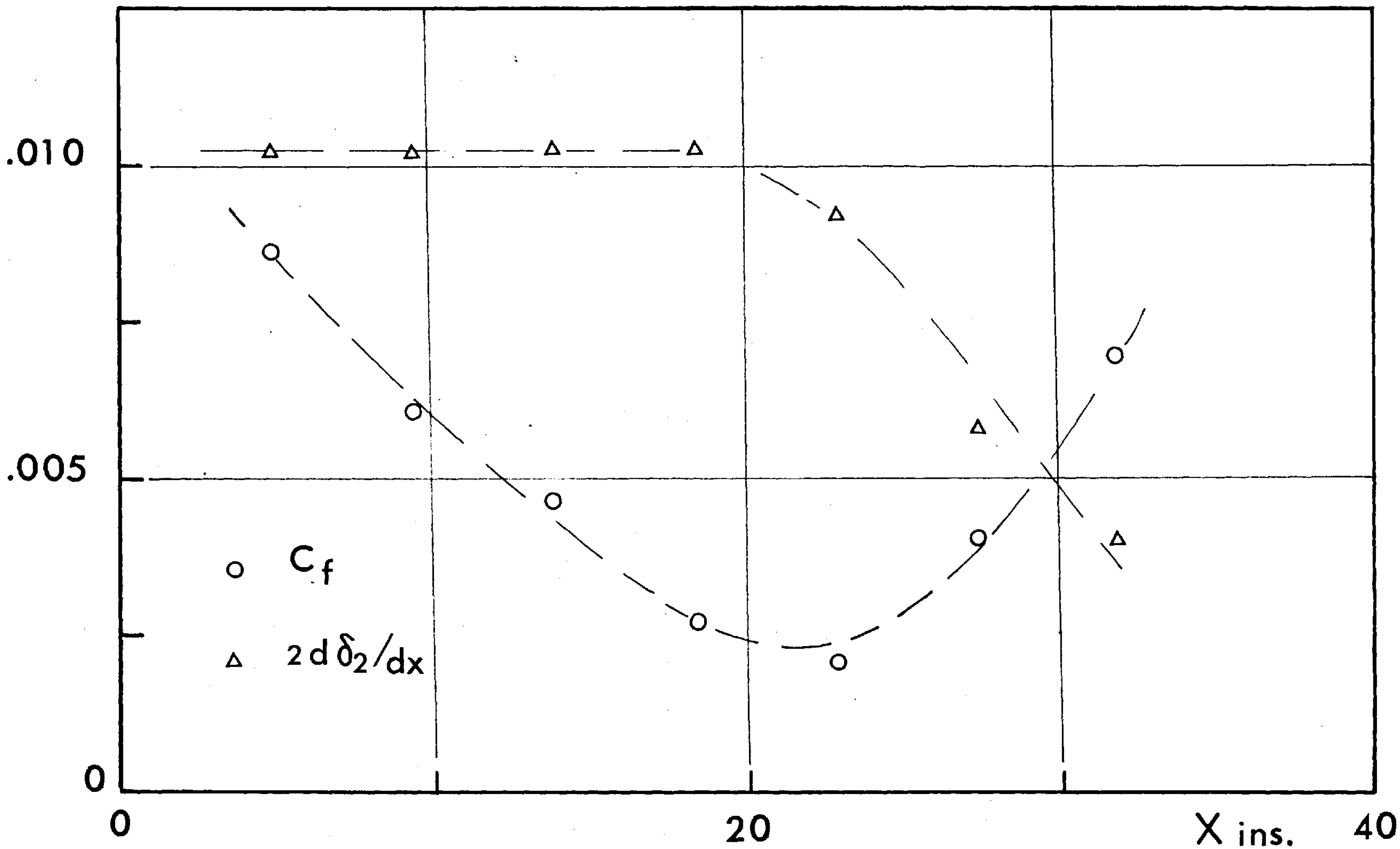

Fig. III. 2.18 _ Skin friction coefficients _ Case II_C .

environments.

When positive pressure gradients were applied, the effect of heating was a noticeable reduction in C_f, while negative pressure gradients were associated with an increase in the skin-friction coefficients with surface heating.

If we consider the definitions of δ_2 and δ_{2u}, and assume that the effect of temperature field on that of the velocity is small, we can then write that,

$$\delta_{2u} > \delta_2 \quad \text{, and hence,}$$

$$\frac{d\delta_{2u}}{dx} > \frac{d\delta_2}{dx} .$$

Similarly, we can deduce that $\delta_1 > \delta_{1u}$ from their respective definitions and the above assumption. This yields,

$$H\left(\equiv \delta_1/\delta_2\right) > H_u\left(\equiv \delta_{1u}/\delta_{2u}\right).$$

A simple substitution in the von-Karman equation would then lead to,

$$\begin{aligned} C_f &\leqq C_{f\,a} \quad \text{if} \quad dP/dx \cong 0 , \\ &< C_{f\,a} \qquad\qquad\qquad > 0, \text{ and,} \\ &> C_{f\,a} \qquad\qquad\qquad < 0 . \end{aligned}$$

(subscript a refers to the adiabatic wall)

We also notice that the pressure gradient severity parameter 'π', is accentuated by surface heating if it was positive. It does not alter significantly if it was negative, as seen from the present experiments.

III.2.5 - Discussion on reference temperature:

A brief discussion will be given, on the possibility of obtaining a method for reference temperature, applicable to rough surfaces in incompressible flow, similar to that generally used for supersonic flow (see (19) for example).

The method, originally derived by Monaghan, consists of referring the viscosity and density of the flow to a 'reference temperature', to allow the use of the formulae of skin-friction coefficients for adiabatic walls. The formula of skin-friction for adiabatic walls, can be written as,

$$C_{f\,a} = \frac{\tau_w}{\frac{1}{2}\rho_e U_e^2} = \frac{C_a}{R^m}$$

where, C and m are constants, and,

R a Reynolds number based upon x or some boundary layer thickness.

When the surface temperature differs from the adiabatic wall temperature, the formula becomes,

$$C_f = \frac{\tau_w}{\frac{1}{2}\rho_r U_e^2} = \frac{C_a}{R_r{}^m}$$

i.e.

$$C_f = C_{f_a} \cdot \left(\frac{T_r}{T_e}\right)^{m(\omega+1)-1}$$

where: $\mu_r/\mu_e = \left(T_r/T_e\right)^{\omega}$.

For a smooth surface in compressible flow, Tr is determined by a semi-emperical formula of the form,

$$T_r \equiv f\left(T_w , T_e , M , P_r \right) .$$

The above functions are obviously not of much use, for two-dimensional incompressible boundary-layers on rough surfaces, with arbitrary pressure gradient. A form, suitable for such an application, is then thought to be,

$$T_r \equiv F\left(k_s , \frac{T_w}{T_e} , R_{\delta_1} , \pi , \frac{\pi}{|\pi|} , P_r\right) .$$

with:
$$C_{f\,a} = \frac{C_o}{(R_{\delta_1})^n} ,$$
$$C_o \equiv F_1(\pi, k_s) , \text{ and,}$$
$$n \equiv F_2(\pi, k_s) .$$

We suggest a form of the function F, based on the previous discussion in § III.2.4, as,

$$\frac{T_r}{T_a} = 1 + A_1 \frac{T_w - T_a}{T_a} + A_2 \frac{\pi^2}{|\pi|} \cdot \frac{T_w - T_a}{T_a} ,$$

where:
$$A_1 \equiv F_3\left(k_s , P_r\right) , \text{ and ,}$$
$$A_2 \equiv F_4\left(k_s , R_{\delta_1} , P_r\right) .$$

A reasonable realistic mathematical derivation of the functions C_o, n, A_1 and A_2 remains complex at present. Semi-emperical expressions can only be possible when enough data for different values of k_s, π and $\frac{T_w}{T_a}$ is collected.

III.2.6 - <u>Presentation of the velocity profiles</u>:

The measured profiles are numerically tabulated in Appendix II, as mentioned earlier.

The form of presenting the profiles, has differed according to authors, even for smooth surfaces, in a search for a single-parameter family.

The profiles were generally expressed as,

$$U/V_0 \equiv f(y/\ell)$$

where: V_0 and ℓ are some velocity and length scales.

The velocity scale was given the values U_e, u_τ or a combination of both, as for the defect profiles for instance. That of length had $\delta, \delta_1, \delta_2, \frac{\nu}{u_\tau}$ or $\frac{\delta_{1u} U_e}{u_\tau}$.

Each of these forms, was associated with a parameter, to specify profiles in arbitrary conditions of pressure gradient. This parameter also varied, and had the forms H, Γ (introduced by Buri (1)), η, G, or Π.

The verification of all these forms is by no means an easy task, but some of the relevant and most frequent will be dealt with.

The parameter chosen by Gruschwitz(1) to define velocity profiles in the presence of pressure gradients was η, where,

$$\eta = 1 - \left(\frac{U_{(y=\delta_2)}}{U_e}\right)^2.$$

Pretsch introduced a universal relation between η and H to suit the experimental results. It can be written as,

$$\eta = 1 - \left[\frac{H-1}{H(H+1)} \right]^{(H-1)} ,$$

with the corresponding velocity profiles expressed as,

$$U/U_e = (y/\delta)^{\frac{1}{n}}$$

where: $n = 2/(H-1)$

When plotting the values of η as measured experimentally against $H_u \; (\equiv \delta_{1u}/\delta_{2u})$ on Fig.III.2.19, a fair agreement can be noticed between experiments and Pretsch's universal function. The scatter involved and the flexibility in the determination of δ, would suggest that this method is not completely adequate for the present results.

The profiles on rough surfaces were also specified, (4) and (6), as $U/Ue = (y / \delta_2)^m$, where m was different from a rough surface to another, but was constant for a particular plate. The range of applicability of such form also seems limited. The authors only considered rough surfaces when no pressure gradient was present.

Nikuradse demonstrated earlier that a velocity

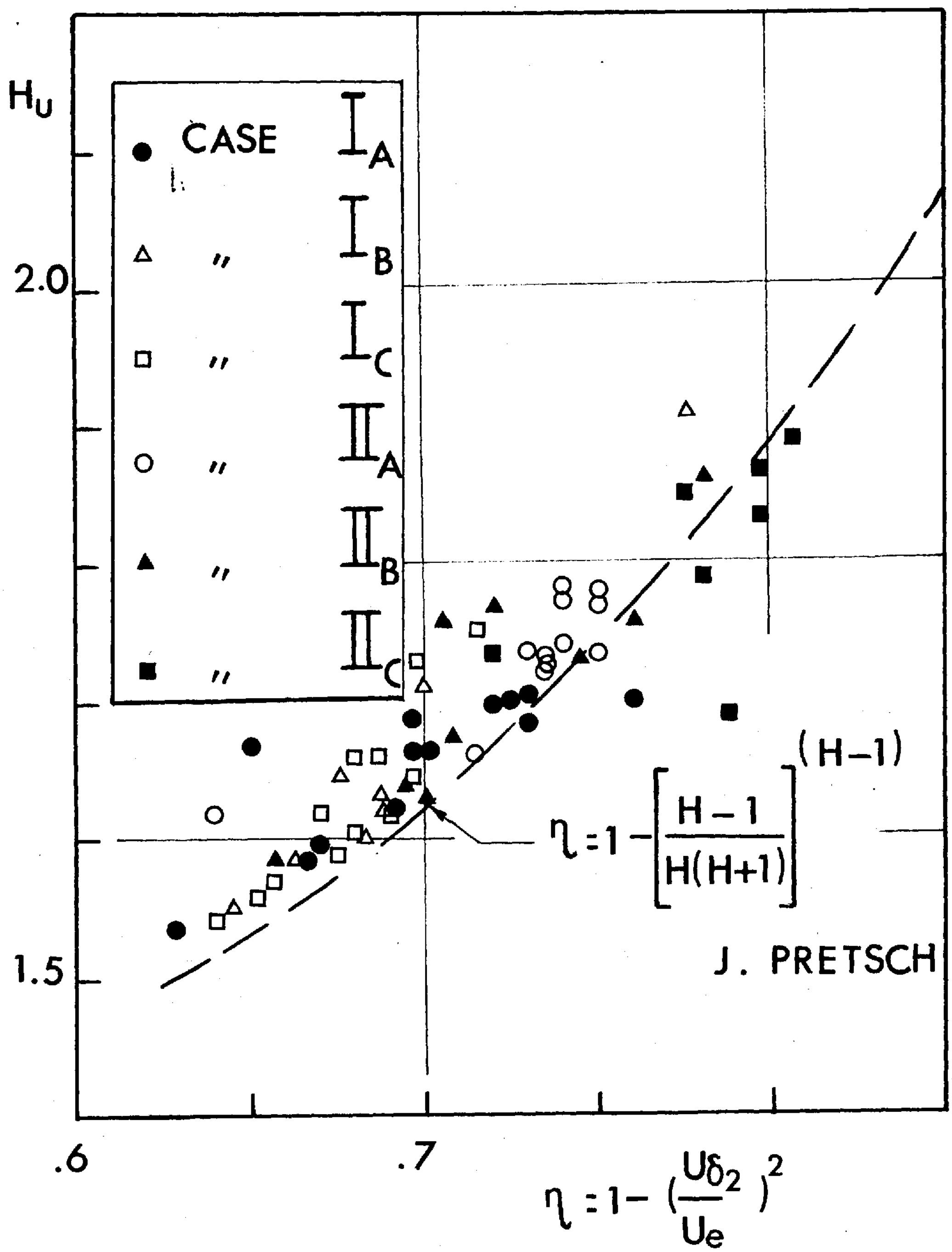

Fig. III. 2.19 _ Relationship between H_u and η.

profile on a rough surface can be represented by the law of the wall, which applies for smooth surfaces, with the difference that the profile for a rough wall is shifted by an amount $\Delta U/u_\tau$ below that of the smooth. This shift was found to be function of R_k $(\equiv k u_\tau/\nu)$. Prandtl and Schlichting verified that fact experimentally for sand roughness. It was also found applicable for wire screens (2), and two-dimensional square ribs (5) and (16).

The velocity profiles of the present study have been plotted in the form $\frac{U}{u_\tau}\left(\frac{y u_\tau}{\nu}\right)$ on Fig. III.2.20 to III.2.25.

These figures show that the linear part is generally confined to a relatively small region, especially for some of the profiles of II_A.

The shift of the linear part $\frac{\Delta U}{u_\tau}\left(k u_\tau/\nu\right)$ is shown on Fig. III.2.26. This figure reveals that the equivalent height of sand roughness for the examined plate, is half the depth of cavities approximately.

The form of presentation used by many authors for smooth and rough surfaces, is the velocity-defect. It can be expressed in the form,

$$(U_e - U)/u_\tau = -\frac{1}{0.4} \operatorname{Ln} \frac{y u_\tau}{\delta_{1u} U_e} + A \quad .$$

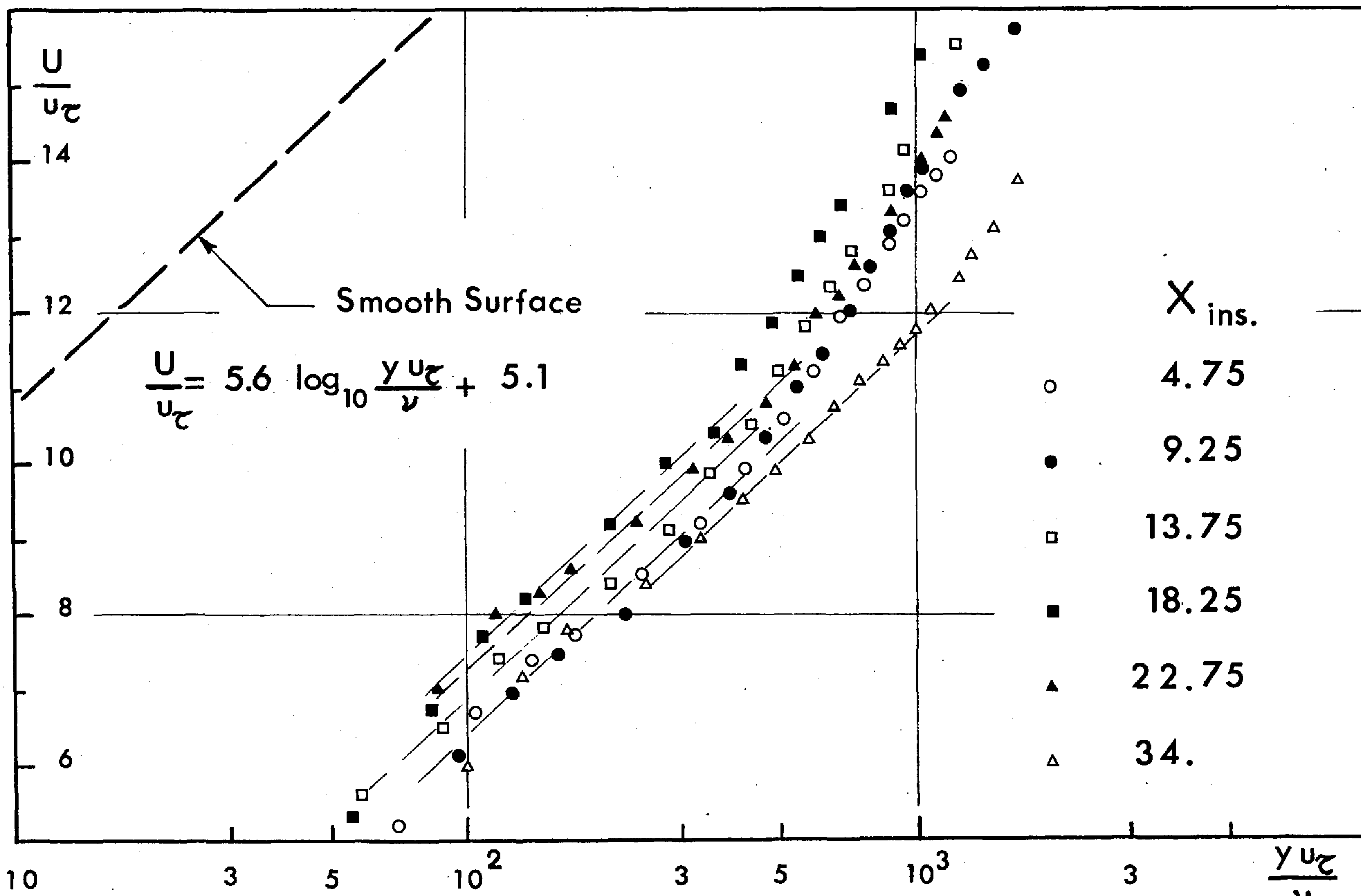

Fig. III.2.20 _ Velocity profiles _ Case I_A .

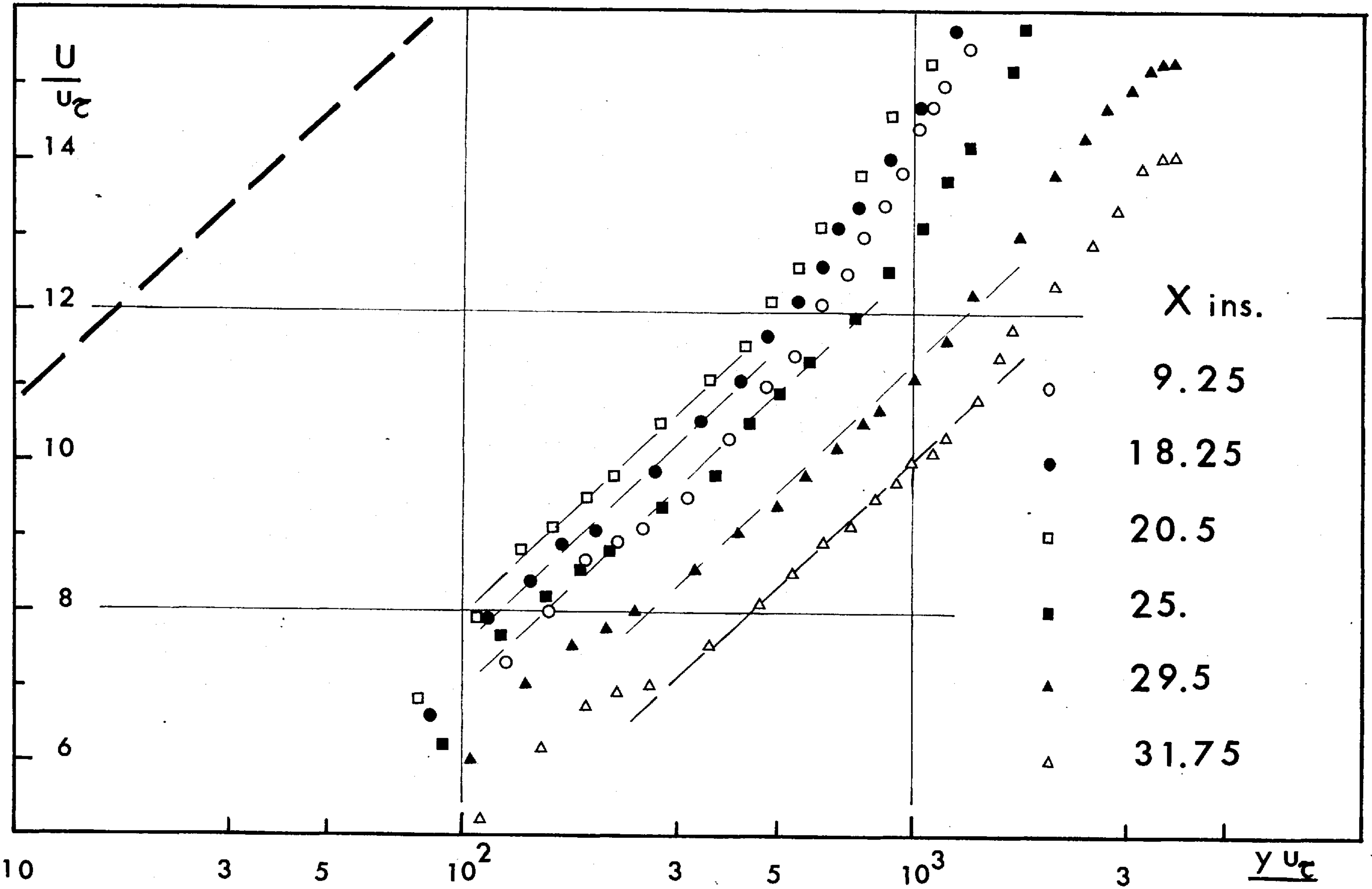

Fig. III.2.21 _ Velocity profiles _ Case I_B .

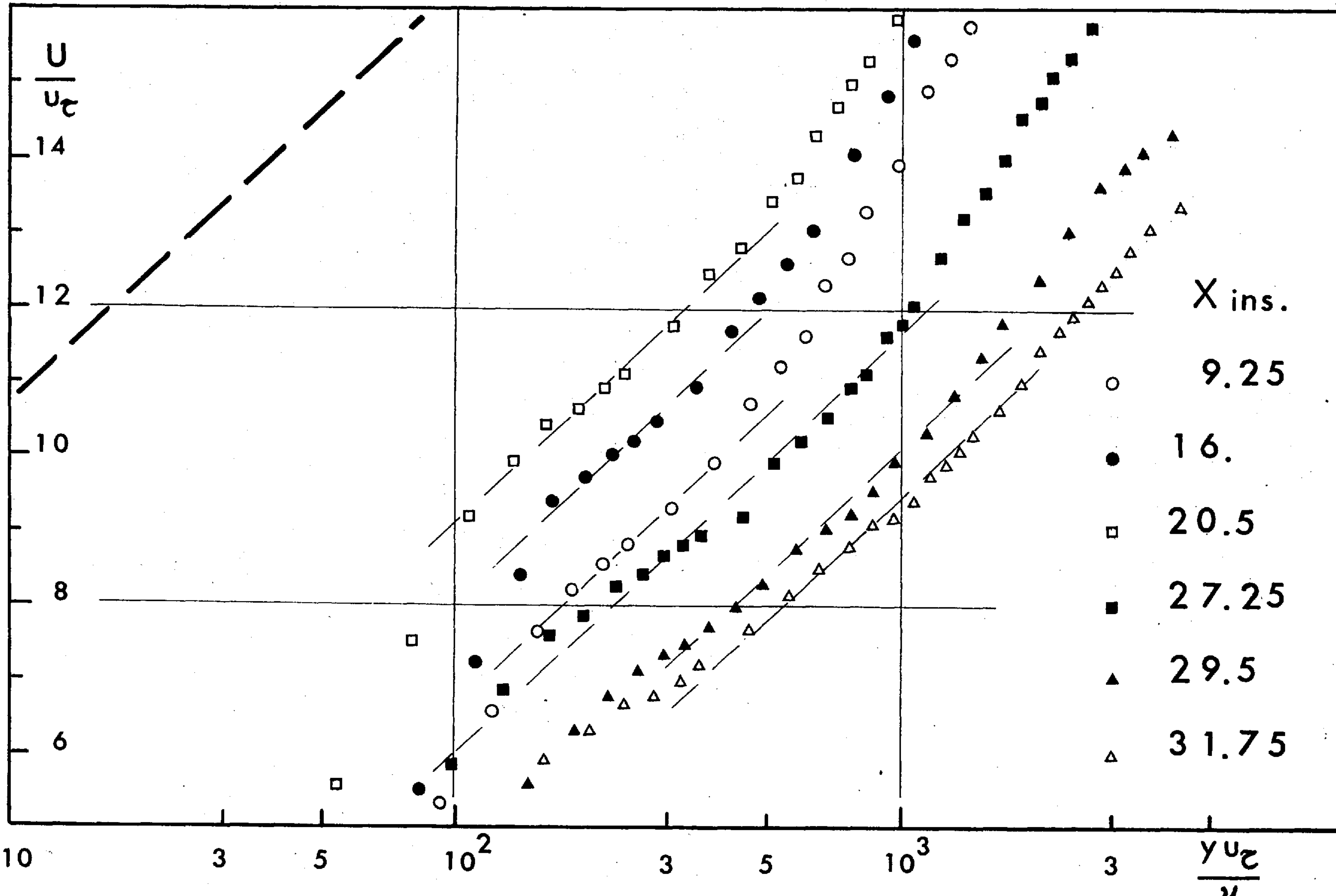

Fig. III. 2. 22 _ Velocity profiles _ Case I_C .

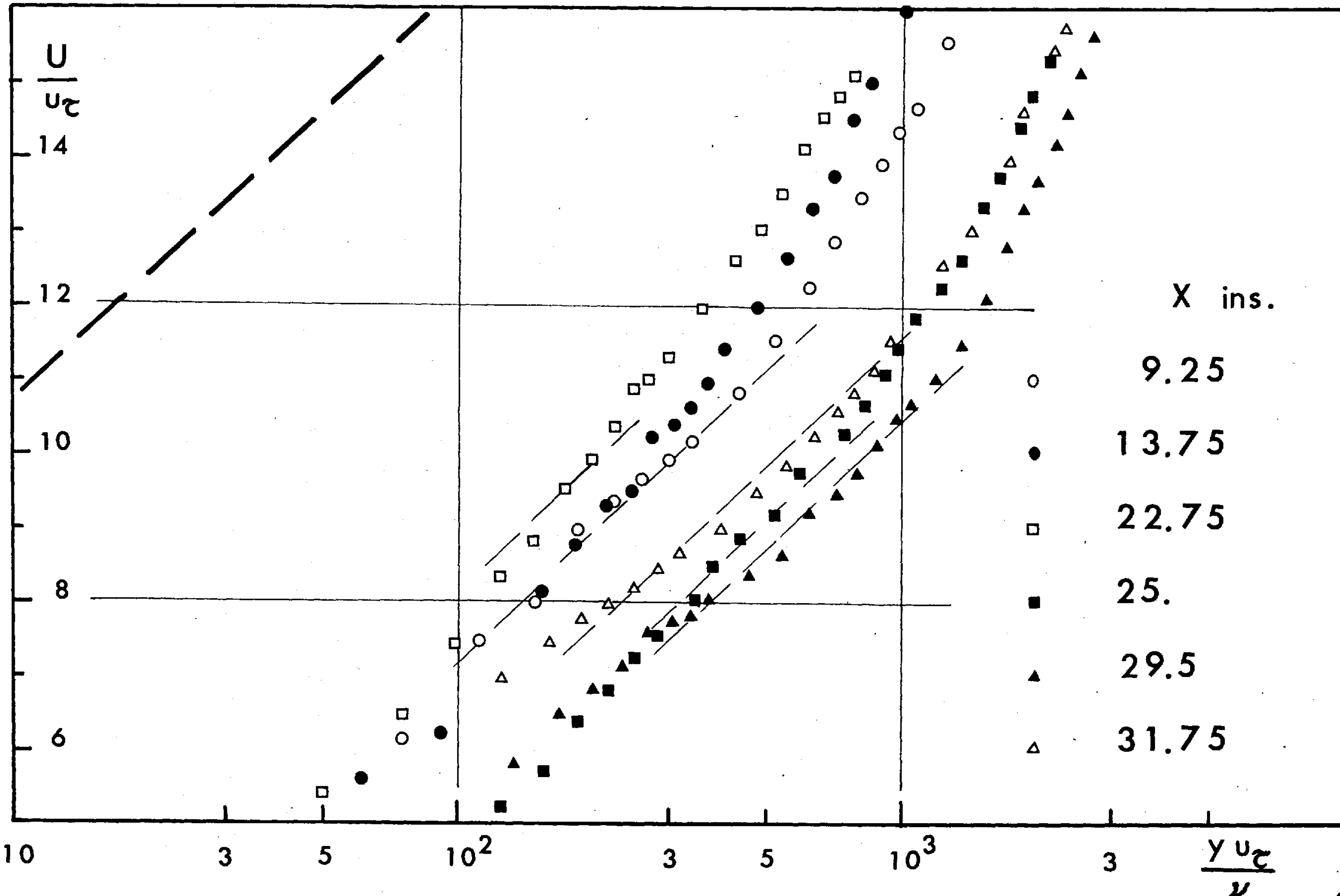

Fig. III.2.23 _ Velocity profiles _ Case II_A .

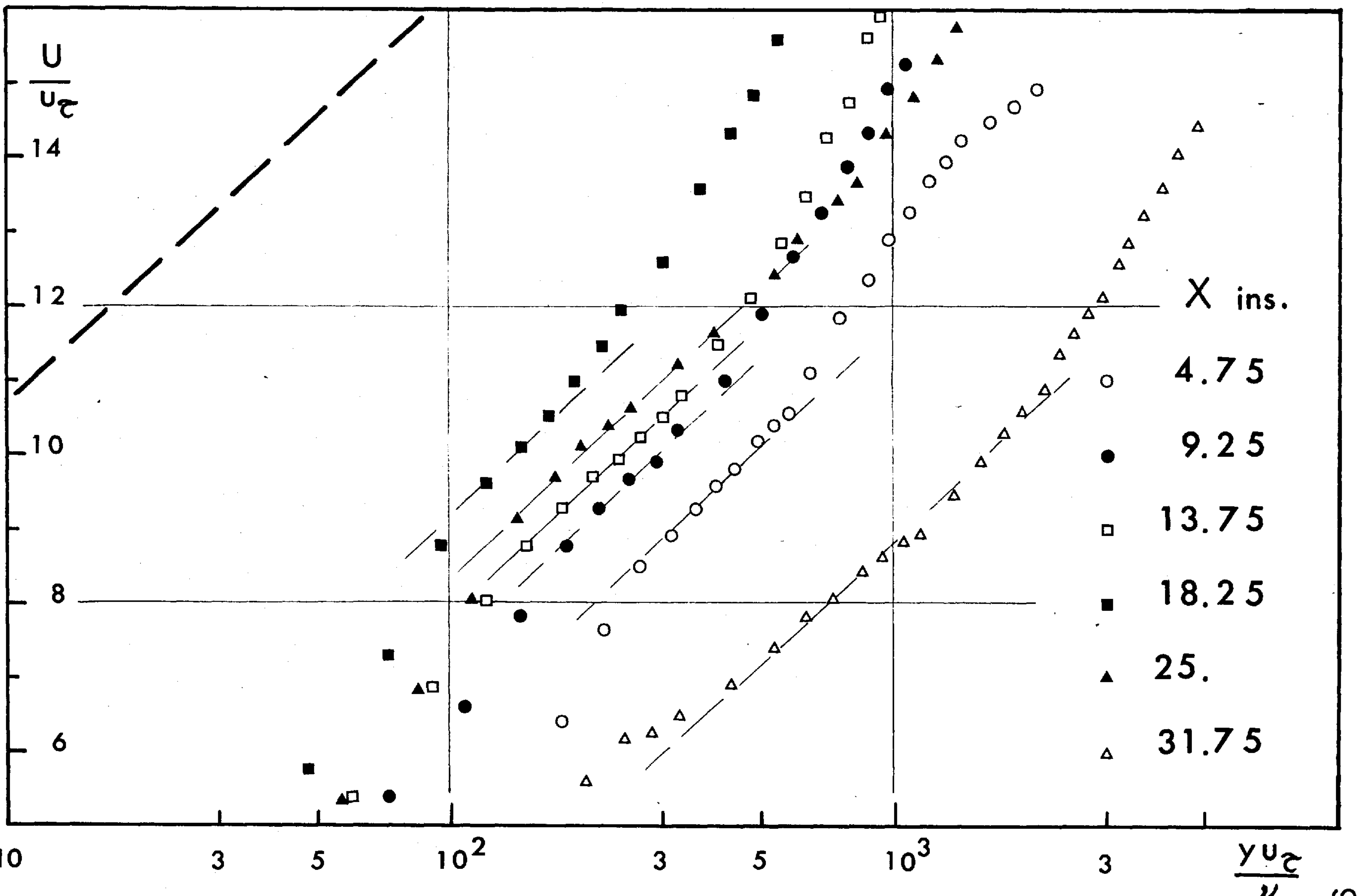

Fig. III.2.24 _ Velocity profiles _ Case II_B .

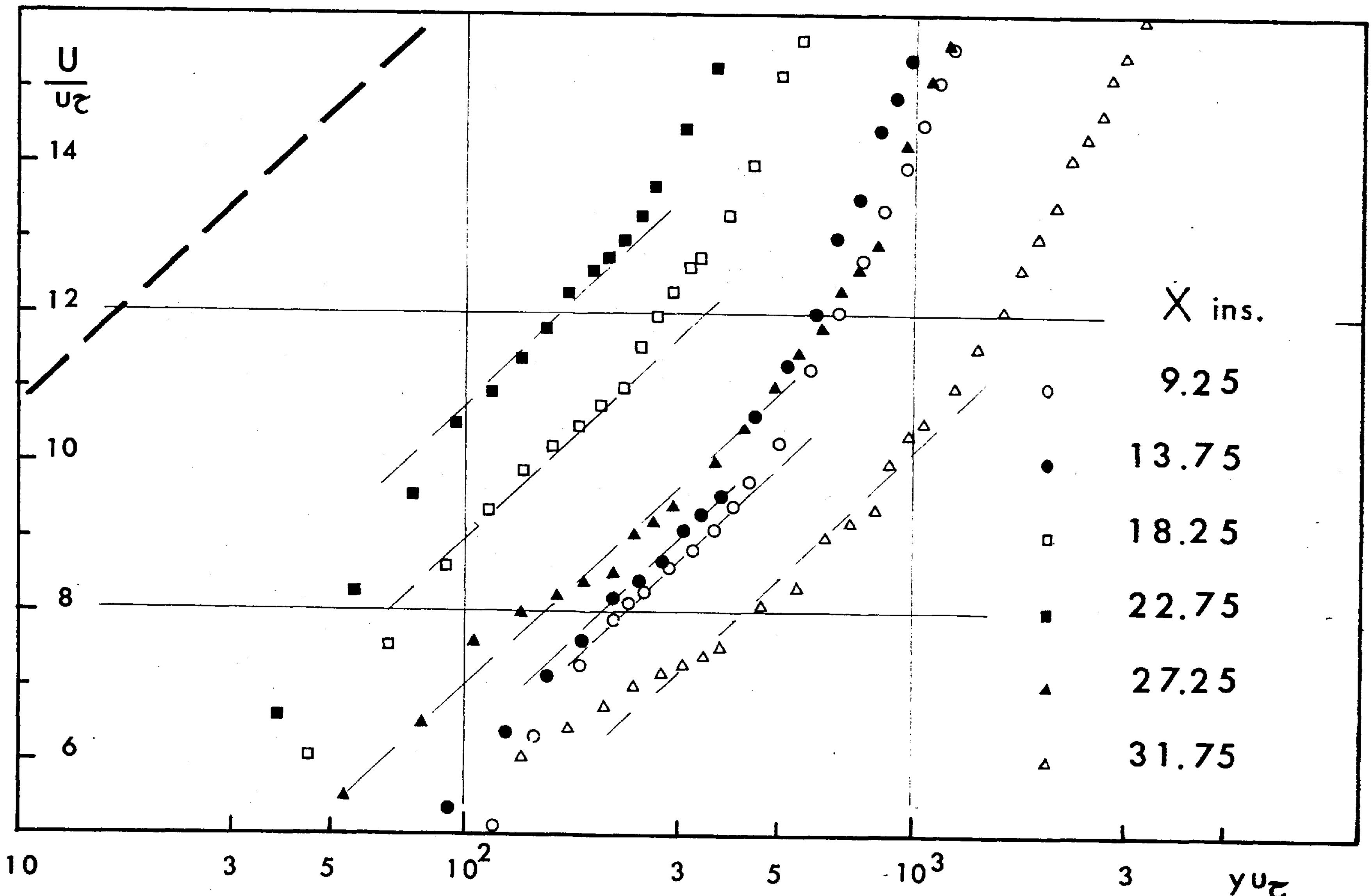

Fig. III.2.25 _ Velocity profiles _ Case II_C

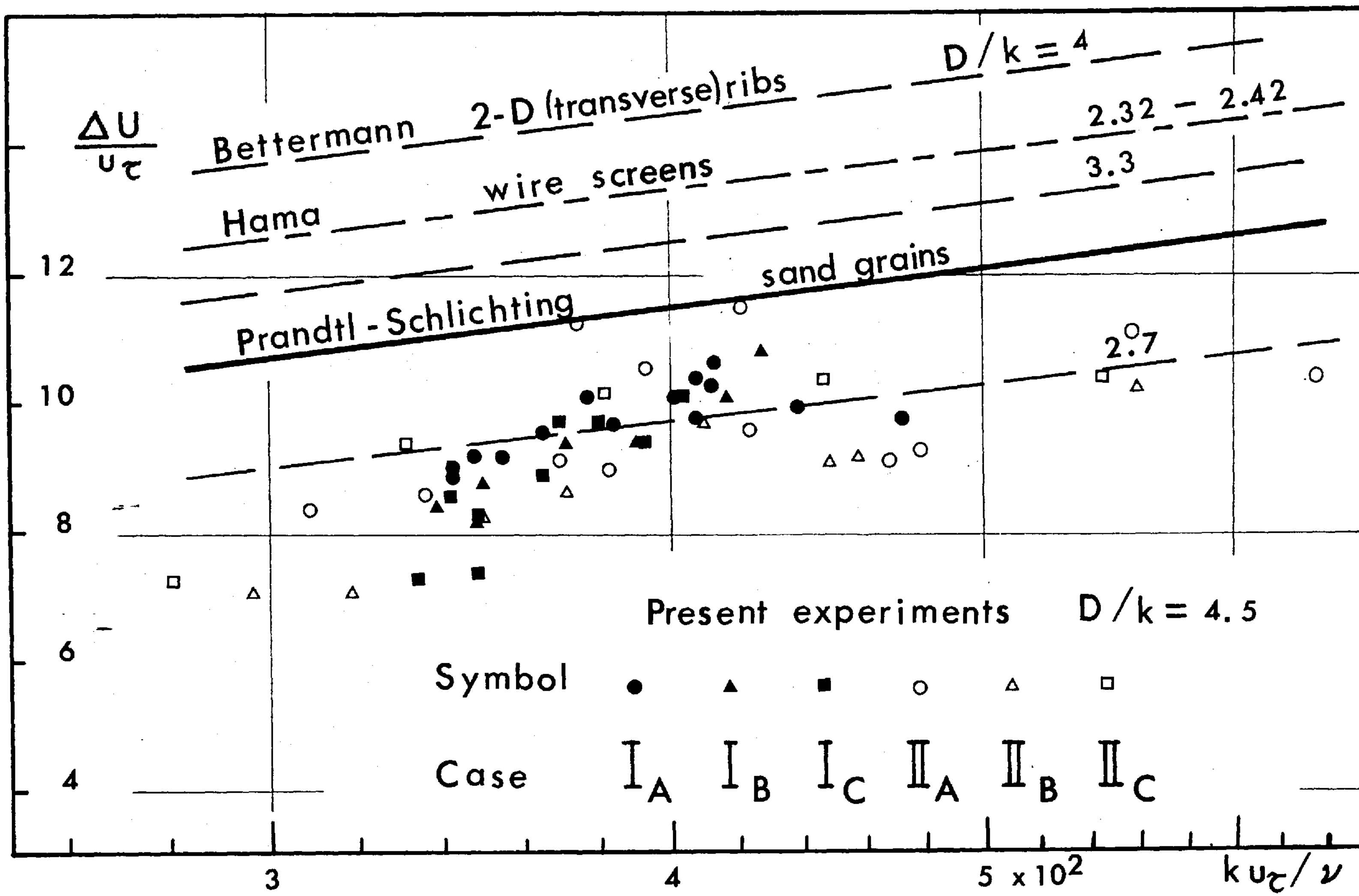

Fig. III. 2. 26 _ Effect of roughness on the law of the wall.

Nikuradse found this semi-logarithmic linear relationship to apply for the regions close to the wall, and outside the viscous sub-layer, for all heights of sand roughness.

Rotta (20), suggested that the value of the constant A appearing in the velocity-defect relation, to be a function of the parameter G, while Mellor (22) retained that $A \equiv A(\Pi, \alpha)$, where α is a parameter introduced by Mellor $\left(\alpha = \dfrac{\Pi\, U_e}{R_{\delta_1} u_\tau} \right)$.

Some velocity profiles of the present work were plotted in the defect form, for various values of G and Π as shown by Fig.III.2.27 to III.2.33.

The velocity-defect presentation is favoured for the present application. This is due to the fact that it covers the regions of boundary layer away from the wall. This presentation is also consistent for smooth and rough surfaces, with G as parameter. This statement will be supported later (see III.2.8).

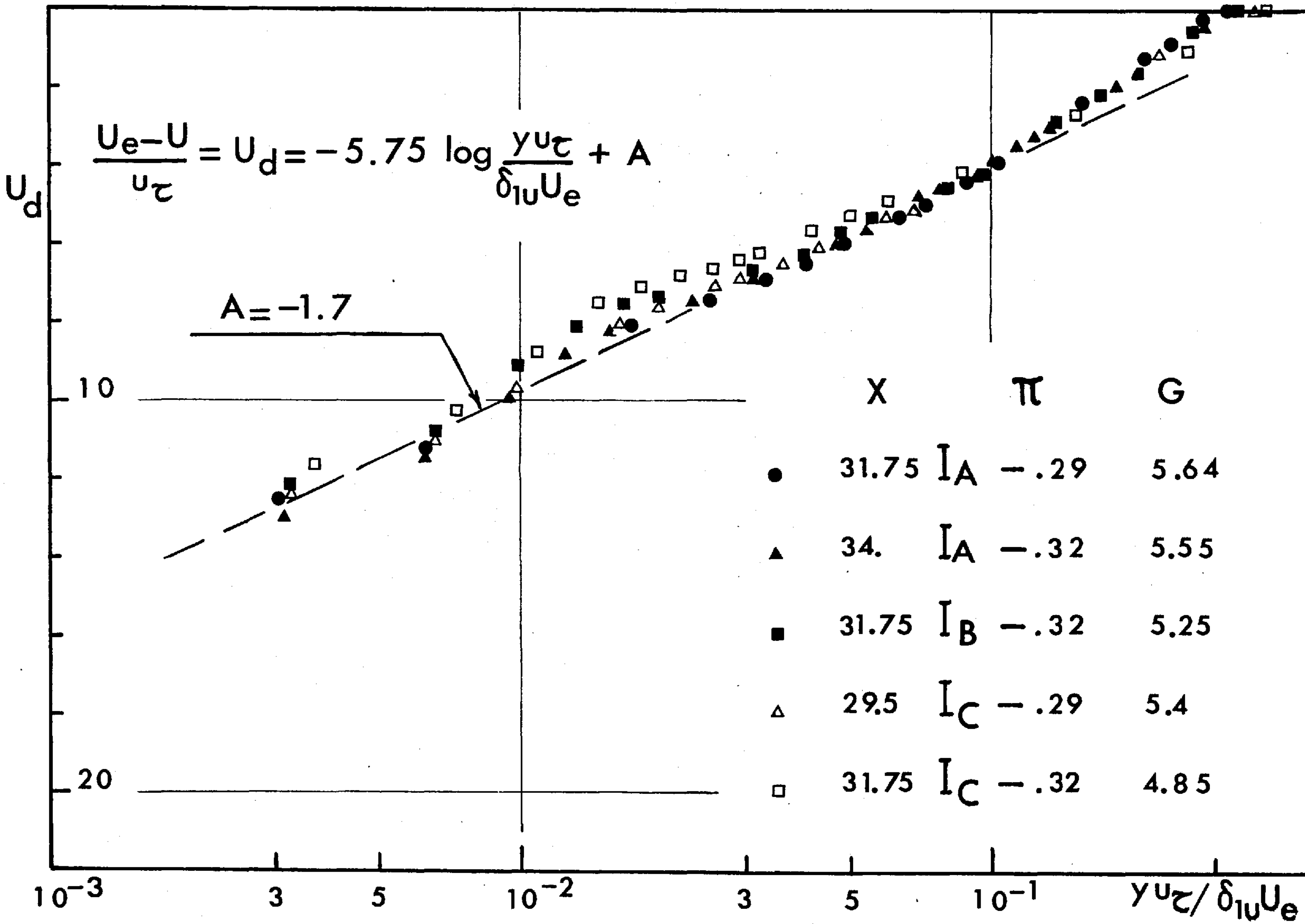

Fig. III.2.27_ Velocity - defect profiles .

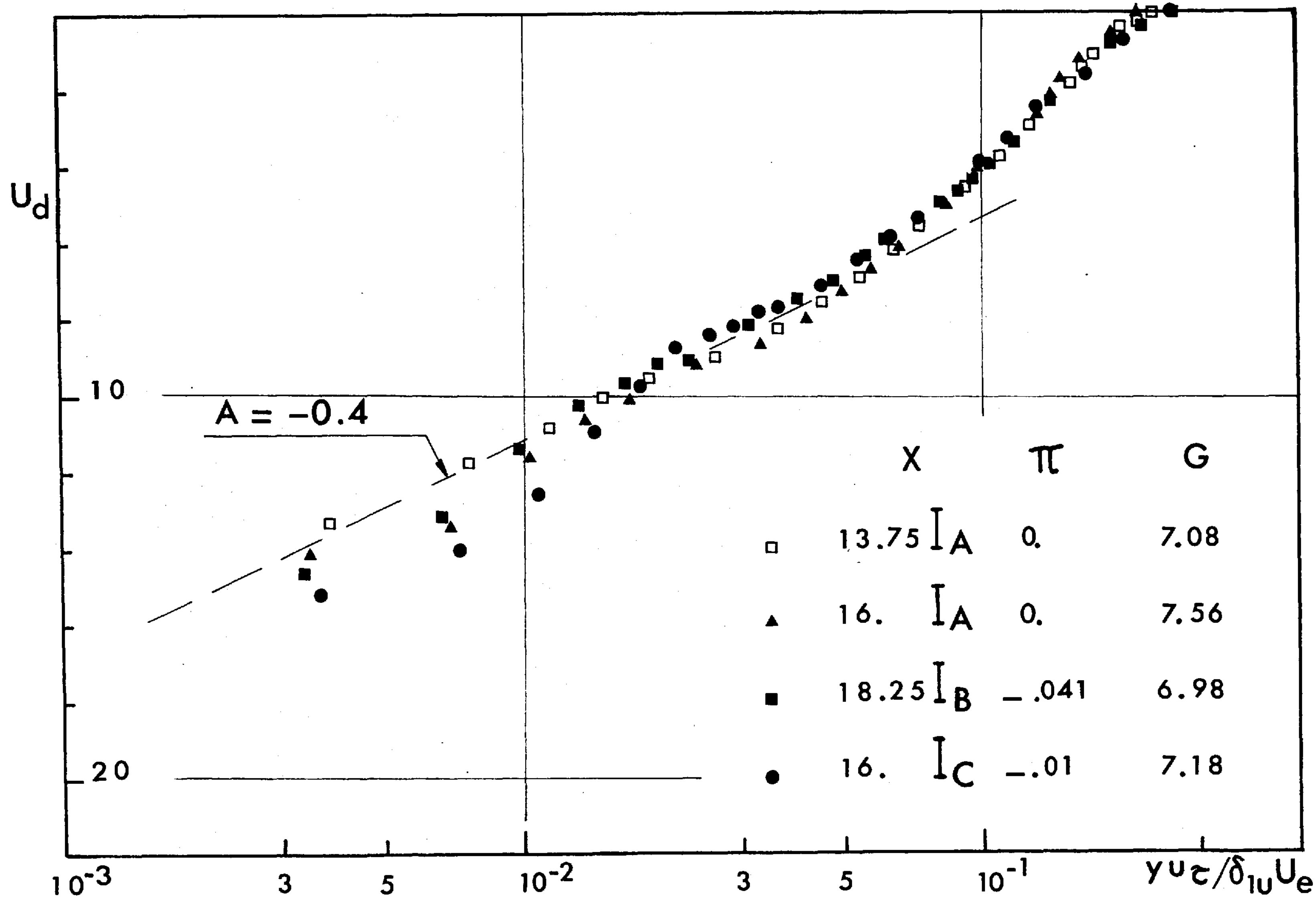

Fig. III.2.28 _ Velocity - defect profiles.

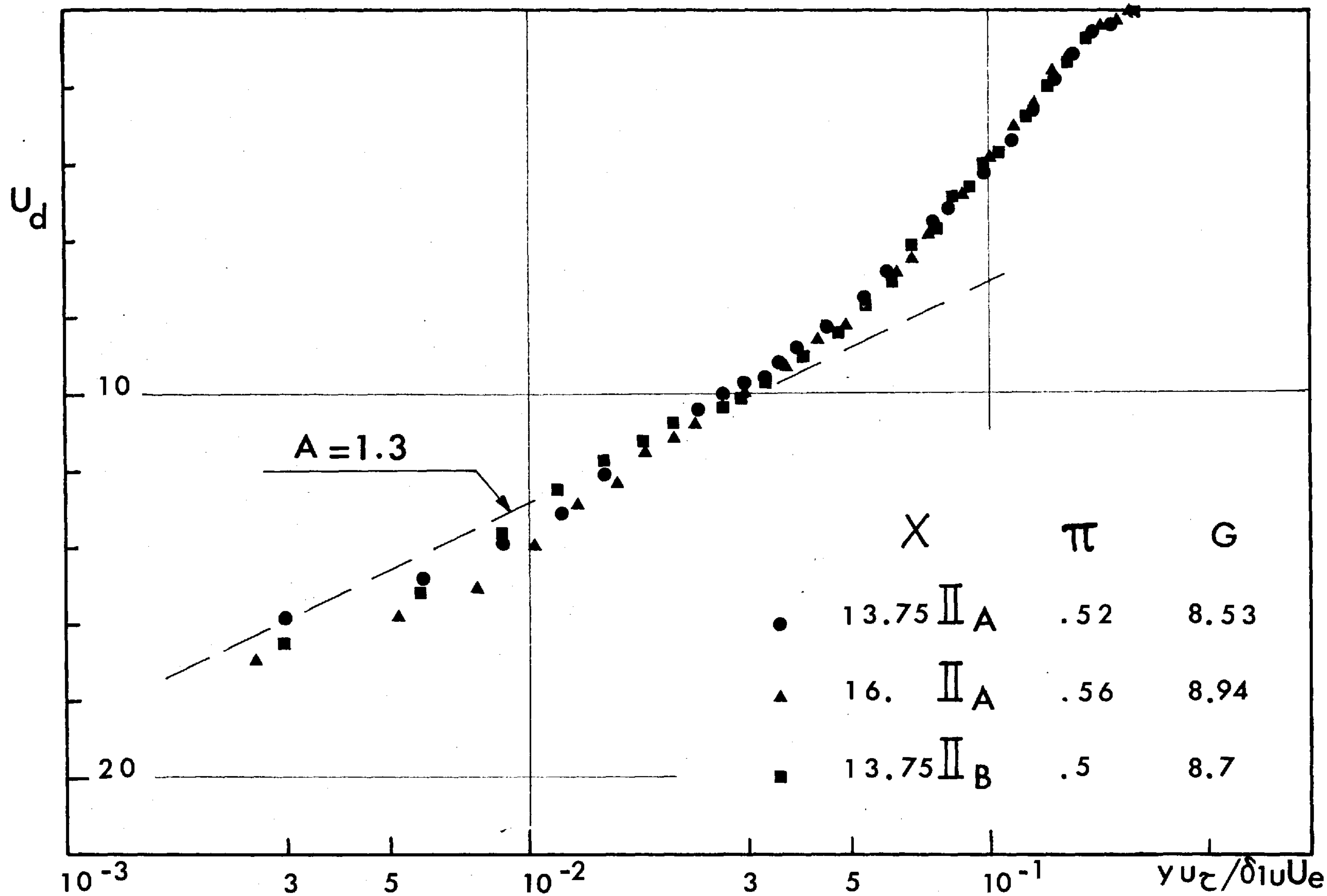

Fig. III. 2. 29 _ Velocity - defect profiles .

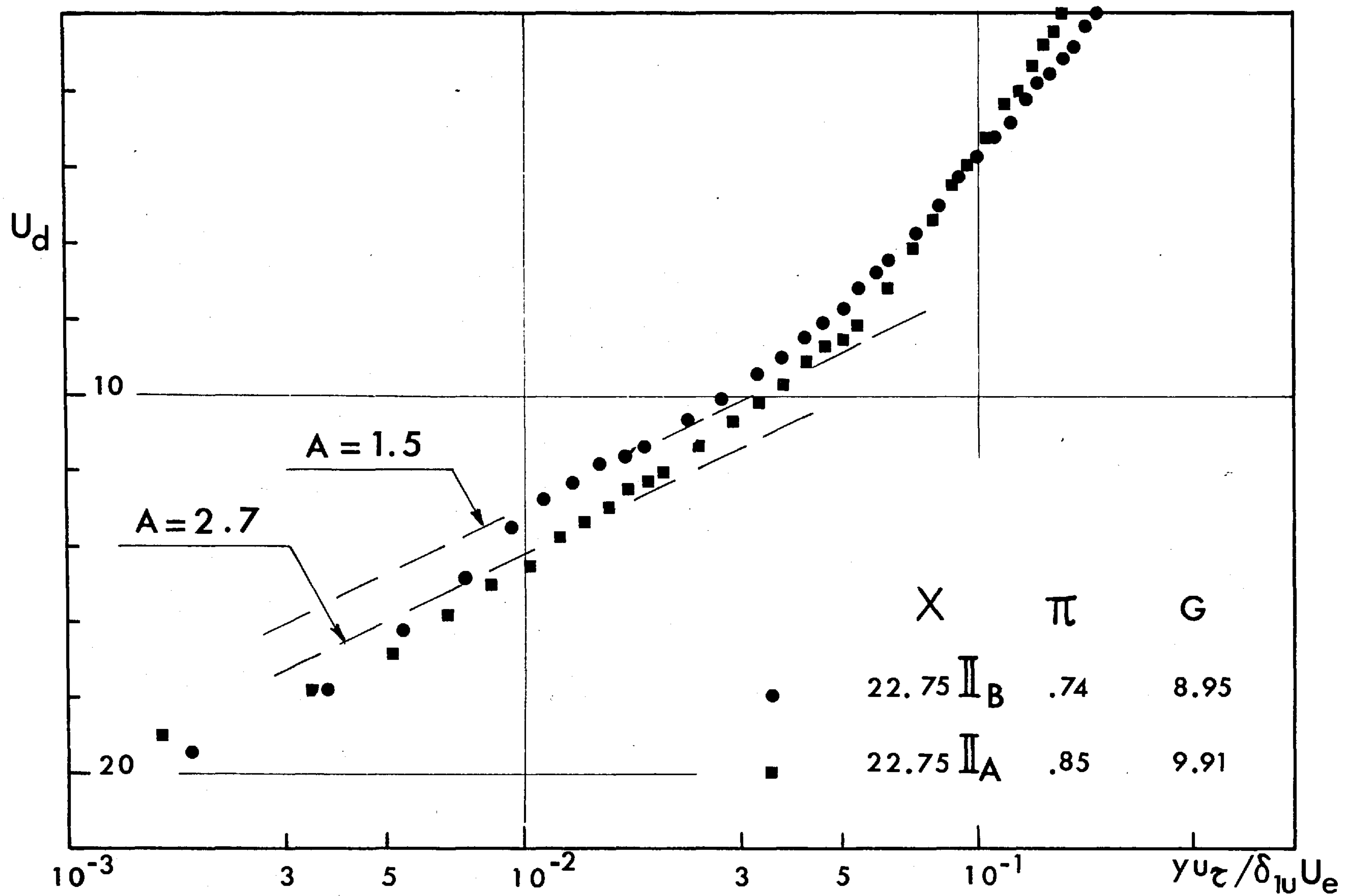

Fig. III. 2.30 _ Velocity - defect profiles .

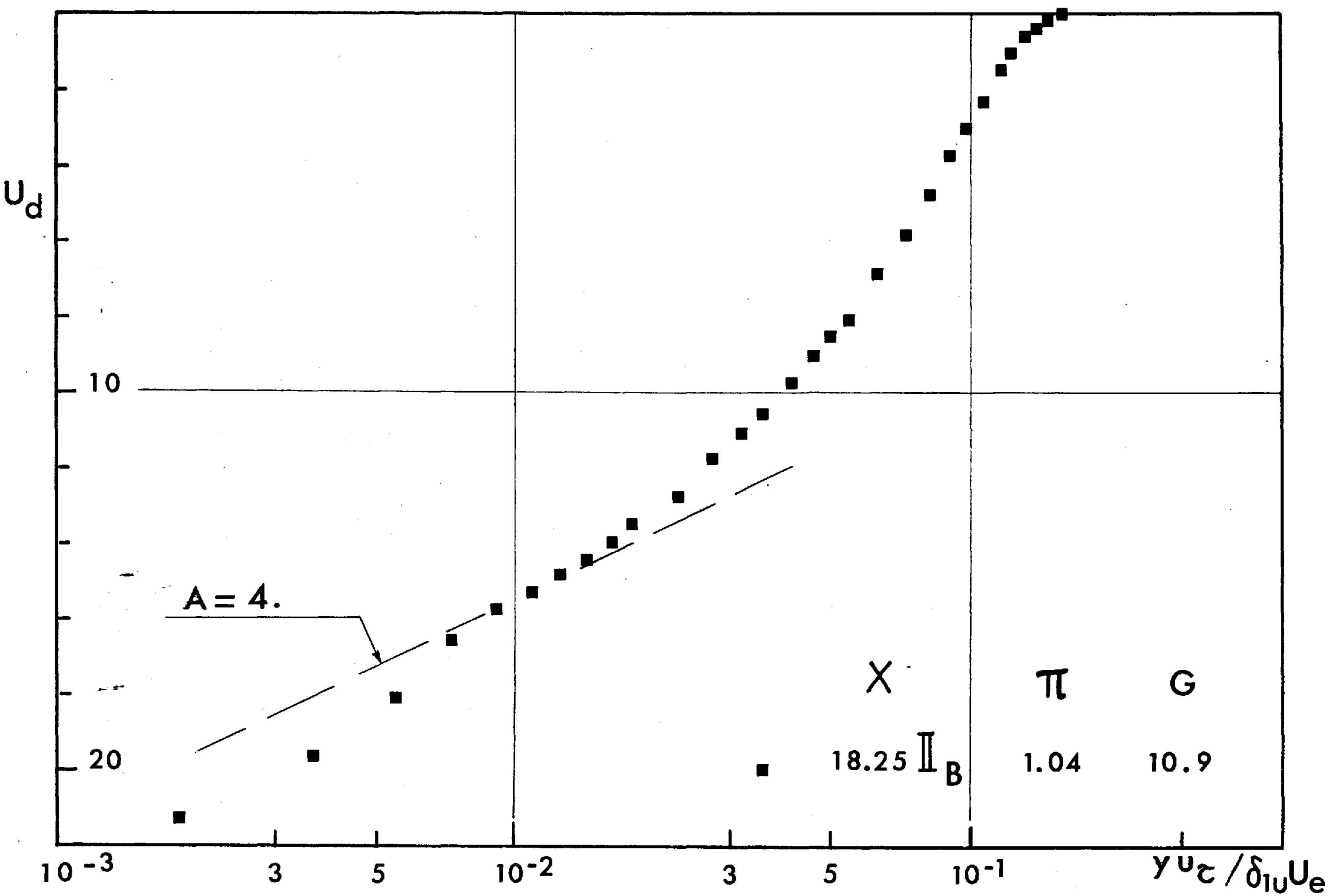

Fig. III. 2. 31_ Velocity - defect profile .

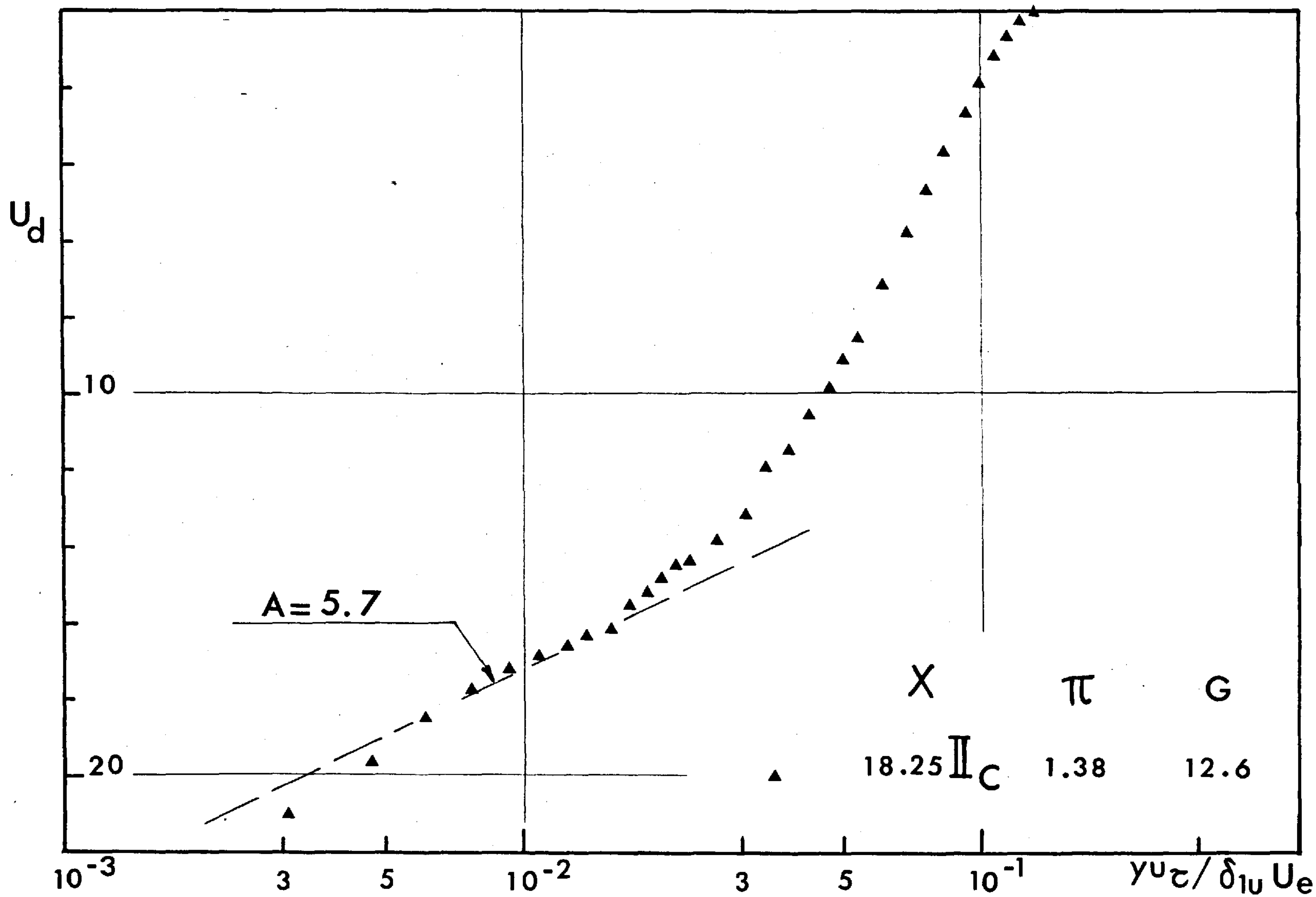

Fig. III. 2.32 _ Velocity - defect profile .

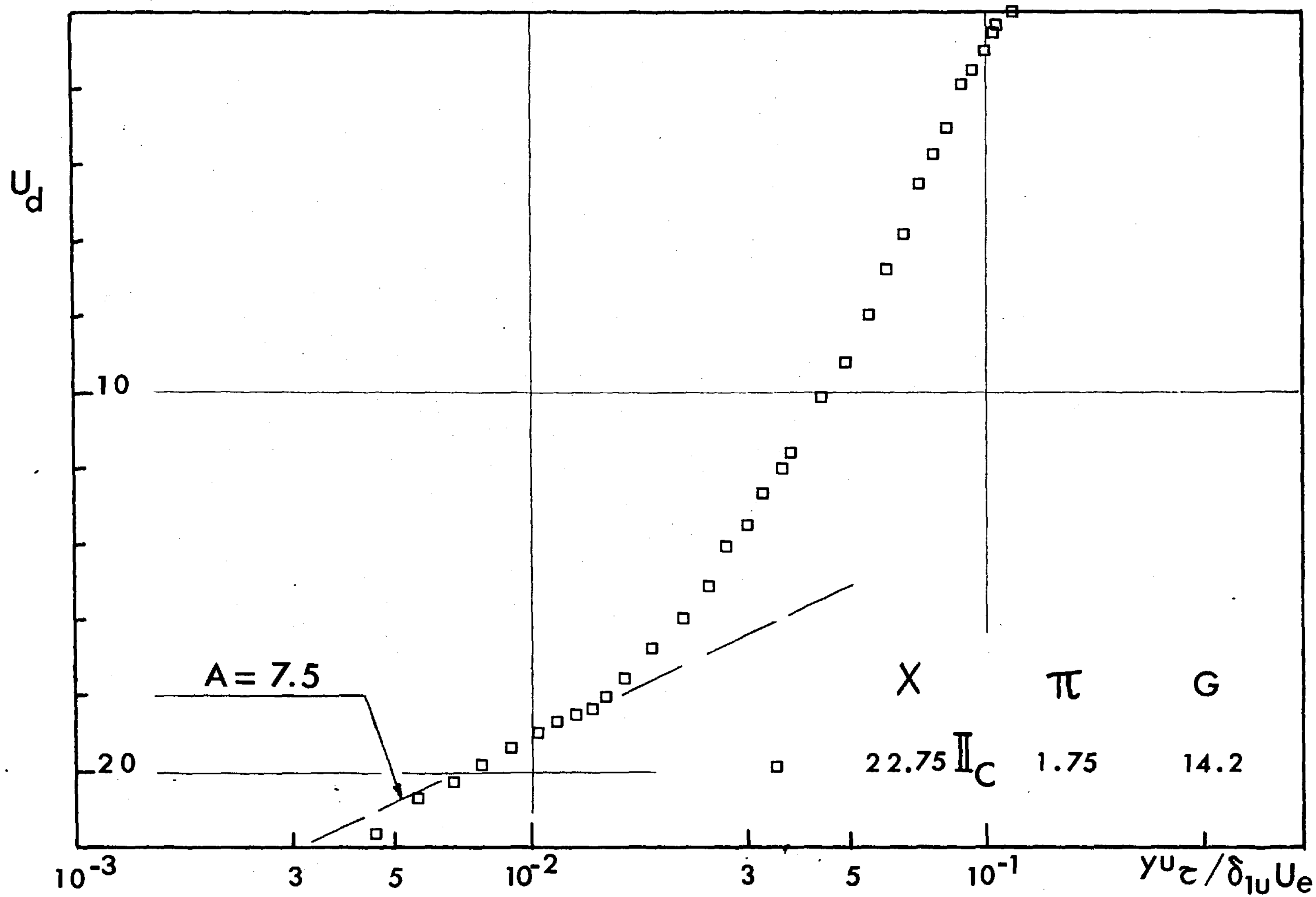

Fig. III.2.33 _ Velocity - defect profile .

III.2.7 – <u>The relation between the velocity profile defect parameter 'G', and the pressure gradient parameter 'Π':</u>

Fig. III.2.23 to III.2.39 show the measured values of G, Π, H and H_u plotted against x*, for the profiles examined.

Further, Fig. III.2.41 show $G(\Pi)$ for the three cases of constant-favourable pressure gradient, and III.2.42 show this relation for the cases of adverse pressure gradient. On Fig. III.2.43, these relations are compared to that of the smooth surface, as given by Nash (27).

In I_A, the value of G continued to rise without noticeable change in Π, until Π was sharply reduced and G followed.

For both I_B and I_C, where the plate was heated, a slight tendency towards equilibrium was exhibited.

In II_A, the values of G were generally higher than those generally quoted for smooth surfaces. As Π is reduced, the value of G decreases, although it departs from the original 'path' towards the end of the plate.

The relation for II_B still follows that of II_A, and shows a 'return' very close to the relation with Π-increasing

* x being the distance measured from the beginning of roughness.

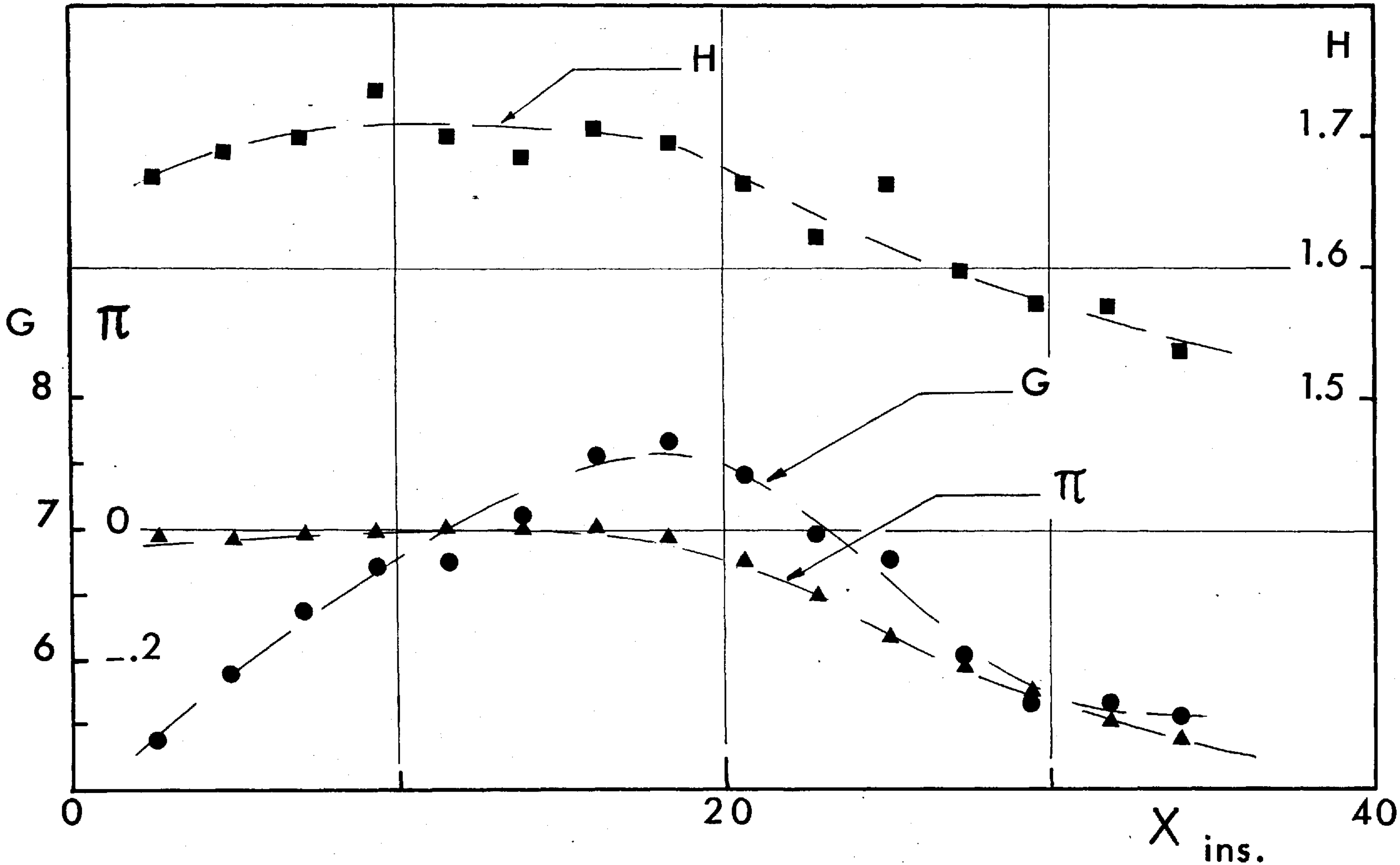

Fig. III. 2.34 _ Variation of G, π and H along X _ Case I_A.

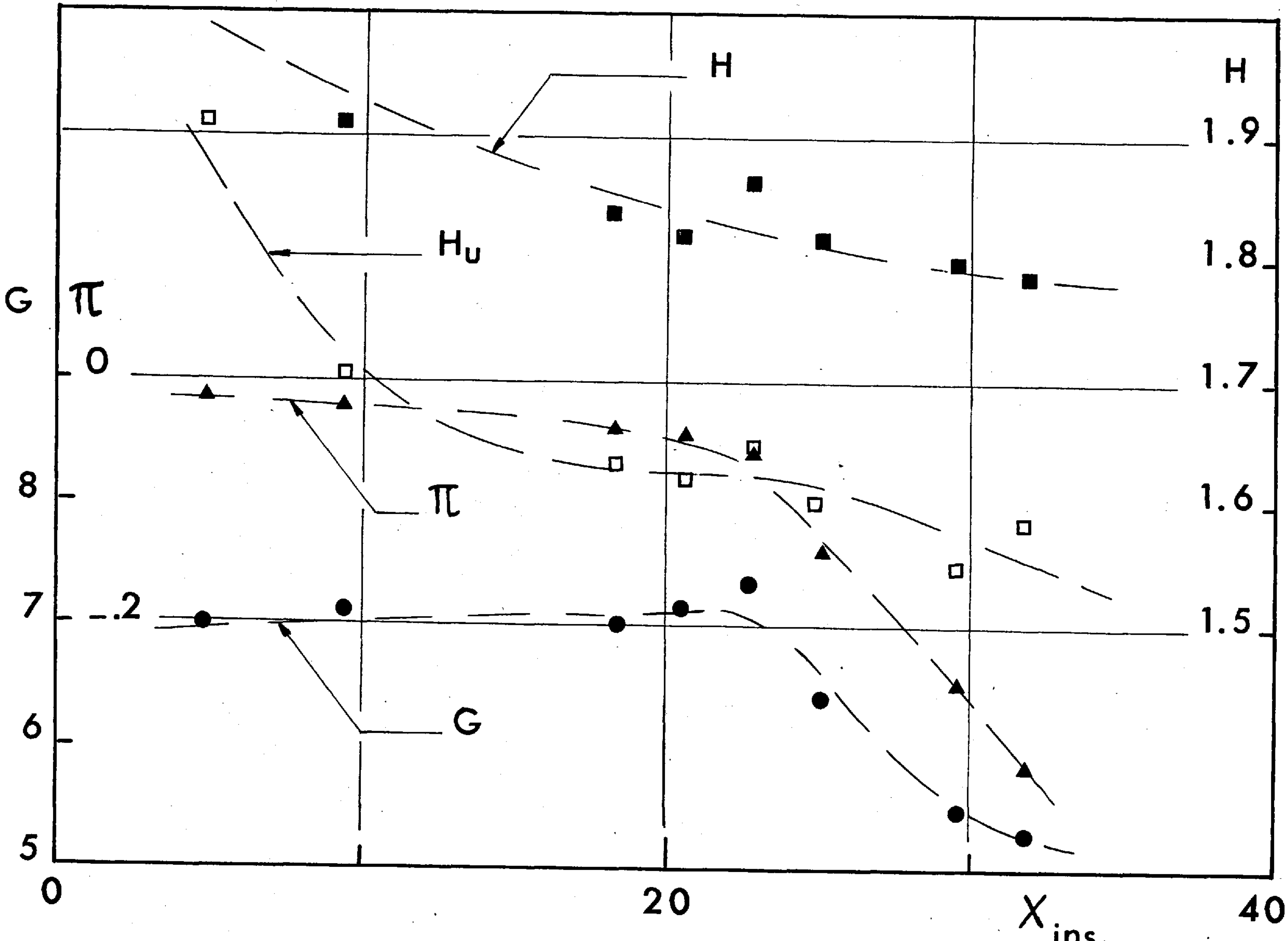

Fig. III. 2.35 _ Variation of G , π, H and H_u along X _ Case I_B .

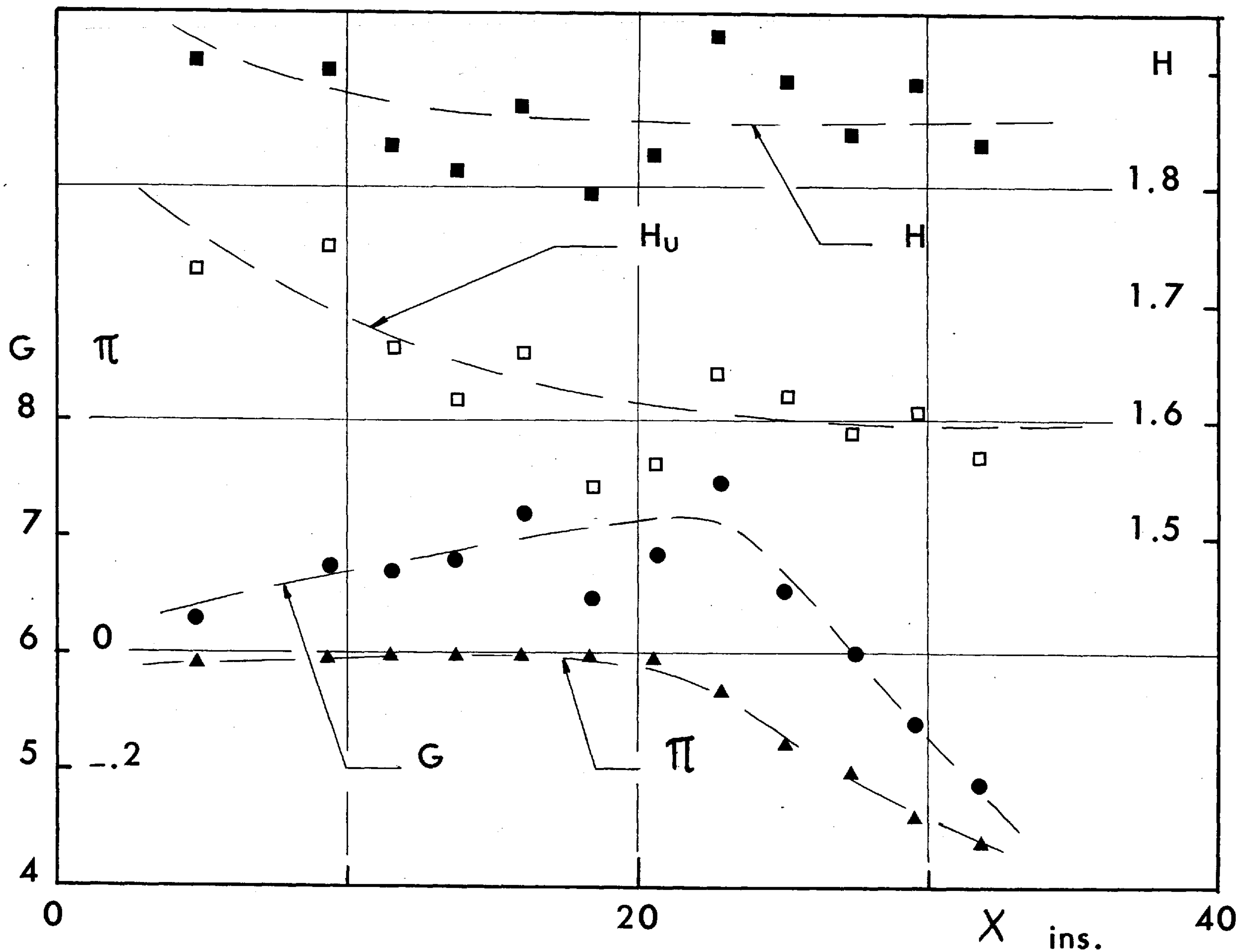

Fig. III. 2. 36 _ Variation of G, Π, H and H_u along X _ Case I_C .

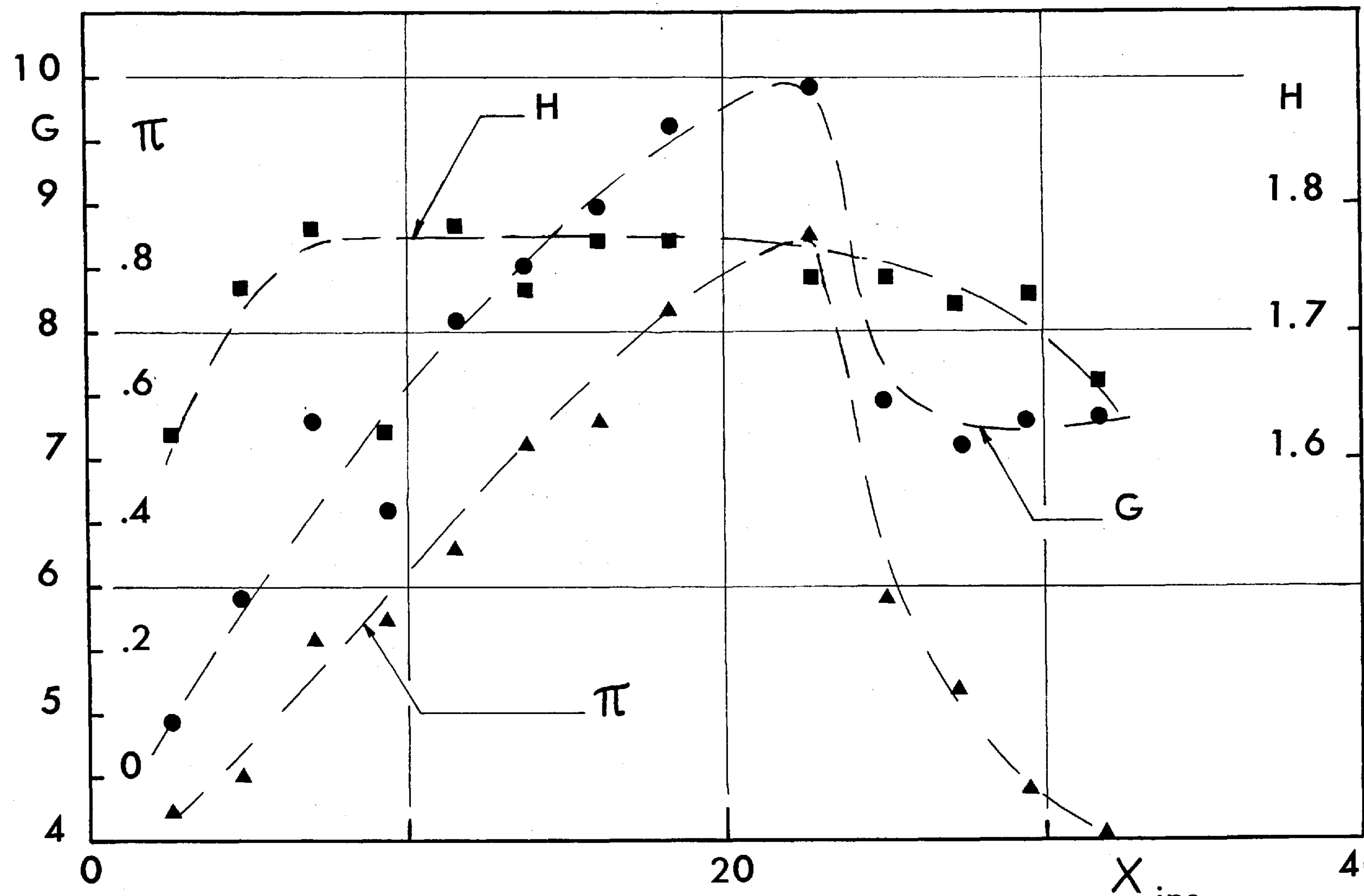

Fig. III.2.37 – Variation of G, Π and H along X – Case II_A.

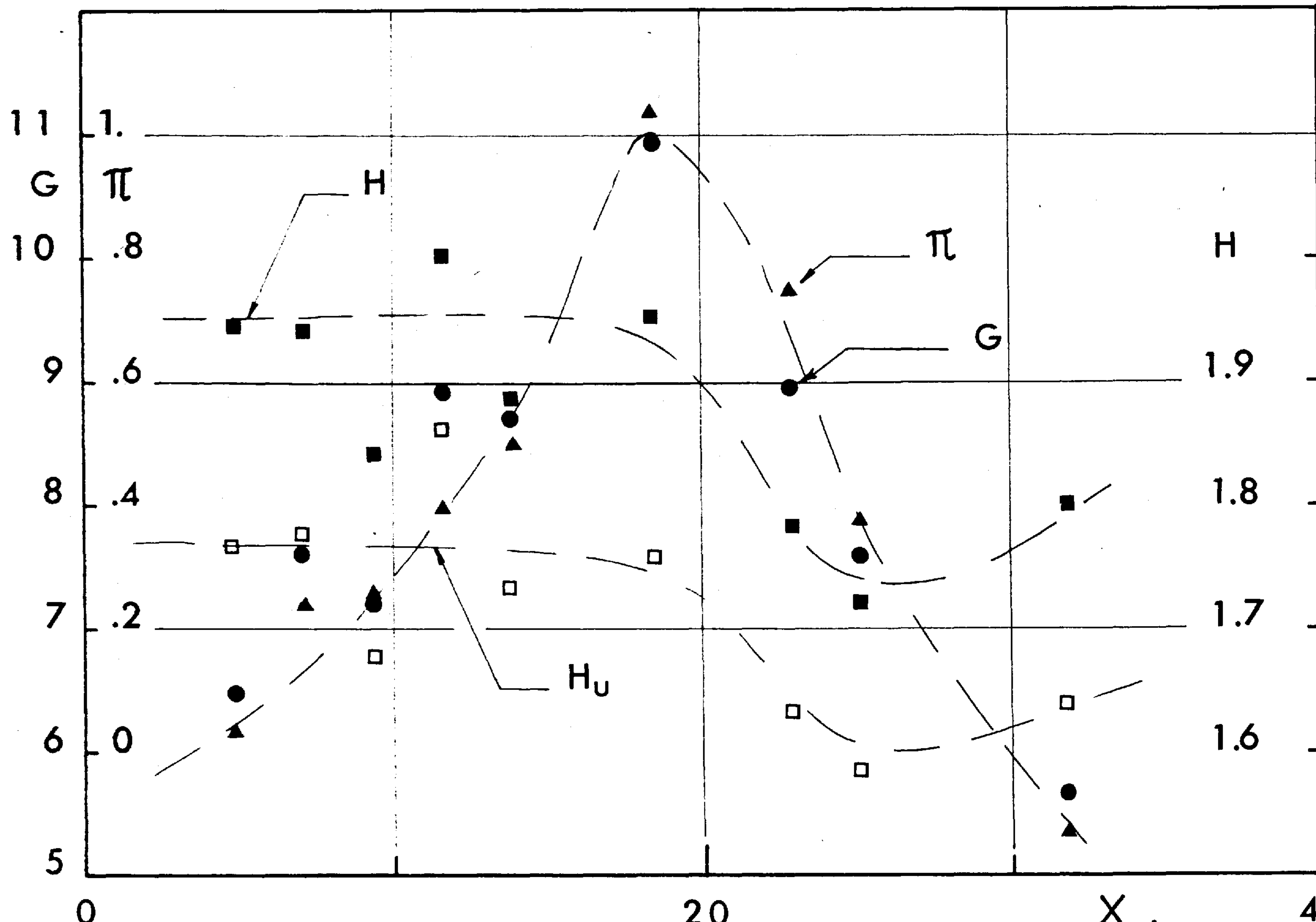

Fig. III.2.38 _ Variation of G, Π, H and H_u along X _ Case II_B.

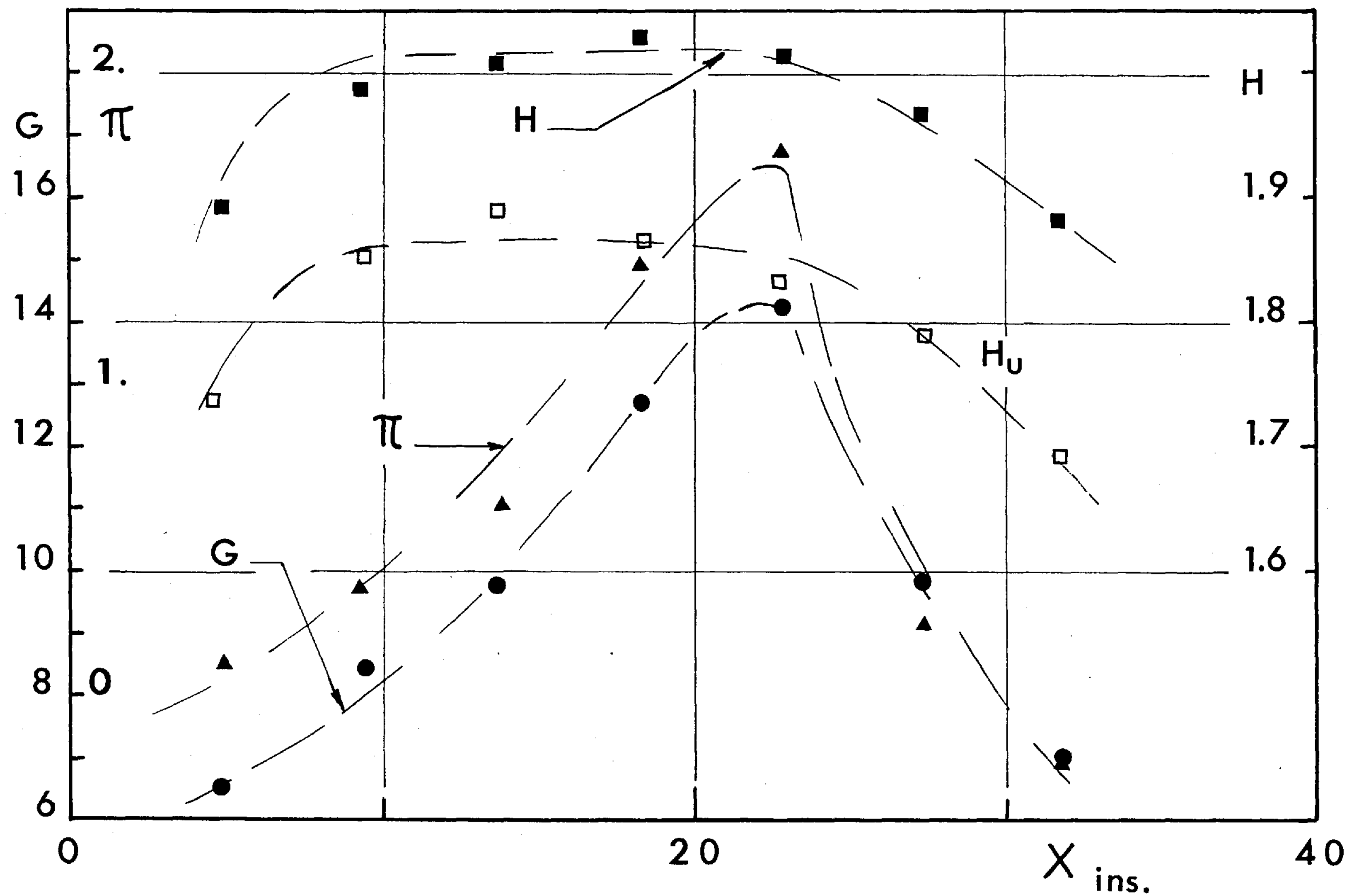

Fig. III.2.39 _ Variation of G, π, H and H_u along X _ Case II_C.

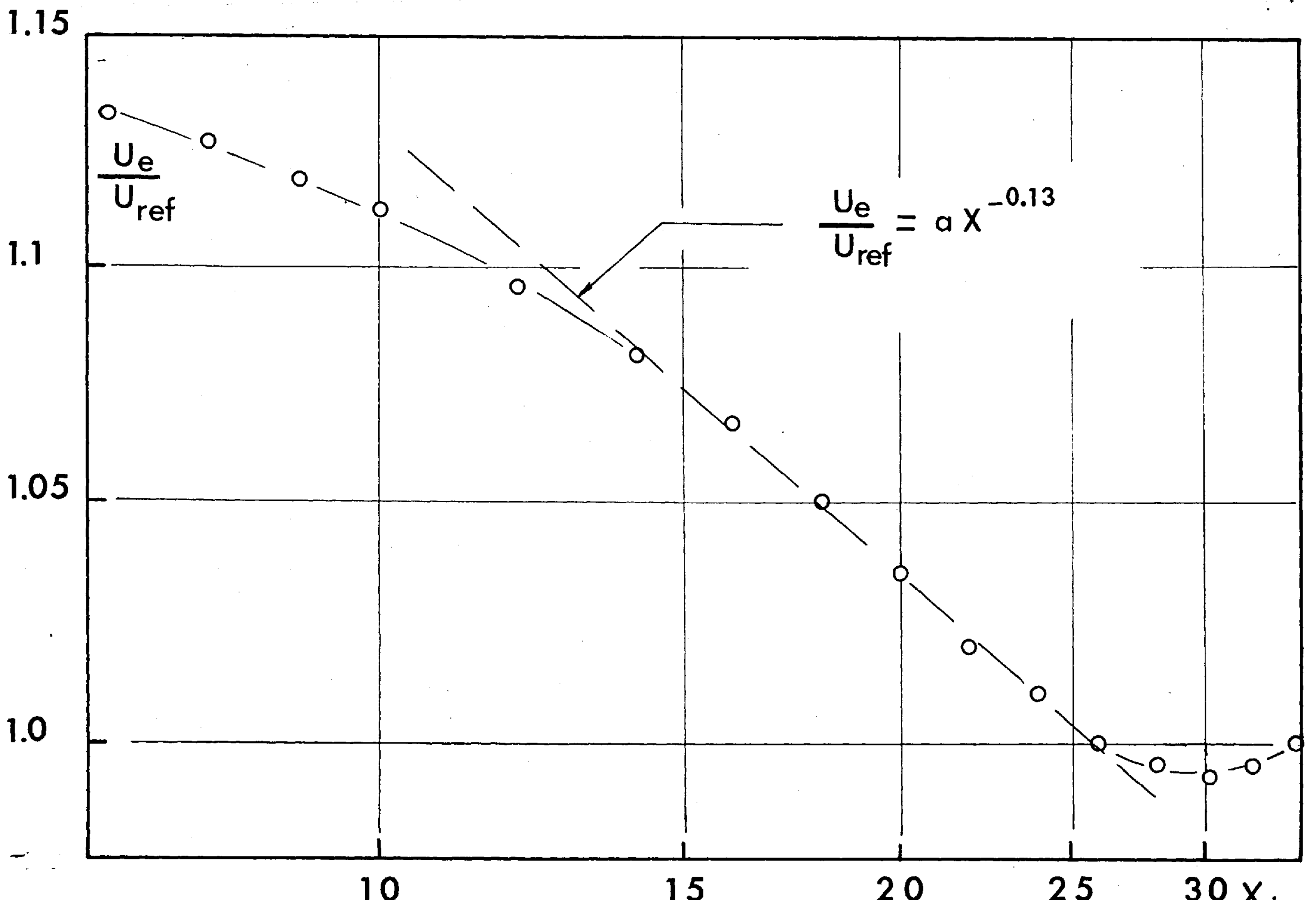

Fig. III. 2.40 _ Variation of free stream velocity along X _Case II A

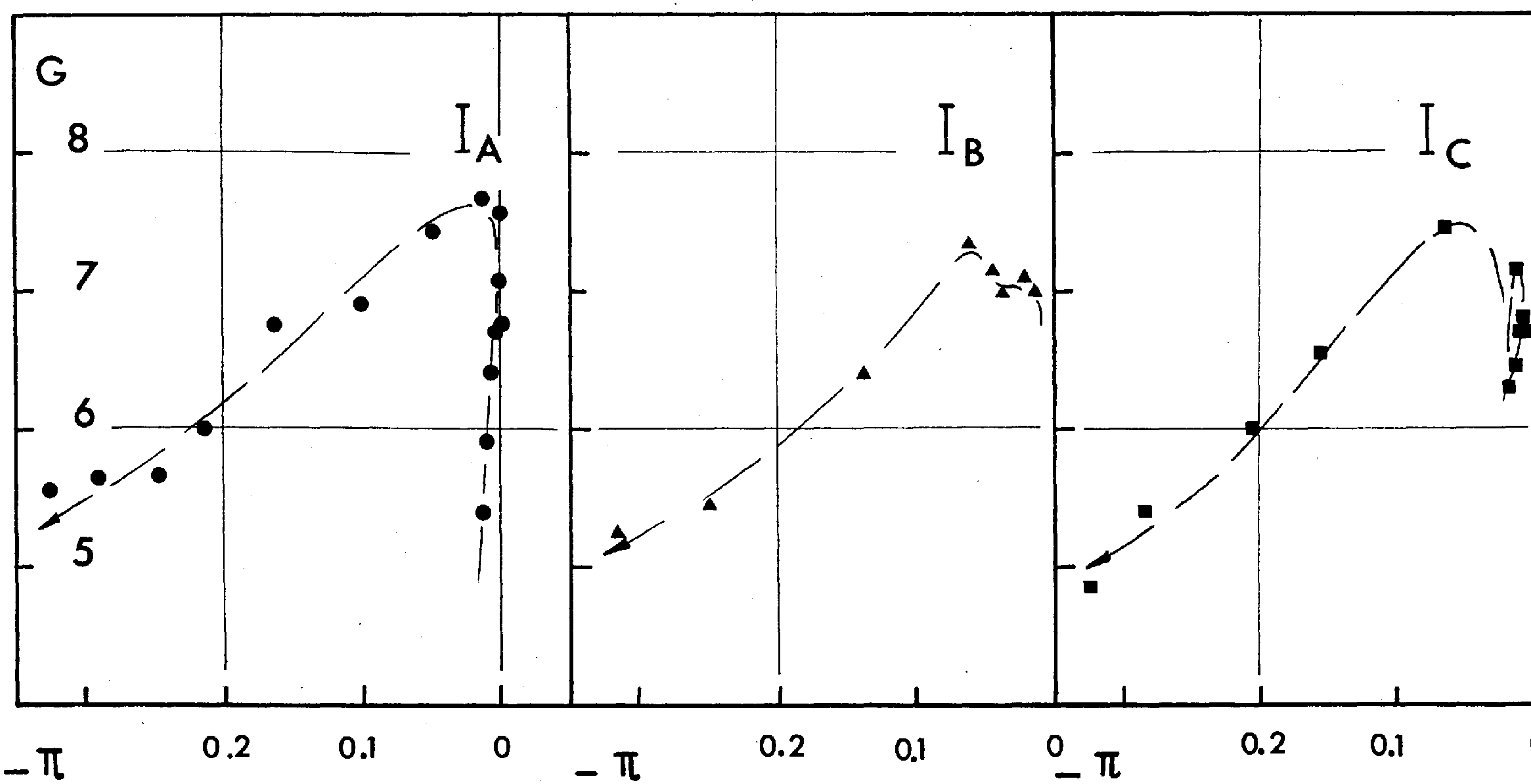

Fig. III.2.41 – $G(\pi)$ – Case I_A, I_B and I_C .

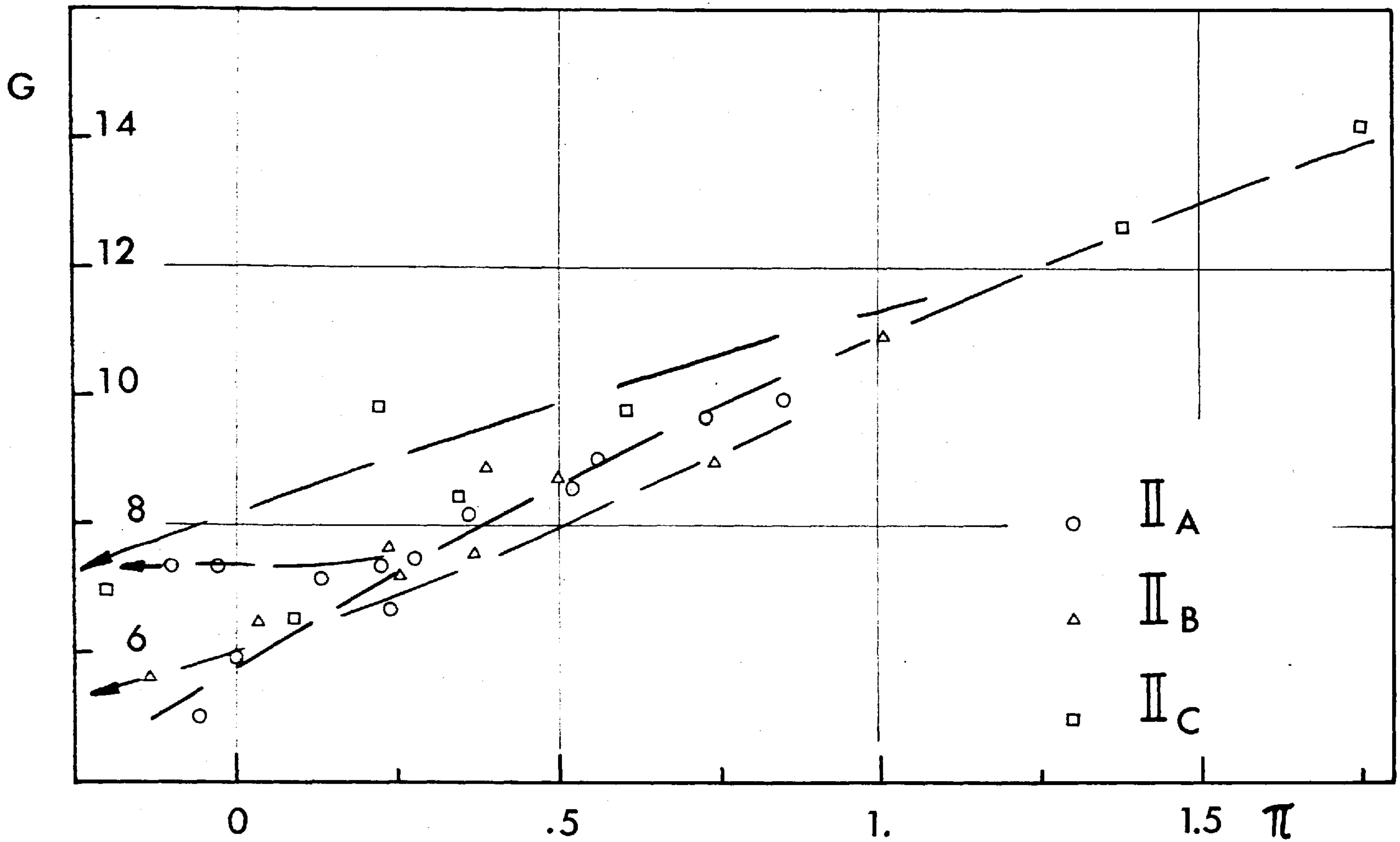

Fig. III. 2.42 _ G(π) _ Case II_A, II_B and II_C .

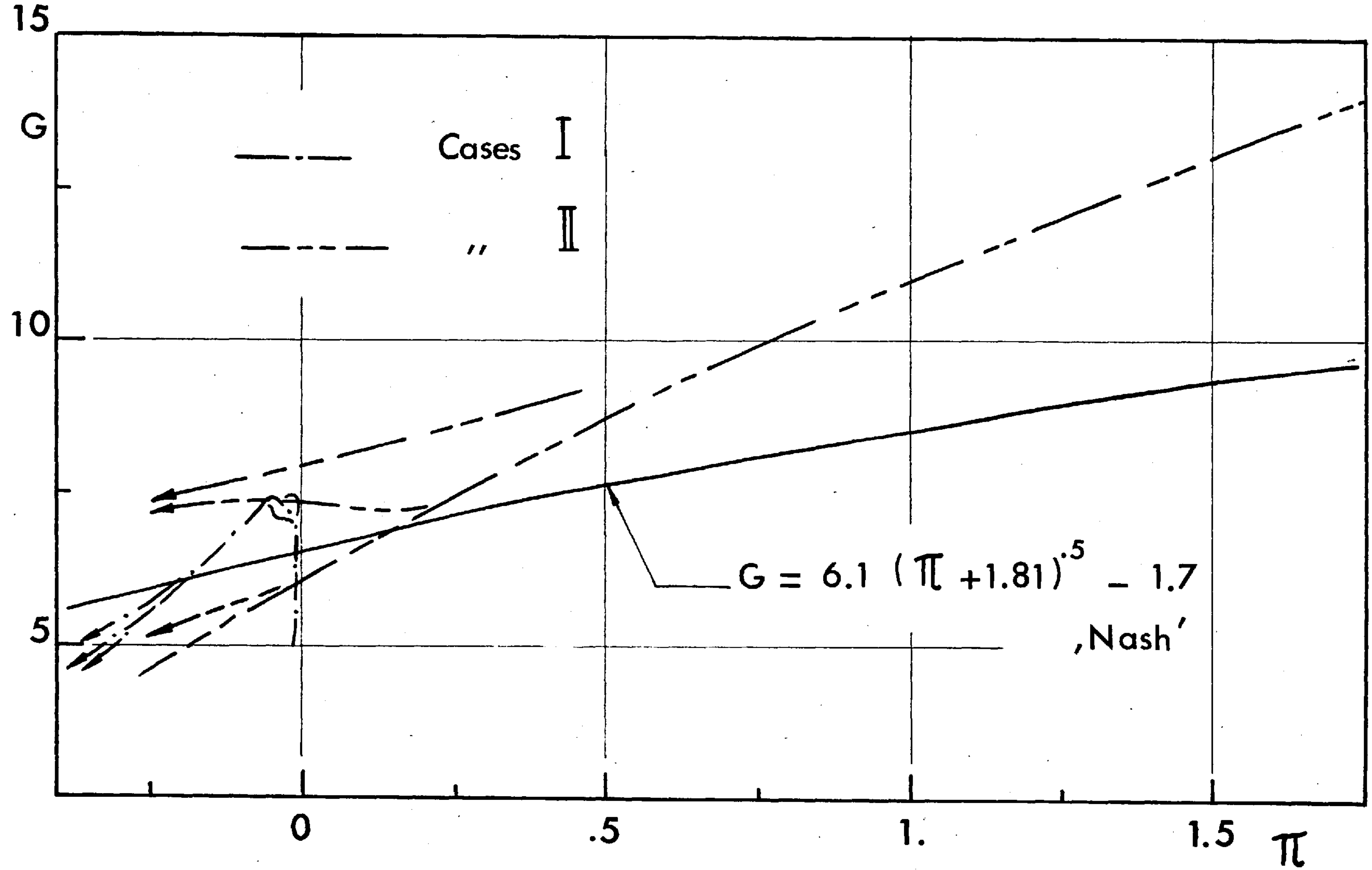

Fig. III.2.43 _ Comparison between obtained results and G(Π) for smooth surfaces.

As for II_C, complete agreement with II_A and II_B is observed, and then continues smoothly for further values of Π. It then reaches the highest values of Π. As Π is reduced, G also decreases as before.

In II_A, II_B, and II_C, the value of G did not continue to rise as the pressure gradient was decreasing in severity. This did not occur in the experiments of Ludwieg and Tillmann reported in (20) and (27).

It appears that the experiments of boundary layer on a smooth surface, passing from the condition $U_e \propto x^{-0.255}$ to $U_e \simeq$ Constant reported in (36), show a similar behaviour to the present results.

The higher values of G found in the present experiments, unlike those for a smooth surface under similar conditions, may be referred to the higher values of H_u for a rough surface. This was already shown in (27). The difference between the values of G for a smooth surface and those for a rough surface become more pronounced when C_f is reduced due to surface heating. This occurred in the present experiments for $\Pi \geqslant 1$.

Further in II_A, adverse pressure gradients with no surface heating, the conditions for equilibrium boundary layers:

$$\frac{d\delta_1}{dx} \left(\text{or } \frac{d\delta_{1u}}{dx} \right) = \text{Constant} ,$$

$$U_e \propto x^{-0.13}$$

(see Fig. III.2.40),

were present for $14'' < x < 26''$, but equilibrium conditions were not achieved.

The lack of equilibrium in both I_A and II_A may be referred to the short length over which the necessary conditions were satisfied. Also the height of roughness was maintained constant in the present experiments, and not the form $k \propto (x - x_0)$ as suggested by Rotta (20).

More useful information about the behaviour of boundary layers on rough surfaces could be achieved by setting equilibrium conditions, and comparing the results with those readily available for smooth surfaces.

III.2.8 - Comparison with some theoretical investigations:

Perry and Joubert (5) have extended the method of computing the skin-friction coefficients adopted by Clauser (18) so as to be applicable for rough surfaces.

The method* consists of assuming that Coles' wake hypothesis is applicable, so that the whole profile could be

* A similar treatment appeared in (16).

described by,

$$\frac{U}{u_\tau} = \frac{1}{\kappa} \mathrm{Ln} \frac{y u_\tau}{\nu} + B - \frac{\Delta U}{u_\tau} + \frac{\pi}{\kappa} \omega(y/\delta) ,$$

ω being the universal wake function, and,

$\frac{\Delta U}{u_\tau}$ the shift of the log. law of the wall for a rough surface.

This could then lead to the relation,

$$\frac{U}{U_e} = \frac{1}{\kappa}\sqrt{\frac{C_f}{2}}\ \mathrm{Ln}\left(\frac{(y_t+\epsilon)\,U_e}{\nu}\right) + \sqrt{\frac{C_f}{2}}\left[\frac{1}{\kappa}\mathrm{Ln}\sqrt{\frac{C_f}{2}} + B - \frac{\Delta U}{u_\tau}\right] + \sqrt{\frac{C_f}{2}}\ \frac{\pi}{\kappa}\,\omega\left(\frac{y}{\delta}\right) .$$

where: y_t is the distance normal to the wall measured from the crest of roughness elements, and,

ϵ the origin correction distance.

According to this equation a set of straight lines representing $\frac{U}{U_e}$ against $\mathrm{Ln}(y_t+\epsilon)$ could be traced having the slopes $\frac{1}{\kappa}\sqrt{\frac{C_f}{2}}$. The experimental results are then plotted in the form $U/U_e(\mathrm{Ln}(y_t+\epsilon))$, and displaced vertically until they conveniently match a particular value of C_f, appropriate for the measured profile.

Unfortunately, this method has its limitations of requiring a fairly large region in conformity with the law of the wall. Hence, it had very limited use for the present work; the same was concluded by the authors(5). Otherwise, the method may retain its merits.

Further, the methods of calculation of the skin-friction coefficients from the formulae used for smooth surfaces clearly prove to be inadequate for the present experiments. This is due to the order of magnitude of the various integral terms and the shape factor H, or H_u, which is higher for a rough surface than for a smooth surface under the same conditions. This is a result of the effect of roughness imposed on the velocity profiles.

For instance, Rotta (20) introduced the formula,

$$\frac{U_e}{u_\tau}\left(R_{\delta_1}\right) = 5.75 \log R_{\delta_1} + 3.7 \quad ,$$

while other formulae, including one by Nash, could be found in (23).

As for the shape of the velocity profiles, Rotta (20) introduced the form,

$$U = \frac{u_\tau}{\kappa}\left(\mathrm{Ln}\,\frac{y u_\tau}{\nu} + 2A\,\frac{y}{\delta}\right) + C\left(\frac{k_r u_\tau}{\nu}\right) \;,$$

$$\text{for} \quad 0 < y < \delta \,,$$

while Coles expressed it, in the same range, as,

$$\frac{U_e - U}{u_\tau} = -\frac{1}{\kappa}\,\mathrm{Ln}\,\frac{y}{\delta} + \frac{B}{\kappa}\left(2 - \omega\left(\frac{y}{\delta}\right)\right) \quad .$$

Rotta then derived analytically the value of the constant of integration 'A' defined by,

$$\frac{U_e - U}{u_\tau} = -5.75 \log \frac{y u_\tau}{\delta_{1u} U_e} + A \;,$$

according to both profiles, and expressed it as function of G.

The values of 'A', determined experimentally in the present work, were found to agree closely with Rotta's relations; or at least that according to Coles' profile. This is shown on Fig.III.2.44.

Mellor (22) on the other hand, introduced a generalized velocity profile, on the basis of an eddy viscosity. It took the form,

$$U = \lim_{\epsilon \to 0}\left[\int_\epsilon \frac{\nu\,\psi(x)}{K^2 y^2}\,dy - \frac{u_\tau}{K}\,\mathrm{Ln}\,\frac{\epsilon\, u_\tau}{\nu}\right] + \frac{2}{K}\left[(u_\tau^2 + P_1 y)^{1/2} - u_\tau\right]$$

$$+ \frac{u_\tau}{K}\,\mathrm{Ln}\left[\frac{4\left[u_\tau^3 (u_\tau^2 + P_1 y)^{1/2} - u_\tau\right]}{\nu P_1 (u_\tau^2 + P_1 y)^{1/2} + u_\tau}\right] ,$$

where, $\psi(x) = \frac{K^2 y^2}{\nu}\frac{\partial U}{\partial y} - \left(\frac{\tau}{\rho}\right)^{1/2}\frac{K y}{\nu}$, and ,
$P_1 = (dP/dx)/\rho$.

Two separate expressions were then derived, the applicability of either being dependent on the value of α $(\equiv \pi U_e / R_{\delta_1} u_\tau)$.

Mellor then related the constant of integration 'A' to π , in the inexplicit form A + B(α). Here B(α) is the constant appearing in the logarithmic law of the wall. It was calculated to be equal to 4.92, 4.9 and 4.94 corresponding to α equal to -0.01, 0 and 0.02 respectively.

Mellor also derived a generalized skin-friction relations in the form,

$$\frac{u_\tau}{U_e} \equiv \frac{u_\tau}{U_e}\left(\pi , R_{\delta_1}\right) .$$

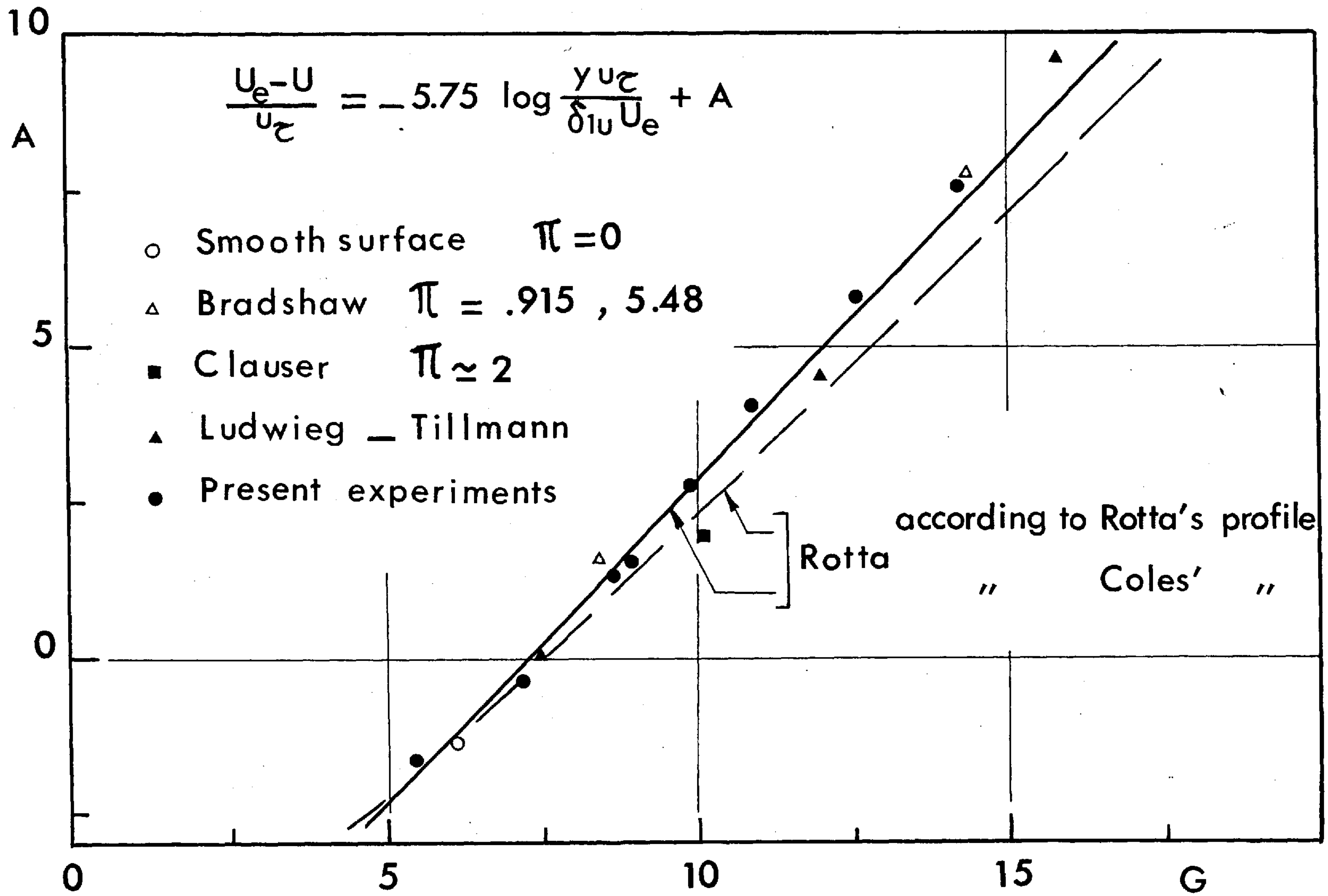

Fig. III. 2.44_ Constant appearing in the expression for the velocity-defect profile as function of G .

The values of 'A' obtained are compared with Mellor's on Fig.III.2.45. It is then evident that good agreement for the range $-0.3 \leq \Pi < 0.8$ exists, while a marked departure from Mellor's predictions occurs for $\Pi \geqslant 0.8$.

As the parameter α in the present experiments was $\leq 3.3 \times 10^{-3}$, it was thought suitable to assume that $B(\alpha)$ may be taken as 4.9 for all the profiles tested. Further, the limited region of linearity parallel to the law of the wall, found for some of the examined profiles as discussed earlier, may be considered unusual for such values of α according to Mellor's analysis for smooth surfaces. For a rough surface this is not necessarily so, considering the differences in $\frac{u_\tau}{U_e}$ or R_{δ_1}, for the two surfaces.

However, to illustrate this difference, Fig.III.2.46, shows a comparison between the obtained results of u_τ/U_e and those of a smooth surface, as given by Mellor, for a value of R_{δ_1} an order of magnitude smaller, almost everywhere.

The value chosen for $B(\alpha)$ does not seem to be the answer for the descripancy presently found with 'A' on Fig. III.2.45. Mellor noted that $B(\alpha)$ is closely related to the behaviour of τ/τ_w outside the viscous

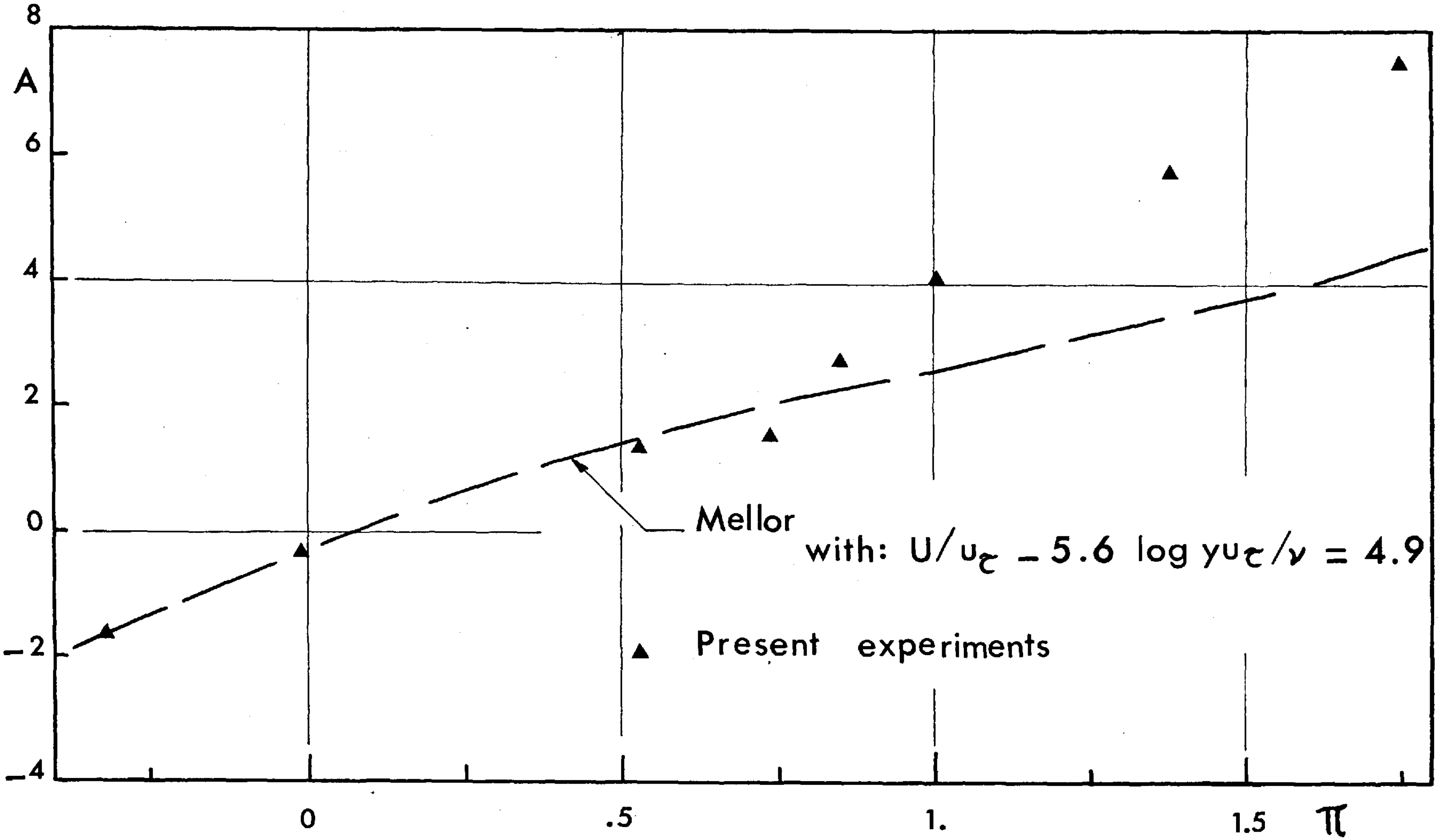

Fig. III.2.45 – Constant appearing in the expression for the velocity-defect profile as function of Π .

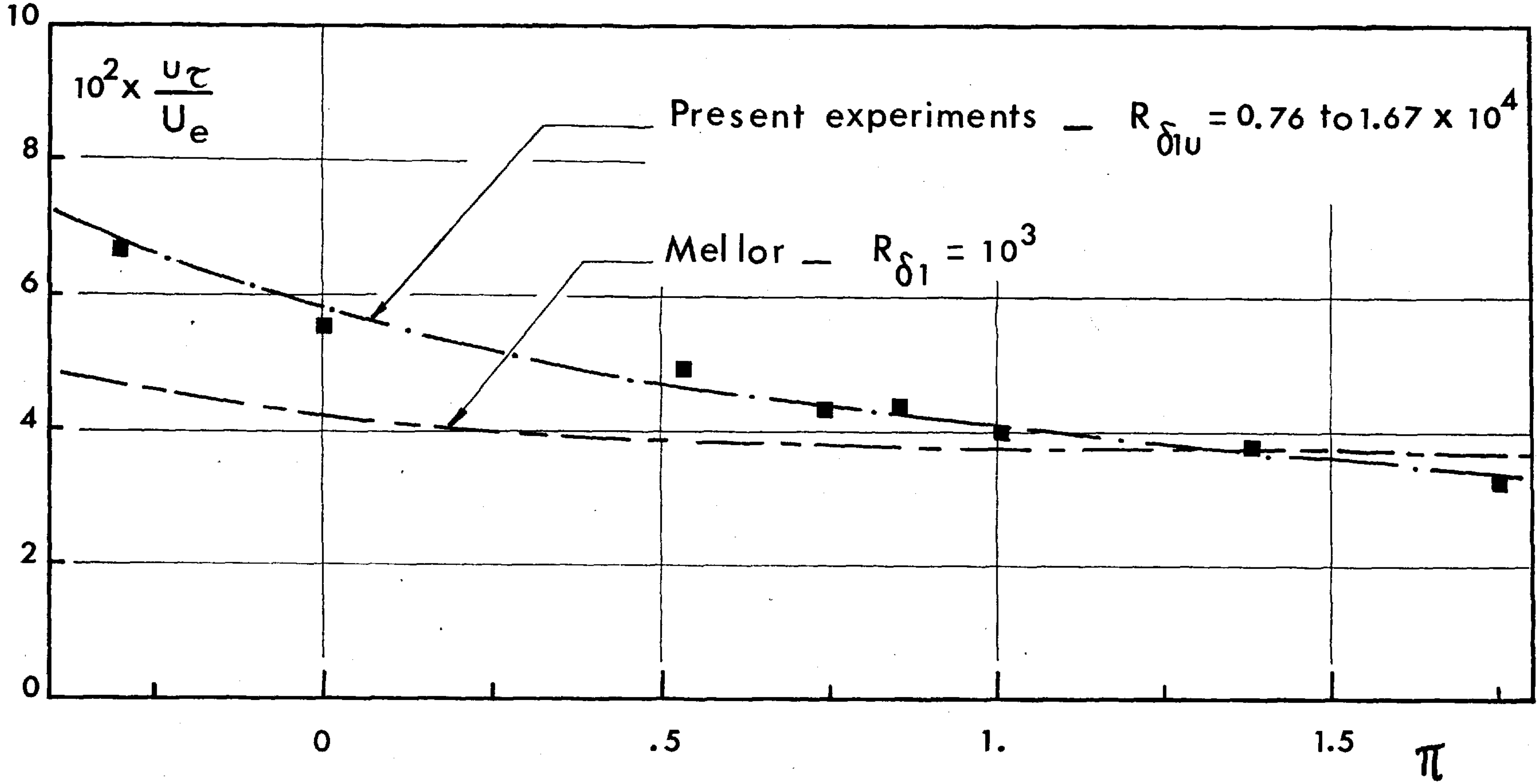

Fig. III.2.46_ Comparison between skin-frictions in the present experiments and those for smooth surfaces .

sublayer. This would differ from 4.9, for $\alpha = 0$, if τ/τ_w does not approach unity in that region. However, in the limited range of the obtained measurements, a rough surface behaves very much like a smooth one, when τ/τ_w is concerned, outside the sublayer. This will appear later on.

The conclusion can be made that if we accept the fact of relating A to G $\left(\equiv G\left(H_u , \frac{U_e}{u_\tau} \right) \right)$ as suggested by Rotta, and not to π as proposed by Mellor, the applicability becomes more general. That is because the relation G(π) varies according to the values of Hu and u_τ/U_e dealt with from one case to another. To relate A directly to G also appears more appropriate, considering the definition of G itself. This conclusion is confirmed by the fact that whenever G (π) of the present experiments agreed with that of the smooth surface, or was not too far from it, both Rotta's and Mellor's predictions were close to the experimental results. Only those of Rotta were applicable when the two relations of G (π) departed significantly.

III.3 - Thermal Boundary Layers:

In this section, the thermal boundary layer and heat-transfer coefficients will be discussed, as the velocity profiles and skin-frictions have been previously dealt with.

III.3.1 - Temperature profiles behind roughness elements:

The heat-transfer behaviour near a rough wall has been modelled by Owen and Thomson (24), who analized the flow pattern on the basis of existence of a horseshoe (secondary flow) eddies surrounding the roughness elements. Doenecke (4) sketched a model of the temperature profile behind a roughness element similar to that shown on Fig. III. 3.1. Unlike the velocity, the temperature profiles start at the solid surface, whether it is the crest of the roughness element or its trough. The shape of the temperature profile measured from the crest of a roughness element might not differ too much from that measured on a smooth surface, did not that the temperature change much more rapidly in the close vicinity of a rough surface than in that of the smooth. The profile behind a roughness element is suggested to have the following regions;

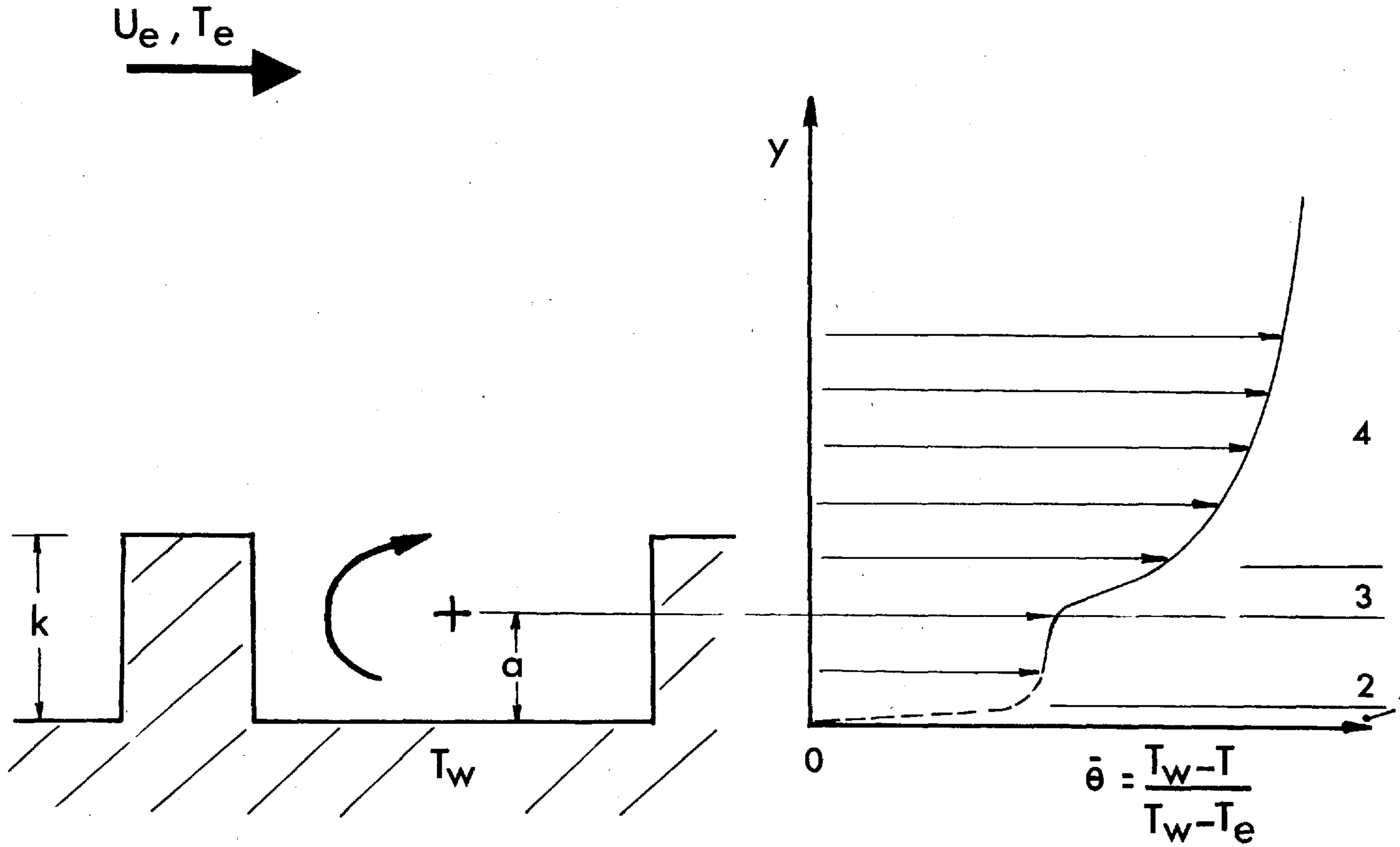

Fig. III.3.1 _ Temperature profiles behind roughness elements.

1. - a region close to the surface, in which the temperature varies rapidly in a fairly thin layer in a manner most likely to be linear, and depending wholly on surface temperature and fluid properties,

2. - a region which forms part of the eddy behind the roughness element, supplied by heat from the former region and dissipates it to the outside flow,

3. - a region which almost coincides in space with the viscous sub-layer of the velocity profile, where the temperature varies according to the local wall temperature, its gradient w.r.t. x and the present velocity field, and,

4. - a region outside the influence of the wall and completely definied by the velocity field and the fluid properties.

The whole temperature profile behind the roughness elements is not altogether feasible with reliable accuracy, without disturbing the delicate structure of the flow; at least for the type and dimensions of the presently studied roughness. The part actually measured was that consisting of the last two regions only, which starts at, or very close to, the origin of the velocity profile.

The origin of the measured profiles was then taken as tha of the velocity profile. This was determined from the measurements of the velocity as described in § III.2.1 earlier on.

The measured profiles are tabulated in Appendix II with their respective velocity profiles.

III.3.2. - Thermal boundary-layer thicknesses:

The boundary layer thermal displacement and enthalpy thicknesses Δ_1 and Δ_2 were calculated simultaneously with the dynamic thickness by the computer, using the method of trapezoids as well.

The obtained values are shown on Fig. III.3.2 to III.3.5, and tabulated numerically in Appendix I.

III.3.3. - Heat-transfer coefficients:

The heat-transfer coefficients of rough surfaces are generally found to be more than those for smooth surfaces, in the same flow and wall temperature conditions.

Although the "rougher" a surface is, the more the value of heat-transfer coefficient is likely to be, it has been already established that the increase in heat transfer due to the presence of roughness is less than the

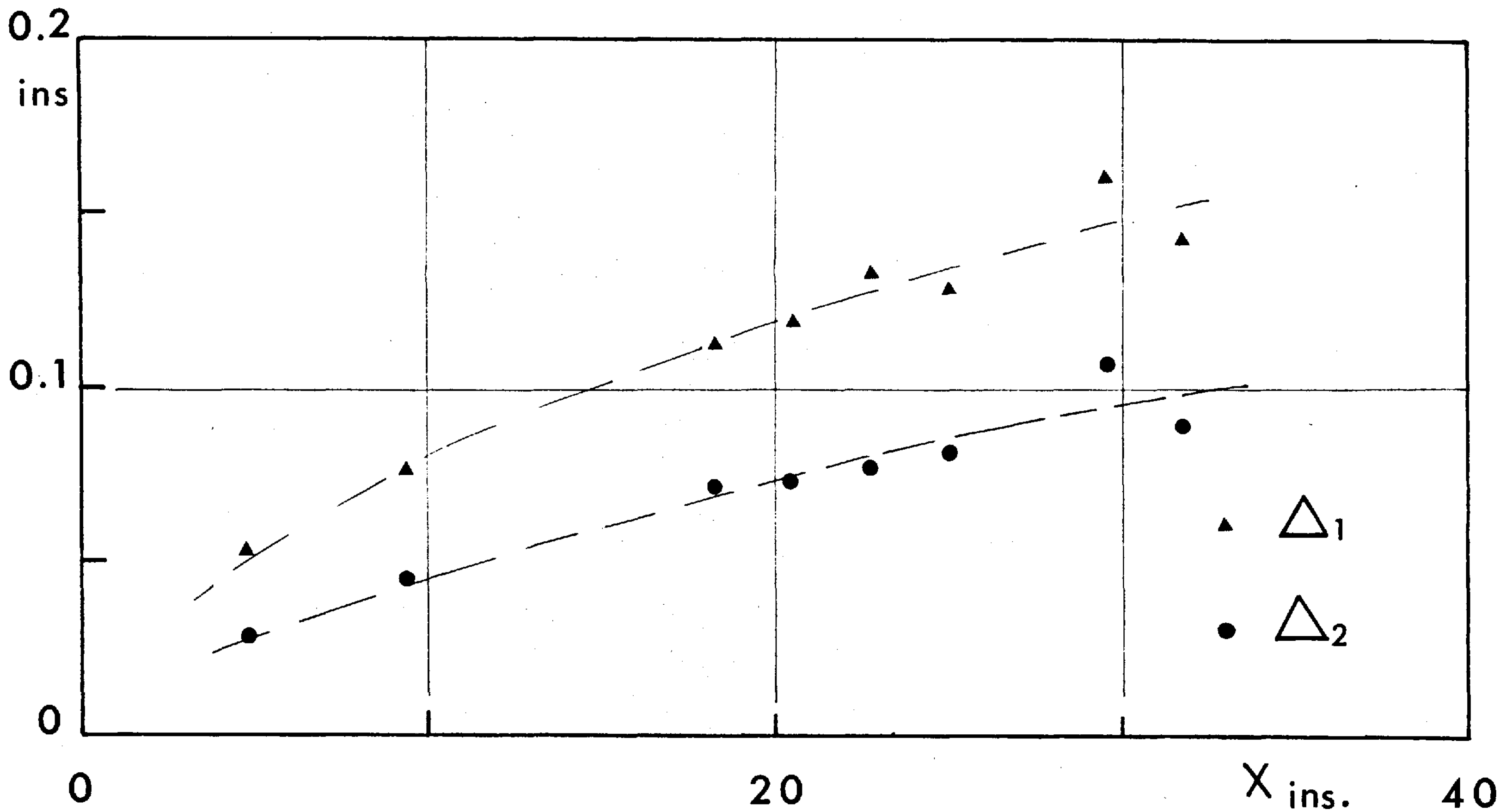

Fig. III.3.2 _ Thermal boundary layer thicknesses _ Case I_B .

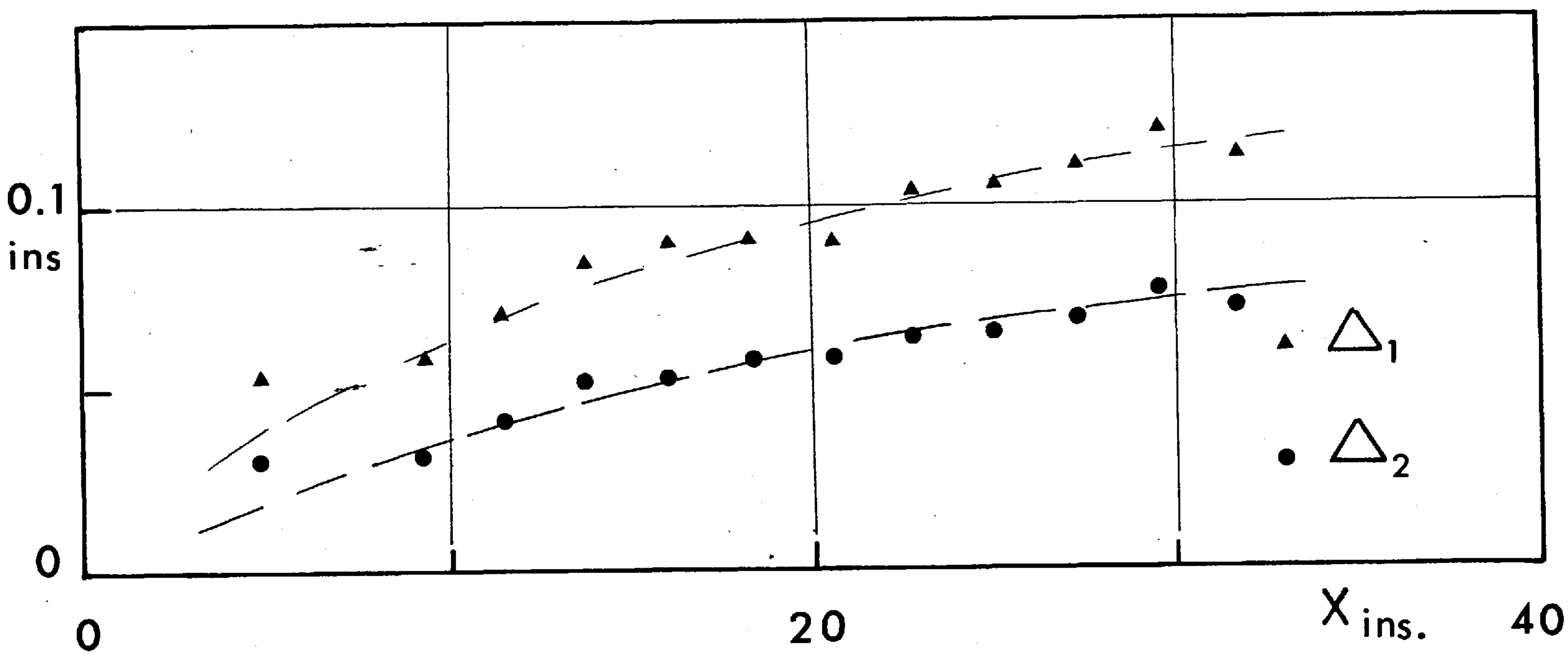

Fig. III.3.3 – Thermal boundary layer thicknesses – Case I_C .

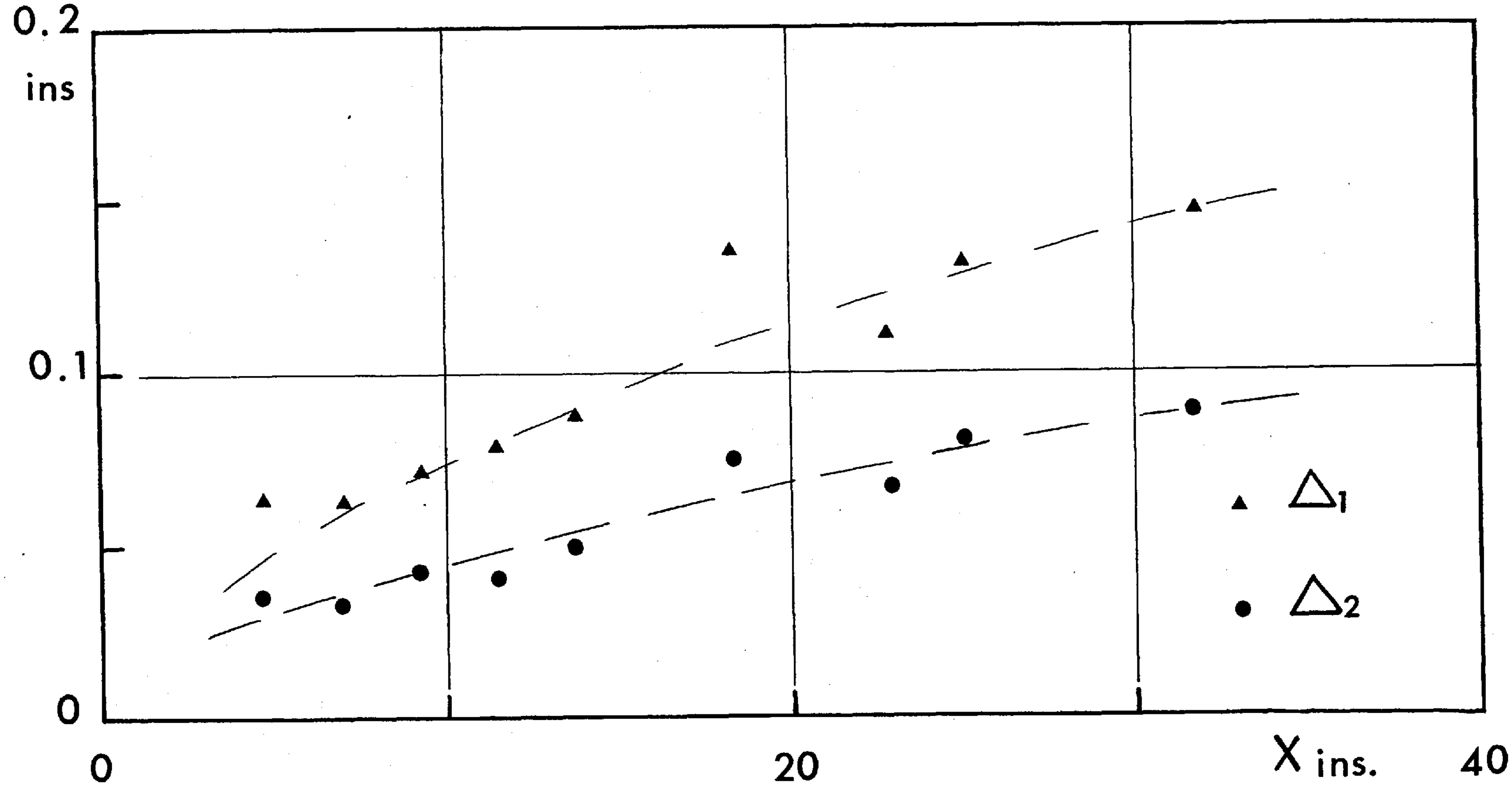

Fig. III.3.4 _ Thermal boundary layer thicknesses _ Case II_B .

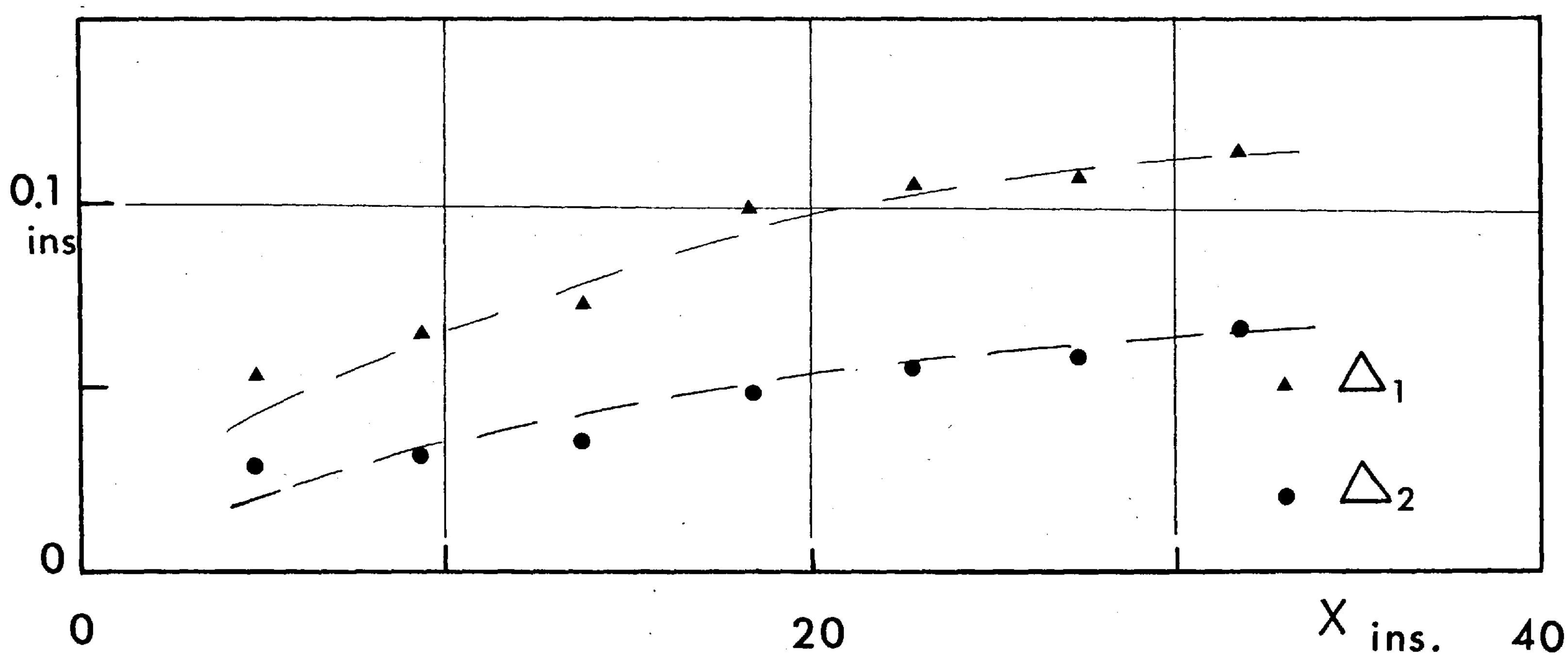

Fig. III.3.5 _ Thermal boundary layer thicknesses _ Case II_C .

increase in skin friction.

In the present experiments, the heat-transfer-coefficients were calculated from the values of the power input to the electric heaters, as described earlier in § II.5.

The calculated coefficients for isothermal heating are plotted on Fig.III.3.6 and III.3.8, together with the graphical differentiations of Δ_2. Good agreement between both results is seen, except near the downstream end of the plate, where the calculated coefficients seem to be higher than the values of $d\Delta_2/dx$.

This is perhaps due to inevitable heat conduction to the 2½ x 2½ in. steel angle supporting the rear end of the plate.

Where the plate temperature undergoes a stepwise variation, Fig. III.3.7 and III.3.9 show the heat-transfer coefficients as calculated by the measured power-input of the heaters, together with the graphical differentiations of Δ_2. This shows a large discrepancy between the two values, which can be reasoned as follows:

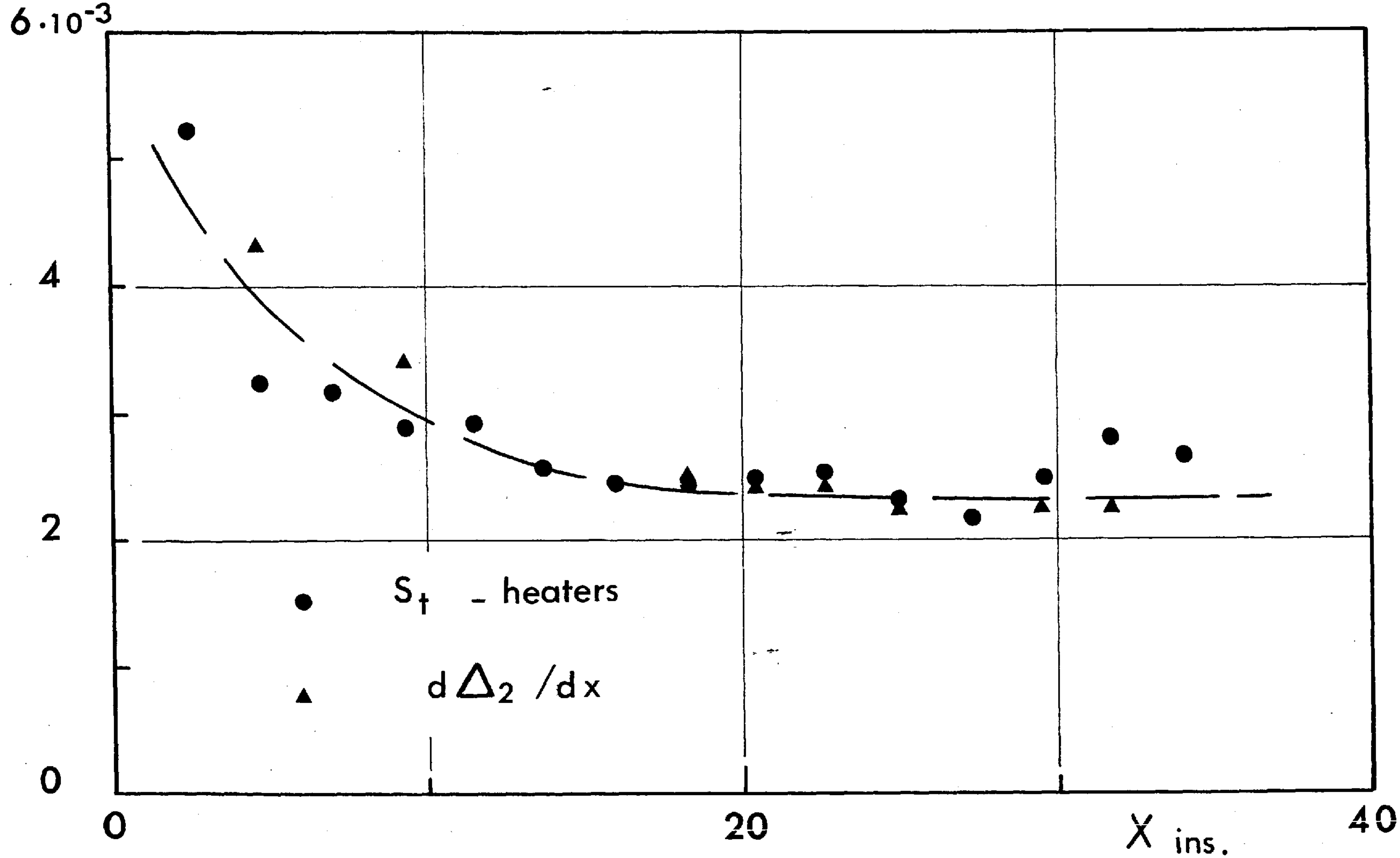

Fig. III.3.6 _ Heat transfer coefficients _ Case I_B .

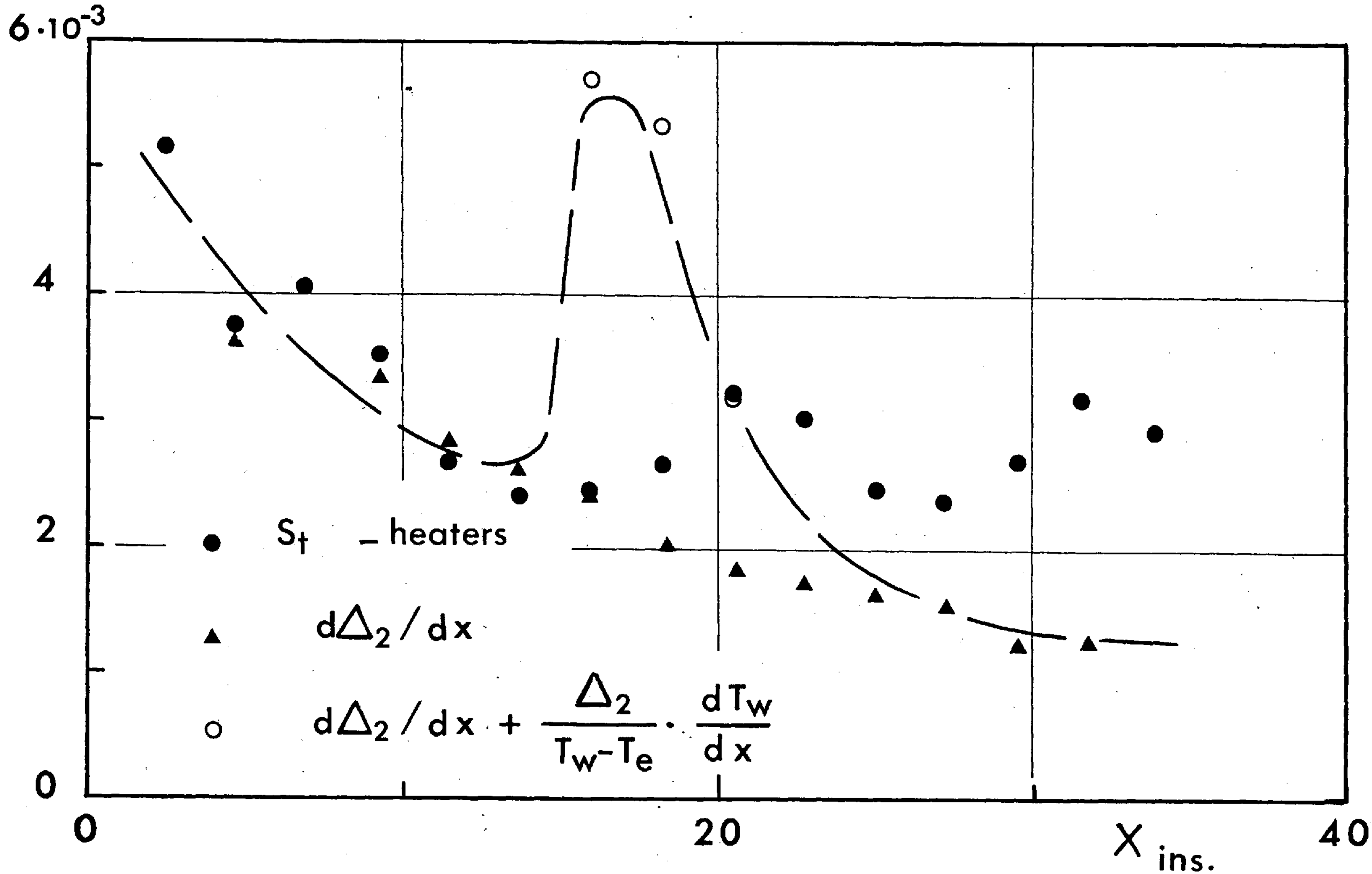

Fig. III.3.7 – Heat transfer coefficients – Case I_C .

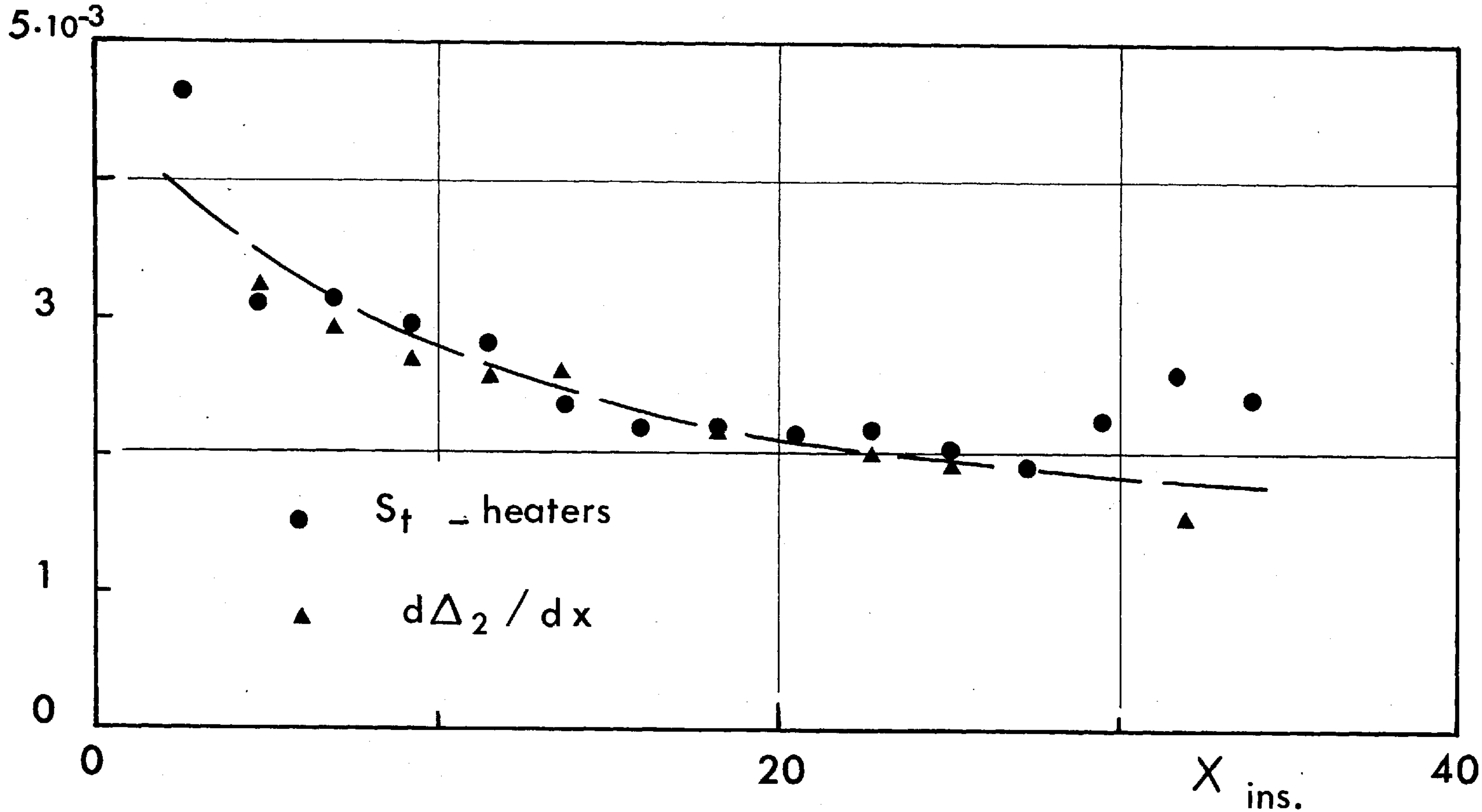

Fig. III.3.8 – Heat transfer coefficients – Case II_B .

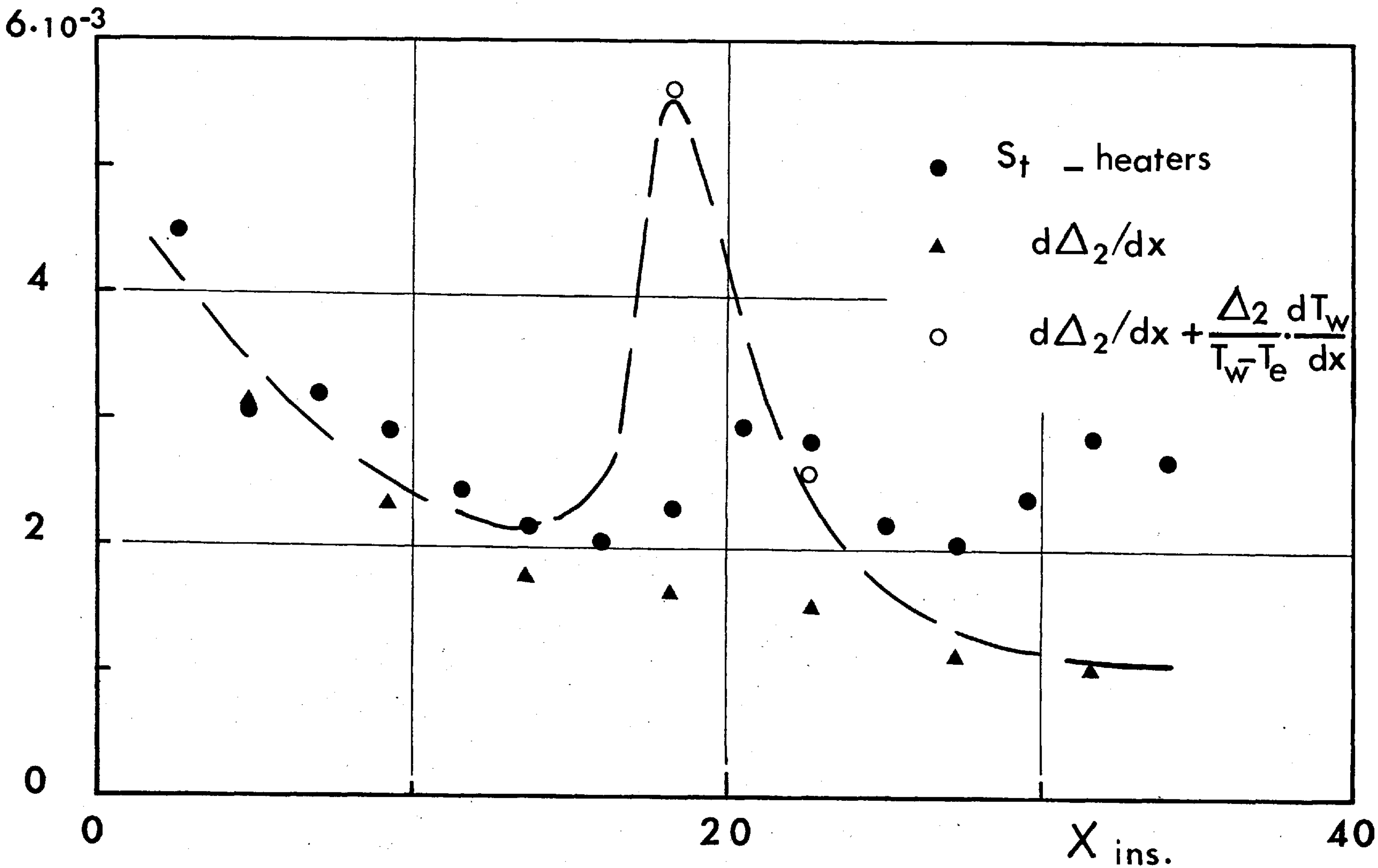

Fig. III.3.9 _ Heat transfer coefficients _ Case II_C .

1. - the heat-transfer coefficients for the flat plate can be generally written as *,

$$S_t \cong \frac{1}{\rho_e U_e c_p (T_w - T_e)} \left[c_p \frac{d}{dx} \rho_e U_e \Delta_2 (T_w - T_e) - \frac{1}{2} \frac{d}{dx} \rho_e U_e^3 \delta_3 \right] .$$

This equation then suggests that the mere term $d\Delta_2/dx$ will not always be representative of the heat-transfer coefficient, and in particular when the wall temperature gradient differs from zero. In the region where dT_w/dx differed from zero in Ic and IIc, the term $\frac{\Delta_2}{T_w - T_e} \cdot (dT_w/dx)$ was added to $d\Delta_2/dx$, as seen on the corresponding figures.

The other terms of the above equation were not taken into account, because they were thought of small effect, compared to the total value of heat-transfer coefficients. Taking into consideration all terms for $x = 18.25$ in IIc, the coefficient was calculated according to the above equation, the result of which was as follows:

term including $dT_w/dx \cong 0.76\ S_t$

" " $d\Delta_2/dx \cong 0.286\ S_t$

terms, " $dU_e/dx \cong -0.044\ S_t$, and,

term " $d\delta_3/dx \cong -0.0013\ S_t$.

*Assuming that the effect of turbulent fluctuations, radiation and natural convection can be neglected compared to forced convection.

2. - In the rear part of the plate, where the surface temperature is approximately 0.1 T_e higher than that of the upstream, there is no guarantee that the heat does not flow by conductivity through the material of the plate. This would result in an apparent rise in the local coefficients at the rear part of the plate, where heat flow to the supporting angle is still present. Alleviation of the steep rise in coefficients at the middle of the plate may be observed.

A quick check on the values of the integration $\int S_t (T_w - T_e)\, dx$ as calculated from the two results may support this view (see Fig. III.3.10).

It can be then suggested that, on the whole, the accuracy of the values which were obtained for the heat-transfer coefficients* was quite good.

The results obtained, and the above discussion, thus indicate that the effect of pressure applied in the present experiments was small, especially when compared to their effect on the skin-friction coefficients.

The more effective parameter was the wall-temperature gradient.

* The chosen values are shown by the broken lines on Fig. III.3.6 to III.3.9

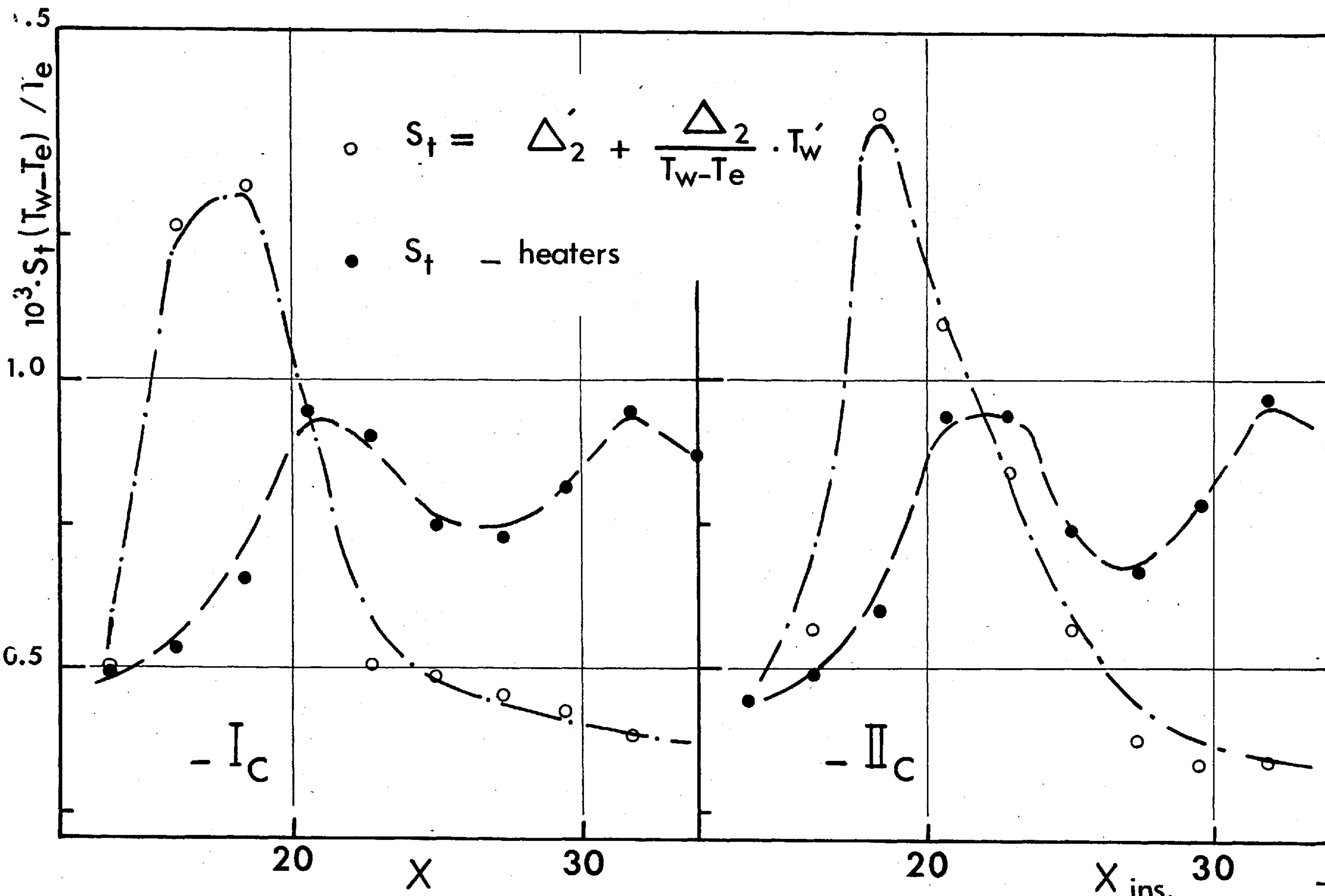

Fig. III.3.10 – Wall heat-input for the Cases I_C and II_C .

The Nusselt numbers were calculated and plotted against R_x*. Fig. III.3.11 represents the isothermal plate, while Fig. III.3.12 concerns the step-heating.

On these figures, the values obtained by Nunner (25) were extrapolated to the presently examined range of R_x.

It is then clear that the values of $Nu(R_x)$ for the isothermal plate were very near to the extrapolated relation shown by Nunner for a value of $k_s = 3.14$ mm. This is approximately twice that value of the present experiments. In the region where dT_w/dx differed from zero, the values of Nu sometimes topped those of k_s, as high as 15 times the present value. The values of Nu afterwards approached those found for smooth pipes.

The free stream temperature for the flat plate is constant, while the core temperature of the pipe is constantly increasing.

*To calculate R_x, 'x' was taken as the distance measured from the beginning of roughness, because this was the beginning of heating. A mean value of $Pr = 0.73$ was taken for all profiles.

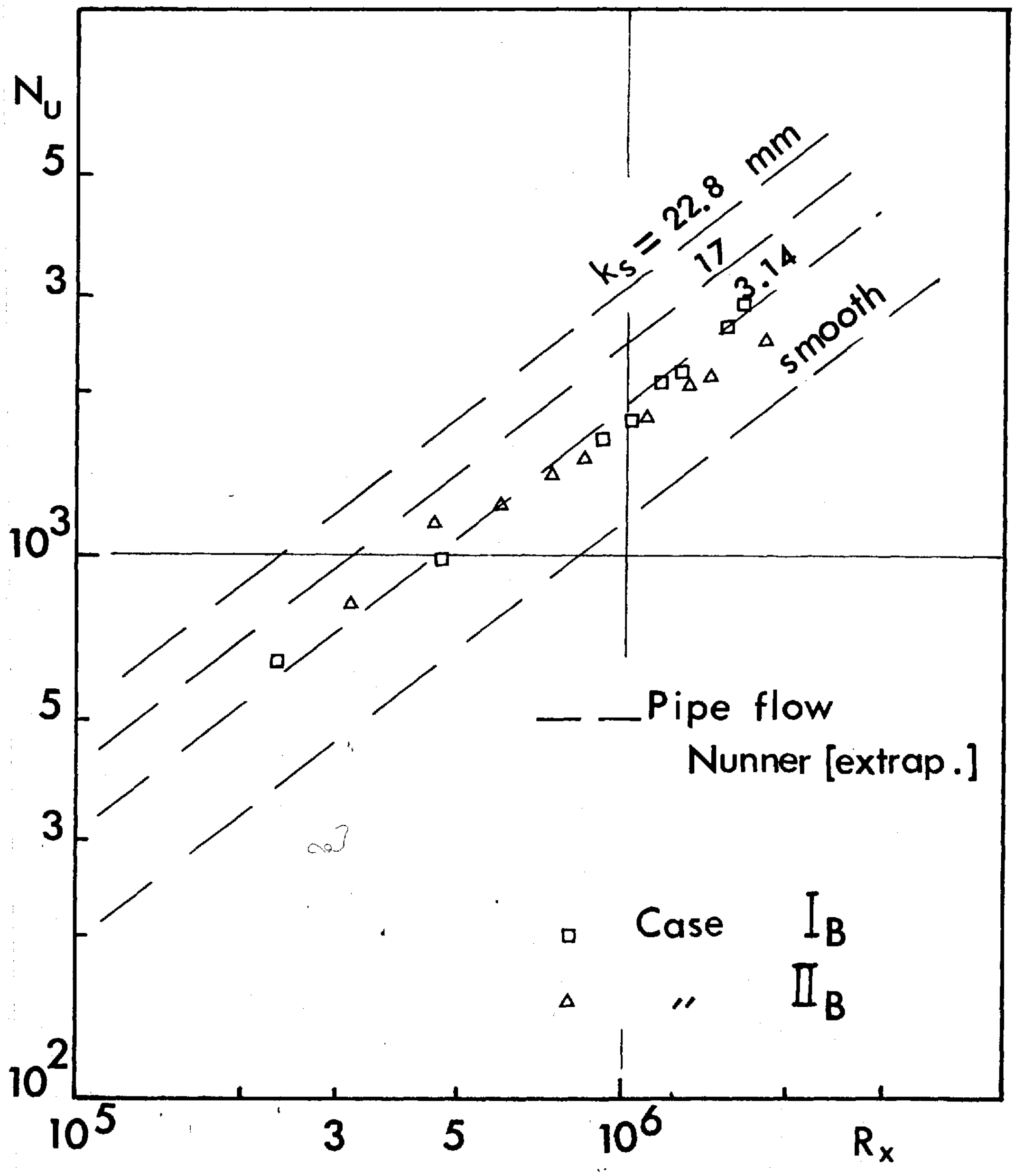

Fig. III.3.11 _ $N_u(R_x)$ for the cases of isothermal heating .

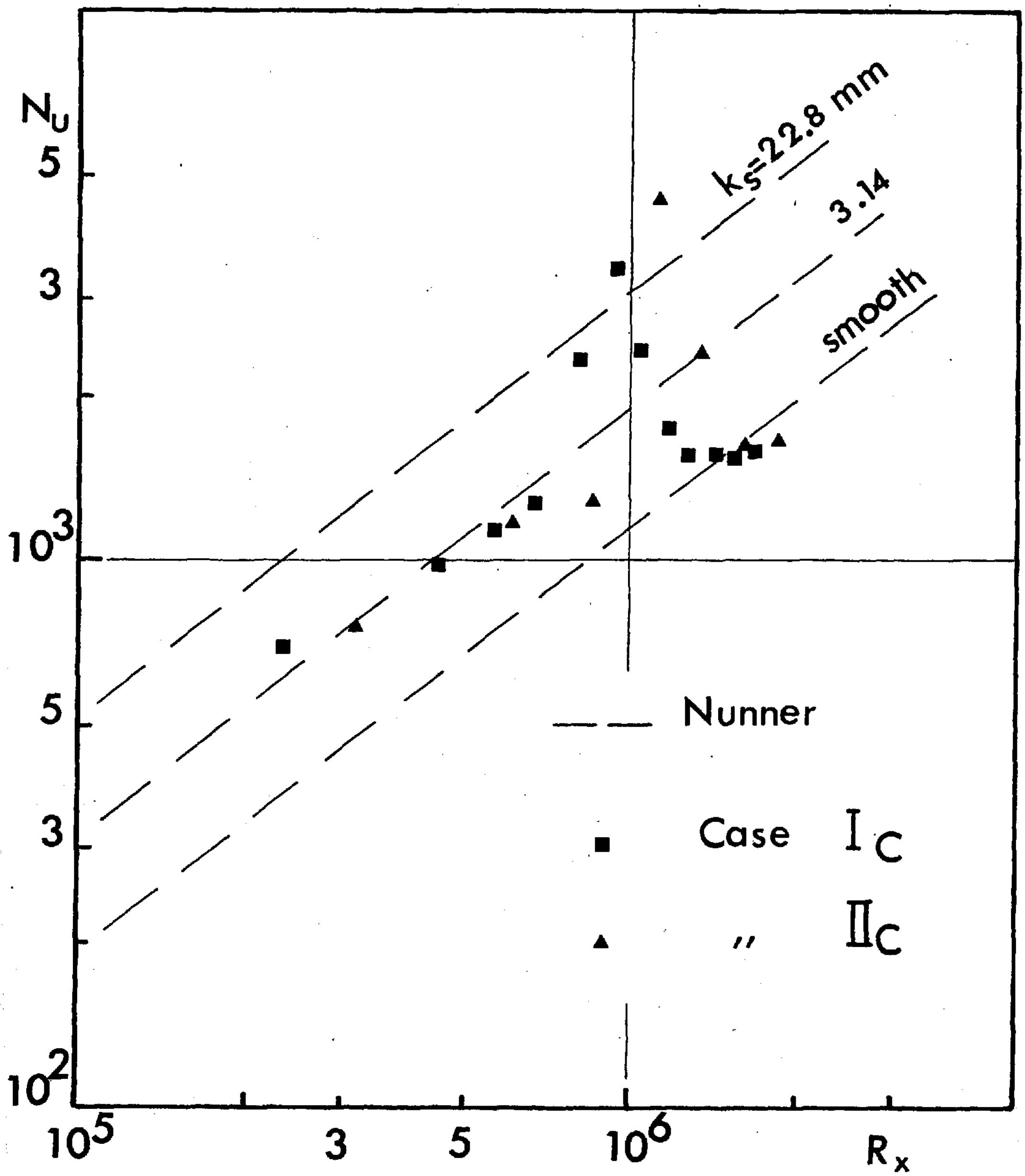

Fig. III. 3.12 _ $N_u(R_x)$ for the cases of step heating.

The effect of an increasing outside temperature being opposite to that of an increasing surface temperature.

Also, the roughness elements used by Nunner were two-dimensional, while that of the present experiments is three-dimensional. This may lead to increase the heat transfer due to the larger area of the surface "wetted" by the air flow. It may also be argued that the three-dimensionality affected the skin-friction, but not the heat-transfer.

Perhaps this accounts for the observation that the isothermal cases approach Nunner's results for $k_s = 3.14$ mm.

Koch (26) has extended Nunner's work for higher values of k_s. His results show that a pipe having a resistance coefficient of 13.33 times that corresponding to Nunner's pipe of $k_s = 22.8$ mm, has only increased the ratio of Nusselt number of the rough pipe to that of the smooth $\left(= \frac{Nu}{Nu_0}\right)$ from 2.6 in Nunner's case to 3.6 approximately.

Further discussion on the relationship between effective roughness and heat-transfer increase will be given in § III.5 later on.

The heat-transfer coefficients of the region dominated by the roughness elements 'B' was calculated by the method of Owen and Thompson (24), where no temperature gradient and little or no pressure gradient was applied. The formula given for the flat plate can be written as:

$$1/S_t = \frac{U_e}{u_\tau}\left(\frac{U_e}{u_\tau} + \frac{1}{B}\right) .$$

The results show close resemblance to those of Nunner (see Fig.III.3.13) which are quoted in (24). They conform with the behaviour of the total hear-transfer coefficients (S_t).

It is interesting that the present theories for smooth surfaces predict higher heat-transfer coefficients after the surface temperature undergoes a stepwise discontinuity, than those of an isothermally heated surface. This is contrary to the results of the present experiments.

This discrepancy is thought to be due mainly to the basic assumptions of similarity between velocity and temperature profiles, the form of velocity profiles chosen, and the disregard for the effect of fluctuations.

Bradshaw et al. (38) recently introduced a method for the calculation of the dynamic boundary layers. They have pointed out the possibility of deducing a parallel method for the thermal boundary layers based upon the turbulent-temperature-fluctuations equation. Such a method might yield more realistic results for experiments like those presently discussed.

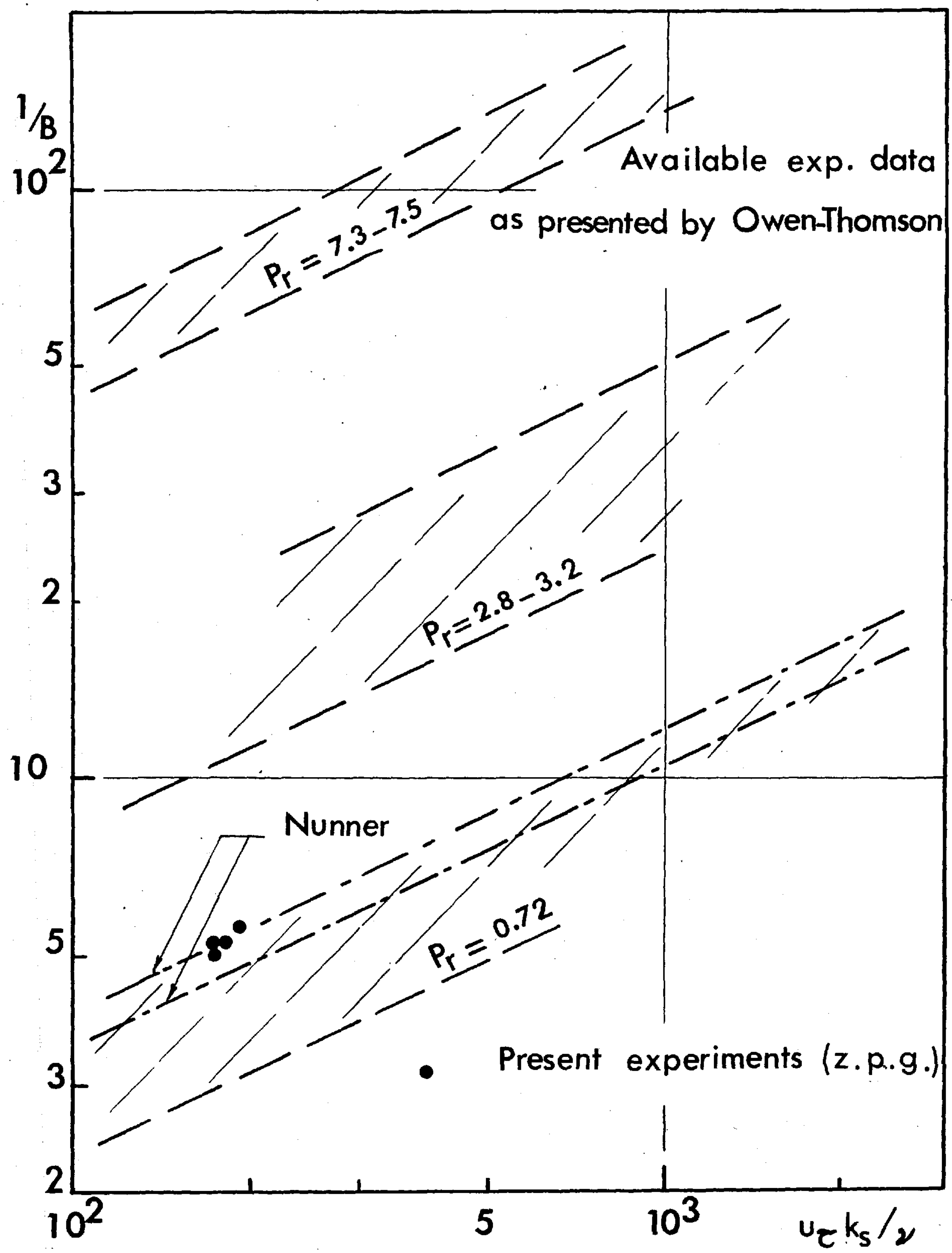

Fig. III.3.13 _ Heat-transfer of roughness-dominated region .

III.3.4 - <u>Presentation of the temperature profiles</u>:

The temperature profiles on a rough surface, as described earlier in § III.3.1, begin at values of $\bar{\theta}\left(=\frac{T_w - T}{T_w - T_e}\right)$ much greater than the corresponding values of U/U_e of the velocity profiles. This difference between the two profiles continues to decrease until it eventually vanishes near the outer edge of the boundary layer, where both $\bar{\theta}$ and U/U_e tend to unity. This observation is already established by the experiments of Brunello (3), Doenecke(4) for the flat plate, and by Nunner's experiments (25) for the pipe flow.

Kestin and Richardson (28) also noted that the effect of roughness may be described as similar to the effect of increase in Prandtl number, except that the increase in Prandtl number affects the temperature profile, while roughness affects the velocity profile.

The limits for the temperature profile are not the same as those for the velocity near the wall. It is then obvious that the Reynolds analogy ($2St/C_f = 1$) does not necessarily apply for a rough surface. Reynolds analogy factor was found to vary between 0.4 to 4.2 approximately in the present experiments. The value for no pressure or surface-temperature gradient was about 0.79.

The effect of roughness, T_w/T_e, dT_w/dx and Π, is best seen from the set of Fig. III.3.14 to III.3.21. below. On each of these figures, we have plotted $\bar{\theta}(y)$ and $U/U_e(y)$ as measured by the hot-wire probe. $\bar{\theta}(y)$ as measured by a 0.5 mm bare-bead thermistor was also included. The thermistor measuring current was such that its temperature was not raised more than 1°C, to avoid the sensitivity to the air speed.

From these profiles it is clear that the effect of T_w/T_e and dT_w/dx was confined to a thin layer close to the 'origin'. The outer part of the profiles was more affected by the velocity field. These figures were also the basis upon which the divisions described in § III.3.1 were chosen.

A unique profile $\bar{\theta}\left(\frac{y}{\Delta_2}\right)$ was found for each plate of (4) and (6). This is not valid in the present work, since both temperature and pressure gradients were applied. However, a comparison is made on Fig. III.3.22 between the present results, at no pressure or wall-temperature gradients, and the results of Doenecke(4) for his plate with two-dimensional square ribs.

Nunner has previously attempted to relate the temperature profiles with surface roughness. He plotted $\frac{U}{U_e}(\bar{\theta})$ and compared the curves obtained with those given by H. Reichardt for different values of P_r. He thus

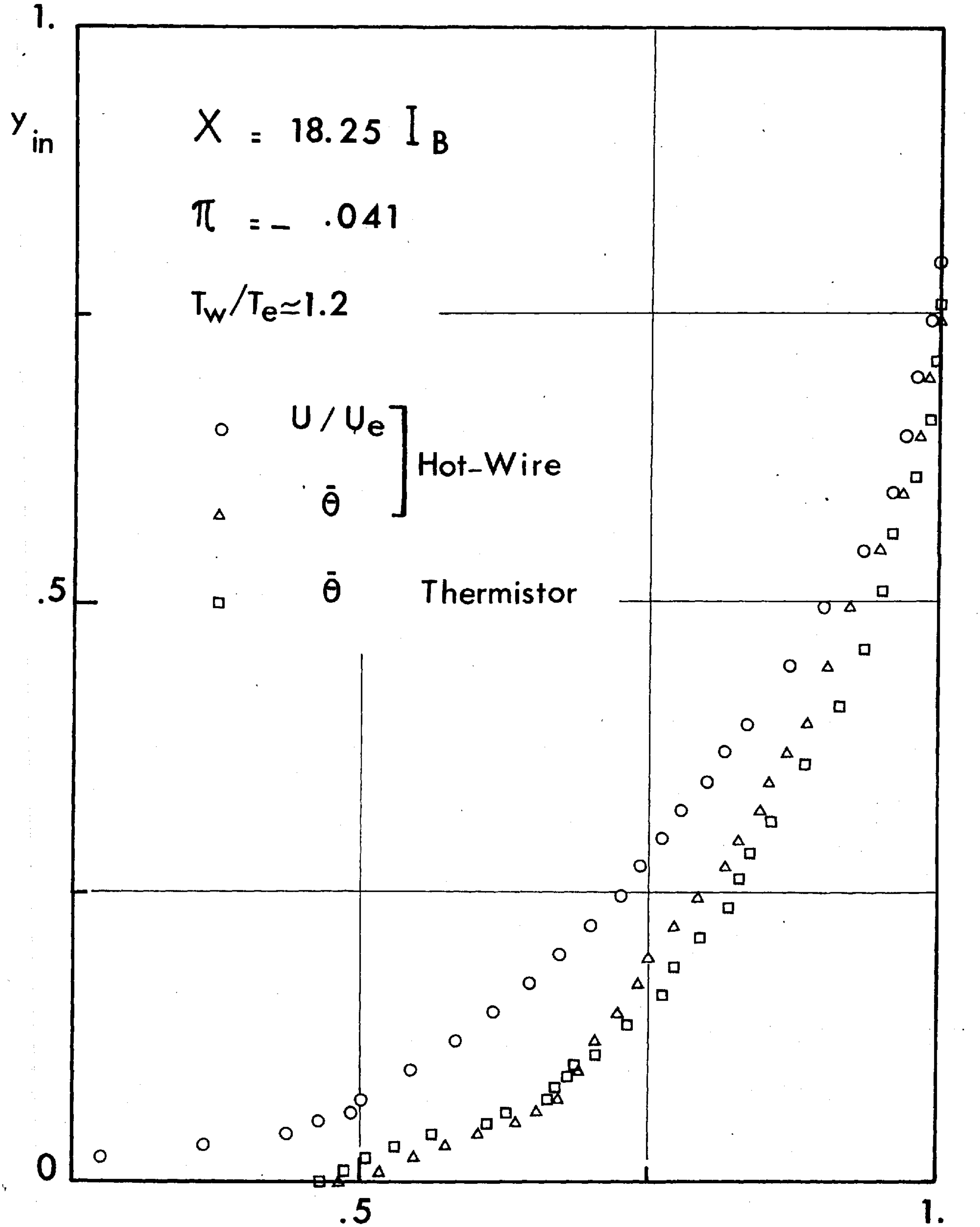

Fig. III. 3.14_Velocity and temperature profiles.

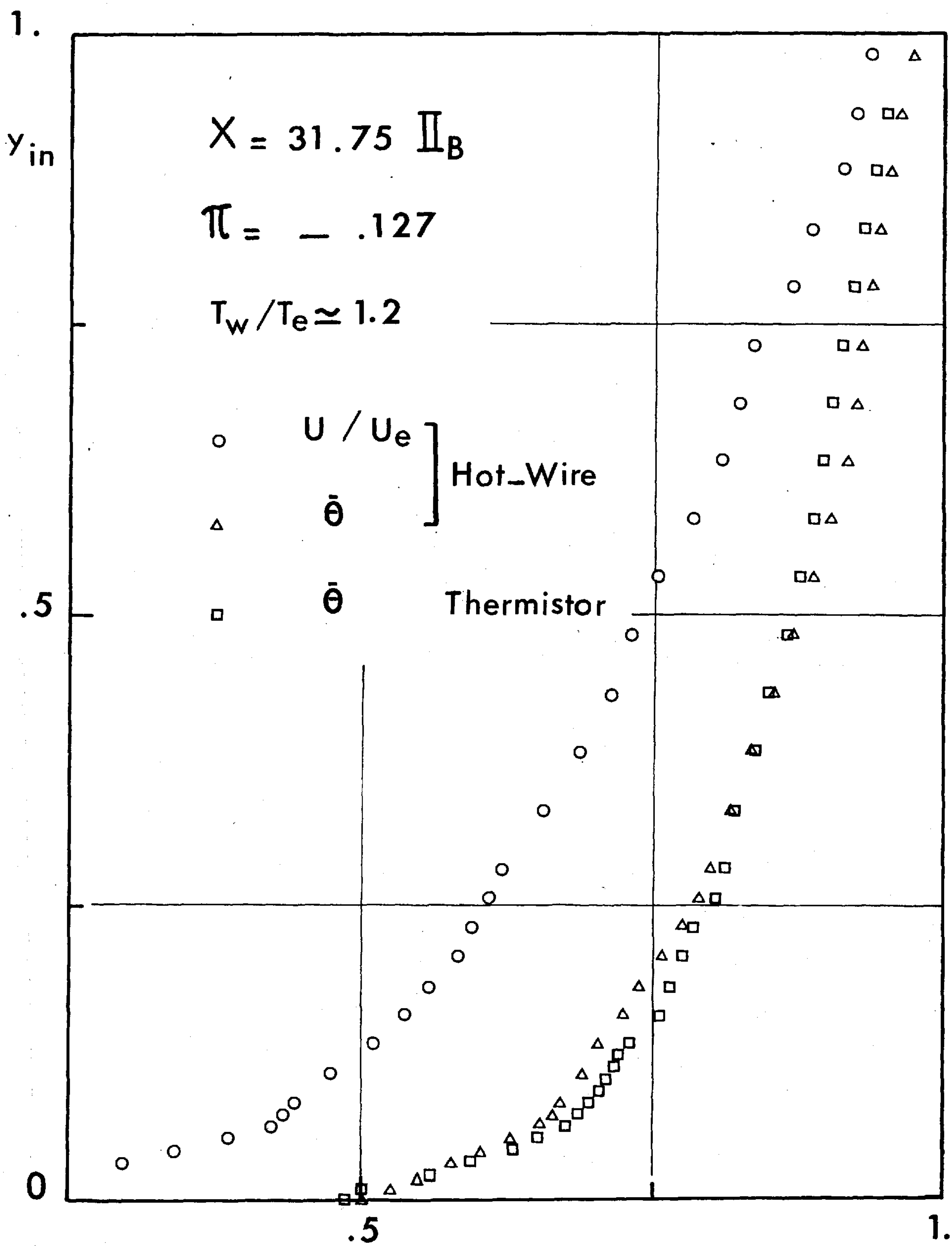

Fig. III. 3.15 – Velocity and temperature profiles.

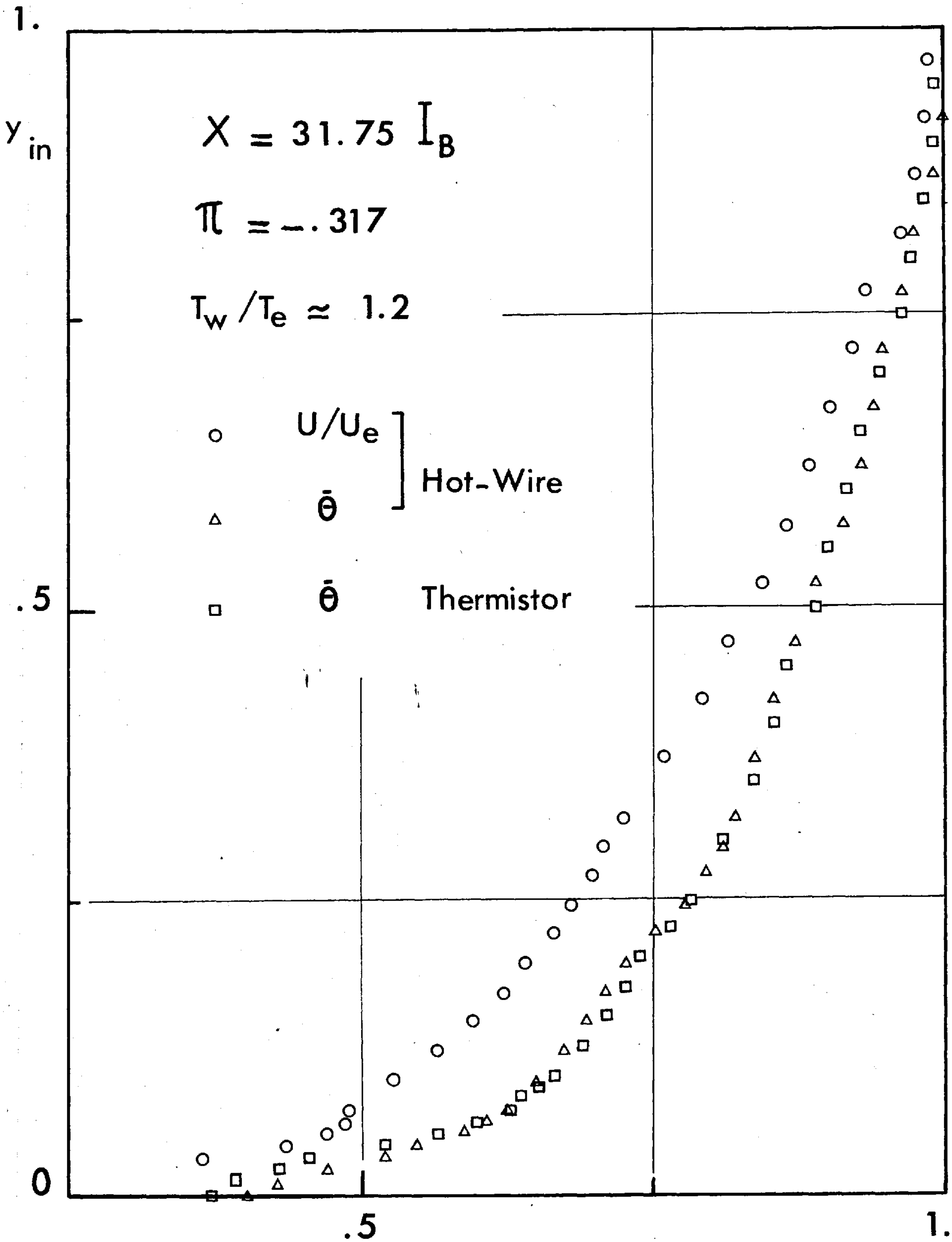

Fig. III.3.16 _ Velocity and temperature profiles.

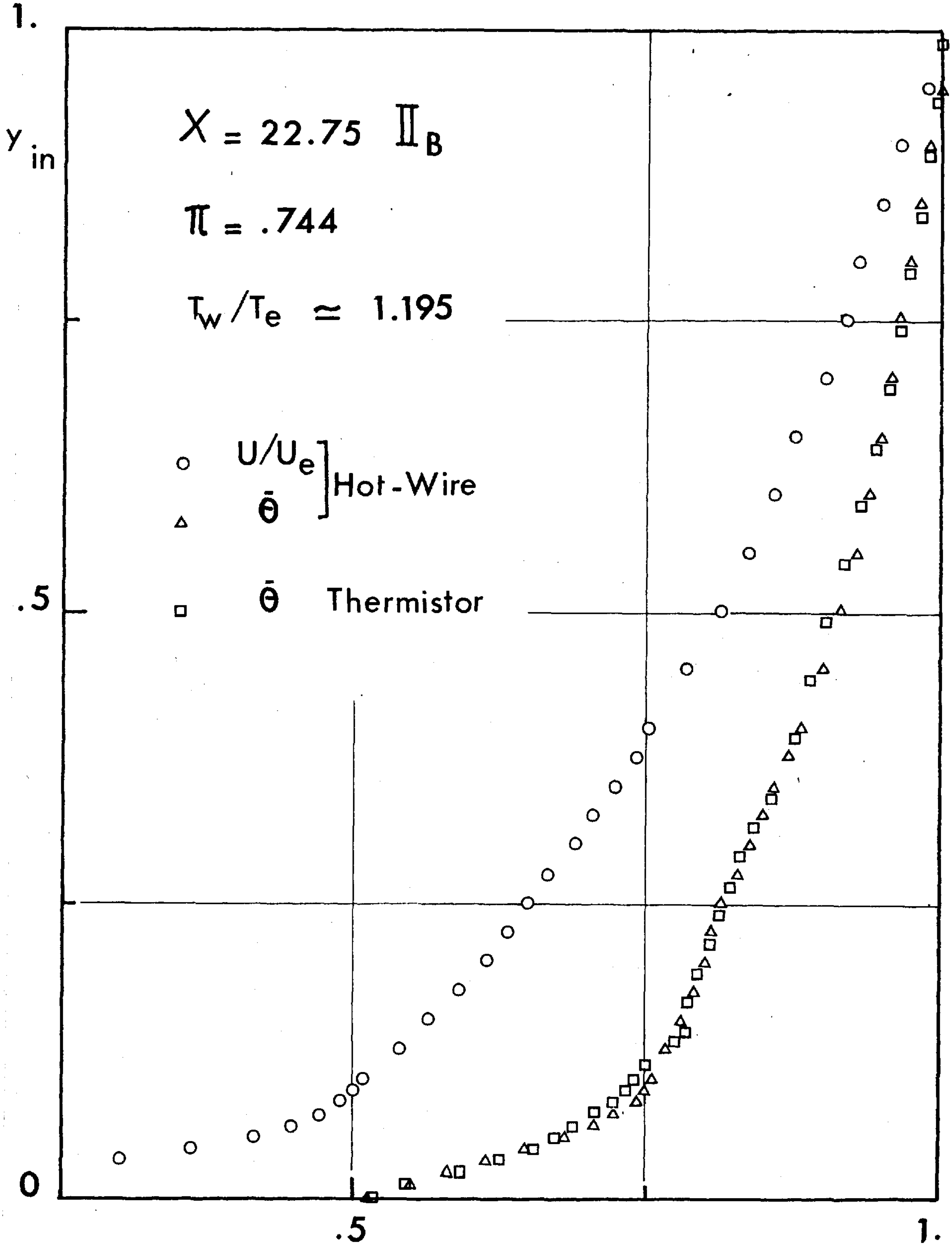

Fig. III. 3.17_Velocity and temperature profiles.

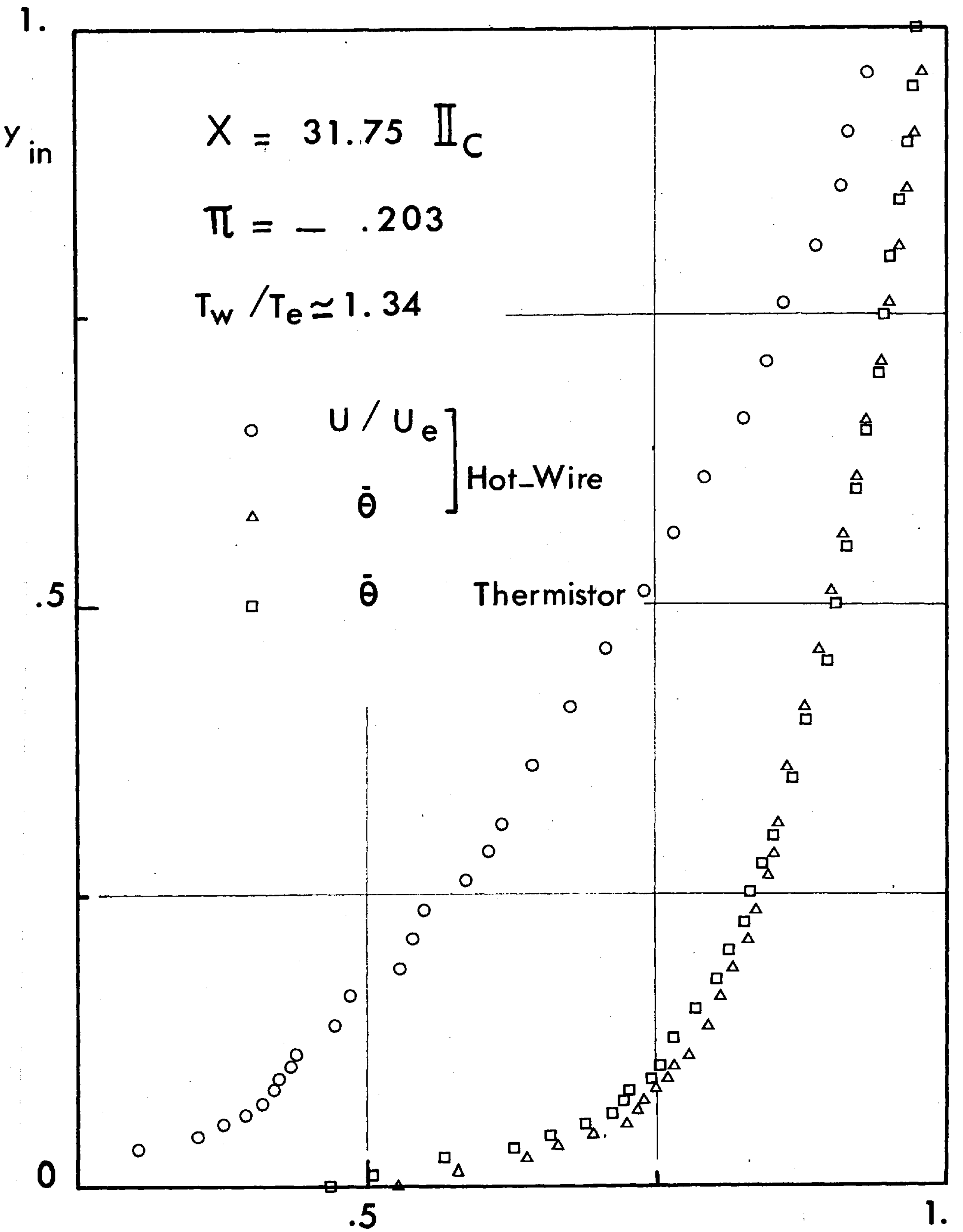

Fig. III. 3.18 _Velocity and temperature profiles.

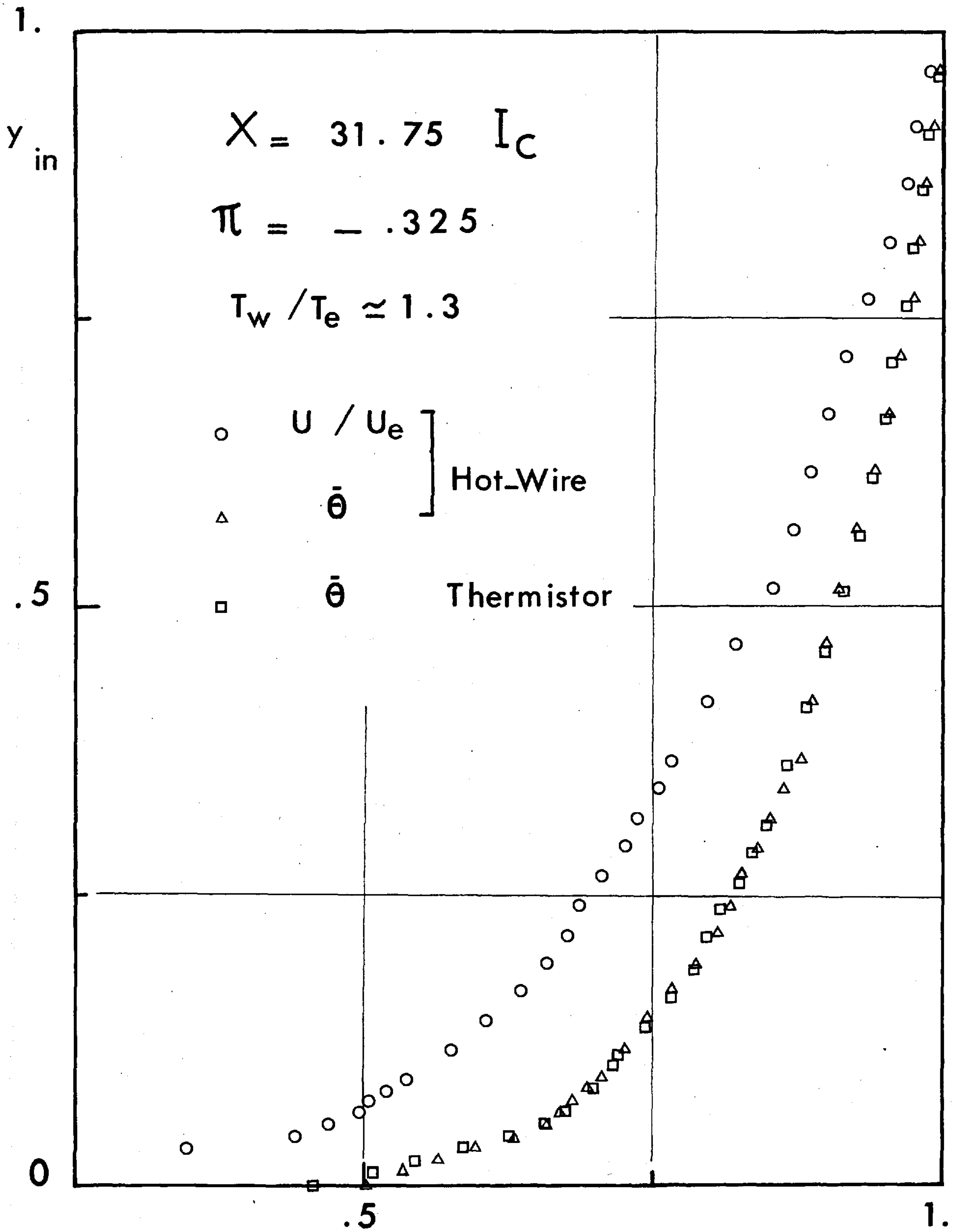

Fig.III.3.19_Velocity and temperature profiles.

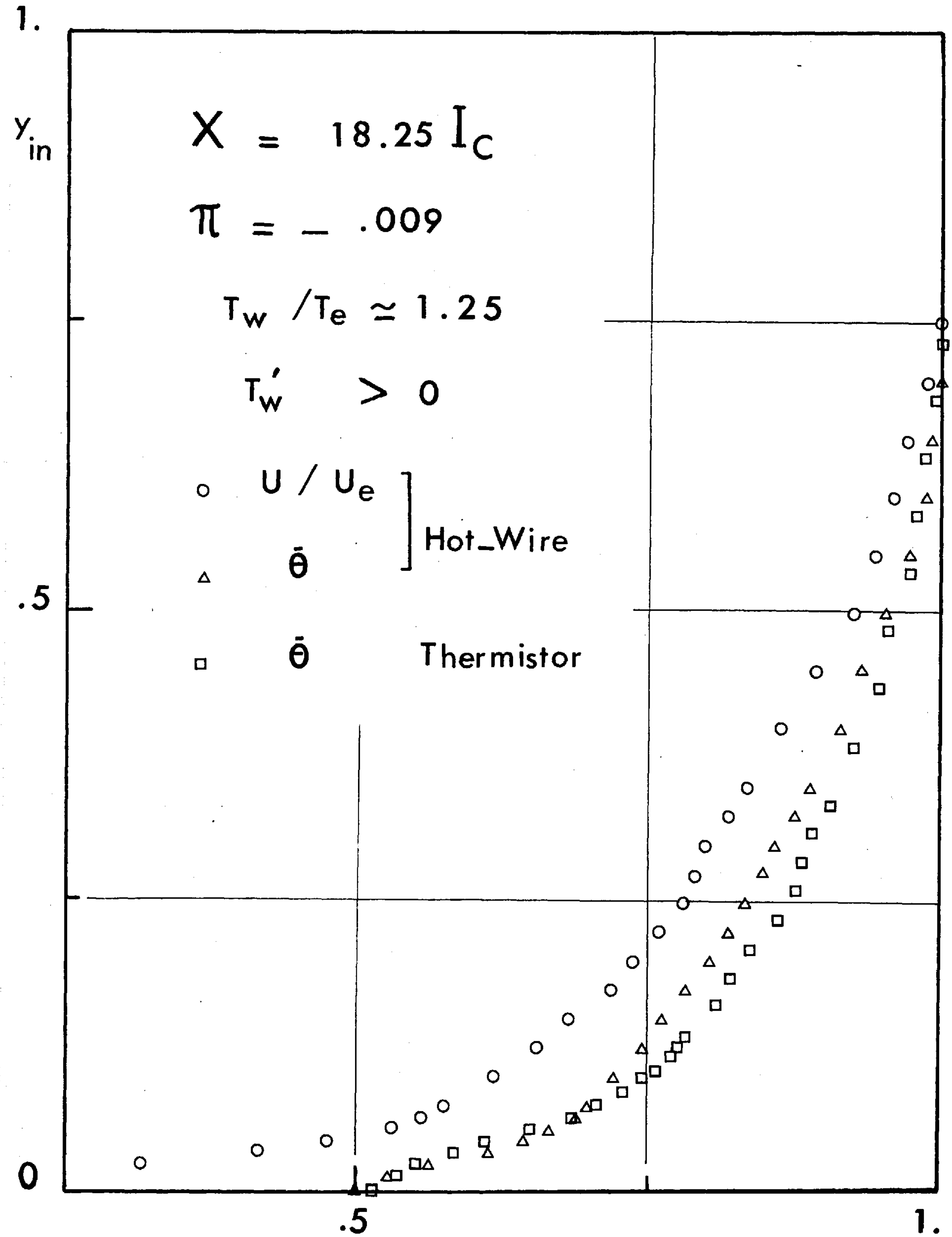

Fig. III. 3. 20_Velocity and temperature profiles.

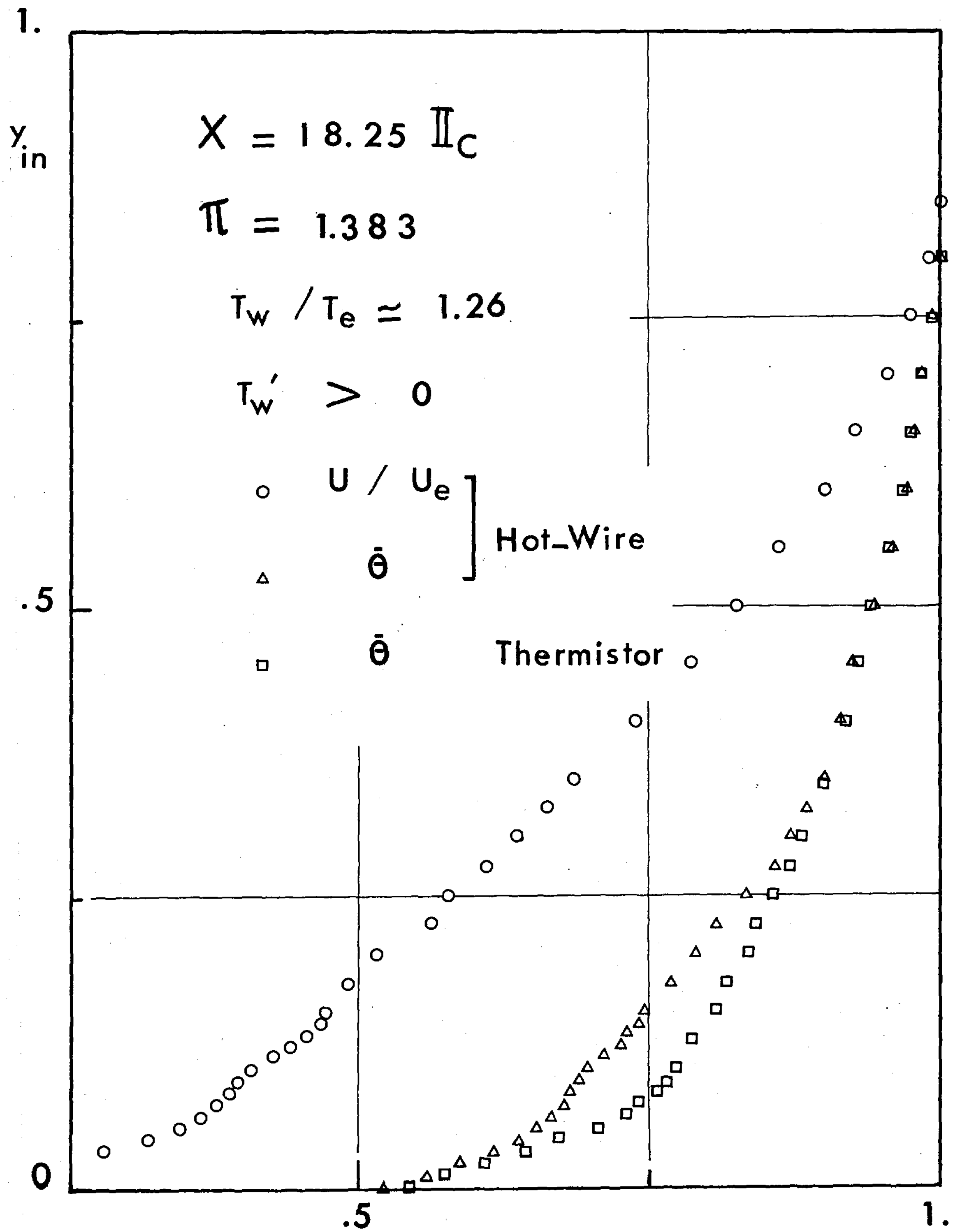

Fig. III. 3.21_Velocity and temperature profiles.

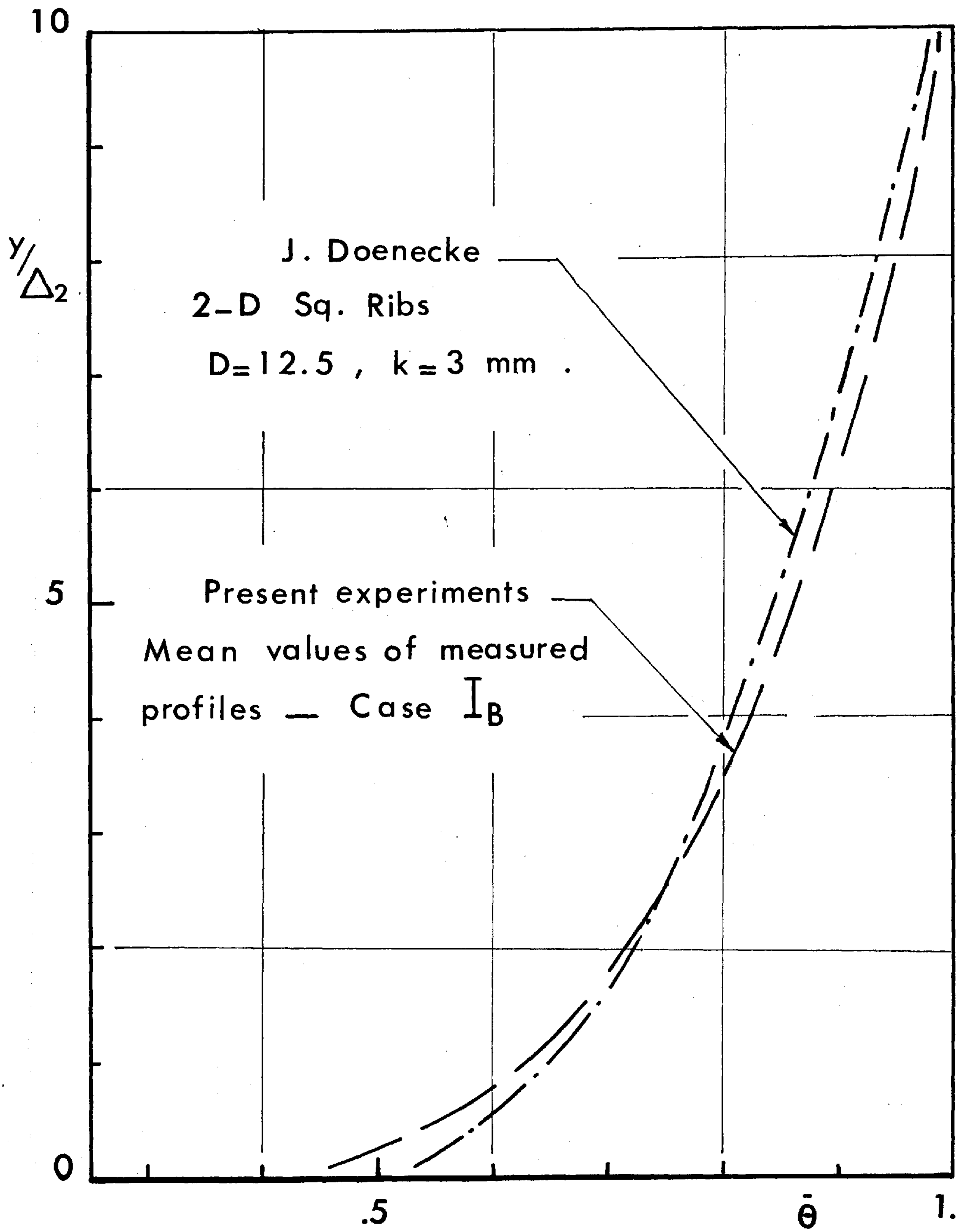

Fig. III.3.22 _ Temperature profiles, $\bar{\theta}(y/\Delta_2)$.

obtained "enlarged or equivalent" values of Pr.

For I_B, the value of $(P_r)_{eq}$ was 3 approximately. This approaches Nunner's value for his pipe with $k_s = 3.14$ mm. The value of $(P_r)_{eq}$ differed from that when boundary layers with pressure and/or wall-temperature gradients were considered.

Deissler (29) introduced the temperature profiles of the form $\theta^+ \left(= \bar{\theta}\ \frac{C_f}{2S_t} \cdot \frac{U_e}{u_\tau}\right) = f\left[\frac{y u_\tau}{\nu}\right]_{Pr}$, which were derived assuming the law of the wall as velocity profile. This might be applicable for a smooth surface, where the velocity profile is universal. It is not necessarily valid for a rough surface, where the location of the semi-logarithmic line depends on $R_k \left(= k_s u_\tau / \nu\right)$.

Instead, we propose a temperature-defect presentation. This would be of the form;

$$-\theta_d^+ = \theta^+ - \theta_e^+ \equiv F\left[\frac{y\, u_\tau}{\Delta_1 U_e}\right] ,$$

where

$$\theta_e^+ = \frac{C_f}{2S_t}\ \frac{U_e}{u_\tau} .$$

This was applied to some of the obtained profiles, covering a range of different pressure gradients, wall temperatures and wall temperature gradients, as shown on Fig. III.3.23. On Fig. III.3.24 two profiles from (4) for rough walls, and one from (3) for a smooth wall, with no pressure or wall-temperature gradients were shown.

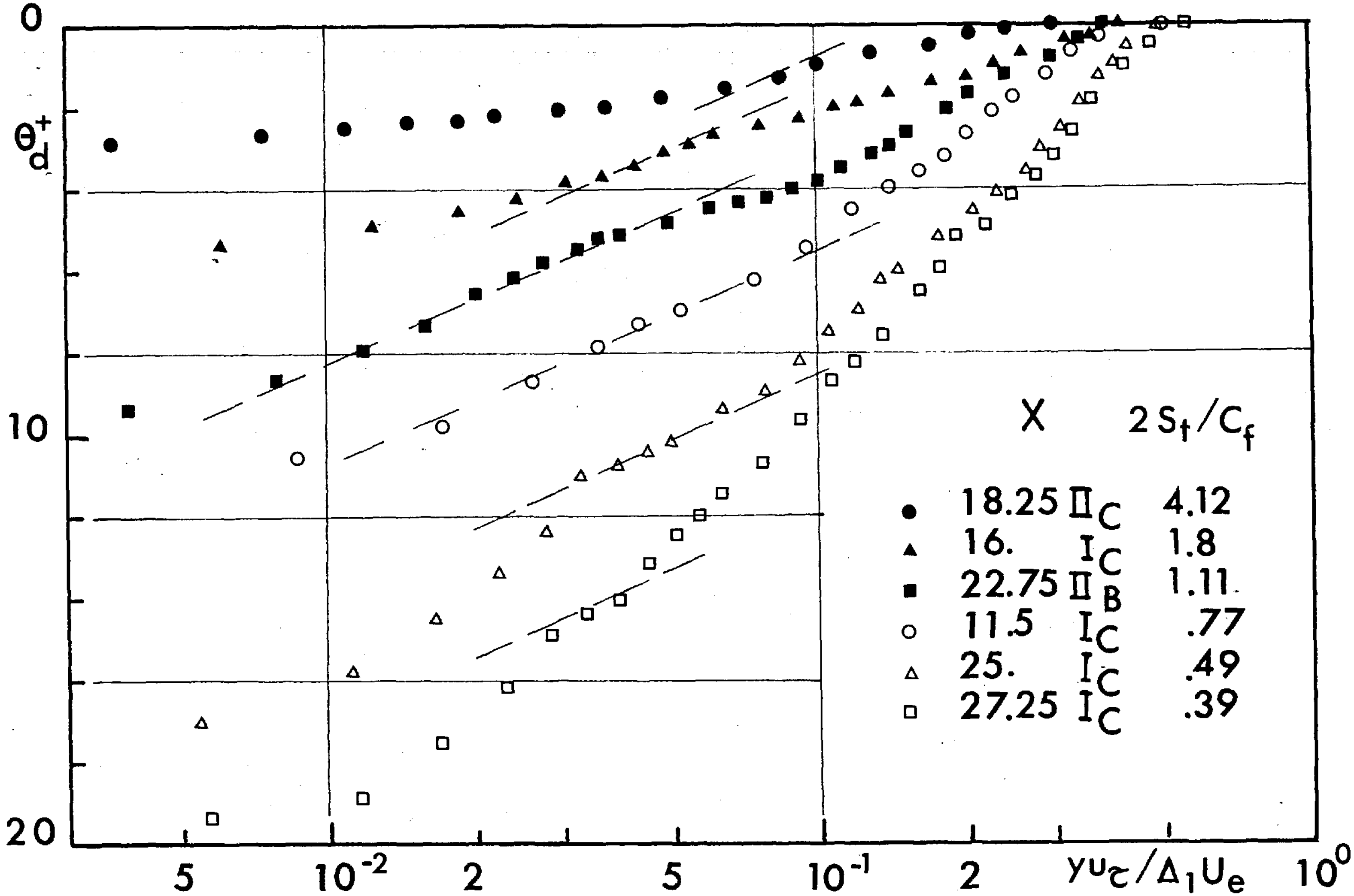

Fig. III. 3.23 _ Temperature-defect profiles.

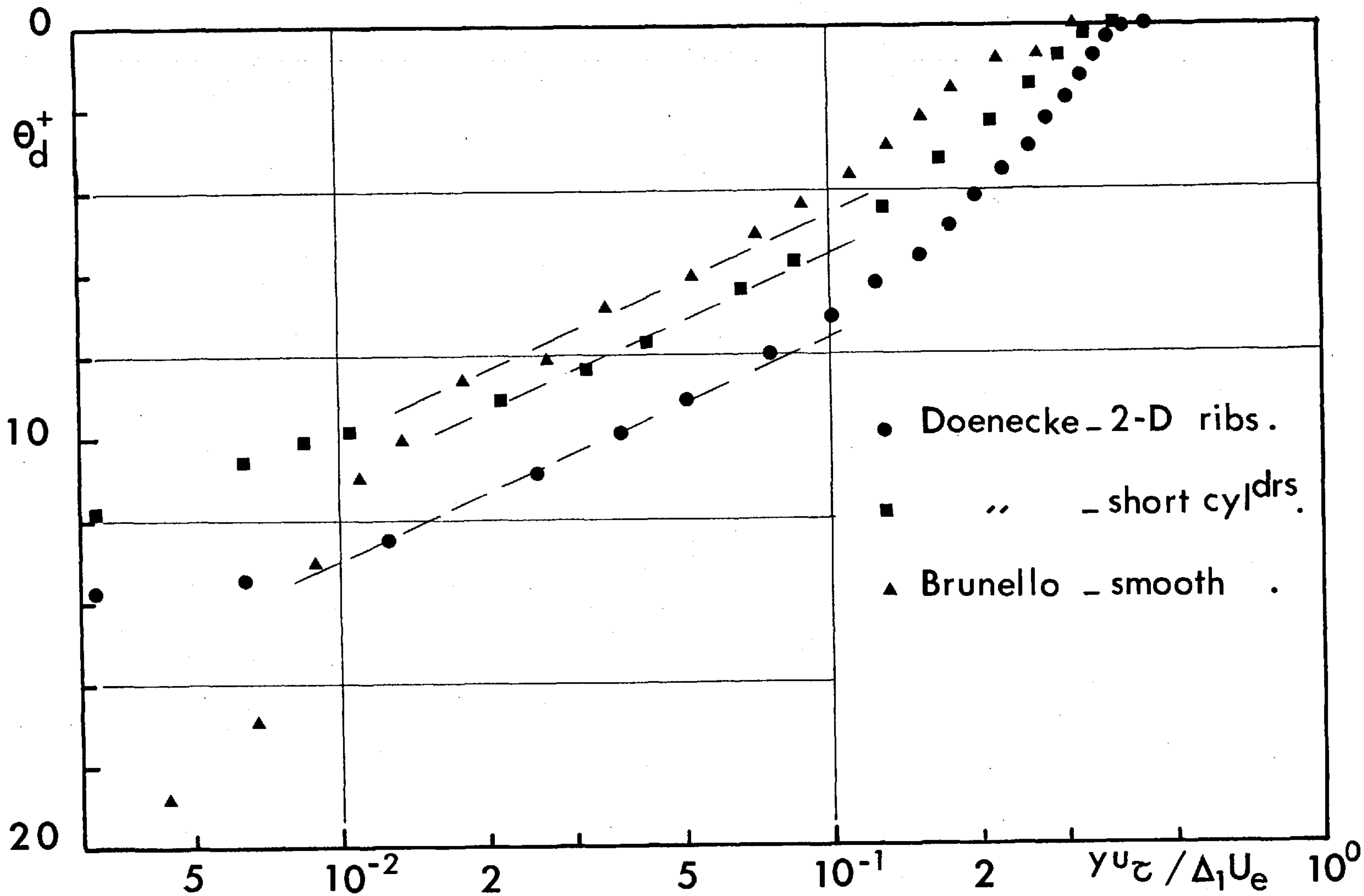

Fig. III. 3. 24 _ Temperature-defect profiles .

These figures show that there exists a layer close to the wall, and outside the viscous sublayer*, in which the relation takes the form,

$$-\theta_d^+ = 5.4 \log \frac{y u_\tau}{\Delta_1 U_e} + A_h \quad .$$

Unlike the velocity-defect, the profiles seem to join the $y u_\tau / \Delta_1 U_e$-axis asymptotically in almost the same region, for all the examined profiles. This was not so with the velocity-defect presentation.

It is also interesting to note that, the slope $d\,\theta_d^+ / d\log\left(\frac{y u_\tau}{\Delta_1 U_e}\right)$ was not always greater in the wall layer than in the 'defect-layer' as it was the case with their velocity profiles.

* This need not be exactly the same as the velocity sublayer.

The empirically determined constant of 5.4 could be a function of Pr, this would be suggested to take the form;

$$\frac{1}{\kappa_h} = (P_r)^n / \kappa$$

with $\kappa_h \simeq 0.425$ (for the present experiments)

$n \simeq 1/7$.

The constant of integration A_h was found to be a consistent function of $2S_t/C_f$ *, as shown in Fig. III.3.25.

The suggested method, undoubtedly needs further verification and discussion, before confirming its validity and limitations.

* Note that the area enclosed by the temperature-defect profile and the two axes would become $C_f/2S_t$, if we can assume that $\rho/\rho_e \simeq 1$.

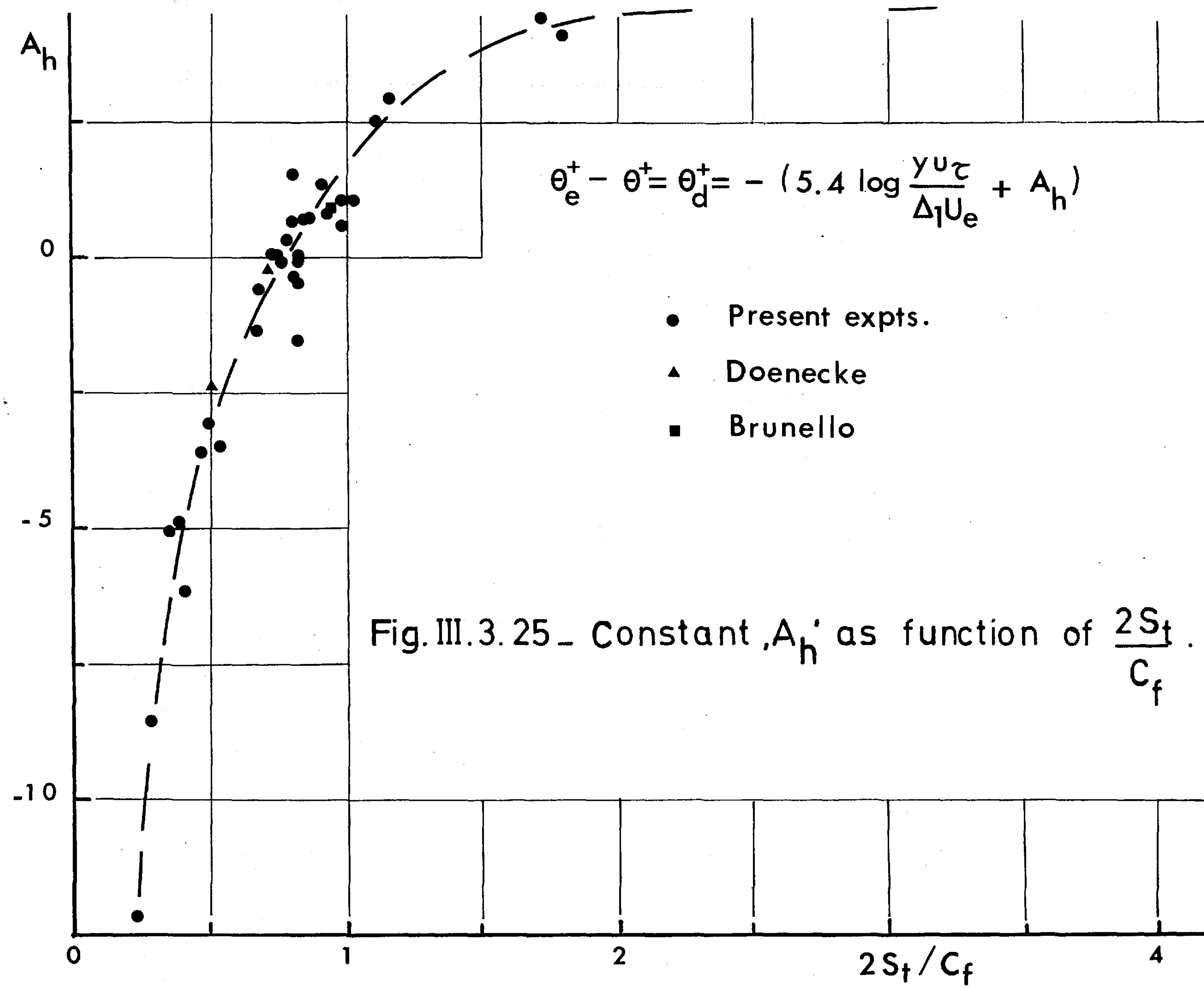

Fig. III.3.25 – Constant 'A$_h$' as function of $\frac{2S_t}{C_f}$.

III.4 - Turbulent Quantities:

The present section which deals with fluctuation measurements is divided into two parts, that dealing with the longitudinal velocity fluctuations, and that concerning Reynolds stress measurements. The latter also includes the study of the effect of surface change.

III.4.1 - Longitudinal Fluctuations:

An example of measurements obtained for longitudinal velocity fluctuations is shown on Fig. III.4.1. They are selected to include boundary layers under the effect of negative, zero or positive pressure gradients in the absence of surface heating. The curve of longitudinal fluctuations for a smooth surface as measured by Klebanoff (1) is also shown. One of the measurements in the presence of surface heating is included on the same figure.

The figure reveals, as expected, that the turbulent fluctuations for the surface examined are higher than those of the smooth surface*.

*Surface roughness was referred to sometimes in literature as "turbulence generator".

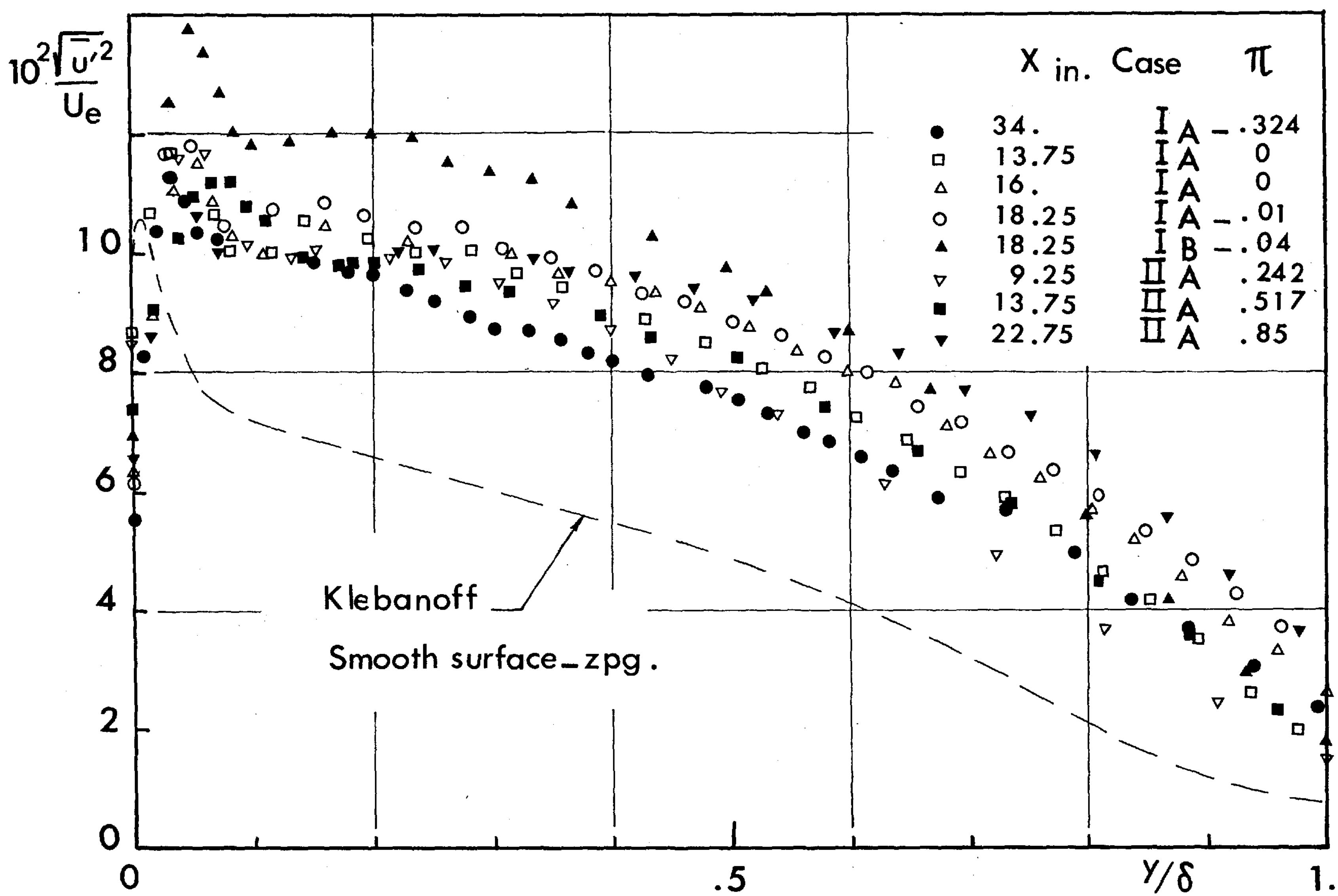

Fig. III.4.1_ Longitudinal component of fluctuations.

More important is the observation of expansion of the 'peak' of longitudinal fluctuations usually occurring at, or very near, the origin of the velocity profiles of smooth surfaces. This may then suggest, with the fact that the origin of the velocity profile behind a roughness element is below the crest (inside the cavities in the present study), that the fluctuations over the crest of the roughness element, which are at least as high as those over a smooth surface, are spread from the downstream edge of the roughness element to the flow behind it.

It is worthwhile noting here that a core diameter of 0.0002 in. was used for few experiments towards the end of this work, because of the 'sometimes incurable' instability of the DISA bridges with 0.0001 in core Wollaston wires. Although they worked quite satisfactorily for mean values, the fluctuations obtained with such wire diameter (a length of 1 mm approximately) did not show this peak feature near the origin of the velocity profiles. They almost agreed with the other measurements in the outer part of the boundary layer. This may be due to the frequency of fluctuations near the origin at its highest. The greater the diameter of the wire, the less the cut-off frequency may be.

Another observation may be made from the above mentioned figure, that velocity fluctuations tend to vanish near, and at, the chosen origin of the velocity profiles. This is a further support to the choice itself.

In the range of the presently applied pressure gradients, their effect on $\overline{u'^2}$ is found to be small.

Finally, the measurements obtained when surface heating was applied show higher values of $\overline{u'^2}$ in the neighbourhood of the origin. This is due to the existence of temperature fluctuations, and the inevitable sensitivity of the wires to them. Generally speaking, the values tend to approach those of the unheated surface away from the wall, where the temperature becomes near its value in the free stream. Probably the temperature fluctuations then diminish.

Unfortunately, the present experiments have not discovered the magnitude of the temperature fluctuations, or their effect on and correlation with those of the velocity. This is mainly due to the necessary electronic apparatus, which is simple in principle, yet relatively elaborate to construct.

III.4.2 - Shear-stress measurements:

Some shear-stress measurements were obtained where no surface heating was applied, by the use of the X -wire probes described earlier in § II.4. The results thus obtained for I_A and II_A are shown on Fig. III.42. and III.4.3 respectively. The accuracy of these measurements was not always completely satisfactory, as is usual. They reveal interesting features of the boundary layers on a rough surface.

The values of shear stresses on the presently examined surface were higher than those of the smooth surface measured earlier by Klebanoff (1), as already anticipated.

The measurements could not be carried out very deeply in the cavity, because of the size of probe relative to the depth of cavity. The shear stress is expected to fall rapidly towards the origin of the velocity profile, as was the case with the longitudinal fluctuations.

Further, the peak shown by the shear-stress measurements conforms and coincides in location with that shown on the longitudinal fluctuations, but is sharper than the peak of $\overline{u'^2}$.

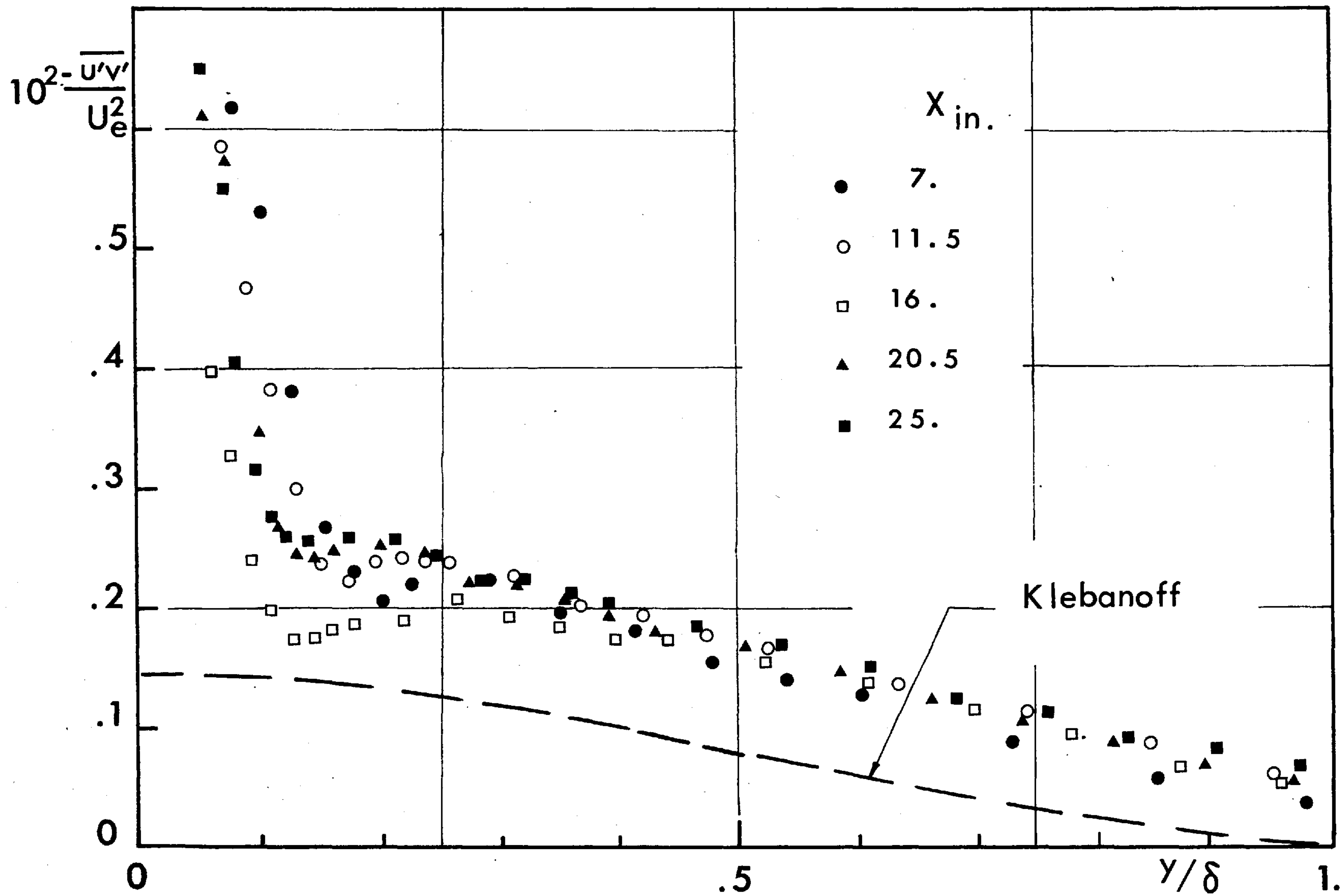

Fig. III.4.2 _ Shear stress profiles _ Case I_A

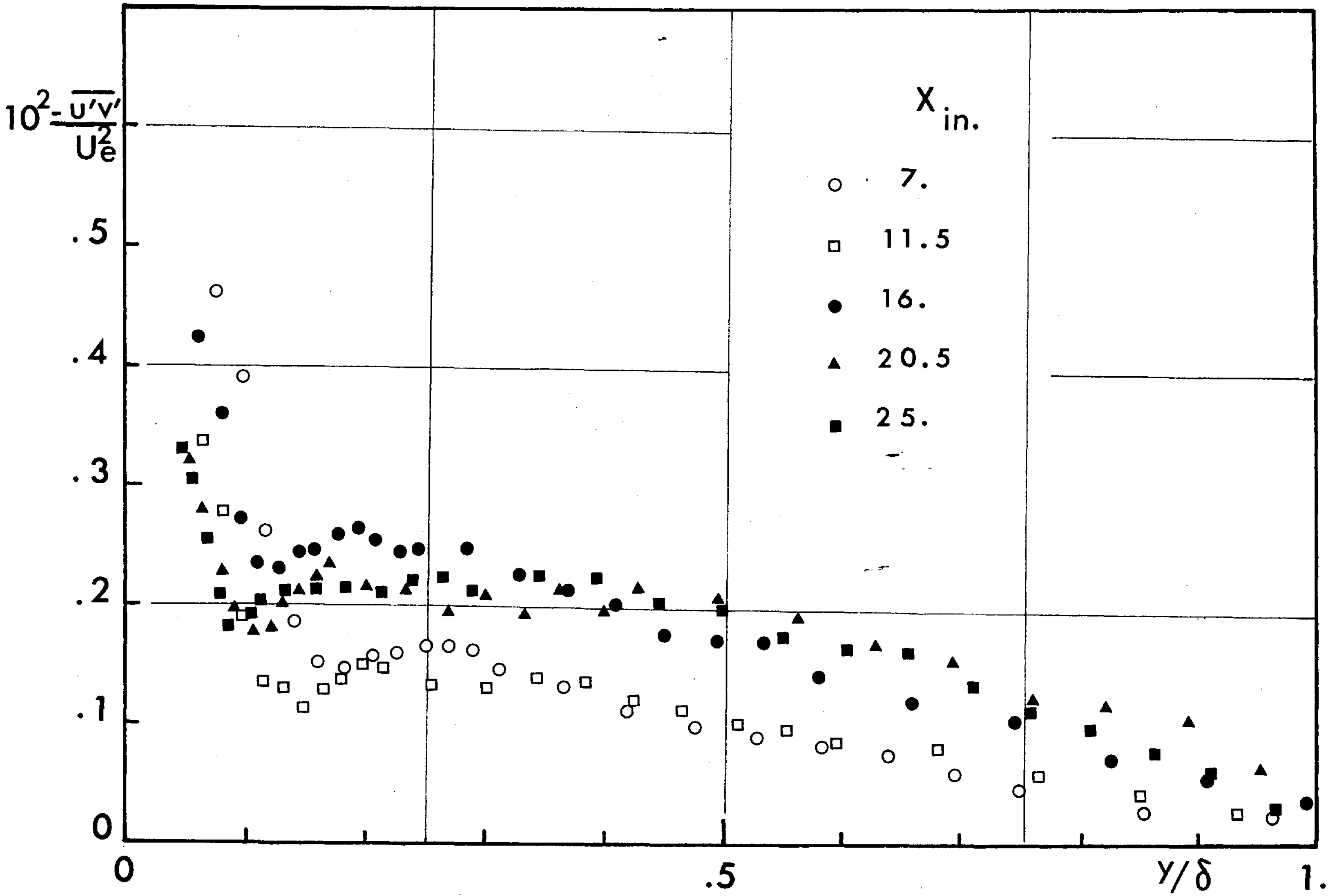

Fig. III.4.3 _ Shear stress profiles _ Case II_A .

This sharp peak is thought to represent the roughness dominated region of the boundary layer, the rest of measurements being similar but slightly higher than those of the smooth surface.

It may be considered also that the shear stresses on the crests of the roughness elements do not differ greatly from those of a smooth surface, with an abrupt increase behind the roughness elements due to their form drag. The momentum differences computed to determine C_f may then represent the mean value of both cases averaged on the basis of the ratio of areas concerned.

If we take a mean value of $\frac{u_\tau}{U_e}$ as about 0.06 for I_A and the peak value of $\left(-\overline{u'v'}/U_e^2\right)$ behind the roughness element to be 0.6×10^{-2}, and the area occupied by the cavities to be $\frac{4}{9}$ and that of the crests $\frac{5}{9}$ of the total area, we then propose that,

$$\frac{4}{9} \times 0.6 \times 10^{-2} + \frac{5}{9} C_c = 0.36 \times 10^{-2}$$

where: C_c is the shear-stress at the crest.

This yields,

$$C_c \cong 0.167 \times 10^{-2} .$$

as compared to 0.15×10^{-2} of the smooth surface.

From the measurements obtained we have chosen the calculation of τ / τ_w profiles, for $\Pi = 0$ and $\Pi = 0.557$ to be compared with the profiles of equilibrium boundary layers on smooth surfaces as given by Mellor and Gibson (21). This is shown on Fig. III.4.4 and III.4.5*.

The values of $\sqrt{\overline{u'^2}} / U_e$ as measured by the single-wire probes are compared with those calculated from the measurements of the X-wire probes on Fig. III.4.6 and III.4.7. This suggests the possible accuracy.

It can then be confirmed that boundary layers on rough surfaces behave generally like those on smooth surfaces, except in the roughness dominated region, as was suggested earlier by Nikuradse.

In a recent publication, Bradshaw, Ferriss and Atwell (38) derived a characteristic method for the calculation of boundary layer development. It was based on the turbulent energy equation, the momentum and the continuity equation. These equations were found to be hyperbolic, with the physical significance that the effect of a small disturbance at a point P is confined to the downstream side of the characteristics through P. "The variables U and $\overline{u'v'}$ could be considered separately from V, and the physical

*The molecular stresses were not included, as $\left[\left(\mu \frac{\partial u}{\partial y}\right)/\tau_w\right]_{max}$ measured 0.05 and 0.04 respectively.

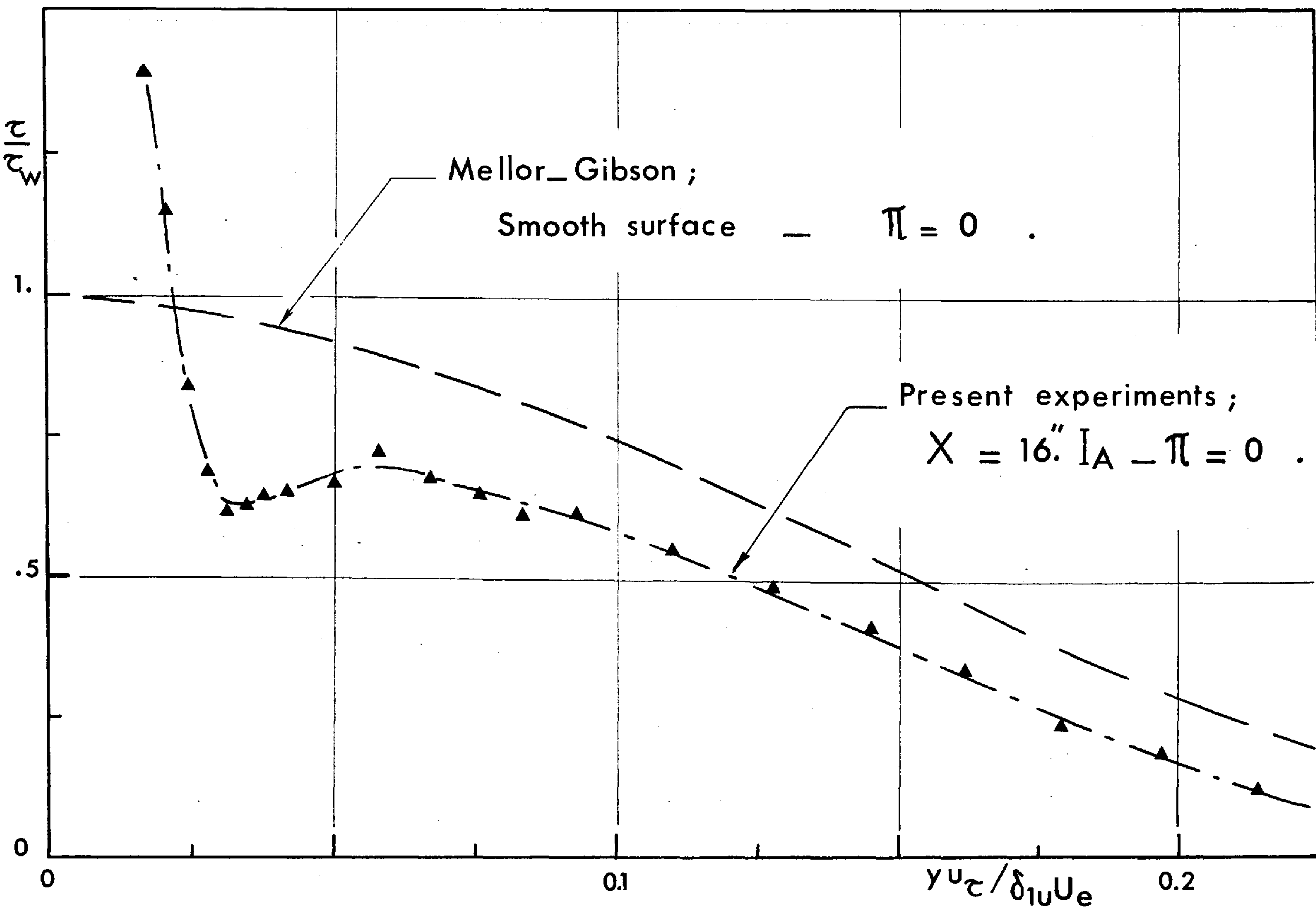

Fig. III.4.4 _ Shear stress profile.

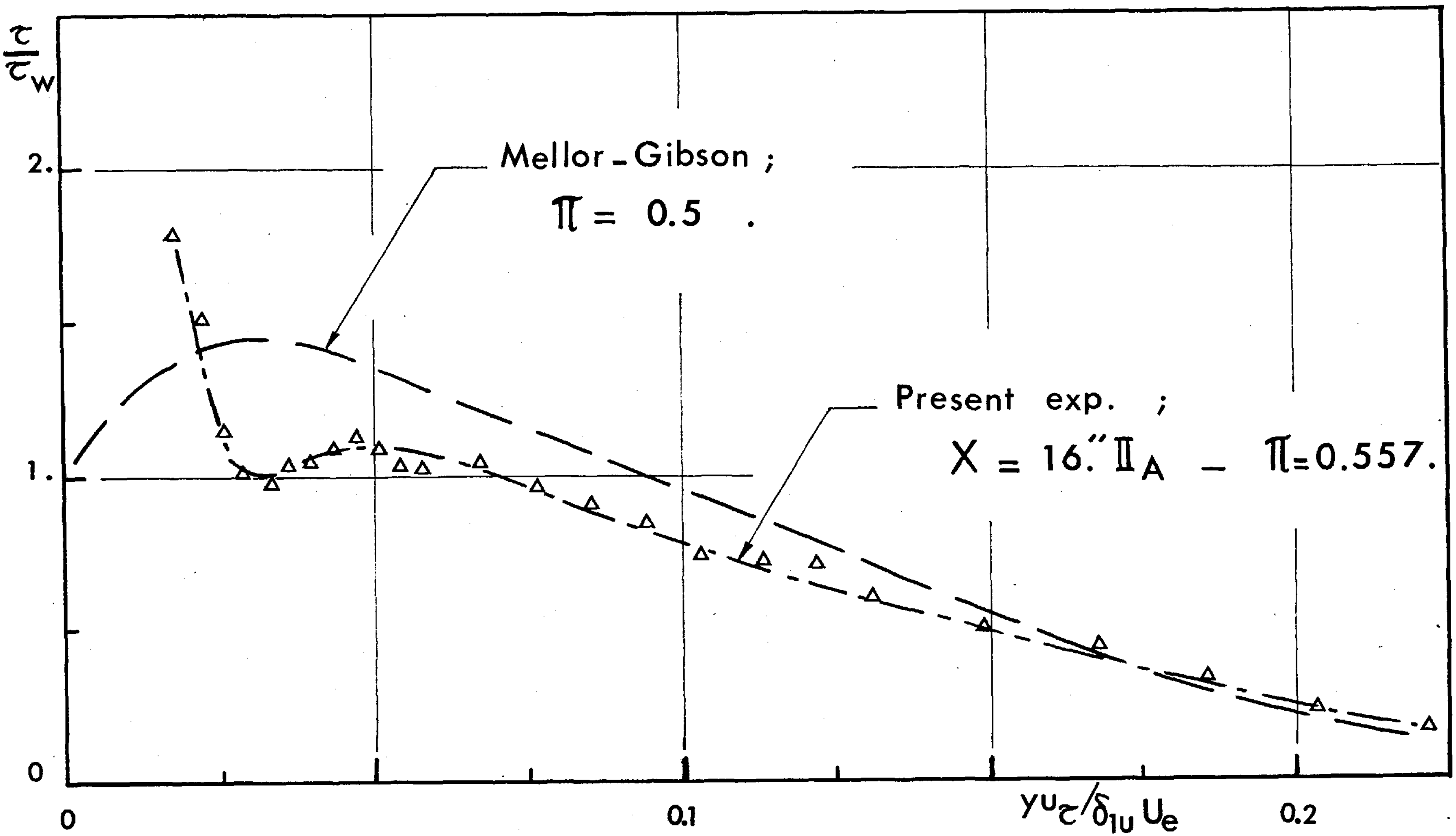

Fig. III.4.5 – Shear stress profile .

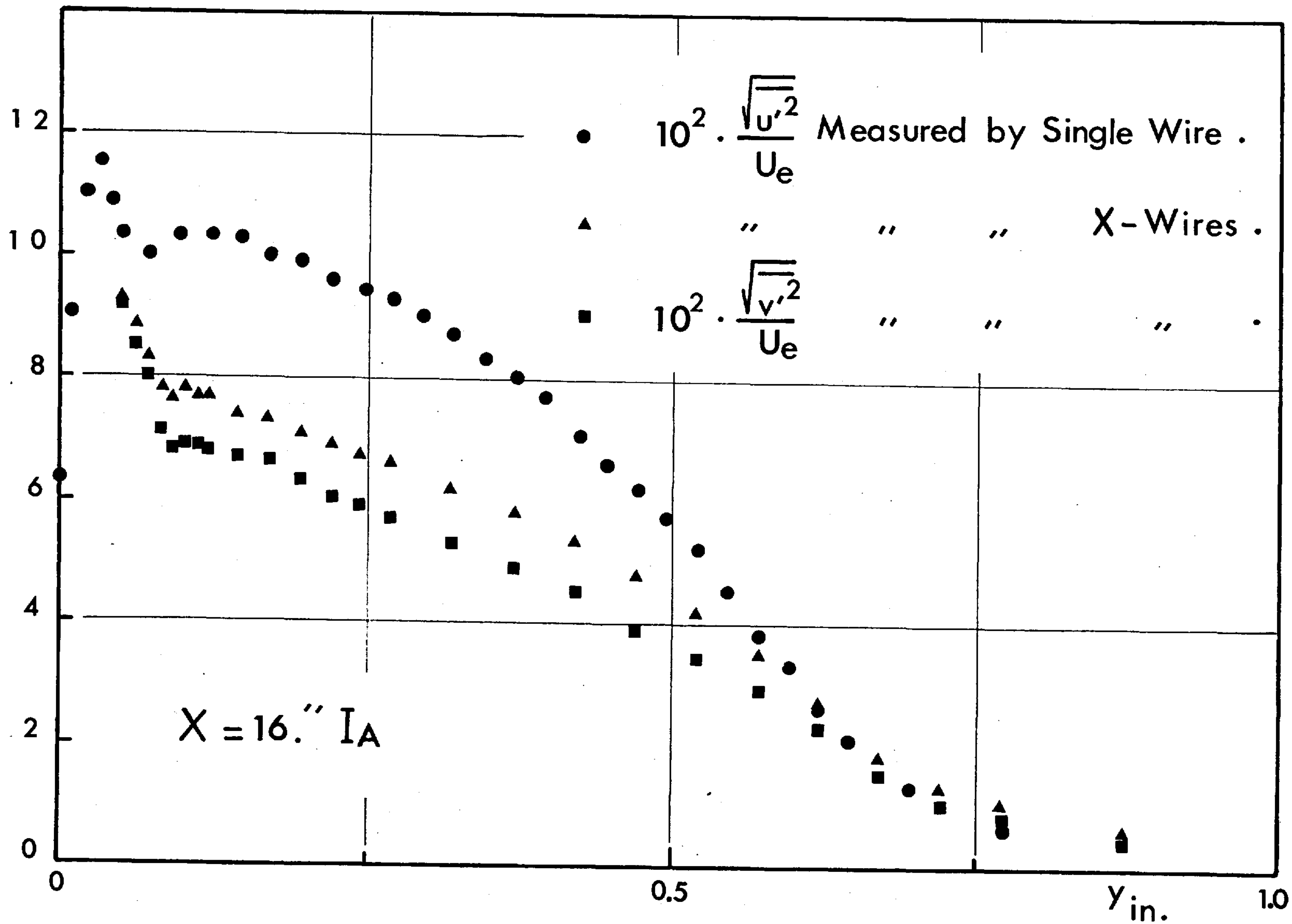

Fig. III.4.6 _ Comparison between single and X-wire results .

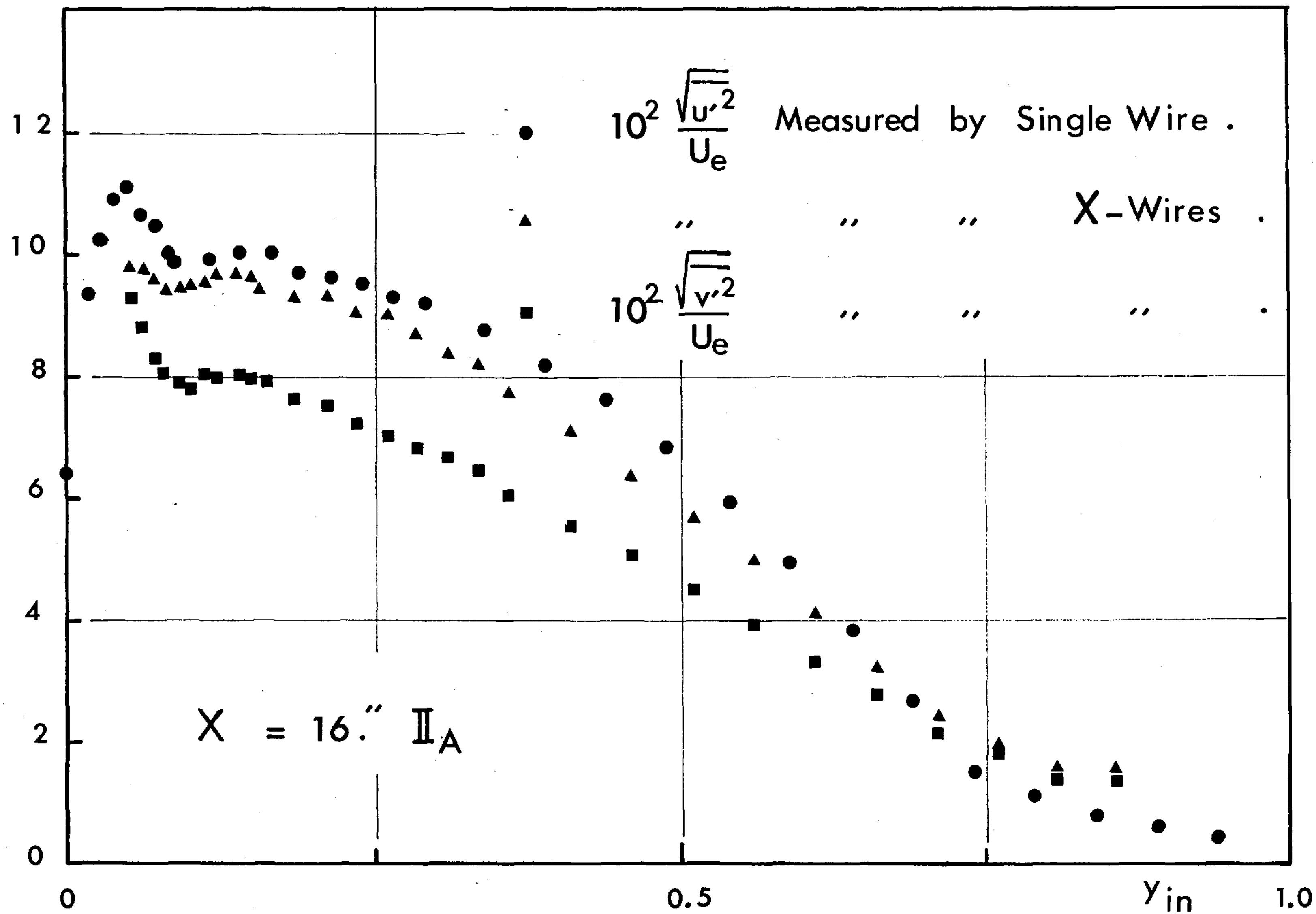

Fig. III.4.7_ Comparison between single and X-wire results .

situation represented by the finite angle between the characteristics is the finite angle of spread of contaminant diffusing from a point source". It was also noted that for homogeneous turbulence, the standard deviation of such a contaminant wake is $\left[\sqrt{\overline{v'^2}}/U\right]\cdot(x-x_o)$ for small values of $(x-x_o)$.

If we consider the spread of fluctuations above the crests, discussed earlier in § III.4.1, the presently found width of peak behind the roughness elements agrees qualitatively with the local values of $\left(\sqrt{\overline{v'^2}}/U\right)(x-x_o)$. The suggested method was applied to smooth surfaces, and agreed satisfactorily with experimental results.

The application of the characteristics method could be extended to rough surfaces, if the functions introduced in the analysis, a_1, L and G defined by:

$$a_1 = \tau / \rho \, \overline{q'^2} ,$$
$$L = L\left(\frac{y}{\delta}\right) = (\tau/\rho)^{3/2} / \nu \, \overline{\left(\frac{\partial u_i'}{\partial x_j}\right)^2} ,$$
$$G = G\left(\frac{y}{\delta}\right) = \left[\frac{\overline{p'v'}}{\rho} + \frac{1}{2}\,\overline{q'^2 v'}\right] \Big/ \left(\frac{\tau_{max}}{\rho}\right)^{\frac{1}{2}} \cdot \frac{\tau}{\rho} ,$$

with,
$$\tau = -\rho\,\overline{u'v'}$$
$$\overline{q'^2} = \overline{u'^2} + \overline{v'^2} + \overline{w'^2}$$

are modified to suit the particular case of a rough surface.

The modification of 'G' may prove to be unnecessary, but a, which was taken constant equal to 0.15 may be slightly reduced*. It is most important that the function $L\left(\frac{y}{\delta}\right)$ describing the dissipation length parameter should be superimposed by a "peak function", spread over the roughness-dominated region $\left(0 < \frac{y}{\delta} \leqslant 0.08\right)$. The maximum value of L is thought to be unconditioned by the local value of $\partial U/\partial y$ only.

It is understood that such an extension of the method to rough surfaces is intended. It is recommended that more measurements of the turbulent quantities should be carried out in the roughness dominated-region and above the crests.

*depending on $\overline{w'^2}$ which was not measured in the present study.

III.4.3 - <u>Effect of abrupt change in surface roughness</u>:

The effect of abrupt change in surface conditions was studied earlier by Jacobs (1) in channel flow, and by Townsend (31) for large scale (meteorological) boundary layers.

In the present experiments, the surface roughness was eliminated temporarily by covering part of the plate with self-adhesive polythene sheet.

Some measurements were taken in I_A and II_A for boundary layers undergoing the change from smooth to rough surface or vice versa.

The measurements obtained are shown on Fig.III.4.8 to III.4.11.

The effect of surface change is seen on these figures to penetrate in the boundary layer from the surface outwards, until eventually, after a considerable distance from the origin of surface change, the variation of the shear-stress across the boundary layer becomes fully representative of the local surface conditions.

This agrees with the behaviour of results obtained by both Jacobs and Townsend. The effect of surface change would not, in general, depend considerably upon the outside flow conditions, as it can be seen from Fig.III.4.12. The presently applied pressure gradients had little effect on the

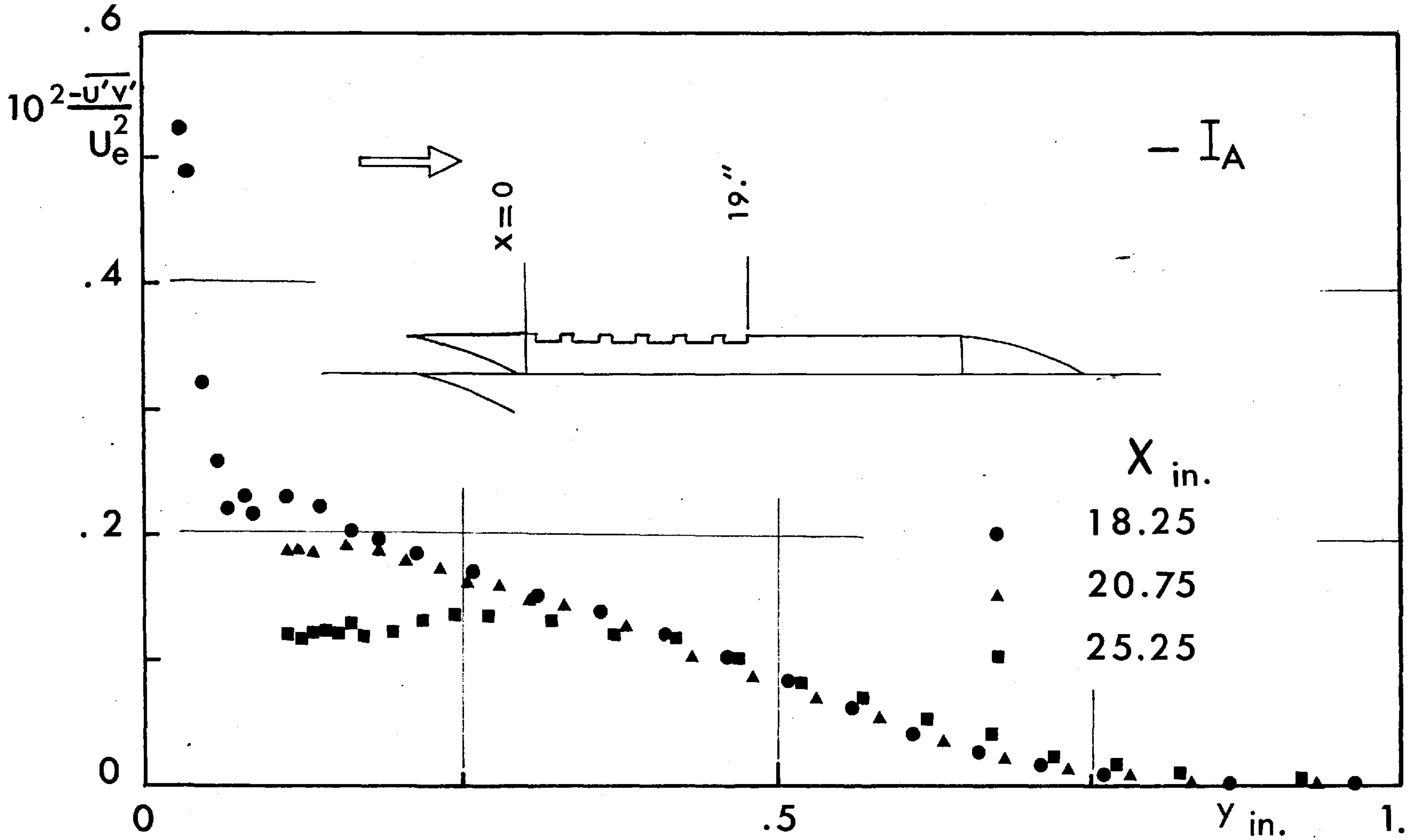

Fig. III.4.8 _ Effect of abrupt change in surface roughness .

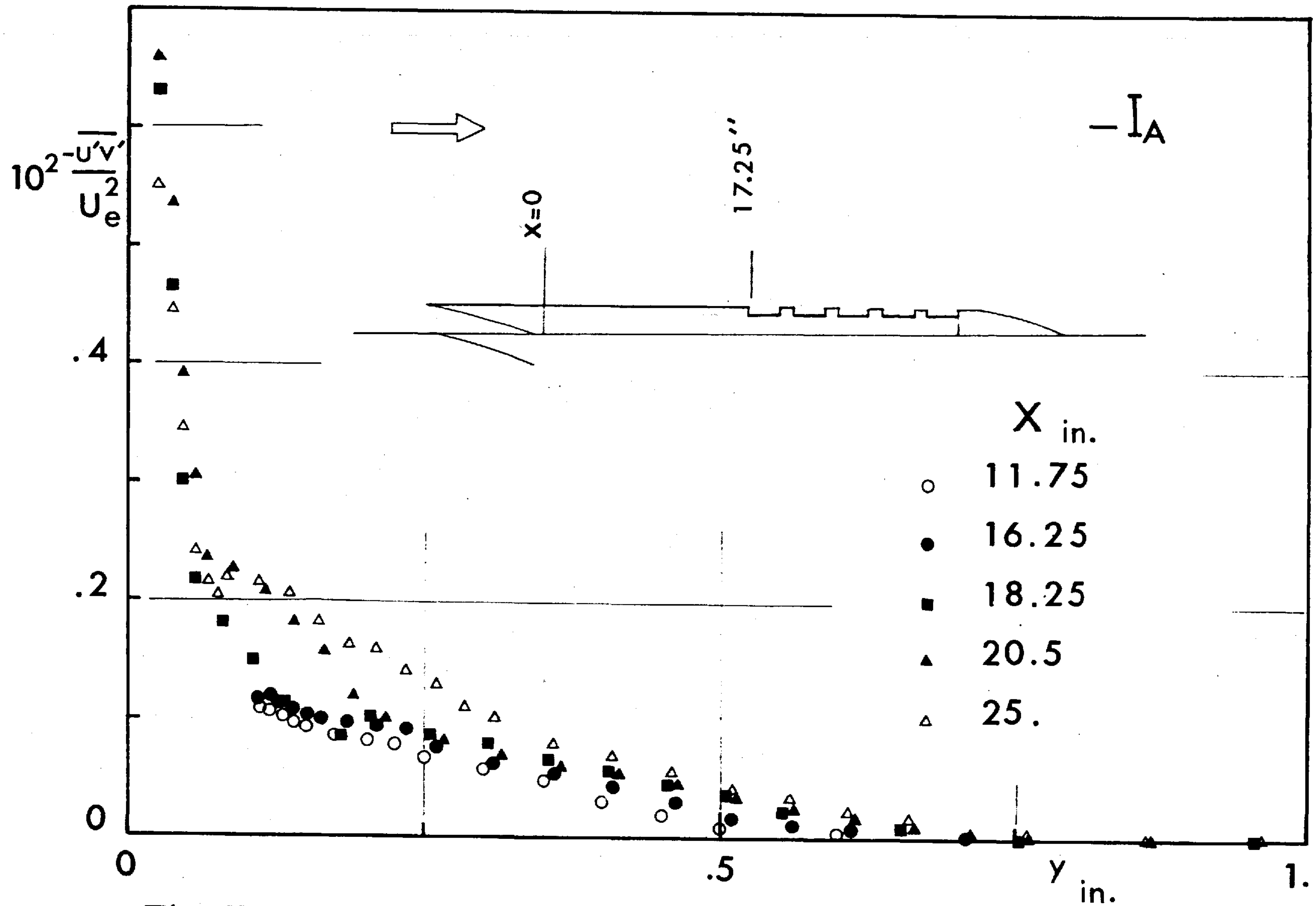

Fig. III.4.9 _ Effect of abrupt change in surface roughness .

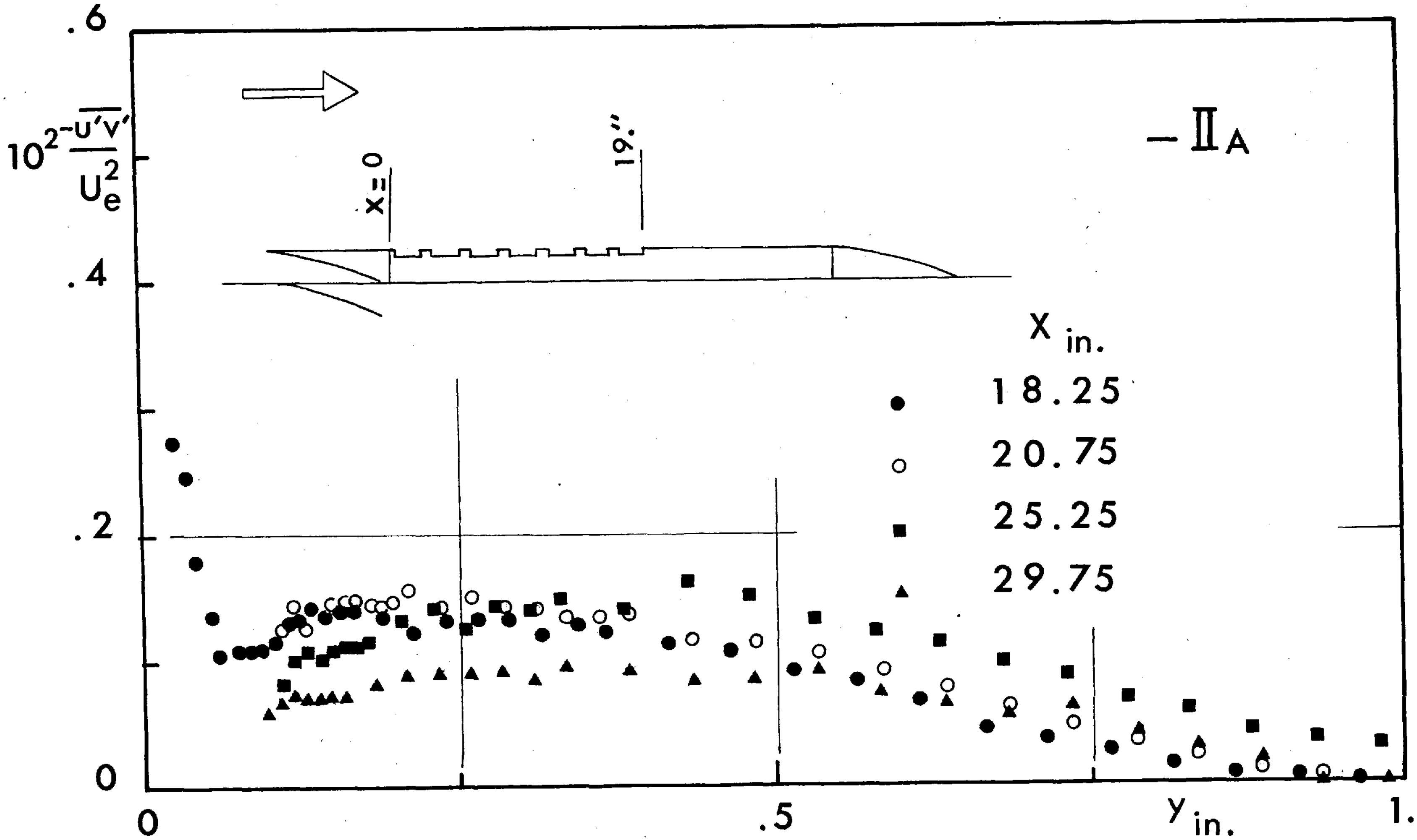

Fig. III.4.10 _ Effect of abrupt change in surface roughness .

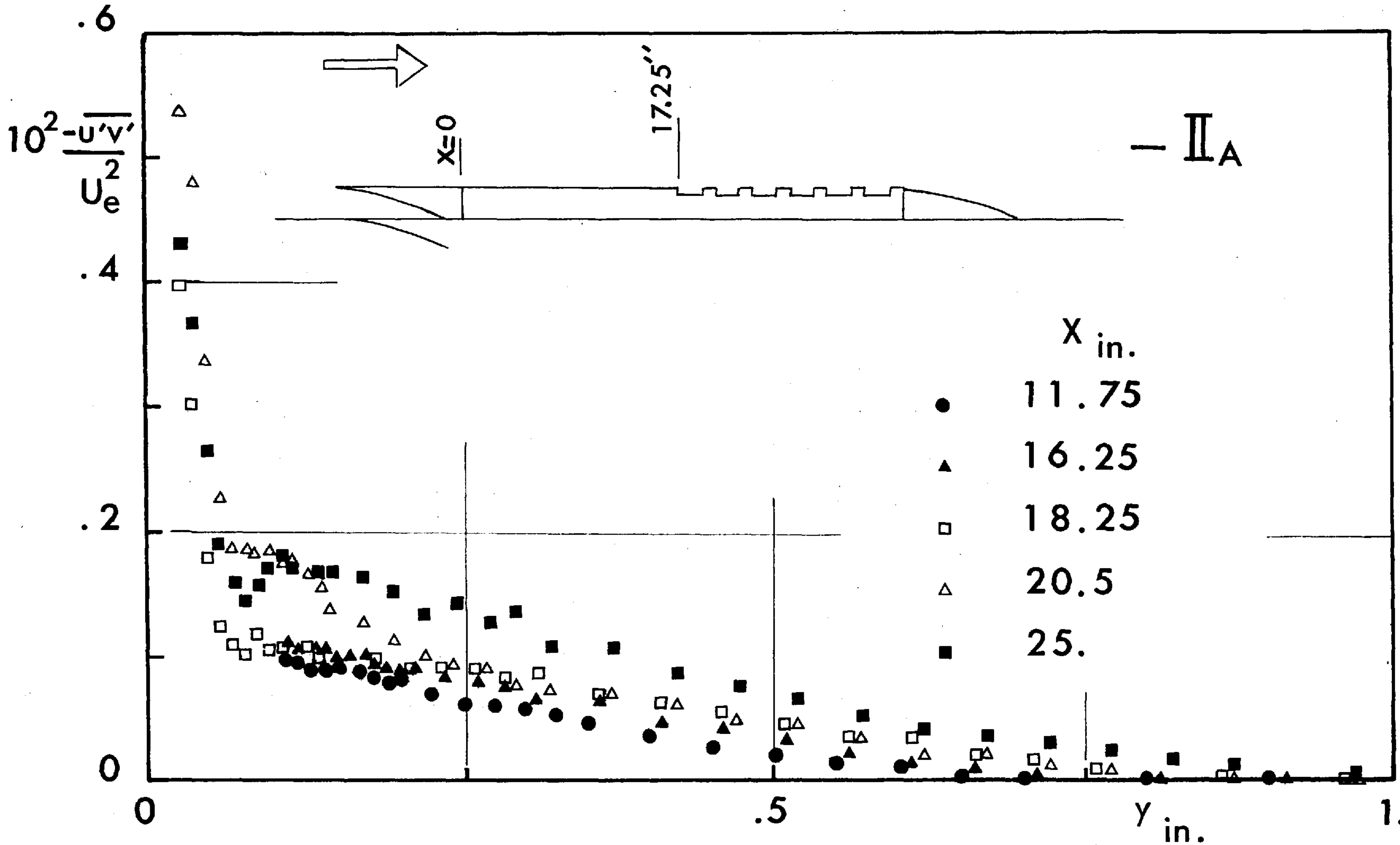

Fig. III.4.11 _ Effect of abrupt change in surface roghness .

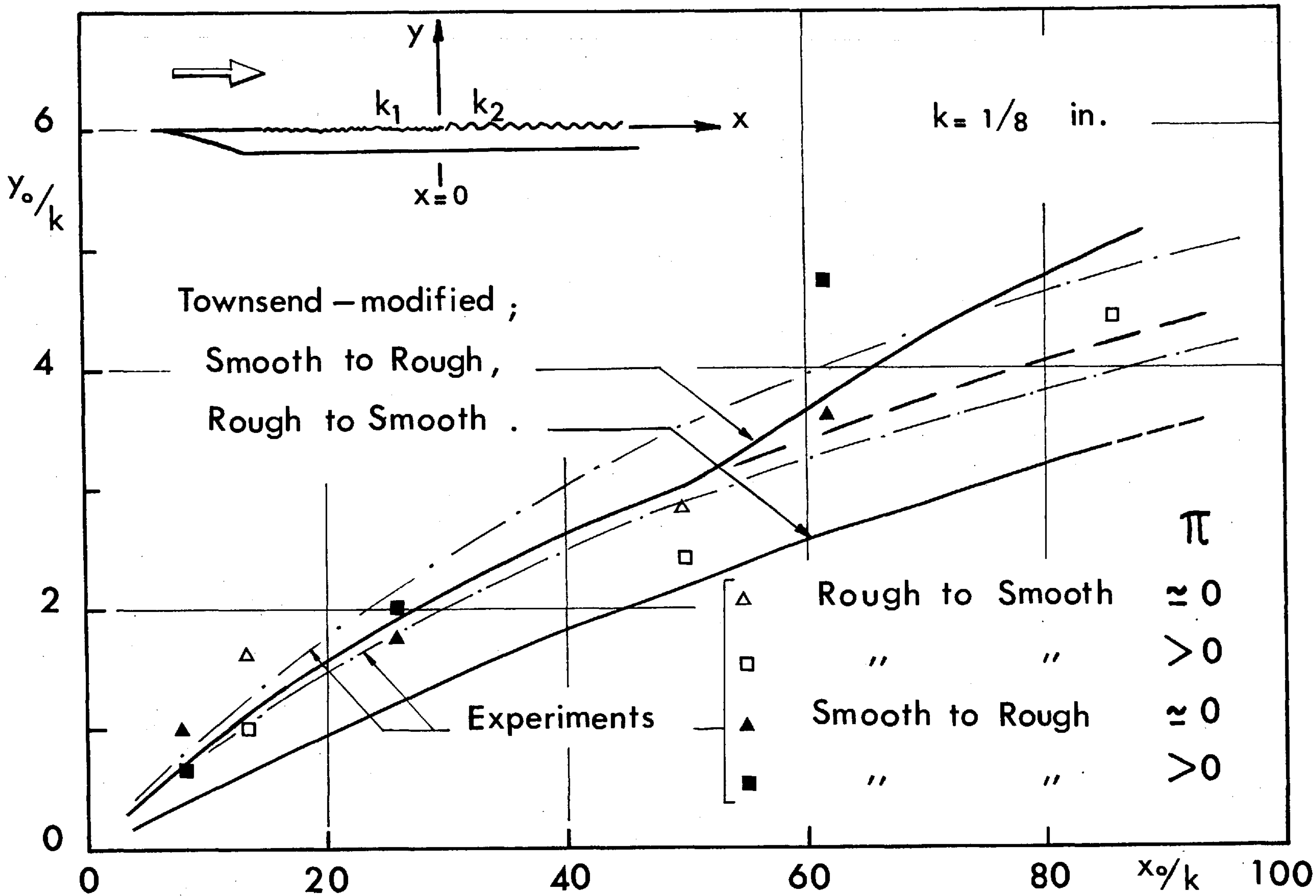

Fig. III.4.12 – Penetration of the effect of abrupt change in surface roughness .

penetration of the effect of surface change in the boundary layer, in the range of this study. In his paper, Townsend (31) explained that a parcel of fluid entering a region of changed rate of strain cannot experience noticeable change in turbulent energy in less time than its turbulent energy $\left(\simeq 3u_\tau^2\right)$ devided by the rate of energy dissipation $\left(= \frac{u_\tau^3}{\kappa y}\right)$. In that time, the parcel would have moved a distance along X equal to the time multiplied by $U(y)$.

He also explained that the same argument applies to fluid parcels at distances which are large, compared with $\frac{3\kappa y}{u_\tau} \cdot U(y)$ which acquire Reynolds stresses according to local rates of shear.

Townsend assumed a velocity profile of the form,

$$U = \frac{u_\tau}{\kappa} \log \frac{y}{k_0}$$

where k_0 is the local roughness height.

This predicted smaller values of X than the presently found.

Considering the range covered in the present study, it was thought suitable to assume, for a rough surface, that the velocity profile takes the form,

$$\frac{U}{u_\tau} = 5.75 \log \frac{y}{k_s} + 8.5 ,$$

where k_s is the equivalent sand-roughness height which was found half the depth of cavities approximately.

This would then result,

$$\left[\frac{x_o}{k}\right]_{\substack{\text{Smooth}\\ \text{to}\\ \text{Rough}}} = 1.2\,\frac{y_o}{k}\left[5.75\log\frac{2y_o}{k} + 8.5\right].$$

Similarly, for a smooth surface, the law of the wall seems an obvious choice, and,

$$\left[\frac{x_o}{k}\right]_{\substack{\text{Rough}\\ \text{to}\\ \text{Smooth}}} = 1.2\,\frac{y_o}{k}\left[5.6\log\frac{y_o u_\tau}{\nu} + 5.1\right].$$

The two relations are shown on Fig. III.4.12, and suggest reasonable agreement with the results obtained.

It might be noted that the analytical curve $\frac{y_o}{k}\left(\frac{x_o}{k}\right)$ for the case 'Smooth to Rough' show a deviation at $y_o/k \simeq 3$. This is only caused by the deviation of the velocity profiles themselves from the linear semi-logarithmic relation suggested above. The relation 'Rough to Smooth' was calculated for a single value of $\frac{u_\tau}{\nu}$ chosen to be 2×10^4, which corresponds to a value of $C_f \approx 2 \times 10^{-3}$.

The present modification is limited by the validity of the suggested forms of velocity profiles, and can only be applied near the origin of surface change, as it is the case here.

III.5 - Comparison between Roughness Geometries:

The selection of a particular type of roughness to suit or to avoid a certain function, depends on its friction and heat characteristics. It is then thought that a scale of comparison needs to be set up for both qualities of momentum and heat transfer of a rough surface.

The obvious momentum scale is thought to be the equivalent height of sand roughness, while the Nusselt number of a smooth surface is chosen for the heat transfer.

The essential difference between a rough and a smooth surface is the existance of eddies behind the roughness elements as described before. It is then suitable to assume that the dynamic and thermal characteristics of rough surfaces depend on these "horseshoe eddies" (24). They are supplied in energy by the outside flow and transfer heat from the surface.

The size of an eddy depends largely on the space behind the roughness elements. This in turn depends on the spacing and distribution of the roughness elements, which can be represented non-dimensionally as the ratio of pitch to height of the roughness elements D/k.

There should exist an arrangement corresponding to the formation of eddies, which could dissipate a maximum energy, as with isotropic turbulence (32). This arrangement is then expected to possessthe highest ratio of k/k_s. It is also expected to transfer heat best from the surface, thus having the highest value of Nu/Nu_o.

The above discussion is supported by Wieghardt's experiments, (33) and (1), who found that the drag of a rough plate has a peak value at a certain roughness arrangement. His roughness elements were circular cavities. However, this is contrary to what was concluded by Ambrose (15), when he experimented on circular cavities and short cylinders in pipes. Ambrose claimed that the resistance increase depends upon the ratio of area occupied by the cavities to the total area, and not related to their size or distribution.

The relation $\frac{D}{k}\left(\frac{k}{k_s}\right)$ is represented for some types of roughness geometries in Fig.III.5.1*, the data for which was taken from (1), (2), (16) and (25).

It can be seen that, at least for the geometries with enough available data, each roughness geometry has a

*A similar representation was shown in a departmental seminar at the Imperial College, given by the author in March 1965.

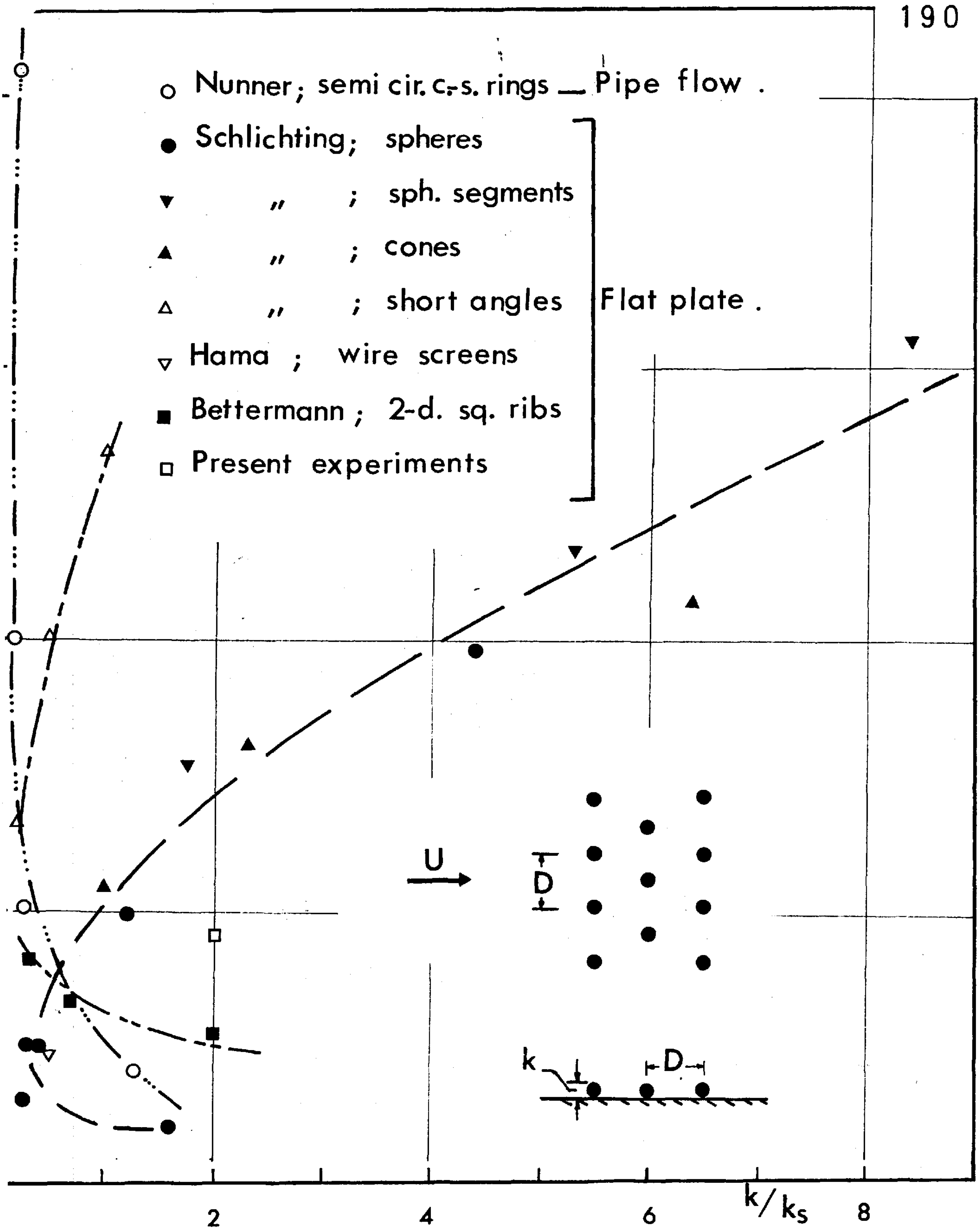

Fig. III. 5.1 _ Comparison between different roughness geometries .

minimum value of k/k_s corresponding to the "roughest" arrangement.

The results of Schlichting for spheres, cones and spherical segments were, very similar, grouped on one curve. Bettermann's results for transverse ribs seem to approach those of Schlichting for short angles.

The present experiments show "smoother" conditions than those of two-dimensional square ribs. This indicates a noticeable effect of three-dimensionality of the roughness geometry, already seen by Fig. III.2.26.

Bettermann (16) has arranged a similar group of information on a set of curves with $\frac{\Delta U}{u_\tau}$ and S_r/S *, at a particular value of $R_k \left(\equiv \frac{k u_\tau}{\nu}\right)$ following a presentation suggested by Stevenson for wire screens (4).

The same conclusions could obviously be reached by either method. The present one was retained for its clarity.

We could trace a locus of the furthest conditions from the origin of Fig. III.5.1 which satisfy the fully rough regime, whenever enough data is collected. The

* S_r being the ratio of area occupied by the roughness elements.

hydraulically smooth surface is represented by $k/k_s \to \infty$ or $D/k \to \infty$.

Richards (34) found in a recent study of roughness induced transition of boundary layers on smooth surfaces in hypersonic flow, that the type of wake generated by the roughness elements was more effective a parameter, than only the height of the elements.

This was clear after he compared transition induced on one hand by a tripping wire, and, on the other, those induced by placing some small thin rectangular triangles normal to the surface at incidence to the outside flow; or a line of small spheres.

This may be an indication that the discussion for subsonic flow, may also be valid for hypersonic speeds, since the basic form exists.

The application to low supersonic speeds may prove to be more complicated. The boundary layer then lacks the simplification of the presence of a considerably smaller mass flow layer as it is the case in hypersonic flow.

The use of rough surfaces, however, for heat exchangers and similar applications may require the increased heat transfer qualities of the surface, with a reasonable increment of the skin-friction associated with it.

It then seemed relevant to study the effect of roughness geometry, especially spacing, on the heat transfer characteristics. The values of Nu/Nuo obtained by Nunner for rough pipes (rings of semi-circular cross-section 4 mm higher than the surface of the pipe) were plotted against D/k, as shown in Fig. III.5.2.

It is then evident that the heat transfer is maximum at the same value of D/k for which k/k_s is minimum (see Fig. III.5.1).

Koch (26) has also represented the values Nu/Nuo against $\overline{m}$ for measurements of rough-pipe flow with D/k as parameter ($\overline{m}$ is the square of the ratio of the inside diameter of the pipe measured from the crest of roughness elements to that measured from the troughs). Koch found that a maximum value of Nu/Nuo exists for each value of D/k at $\overline{m} \simeq 0.3$.

The values of D/k covered on the presentation of Koch ranged from 10 to 200, with Nu/Nuo, for a certain value of $\overline{m}$, decreasing as D/k increases. As he had represented earlier the resistance coefficients as a function of D/k, for different values of $\overline{m}$ as parameter, it was seen that the resistance coefficients pass by a maximum at D/k $\simeq$ 10, similar to Nunner's experiments. It is then reasonable to

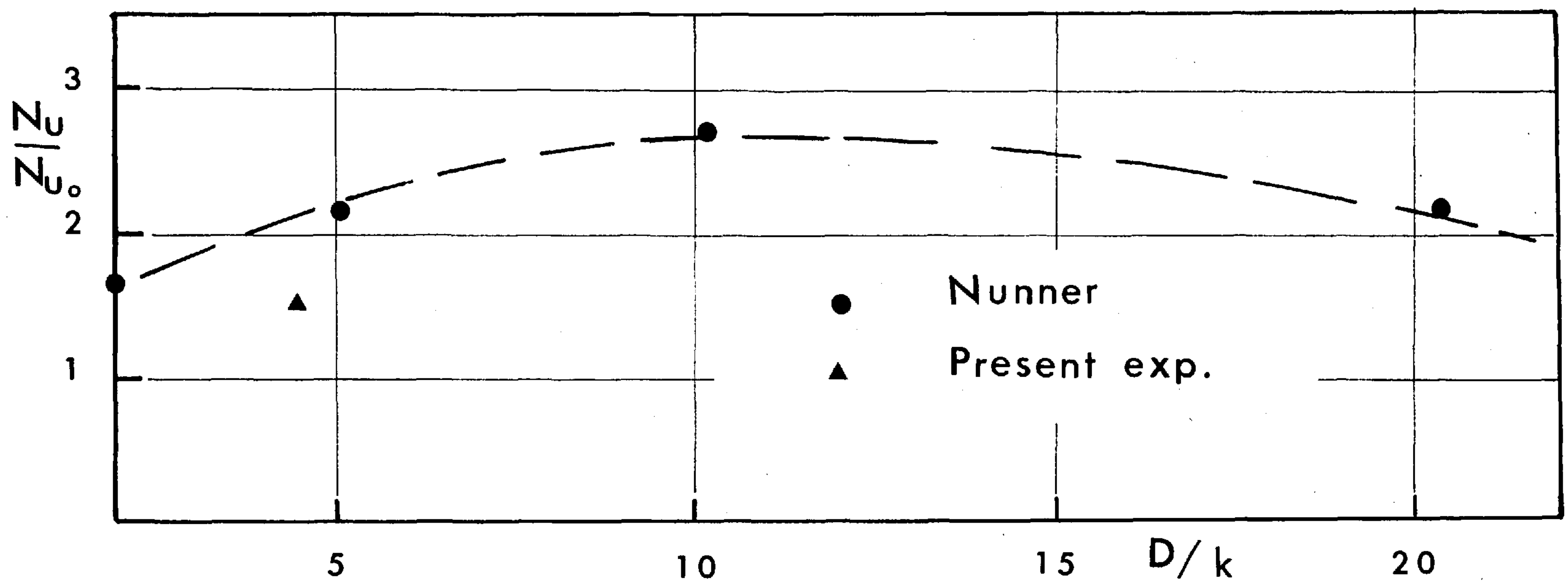

Fig. III.5.2 _ Effect of roughness-spacing on heat transfer .

assume that, for the values of D/k less than 10, the curves of Nu/Nuo are lower than that for $D/k \simeq 10$.

This means that there exists a certain roughness arrangement for which Nu/Nuo is maximum-maximum. This would be, in Kock's case, the roughness satisfying both $D/k \simeq 10$ and $\bar{m} \simeq 0.3$*. The friction coefficient is also expected to be at utmost height.

Nunner's experiments were plotted in the form $(Nu/Nu_o)[k/k_s]$ on Fig. III.5.3. It is then clear that the increase in friction is more important than the increase in heat transfer.

* For flat plates the two conditions would be a value of D/k at a certain height k.

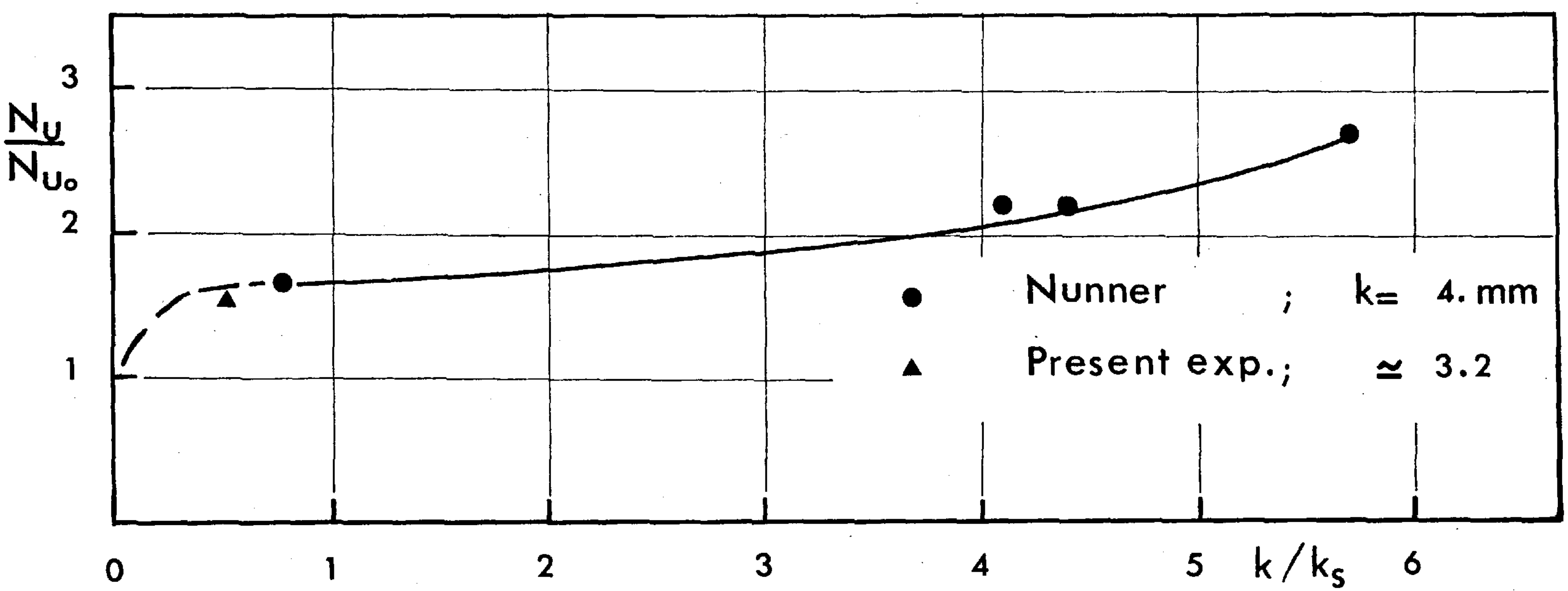

Fig. III.5.3 _ Comparison between the variation of effective roughness and the increase in heat transfer .

IV - CONCLUSIONS

IV.1 - Concluding Remarks:

The following conclusions are deduced from the present work, which was carried out to examine the behaviour of boundary layers on a surface with square cavities as roughness elements, in the presence of pressure gradient and surfacing heating.

1. The velocity profiles behind roughness elements, whether cavities of protrusions, take similar forms, and the origin of the profiles is situated below the crest of the protrusion or the top of cavity,

2. The effect of surface heating on the skin-friction coefficients depends on the pressure gradient present, whether negative, zero or positive,

3. The form of the velocity profile which had the greatest application in the experiments of the present work, was the velocity-defect profile, with G as parameter,

4. The relation G (π) for a rough surface need not be similar to that of a smooth surface. This is due to the velocity profile shape factor Hu being higher than that of a smooth surface. Generally, higher values of G are found,

5. The effect of pressure gradients applied in the present experiment on the heat-transfer coefficients were very small, especially when compared with their effect on the skin-friction coefficients. The effect of surface temperature gradient was more important,

6. The form of the temperature profile which had the greatest application in the experiments of the present work, was the temperature-defects profile, with $2 S_t / C_f$ as parameter.

7. The peak of longitudinal fluctuations found in the viscous sublayer over smooth surfaces is smaller in width than that found with the rough surface tested,

8. In the range of the present experiments, the effect of pressure gradients on the longitudinal fluctuations was very small, especially near the wall,

9. τ / τ_w as measured across the boundary layer over the present surface was similar to that of a smooth surface, except in the vicinity of the origin. Here the values were considerably higher than those of the smooth surface,

10. The penetration of the effect of abrupt change in surface conditions spreads from the surface, with small effect from the presently applied pressure gradients,

11. It seems by comparison of the present results with those obtained for two-dimensional roughness geometries, that the three-dimensionality of the roughness elements reduces the friction and, perhaps, increases the heat coefficients,

12. There exists a certain roughness arrangement for each goemtry which renders the maximum skin-friction and heat-transfer coefficients.

IV. 2 - Suggestions for Future Work:

A few suggestions will now be given for the extension of the work. They include the following fields;

1. Spectrum analysis of the fluctuating velocity components for various roughness geometries under different conditions of pressure gradients,

2. The behaviour of G (π) relationship, with values of π higher than the presently achieved,

3. The development and verification of the proposed temperature-defect presentation,

4. The temperature fluctuation measurement and their correlation with those of the velocity,

5. The development of a characteristics method for the prediction of heat transfer,

6. The development of an accurate measuring technique with the characteristics of drift-free and robustness.

V - REFERENCES

1. H. SCHLICHTING: "Boundary layer theory", Trans. by J. Kestin, McGraw-Hill (1960).

2. F.R. HAMA: "Boundary layer characteristics for smooth and rough surfaces". Soc. of Naval Arch. and Marine Eng.Trans. - Vol. 62 p.333 (1954).

3. G. BRUNELLO: "Contribution à l'étude de la convection forcée de la chaleur sur des parois rugueuses", Pub. Sc. et Tech. du Min. de l'Air (France) No.332 (1957).

4. J. DOENECKE: "Contribution à l'étude de la convection forcée turbulente le long de plaques rugueuses", Dr. Ing. Thesis, Paris Univ. (1963).

5. A.E.PERRY and P.N.JOUBERT "Rough-wall boundary layers in adverse pressure gradients", J.F.M. - Vol.17 part 2 (Oct 1963).

6. D.Bettermann: F. BRUN, and P. GOUGAT "Distribution des vitesses et des températures dans la couche limite des plaques rugueuses", Compte Rendue Acad. des Sc. Paris - Vol. 258-4 p 1151 (Jan. 1964).

7. DISA "Constant temperature anemometer type 55 A 01 description and operating instructions manual".

8. R.D. COOPER and M.D. TULIN "Turbulence measurements with hot-wire anemometer", AGARDograph 12.

9. SUNG-CHING LIN: "Measurement of flow characteristics by the hot film technique", Ph.D.Thesis, Iowa Univ. (1955).

10. DISA "Random signal indicator and correlator type 55 A 06 description and operating instructions manual".

11. CAPE IND. and ASBESTOS PRODUCTS LTD. "Caposite", Catalogue No. CAC/2/3/62.

12. C.A.G. WEBSTER : "An Experimental study of turbulence in a density stratified shear flow", Chapter III, Ph.D.Thesis, Manchester Univ. (1962).

13. M.I.I.RASHED: "Two dimensional boundary layers with heat and mass transfer", Copyright 1963 by the author.

14. P.BRADSHAW: and R.F.JOHNSON "Turbulence measurements with hot wire anemometers", Notes on App. Sci. No.33 (1963).

15. H.H. AMBROSE: The effect of character of surface roughness on velocity distribution and boundary resistance", Tennessee Univ. Rep. - Contract Nonr 811/03, Office of Nav. Res. USA (1953).

16. D.BETTERMANN: "Contribution à l'étude de la couche limite turbulente le long de plaques rugueuses", Rep. No. 65-6 C.N.R.S. Meudon (June 1965).

17. C.T.HEWSON: "The growth and separation of a turbulent boundary layer", Ph.D.Thesis, Cambridge Univ. (1949).

18. F.H. CLAUSER: "Turbulent boundary layers in adverse pressure gradients", Jour. of Aero Sci. - Vol. 21 no 2 (1954).

19. R.MICHEL: "Resultats sur la couche limite turbulente aux grandes vitesses", Pub. O.N.E.R.A. No. 102 (1961).

20. J.C. ROTTA: "Incompressible turbulent boundary layers", Coll.Inter. du C.N.R.S. No. 108, Mech. de la turbulence, Marseille (1961).

21. G.L. MELLOR and D.M.GIBSON "Equilibrium turbulent boundary layers", J.F.M. - Vol. 24 part 2 (Feb 1966).

22. G.L.MELLOR "The effect of pressure gradients on turbulent flow near a smooth wall", J.F.M. - Vol. 24 part 2 (Feb 1966).

23. J.F. NASH: "A note on skin-friction laws for incompressible turbulent boundary layers", N.P.L. Aero Rep. 1135 (1964).

24. P.R.OWEN and W.R.THOMSON "Heat transfer across rough surfaces", J.F.M. - Vol.15 part 3 (March 1963).

25. W. NUNNER: "Wärmeübergang und Druckabfall in Rauhen Rohren", VDI Forschungsheft 455, Ausgabe B, Band 22 (1965).

26. R.KOCH : "Druckverlust und Wärmeübergang beiverwirbelter Strömung", VDI Forschungsheft 469, Ausgabe B, Band 24 (1958).

27. J.F. NASH : "Turbulent boundary layer behaviour and the auxiliary equation", N.P.L. Aero Rep. 1137 (1965).

28. J. KESTIN : and P.D.RICHARDSON "Heat transfer across turbulent incompressible boundary layers" , Int. J.H.M. Transfer - Vol. 6 p.147 (1963).

29. R.G. DEISSLER : "Analysis of turbulent heat transfer, masstransfer, and friction in smooth tubes at high Prandtl and Schmidt numbers, NACA TN 3145 (1954).

30. A.I.El-GAWHARY: "Turbulent flow past rough walls and the movement of grains on stream beds", Ph.D.Thesis, London Univ. (1963).

31. A.A. TOWNSEND: "Self-preserving flow inside a turbulent boundary layer", J.F.M. - Vol 22 part 4 (1965).

32. J.O. HINZE : "Turbulence - An introduction to its mechanism and theory", McGraw-Hill (1959).

33. K. WIEGHARDT : "Erhöhung des Turbulenten Reibungswiderstandes durch Oberflächenströrungen", Forschungshafte für Schiffstechnik 1, p 65-81 (1953).

34. B.E.RICHARDS : Private communication (1965).

35. E.A. BRUN : "Introduction à l'étude de la couche limite". Gauthier-Villars (1955).

36. P. BRADSHAW and D.H. FERRISS : "The response of a retarded equilibrium turbulent boundary layer to the sudden removal of pressure gradient", N.P.L. Aero Rep. 1145 (1965).

37. P. BRADSHAW : "Inactive motion and pressure fluctuations in turbulent boundary layers", N.P.L. Aero Re . 1172 (1965).

38. P. BRADSHAW : D.H. FERRIS, and N.P. ATWELL "Calculation of boundary layer development using the turbulent energy equation", N.P.L. Aero Rep. 1182 (1966).

39. P. BRADSHAW : "The turbulence structure of equilibrium boundary layers", N.P.L. Aero Rep. 1184 (1966).

40. D. COLES : "The law of the wake in turbulent boundary layer", J.F.M. - Vol. 1 part 2 (1956).

41. M.W. RUBESIN : "The effect of an arbitrary surface - temperature variation along a flat plate on the convective heat transfer in an incompressible turbulent boundary layer", NACA TN 2345 (1951).

42. D.B. SPALDING : "Heat transfer to a turbulent stream from a surface with a stepwise discontinuity in wall temperature", Int. Dev. in Heat Transfer Part II p 439, ASME (1961).

43. D.S. JOHNSON: "Velocity and temperature fluctuation measurement in a turbulent boundary layer downstream of a stepwise discontinuity in wall temperature", J. App. Mech. - Vol. 26 pp 325-336 (1959).

44. E.R.G. ECKERT, J.P. HARTNETT, and R. BIRKEBAK "Simplified equations for calculating local and total heat flux to nonisothermal surfaces", J. Aero. Sci. - Vol. 24 pp 549-551 (1957).

45. W.J. McCROSKEY: "Effect of a stepwise distribution of heat transfer on the supersonic flow over a flat plate", TCEA NT 13 (1963).

LIST OF FIGURES

APPENDIX I

I.1 - CASE I_A - Favourable Pressure Gradient, with No Surface Heating

x	δ_1	δ_2	δ_3
2.5	0.0735	0.044	0.075
4.75	0.0915	0.0543	0.0908
7.0	0.104	0.0612	0.102
9.25	0.1237	0.0713	0.1183
11.5	0.1341	0.079	0.1316
13.75	0.1517	0.09	0.1494
16.0	0.1587	0.093	0.1546
18.25	0.165	0.0974	0.1621
20.5	0.183	0.1098	0.183
22.75	0.1851	0.1141	0.1915
25.0	0.2003	0.1205	0.2014
27.25	0.1931	0.1209	0.2048
29.5	0.1945	0.124	0.2106
31.75	0.2056	0.1312	0.2236
34.0	0.2025	0.132	0.2269

* All values in Appendix I are in inches.

I.2 - CASE I_B - Favourable Pressure Gradient, with Isothermal Heating

x	δ_1	δ_2	δ_3	δ_{1u}	δ_{2u}	δ_{3u}	Δ_1	Δ_2
4.75	0.1009	0.0481	0.0799	0.0955	0.0499	0.0826	0.0519	0.028
9.25	0.1286	0.0674	0.1132	0.1201	0.0702	0.1175	0.0748	0.0441
18.25	0.1807	0.0985	0.1663	0.1673	0.1026	0.1729	0.1111	0.0697
20.5	0.1897	0.1045	0.1773	0.176	0.1088	0.1842	0.1181	0.073
22.75	0.1944	0.1045	0.1765	0.1807	0.1091	0.1838	0.1317	0.0778
25.	0.204	0.1123	0.1909	0.1878	0.1173	0.1989	0.1287	0.0813
29.5	0.2172	0.121	0.2072	0.1966	0.1268	0.2167	0.161	0.1063
31.75	0.2311	0.1296	0.2211	0.2138	0.135	0.2296	0.1417	0.0888

I.3 - CASE I_C - Favourable Pressure Gradient, with Step Heating

x	δ_1	δ_2	δ_3	δ_{1u}	δ_{2u}	δ_{3u}	Δ_1	Δ_2
4.75	0.1019	0.0534	0.0898	0.0961	0.0554	0.0929	0.0537	0.0302
9.25	0.1331	0.0701	0.1168	0.1268	0.0724	0.1203	0.0588	0.0319
11.5	0.1376	0.075	0.1264	0.1294	0.0779	0.1309	0.0704	0.0409
13.75	0.1483	0.0817	0.1383	0.1377	0.0852	0.1439	0.0849	0.0516
16.	0.1655	0.0886	0.1501	0.1535	0.0924	0.1561	0.0897	0.0534
18.25	0.1559	0.0868	0.1497	0.1404	0.0913	0.1569	0.0895	0.0586
20.5	0.1752	0.0959	0.1653	0.157	0.1012	0.1738	0.0895	0.058
22.75	0.2047	0.1059	0.1793	0.1844	0.1121	0.1891	0.1024	0.0637
25.	0.2143	0.1135	0.1929	0.1939	0.1197	0.2029	0.1053	0.0656
27.25	0.2232	0.121	0.2058	0.2028	0.1274	0.216	0.1107	0.0688
29.5	0.2402	0.1272	0.2168	0.2157	0.1345	0.2285	0.1209	0.0764
31.75	0.2314	0.1259	0.2162	0.2085	0.1327	0.2272	0.1132	0.0720

I.4 - CASE II_A - Adverse Pressure Gradient, with No Surface Heating

x	δ_1	δ_2	δ_3
2.5	0.0674	0.0416	0.0713
4.75	0.0959	0.0553	0.0923
7.	0.11	0.0618	0.1031
9.25	0.1161	0.0717	0.1207
11.5	0.1448	0.0812	0.1341
13.75	0.1693	0.0977	0.1613
16.	0.1899	0.1071	0.1763
18.25	0.214	0.121	0.1983
22.75	0.2518	0.1448	0.2379
25.	0.2718	0.1564	0.2578
27.25	0.3035	0.1766	0.2909
29.5	0.2993	0.1733	0.2849
31.75	0.2949	0.1778	0.2952

I.5 - CASE II_B - Adverse Pressure Gradient with Isothermal Heating

x	δ_1	δ_2	δ_3	δ_{1u}	δ_{2u}	δ_{3u}	Δ_1	Δ_2
4.75	0.101	0.0519	0.0873	0.0949	0.0539	0.0904	0.0623	0.0355
7.	0.1249	0.0644	0.108	0.1184	0.0668	0.1116	0.0622	0.0336
9.25	0.128	0.0695	0.1166	0.1206	0.072	0.1206	0.0709	0.0415
11.5	0.1644	0.0821	0.1347	0.1574	0.0848	0.1388	0.0789	0.04
13.75	0.1758	0.0934	0.1544	0.1671	0.0965	0.1594	0.0885	0.0494
18.25	0.2304	0.1182	0.1951	0.2165	0.1233	0.2029	0.135	0.0755
22.75	0.248	0.1394	0.235	0.2345	0.1439	0.2421	0.111	0.0666
25.	0.2617	0.1521	0.2573	0.2474	0.1567	0.2646	0.1314	0.0812
31.75	0.3081	0.1711	0.287	0.2906	0.1771	0.2963	0.1472	0.0876

I.6 - CASE II_C - Adverse Pressure Gradient, with Step Heating

x	δ_1	δ_2	δ_3	δ_{1u}	δ_{2u}	δ_{3u}	Δ_1	Δ_2
4.75	0.1012	0.0536	0.0899	0.0962	0.0555	0.0927	0.0522	0.0285
9.25	0.1572	0.0792	0.1295	0.151	0.0817	0.1333	0.0637	0.0323
13.75	0.2003	0.0993	0.1609	0.1934	0.1023	0.1653	0.0735	0.0354
18.25	0.2521	0.1243	0.201	0.2405	0.1292	0.2083	0.0978	0.0492
22.75	0.3013	0.1495	0.2434	0.2847	0.1559	0.2531	0.1036	0.0555
27.25	0.3147	0.1601	0.2611	0.2977	0.1666	0.271	0.1069	0.0582
31.75	0.3276	0.1744	0.2899	0.3073	0.1815	0.301	0.114	0.0657

APPENDIX II

II.1 - CASE I_A

x = 2.5 ins		4.75		7.0		9.25	
Y	U	Y	U	Y	U	Y	U
0	79	0	119	0	105	0	96
10	185	10	225	10	232	10	184
20	395	20	359	20	364	20	292
30	523	30	463	30	444	30	389
40	586	40	512	40	482	40	440
50	608	50	534	65	534	50	474
75	675	70	588	90	585	70	506
100	717	95	635	115	635	95	567
125	761	120	685	140	689	120	608
150	804	145	729	165	731	145	656
175	852	170	777	190	778	170	698
200	884	195	824	215	809	195	723
225	909	220	852	240	841	220	761
250	936	245	888	265	872	245	799
275	952	270	911	290	903	270	828
300	968	295	938	315	925	295	862
325	990	320	954	340	949	320	881
350	994	345	970	365	955	345	904
375	1000	370	986	390	979	370	920
		395	996	415	992	395	950
		420	1000	440	992	420	962
				465	1000	445	970
						470	980
						495	1000

CASE I_A (Cont.)

x = 11.5 ins		13.75		16.0		18.25	
Y	U	Y	U	Y	U	Y	U
0	96	0	153	0	100	0	95
10	193	10	234	10	173	10	177
20	316	20	321	20	264	20	286
30	400	30	375	30	358	30	362
40	452	40	425	40	415	40	411
65	500	50	448	50	446	50	441
90	541	70	484	70	495	75	491
115	594	95	525	95	526	100	537
140	625	120	566	120	563	125	564
165	667	145	604	145	601	150	607
190	698	170	644	170	627	175	635
215	735	195	677	195	667	200	668
240	761	220	709	220	694	225	696
265	794	245	735	245	726	250	720
290	816	270	756	270	755	275	742
315	843	295	781	295	779	300	761
340	879	320	811	320	801	325	785
365	895	345	829	345	821	350	809
390	910	370	856	370	839	375	824
415	926	395	882	395	856	400	847
440	950	420	892	420	877	425	870
465	964	445	917	445	903	450	887
490	970	470	933	470	922	475	907
515	980	495	949	495	930	500	927
540	988	520	967	520	949	525	941
565	1000	545	975	545	955	550	949
		570	975	570	975	575	959
		595	984	595	979	600	977
		620	994	620	990	625	992
		645	994	645	1000	650	992
		670	1000			675	992
						700	1000

CASE I_A (Cont.)

x = 20.5 ins		22.75		25.0		27.25	
Y	U	Y	U	Y	U	Y	U
0	122	0	120	0	102	0	105
10	191	10	212	10	161	10	173
20	277	20	315	20	252	20	270
30	354	30	391	30	340	30	385
40	419	40	444	40	401	40	428
50	451	50	459	50	444	60	488
60	468	60	479	60	466	85	523
70	487	85	512	35	497	110	558
90	515	110	551	110	536	135	591
115	550	135	575	135	561	160	617
140	579	160	599	160	587	185	642
165	602	185	631	185	610	210	667
190	629	210	670	210	640	235	681
215	650	235	681	235	670	260	709
240	680	260	703	260	691	285	723
265	709	285	720	285	703	310	742
290	724	310	740	310	720	335	755
315	743	335	756	335	739	360	777
340	763	360	779	360	756	385	793
365	777	385	797	385	772	410	810
390	799	410	811	410	786	435	825
415	826	435	827	435	802	460	839
440	843	460	851	460	829	485	852
465	867	485	870	485	851	510	869
490	886	510	887	510	861	535	881
515	894	535	893	535	872	560	891
540	903	560	904	560	877	585	899
565	919	585	921	585	891	610	907
590	938	610	937	610	912	635	915
615	952	635	947	635	929	660	930
640	964	660	954	660	947	685	937
665	972	685	964	685	954	710	947
690	982	710	970	710	966	735	955
715	988	735	980	735	972	760	967
740	1000	760	990	760	982	785	975
		785	990	785	990	810	979
		810	1000	810	1000	835	985
						860	990
						885	998
						910	1000

CASE I_A (Concluded)

x = 29.5 ins

Y	U
0	141
10	220
20	311
30	391
40	438
65	502
90	533
115	567
140	607
165	628
190	648
215	669
240	691
265	712
290	730
315	746
340	758
365	775
390	790
415	803
440	818
465	835
490	848
515	861
540	869
565	887
590	891
615	904
640	912
665	924
690	938
715	949
740	959
765	969
790	977
815	981
840	981
865	981
890	988
915	992
940	996
965	1000

31.75

Y	U
0	122
10	190
20	274
30	366
55	479
80	522
105	555
130	582
155	614
180	646
205	656
230	679
255	696
280	715
305	735
330	749
355	765
380	778
405	794
430	807
455	820
480	838
505	849
530	853
555	859
580	866
605	882
630	895
655	905
680	914
705	922
730	930
755	936
780	944
805	954
830	960
855	970
880	976
905	984
930	994
955	994
980	994
1005	1000

34.0

Y	U
0	105
10	176
20	274
30	376
40	448
50	488
75	529
100	568
125	599
150	621
175	647
200	675
225	697
250	712
275	724
300	738
325	755
350	775
375	782
400	797
425	811
450	824
475	839
500	846
525	854
550	863
575	869
600	878
625	886
675	909
725	930
775	938
825	948
875	964
925	972
975	988
1025	1000

II.2 - CASE I_B

x = 4.75 ins

Y	U	T
0	86	483
10	123	517
20	183	569
30	287	621
40	395	655
50	484	690
60	543	724
70	566	759
85	606	795
110	655	819
135	715	845
160	768	871
185	823	888
210	861	905
235	890	922
260	929	940
285	949	957
310	959	974
335	969	983
360	979	1000
410	1000	

9.25

Y	U	T
0	107	483
10	167	509
20	255	534
30	362	569
40	454	603
50	503	638
60	540	664
70	555	690
80	566	707
100	594	733
125	642	759
150	683	784
175	710	810
200	752	828
225	779	853
250	810	871
275	834	897
300	862	914
325	901	931
350	916	948
375	932	966
425	970	983
475	980	991
525	990	1000
575	1000	

18.25

Y	U	T
0	118	483
10	190	517
20	274	552
30	366	578
40	438	603
50	465	638
60	494	655
70	501	672
95	545	690
120	584	707
145	616	724
170	648	741
195	673	750
220	699	772
245	725	793
270	742	816
295	760	828
320	778	845
345	802	853
370	815	871
395	833	888
445	871	905
495	900	922
545	935	948
595	957	966
645	969	983
695	980	991
745	990	1000
795	1000	

CASE I_B (Cont.)

x = 20.5 ins

Y	U	T
0	101	439
10	174	474
20	266	509
30	365	535
40	424	561
50	473	579
60	487	605
70	509	623
80	524	640
105	563	667
130	594	684
155	619	711
180	652	728
205	677	754
230	703	781
255	721	807
280	739	825
305	766	842
330	784	860
355	803	877
405	821	895
455	859	912
505	895	930
555	918	947
605	949	956
655	965	970
705	971	982
755	979	991
805	985	1000
855	994	
905	1000	

22.75

Y	U	T
0	145	385
10	182	404
20	222	423
30	285	442
40	342	471
50	384	500
60	442	529
70	481	558
95	554	587
120	580	615
145	624	644
170	651	673
195	669	712
220	688	740
245	717	769
270	736	798
320	746	827
370	806	846
420	847	885
470	858	913
520	890	933
570	911	962
620	944	990
670	955	1000
720	977	
770	1000	

25.0

Y	U	T
0	86	450
10	153	475
20	266	508
30	364	542
40	449	567
50	481	583
60	499	617
70	513	633
95	551	650
120	577	675
145	614	700
170	638	725
195	663	742
220	672	767
245	697	783
270	715	800
295	732	825
345	768	842
395	804	858
445	832	883
495	861	900
545	890	917
595	923	933
645	939	950
695	949	967
745	965	983
795	979	992
845	990	1000
895	1000	

CASE I_B (Concluded)

x = 29.5 ins

Y	U	T
0	109	397
10	179	431
20	299	466
30	395	500
40	456	534
50	491	560
60	506	578
70	521	586
95	559	612
120	590	638
145	614	664
170	638	690
195	663	707
220	685	724
245	697	741
270	715	759
295	723	767
345	759	793
395	795	810
445	823	828
495	851	845
545	870	862
595	899	888
645	909	914
695	935	940
745	949	957
795	959	974
845	969	988
895	975	1000
945	990	
995	1000	

31.75

Y	U	T
0	82	402
10	148	427
20	238	470
30	363	521
40	435	547
50	470	590
60	484	607
70	491	624
95	528	650
120	567	675
145	597	692
170	623	709
195	639	726
220	664	752
245	682	778
270	699	795
295	707	812
320	725	821
370	759	838
420	798	855
470	816	872
520	845	889
570	864	915
620	883	932
670	903	940
720	923	949
770	933	966
820	963	974
870	973	988
920	977	1000
970	983	
1020	1000	

II.3 - CASE I_C

x = 4.75 ins			9.25			11.5		
Y	U	T	Y	U	T	Y	U	T
0	122	466	0	108	492	0	109	483
10	189	500	10	156	525	10	181	517
20	259	534	20	243	559	20	289	550
30	365	578	30	330	610	30	387	600
40	453	629	40	409	644	40	456	642
50	528	672	50	475	678	50	516	667
60	577	707	60	511	712	60	531	683
70	616	741	70	535	746	85	579	717
95	650	784	80	551	763	110	611	750
120	684	828	90	565	788	135	645	792
145	729	862	100	582	805	160	680	817
170	765	888	125	617	831	185	715	833
195	812	905	150	669	847	210	743	850
220	841	922	175	700	873	235	770	875
245	875	940	200	725	890	260	799	900
295	931	966	225	766	907	285	808	917
345	964	983	250	789	924	335	861	942
395	983	991	275	828	932	385	907	967
445	1000	1000	325	868	949	435	948	983
			375	930	966	485	970	992
			425	957	983	535	987	1000
			475	985	1000	585	1000	
			525	1000				

CASE I_C (Cont.)

x = 13.75 ins

Y	U	T
0	134	484
10	204	516
20	301	548
30	409	581
40	459	613
50	504	637
75	567	661
100	593	694
125	633	726
150	668	758
175	694	790
200	712	815
225	740	839
250	766	855
275	797	879
300	816	895
350	855	919
400	887	944
450	926	968
500	957	984
550	972	992
600	987	1000
650	1000	

16.0

Y	U	T
0	112	433
10	162	463
20	222	507
30	306	552
40	399	582
50	465	619
60	519	642
70	536	672
80	552	694
90	565	716
100	577	739
125	603	761
150	647	776
175	673	806
200	697	821
225	721	836
275	779	866
325	819	888
375	860	910
425	891	933
475	913	955
525	936	970
575	956	985
625	978	993
675	989	1000
725	1000	

18.25

Y	U	T
0	137	503
10	224	529
20	319	567
30	415	605
40	476	643
50	533	669
60	556	688
70	575	701
95	619	720
120	655	745
145	683	764
170	720	783
195	739	803
220	761	822
245	781	834
270	791	847
295	801	860
320	822	879
345	836	892
395	864	917
445	896	936
495	928	955
545	946	975
595	962	987
645	973	994
695	991	1000
745	1000	

CASE I_C (Cont.)

x = 20.5 ins			22.75			25.0		
Y	U	T	Y	U	T	Y	U	T
0	120	521	0	103	521	0	81	505
10	183	553	10	158	543	10	144	527
20	291	585	20	233	574	20	236	559
30	393	617	30	311	606	30	343	591
40	481	649	40	392	638	40	421	624
50	522	681	50	451	681	50	471	656
60	547	707	60	479	691	60	493	677
70	556	723	70	493	707	70	504	699
80	573	734	80	514	718	80	509	710
90	582	745	90	523	729	90	523	720
115	618	761	100	538	739	115	561	742
140	655	777	125	569	750	140	590	753
165	674	793	150	600	766	165	618	774
190	702	809	175	641	777	190	643	796
215	722	819	200	659	798	215	669	806
240	752	835	225	683	809	240	686	828
265	772	851	250	705	819	265	713	839
290	788	867	275	726	835	315	742	860
315	803	878	325	771	851	365	777	876
365	834	894	375	808	872	415	814	892
415	866	915	425	836	904	465	843	909
465	888	931	475	864	915	515	872	919
515	912	947	525	894	931	565	902	935
565	932	963	575	913	947	615	922	952
615	948	979	625	943	957	665	949	968
665	959	989	675	963	973	715	955	978
715	972	995	725	971	989	765	963	984
765	982	1000	775	977	995	815	974	989
815	1000		825	988	1000	865	984	995
			875	1000		915	990	1000
						965	1000	

CASE I_C (Concluded)

x = 27.25 ins			29.5			31.75		
Y	U	T	Y	U	T	Y	U	T
0	110	506	0	90	505	0	68	503
10	179	528	10	141	537	10	128	534
20	267	545	20	229	568	20	235	566
30	360	573	30	319	600	30	345	598
40	424	607	40	388	626	40	439	630
50	470	635	50	440	653	50	471	661
60	486	652	60	471	663	60	496	672
70	510	663	70	495	679	70	504	683
80	518	680	80	511	689	80	521	693
90	535	697	90	520	695	90	538	704
100	543	708	100	536	705	115	574	725
110	552	719	110	545	721	140	604	746
135	569	742	135	576	737	165	634	767
160	613	764	160	606	753	190	657	788
185	631	787	185	630	763	215	676	804
210	649	798	210	643	779	240	686	815
235	677	815	235	661	795	265	706	825
260	687	826	260	690	811	290	726	841
285	715	843	285	699	821	315	736	852
310	725	854	310	719	837	340	752	862
335	745	871	360	754	858	365	767	878
385	784	882	410	789	874	415	794	889
435	815	899	460	820	884	465	820	899
485	836	910	510	841	905	515	852	910
535	868	921	560	862	916	565	872	926
585	900	938	610	881	932	615	885	942
635	911	955	660	905	947	665	901	952
685	933	966	710	928	958	715	919	963
735	944	978	760	948	968	765	935	974
785	962	983	810	959	974	815	953	979
835	973	989	860	966	979	865	969	984
885	984	992	910	975	984	915	976	989
935	989	997	960	982	992	965	988	995
985	993	1000	1010	986	997	1015	991	1000
1035	1000		1060	991	1000	1065	1000	
			1110	1000				

II.4 - CASE II_A

x = 2.5 ins		4.75		7.0		9.25	
Y	U	Y	U	Y	U	Y	U
0	150	0	181	0	138	0	173
10	250	10	240	10	181	10	260
20	369	20	301	20	236	20	356
30	493	30	350	30	304	30	438
40	589	40	417	40	383	40	464
50	638	50	478	50	441	50	521
60	673	60	521	60	494	60	543
70	703	70	560	70	537	70	561
80	721	80	590	80	577	80	575
90	744	90	620	90	599	90	590
100	761	100	643	100	622	115	628
125	805	110	672	110	643	140	670
150	840	120	684	120	652	165	711
175	877	145	740	130	679	190	748
200	902	170	790	155	724	215	781
225	912	195	828	180	766	240	807
250	927	220	864	205	803	265	834
275	948	245	892	230	829	290	851
300	957	270	910	255	856	340	902
325	1000	295	930	280	884	390	943
		320	945	305	912	440	968
		370	972	330	925	490	981
		420	988	380	957	540	990
		470	1000	430	987	590	1000
				480	991		
				530	1000		

CASE II_A (Cont.)

x = 11.5 ins		13.75		16.0		18.25	
Y	U	Y	U	Y	U	Y	U
0	134	0	156	0	132	0	130
10	188	10	210	10	174	10	171
20	231	20	264	20	227	20	223
30	292	30	309	30	265	30	281
40	344	40	349	40	318	40	330
50	391	50	402	50	371	50	375
60	430	60	434	60	400	60	400
70	473	70	461	70	436	70	422
80	506	80	480	80	456	80	440
105	553	90	506	90	474	90	460
130	593	100	515	115	513	100	467
155	635	110	525	140	548	125	498
180	668	120	545	165	582	150	534
205	706	130	566	190	602	175	566
230	741	155	594	215	636	200	587
255	765	180	627	240	666	250	641
280	789	205	659	265	690	300	684
305	829	230	682	290	717	350	723
330	853	255	719	340	765	400	772
380	896	280	744	390	814	450	808
430	931	330	792	440	853	500	849
480	967	380	830	490	880	550	888
530	976	430	871	540	924	600	918
580	995	480	910	590	945	650	945
630	1000	530	946	640	982	700	972
		580	972	690	983	750	991
		630	982	740	991	800	992
		680	1000	790	1000	850	1000

CASE II_A (Cont.)

x = 22.75 ins		25.0		27.25		29.5	
Y	U	Y	U	Y	U	Y	U
0	139	0	139	0	100	0	98
10	182	10	171	10	146	10	142
20	231	20	214	20	212	20	209
30	277	30	243	30	275	30	272
40	317	40	295	40	342	40	335
50	356	50	323	50	373	50	372
60	377	60	363	60	393	60	392
70	408	70	387	70	417	70	410
80	426	80	412	80	426	80	434
90	444	90	429	90	435	90	442
100	465	100	439	100	444	100	451
110	471	110	456	110	456	110	461
120	483	120	483	120	467	135	482
145	512	130	492	130	479	160	494
170	539	140	502	155	501	185	531
195	559	165	522	180	519	210	543
220	579	190	552	205	534	235	560
245	605	215	563	230	554	260	580
270	622	240	584	255	568	285	602
295	634	265	605	280	578	310	614
320	648	290	627	305	602	360	632
370	691	315	649	330	617	410	660
420	738	340	671	380	658	460	696
470	766	390	695	430	676	510	738
520	804	440	716	480	708	560	764
570	830	490	758	530	746	610	790
620	857	540	781	580	776	660	815
670	897	590	821	630	801	710	841
720	912	640	844	680	822	760	871
770	941	690	871	730	853	810	898
820	963	740	900	780	878	860	925
870	981	790	930	830	901	910	944
920	1000	840	945	880	918	960	955
		890	960	930	942	1010	974
		940	975	980	959	1060	991
		990	985	1030	966	1110	1000
		1040	1000	1080	981		
				1130	1000		

CASE II_A (Concluded)

x = 31.75 ins

Y	U
0	113
10	178
20	266
30	337
40	379
50	403
60	421
70	433
80	446
90	458
100	469
125	486
150	513
175	532
200	554
225	574
250	585
275	603
300	624
350	642
400	680
450	706
500	726
550	756
600	796
650	809
700	839
750	854
800	884
850	902
900	920
950	941
1000	957
1050	974
1100	989
1150	996
1200	1000

II.5 - CASE II_B

x = 4.75 ins			7.0			9.25		
Y	U	T	Y	U	T	Y	U	T
0	123	460	0	101	474	0	151	481
10	186	480	10	151	509	10	223	519
20	243	500	20	216	544	20	302	558
30	329	540	30	302	579	30	369	587
40	430	580	40	391	614	40	437	615
50	512	620	50	472	649	50	490	635
60	568	650	60	512	675	60	518	673
70	597	680	70	542	702	70	539	692
80	619	710	80	554	728	80	554	712
90	642	730	90	575	746	90	580	721
100	657	750	100	595	763	115	616	750
110	680	770	110	612	781	140	667	769
120	696	780	135	665	807	165	708	808
130	707	800	160	704	825	190	741	837
145	744	820	185	769	851	215	775	865
170	794	850	210	782	877	240	801	894
195	828	880	235	814	904	265	836	923
220	863	910	260	837	930	290	854	933
245	890	930	285	863	947	340	899	952
270	917	950	310	890	965	390	927	971
295	935	960	335	908	974	440	965	981
320	953	970	360	935	982	490	986	990
345	963	980	410	953	991	540	994	1000
370	972	990	460	976	1000	590	1000	
395	976	996	510	1000				
420	985	1000						
470	1000							

CASE II_B (Cont.)

x = 11.5 ins			13.75			18.25		
Y	U	T	Y	U	T	Y	U	T
0	95	431	0	144	471	0	119	417
10	133	461	10	194	500	10	161	444
20	197	500	20	262	529	20	226	472
30	266	539	30	334	558	30	288	500
40	325	569	40	391	587	40	345	519
50	384	608	50	428	615	50	379	537
60	413	627	60	453	654	60	397	556
70	448	657	70	472	673	70	414	574
80	467	676	80	485	692	80	433	593
90	492	706	90	499	712	90	451	602
100	504	725	100	512	721	100	470	611
110	514	745	110	526	731	125	496	630
120	537	765	135	561	750	150	536	657
145	578	784	160	589	769	175	564	685
170	617	814	185	626	798	200	585	713
195	663	833	210	657	827	225	614	741
220	700	853	235	696	846	250	644	769
245	731	882	260	720	865	275	666	787
270	759	902	285	760	885	300	682	815
295	794	912	310	773	894	350	729	852
320	819	931	335	802	904	400	769	880
370	860	951	360	819	923	450	810	898
420	903	961	410	866	942	500	853	917
470	955	980	460	902	952	550	879	935
520	978	990	510	935	971	600	915	944
570	994	1000	560	963	981	650	941	963
620	1000		610	985	990	700	959	972
			660	994	1000	750	978	981
			710	1000		800	985	991
						850	992	1000
						900	1000	

CASE II_B (Concluded)

x = 22.75 ins			25.0			31.75		
Y	U	T	Y	U	T	Y	U	T
0	126	513	0	162	442	0	102	500
10	164	546	10	203	481	10	157	526
20	235	580	20	260	519	20	218	552
30	299	613	30	335	558	30	297	578
40	360	647	40	394	587	40	341	603
50	416	681	50	447	625	50	389	629
60	449	706	60	474	654	60	426	655
70	469	723	70	496	683	70	433	664
80	490	739	80	505	702	80	446	672
90	498	748	90	519	712	105	477	690
100	508	756	115	546	731	130	514	707
125	540	765	140	570	740	155	538	724
150	563	782	165	592	760	180	557	741
175	590	790	190	607	769	205	584	759
200	613	798	215	631	788	230	596	776
225	632	807	240	638	808	255	610	793
250	648	815	265	654	827	280	620	802
275	664	832	290	667	837	330	656	819
300	689	840	340	699	856	380	689	836
325	706	849	390	723	869	430	713	853
350	723	857	440	748	885	480	733	871
375	740	874	490	770	894	530	755	888
400	750	882	540	803	904	580	786	905
450	783	899	590	831	913	630	807	917
500	814	916	640	849	923	680	825	926
550	837	929	690	873	932	730	838	931
600	857	941	740	895	942	780	870	940
650	874	950	790	914	952	830	889	948
700	903	958	840	942	962	880	917	957
750	922	966	890	952	971	930	926	966
800	931	975	940	961	981	980	941	974
850	951	983	990	971	990	1030	957	983
900	966	992	1040	980	1000	1080	975	991
950	990	1000	1090	1000		1130	988	997
1000	1000					1180	1000	1000

II.6 - CASE II_C

x = 4.75 ins

Y	U	T
0	131	423
10	197	481
20	296	538
30	386	596
40	481	654
50	519	683
60	539	712
70	566	731
80	580	750
90	608	769
100	629	788
125	688	827
150	745	865
175	789	894
200	830	913
225	872	933
250	894	952
275	915	971
300	932	981
350	959	990
400	985	1000
450	1000	

9.25

Y	U	T
0	121	522
10	161	558
20	216	593
30	280	628
40	347	664
50	402	690
60	433	708
70	454	726
80	473	735
90	485	743
100	500	752
110	517	770
120	536	788
130	544	796
140	563	805
165	617	832
190	660	858
215	697	880
240	735	903
265	766	920
290	797	938
315	829	947
340	854	956
390	904	973
440	947	982
490	974	991
540	986	1000
590	1000	

13.75

Y	U	T
0	109	500
10	159	535
20	218	579
30	258	623
40	306	658
50	341	684
60	365	711
70	393	728
80	405	737
90	417	746
100	437	754
110	447	763
120	459	772
145	510	798
170	544	816
195	578	833
220	628	851
245	650	868
270	695	886
295	718	912
320	741	930
370	797	947
420	848	965
470	881	974
520	933	982
570	955	991
620	980	1000
670	1000	

CASE II_C (Cont.)

x = 18.25 ins			22.75			27.25		
Y	U	T	Y	U	T	Y	U	T
0	126	522	0	105	580	0	103	524
10	175	558	10	163	608	10	177	565
20	223	587	20	212	636	20	247	612
30	278	616	30	265	670	30	292	659
40	318	638	40	307	699	40	340	688
50	344	652	50	337	716	50	357	706
60	363	667	60	350	727	60	369	718
70	377	674	70	365	739	70	374	729
80	388	681	80	378	744	80	380	735
90	397	688	90	392	756	90	404	753
100	405	696	100	402	761	100	413	765
110	426	710	110	408	767	110	423	771
120	440	725	120	415	773	135	448	788
130	453	732	130	426	778	160	467	806
140	465	739	140	438	784	185	494	818
150	469	746	165	463	795	210	514	829
175	490	768	190	489	807	235	528	841
200	516	790	215	516	818	260	549	853
225	560	812	240	550	830	285	563	859
250	576	833	265	569	841	310	578	865
275	611	855	290	593	852	360	637	876
300	634	870	315	615	858	410	676	888
325	662	884	340	630	864	460	698	900
350	684	899	390	675	875	510	732	906
400	738	913	440	706	892	560	782	918
450	786	928	490	746	909	610	816	929
500	826	942	540	782	926	660	842	941
550	863	961	590	813	938	710	860	953
600	903	971	640	856	949	760	896	965
650	929	978	690	882	960	810	924	971
700	955	986	740	903	966	860	942	976
750	974	993	790	939	977	910	951	982
800	991	1000	840	948	983	960	970	992
850	1000		890	965	989	1010	985	995
			940	981	994	1060	992	1000
			990	991	1000	1110	1000	
			1040	1000				

CASE II_C (Concluded)

$x = 31.75$ ins

Y	U	T
0	93	528
10	158	583
20	218	639
30	302	667
40	357	694
50	377	722
60	395	733
70	410	739
80	420	750
90	426	761
100	433	767
110	441	778
135	473	794
160	486	806
185	528	817
210	540	828
235	550	833
260	587	844
285	606	850
310	617	856
360	644	867
410	676	878
460	707	889
510	738	900
560	764	911
610	790	922
660	825	933
710	843	944
760	861	950
810	889	961
860	907	966
910	917	972
960	934	977
1010	945	984
1060	951	989
1110	975	992
1160	984	997
1210	994	1000
1260	1000	